

Copyright

by

Yang Du

2016

**The Dissertation Committee for Yang Du Certifies that this is the approved version  
of the following dissertation:**

**Amine Solvent Development for Carbon Dioxide Capture**

**Committee:**

---

Gary T. Rochelle, Supervisor

---

Isaac C. Sanchez

---

James E. Critchfield

---

Gyeong S. Hwang

---

Eric Chen

**Amine Solvent Development for Carbon Dioxide Capture**

**by**

**Yang Du, B.S.; M.S.; M.S.E**

**Dissertation**

Presented to the Faculty of the Graduate School of

The University of Texas at Austin

in Partial Fulfillment

of the Requirements

for the Degree of

**Doctor of Philosophy**

**The University of Texas at Austin**

**May 2016**

## **Dedication**

To my father, who has always been proud of me, but could not see this dissertation completed;

To my mother, who has been my role-model for hard work and integrity, and who has always given me her unconditional love and support.

## **Acknowledgements**

I would like to express my sincere gratitude to Dr. Gary T. Rochelle for being an incredibly knowledgeable and supportive supervisor for me throughout my entire Ph.D. study. I have always benefited from his constructive advice when I met difficulties in my research. He helped me through many tough times in my life, which I have no way but hard work to repay him. He is also a great role model for me. His genuinely cares about his students, creative but pragmatic thinking, and strong sense of family and social responsibility, as well as his passion for wilderness, have deeply influenced me. He warned me when I first met him that choosing an adviser is like getting married. Now I can say my Ph.D. journey with Dr. Rochelle was full of joy and fruit.

I need to thank my Ph.D. committee members, Prof. Isaac Sanchez, Prof. Gyeong Hwang, Dr. Jim Critchfield, and Dr. Eric Chen for their valuable time and insightful inputs for my work. They enabled me to have a more comprehensive and deeper view of my research.

I want to thank Maeve Cooney for her tremendous assistance throughout my graduate school career. She has been very patient and efficient helping me in editing all of my reports and papers, as well as helping me meet many key deadlines. I would like to extend my thanks to all the supporting staff at UT-Austin: Jim Smitherman and Butch Cunningham for experimental equipment design and trouble-shooting; Steve Sorey for NMR measurement; Randy Rife for IT support; Kevin Haynes and Eddie Ibarra for chemicals ordering and shipping; T Stockman and Kate Baird for their assistance throughout my graduate school career.

I am deeply indebted to Dr. Isaac Sanchez for supporting me, as a graduate advisor, during one of my hardest times in life. He not only chose to trust me, but also gave me valuable advices. I also want to thank Dr. Benny Freeman for making me learn a valuable life lesson the hard way.

I have benefited a lot from the following courses which made me become a true chemical engineer from an environmental scientist: 1) “Advanced Analysis for Chemical Engineers” by Dr. Isaac Sanchez; 2) “Chemical Reactor Analysis and Design” by Dr. Hal Alper; 3) “Transport Phenomena” by Dr. Maša Prodanović; 4) “Optimization: Theory/Practice” by Dr. Juan Ruiz. I also enjoyed the class “Proton and C13 Spectroscopy” by Dr. Ben Shoulders which was very helpful for my research.

I have been very lucky to have the opportunity working with many great graduate students in our research group. I am really grateful to have Steven Fulk as my lab mate. Steven spent a substantial amount of time helping me in running and maintaining the FTIR system. His broad knowledge and striving for perfection are very impressive and inspiring. Brent Sherman gave me a tremendous help in developing Aspen Plus® model from scratch. He was always willing to spend his time patiently helping me with his excellent knowledge of modeling and great teaching skills. Lynn Li taught me how to perform the Wetted-Wall Column experiment and other basic experiments when I was still a newbie in the group. Lynn was always thoughtful and gave me valuable advice when I met difficulties in research and in life. Omkar Namjoshi showed me how to run degradation experiment and analyze samples. Omkar is the master of various analytical apparatus in our lab, and his advice for experimental planning and design benefited me a lot. Alex Voice, Paul Nielsen and Kent Fischer have given many helps on my oxidation experiments and sample analysis. Yu-Jeng Lin taught me a lot about process simulation and optimization. Nathan Fine’s passion for innovation inspired me a lot. I would also

like to thank all other colleagues: Dr. Eric Chen, Mandana Ashouripashaki, Qing Xu, Jorge Plaza, Chao Wang, Thu Nguyen, Peter Frailie, Darshan Sachde, Matt Walters, Tarun Madan, Matt Beaudry, Di Song, Ye Yuan, Yue Zhang, and Junyuan Ding. It has been a great pleasure working with them on a daily basis.

I want to give special thanks to my colleague, Ye Yuan, and my undergraduate research assistants, Nathan Kwan and Yukai Wang. We have worked closely as a team. Without their help, it was not possible for me to get so much work done.

I also need to thank Dr. Arlinda Ciftja from NTNU who measured the  $pK_a$  of HMPD for us.

Last but definitely not least, I wanted to thank my families. The unselfish and unconditional love from my parents have always been my strongest support during my hard time. They always support my decision and believe I will succeed. I am so lucky to marry Yao, the girl who I fell in love with at first sight and who has accompanied me through all life's ups and downs in the past ten years. Without her understanding and the great support, I would not have focused on my research. I also want to thank my parents-in-law for helping take care of my mom.

# **Amine Solvent Development for Carbon Dioxide Capture**

Yang Du, Ph.D.

The University of Texas at Austin, 2016

Supervisor: Gary T. Rochelle

36 novel aqueous piperazine (PZ)-based amine blends for CO<sub>2</sub> capture from flue gas were screened for their thermal degradation, amine volatility, CO<sub>2</sub> cyclic capacity, and CO<sub>2</sub> absorption rate at normal operating conditions. These amines include 7 imidazoles, 8 cyclic and long-chain diamines, 12 tertiary amines, 4 hindered amines, 3 hindered and tertiary amino acids, and 2 ether amines that were selected based on known amine structure-property relationships and their potential for industrial application. 18 thermally stable PZ-based amine blends were identified with proposed degradation mechanisms. 14 novel tertiary and hindered amines were found to have a lower volatility than 2-amino-2-methyl-1-propanol (AMP). A group contribution model to predict amine volatility was developed. In a PZ/tertiary amine, the optimum pK<sub>a</sub> of the tertiary amine was around 9.1 to give the highest CO<sub>2</sub> cyclic capacity. A generic model for PZ/tertiary amines was developed in Aspen Plus<sup>®</sup>, which can predict the CO<sub>2</sub> vapor-liquid-equilibrium based on the pK<sub>a</sub> of the tertiary amine in blend. To a lesser degree than pK<sub>a</sub>, the polarity of the tertiary amine also affects the CO<sub>2</sub> solubility of the blend. CO<sub>2</sub> absorption rates of most 2.5 m PZ/2.5 m tertiary amines are slightly lower than 2.5 m PZ itself, due to the higher viscosity of the blends, but they still absorb CO<sub>2</sub> much faster than 7 m monoethanolamine (MEA).

2 m PZ/3 m 4-hydroxy-1-methylpiperidine (HMPD) is the blend that shows the best overall properties for thermal stability, amine volatility, CO<sub>2</sub> cyclic capacity, and CO<sub>2</sub> absorption rate. 2 m PZ/3 m HMPD also has a much better solid solubility than 5 m PZ. The capital and energy cost for flue gas CO<sub>2</sub> capture using 2 m PZ/3 m HMPD is expected to be much lower than that using 7 m MEA, while comparable to that using 5 m PZ.

Thermally degraded diglycolamine<sup>®</sup> (DGA<sup>®</sup>)/dimethylaminoethoxyethanol (DMAEE) was found to have a better performance for CO<sub>2</sub> capture than the original solvent. At high temperature, DGA<sup>®</sup>/DMAEE reaches equilibrium with its major degradation product, methylaminoethoxyethanol (MAEE). The production of MAEE enhances the CO<sub>2</sub> absorption rate, while maintaining the CO<sub>2</sub> capacity of the original solvent.

## Table of Contents

List of Tables .....	xv
List of Figures .....	xx
Chapter 1: Introduction .....	1
1.1 Global Warming and CO <sub>2</sub> Emission .....	1
1.2 Amine Scrubbing Technology for CO <sub>2</sub> Capture .....	1
1.3 Solvent Development .....	2
1.4 Review of Relevant Literature .....	4
1.5 Research Objectives .....	6
Chapter 2: Thermal Degradation of Novel Piperazine/Amine Blends for CO <sub>2</sub> Capture .....	7
2.1 Introduction .....	7
2.2 Experimental Methods .....	10
2.2.1 Solution preparation .....	10
2.2.2 Experimental Approach .....	10
2.2.3 Analytical Tools - Cation and Anion Chromatography .....	11
2.2.4 Thermal degradation model .....	11
2.3 Results and Discussion .....	12
2.3.1 PZ/Imidazoles .....	12
2.3.2 PZ/Diamines .....	17
2.3.3 PZ/Tertiary amines .....	22
2.3.4 PZ/Hindered amines .....	26
2.3.5 PZ/Amino acids and PZ/Ether amines .....	27
2.4 Conclusions .....	29
2.5 Recommendations .....	30
2.6 Acknowledgements .....	31
Chapter 3: Volatility of Amines for CO <sub>2</sub> Capture .....	32
3.1 Introduction .....	32

3.2	Experimental Methods .....	34
3.2.1	Solution preparation.....	34
3.2.2	Amine volatility measurement.....	35
3.2.3	Henry's law constant.....	37
3.2.4	Experimental validation .....	38
3.3	Results and Discussion .....	39
3.3.1	Henry's law constant.....	39
3.3.2	Amine partial pressure ( $P_{am}$ ) of tertiary and hindered amines ....	46
3.3.3	Correlation between $H_{am}$ and $P_{am}$ of tertiary and hindered amines at nominal lean loading for coal-fired flue gas .....	52
3.4	Conclusions.....	53
3.5	Acknowledgements.....	54
Chapter 4: CO <sub>2</sub> Capacity and Absorption Rate of Novel Piperazine/Amine Blends .....		55
4.1	Introduction.....	56
4.2	Experiment Methods.....	59
4.2.1	Solution preparation.....	59
4.2.2	Viscosity measurement .....	60
4.2.3	CO <sub>2</sub> solubility by FTIR.....	60
4.2.4	CO <sub>2</sub> solubility and absorption rate by WWC.....	60
4.3	Results and Discussion .....	63
4.3.1	CO <sub>2</sub> solubility of PZ/tertiary amines.....	63
4.3.1.1	Effect of $pK_a$ of tertiary amines.....	63
4.3.1.2	Effect of solution polarity .....	66
4.3.2	Generic Aspen Plus <sup>®</sup> model.....	67
4.3.3	Comparison between PZ/tertiary amine and PZ/hindered amine.....	69
4.3.4	CO <sub>2</sub> absorption rate of PZ/tertiary amines.....	70
4.3.5	Proposed PZ/tertiary amines for CO <sub>2</sub> capture from flue gas .....	73
4.4	Conclusions.....	75
4.5	Acknowledgements.....	76

Chapter 5: Thermal Degradation of Piperazine/4-Hydroxy-1-methylpiperidine	77
5.1 Introduction	77
5.2 Experiment Methods	79
5.2.1 Solution preparation	79
5.2.2 Experimental Approach	79
5.2.3 Analytical Tools - Cation Chromatography	80
5.3 Results and Discussion	80
5.3.1 Degradation Mechanism and Products	80
5.3.2 Effect of Process Conditions	84
5.3.2.1 Effect of CO <sub>2</sub> loading	85
5.3.2.2 Effect of solvent composition	86
5.3.2.3 Effect of temperature	87
5.3.3 Comparison between PZ/HMPD and PZ/MDEA	89
5.3.4 Potential environmental issues of 1,4 DMPZ	94
5.4 Conclusions	97
5.5 Acknowledgements	97
Chapter 6: Piperazine/4-Hydroxy-1-methylpiperidine for CO <sub>2</sub> Capture	98
6.1 Introduction	98
6.2 Experimental Methods	100
6.2.1 Solution preparation	100
6.2.2 Viscosity measurement	101
6.2.3 Amine volatility	101
6.2.4 CO <sub>2</sub> solubility and absorption rate	101
6.2.5 Solid Solubility	102
6.2.6 Oxidative Degradation	102
6.3 Results and Discussion	103
6.3.1 Amine volatility	103
6.3.2 Viscosity	104
6.3.3 CO <sub>2</sub> capacity and absorption rate	105
6.3.4 Solid solubility	109

6.3.5	CO <sub>2</sub> solubility in 2 m PZ/3 m HMPD at 20 – 160 °C .....	112
6.3.6	Oxidative stability and thermal stability .....	113
6.3.7	Synthesis and cost of HMPD .....	114
6.4	Conclusions.....	115
Chapter 7:	Thermally Degraded Diglycolamine <sup>®</sup> /Dimethylaminoethoxyethanol for CO <sub>2</sub> Capture .....	116
7.1	Introduction.....	116
7.2	Experimental Methods .....	118
7.2.1	Solution preparation.....	118
7.2.2	Thermal degradation .....	119
7.2.3	Analytical Tools - Cation Chromatography.....	119
7.2.4	Viscosity measurement .....	120
7.2.5	CO <sub>2</sub> solubility and absorption rate .....	120
7.3	Results and Discussion .....	121
7.3.1	Degradation of DGA <sup>®</sup> and DMAEE in Acidified Solution .....	121
7.3.2	Degradation of DGA <sup>®</sup> in CO <sub>2</sub> Loaded Solution.....	122
7.3.3	Degradation of DGA <sup>®</sup> /DMAEE in Acidified Solution.....	124
7.3.4	Degradation of DGA <sup>®</sup> /DMAEE in CO <sub>2</sub> -loaded solution.....	127
7.3.5	Loss of effective amine in degraded DGA <sup>®</sup> /DMAEE .....	128
7.3.6	CO <sub>2</sub> Cyclic Capacity and Absorption Rate .....	129
7.3.7	CO <sub>2</sub> Solubility in 1.75 m DGA <sup>®</sup> /1.75 m MAEE/3.50 m DMAEE at 20 – 160 °C .....	133
7.4	Conclusions.....	135
7.5	Recommendations.....	136
7.6	Acknowledgements.....	136
Chapter 8:	Conclusions and Recommendations .....	137
8.1	Conclusions.....	137
8.2	Recommendations.....	141

Appendix A: Thermal Degradation Data for Chapter 2.....	144
Appendix B: Detailed WWC data.....	149
Appendix C: Thermal Degradation Data for DGA <sup>®</sup> /DMAEE.....	173
References.....	177

## List of Tables

Table 2.1:	Summary of $k_1$ , $E_A$ , and $T_{\max}$ for 2 m PZ/2 m imidazoles with 0.2 mol CO <sub>2</sub> /mole alkalinity.....	15
Table 2.2:	Summary of $k_1$ , $E_A$ , and $T_{\max}$ for 2 m PZ/2 m diamines with 0.2 mol CO <sub>2</sub> /mole alkalinity.....	22
Table 2.3:	Summary of $k_1$ , $E_A$ , and $T_{\max}$ for 2 m PZ/2 m tertiary amines with 0.2 mol CO <sub>2</sub> /mole alkalinity. ....	25
Table 2.4:	Summary of $k_1$ , $E_A$ , and $T_{\max}$ for 2 m PZ/2 m hindered amines with 0.2 mol CO <sub>2</sub> /mole alkalinity. ....	26
Table 2.5:	Summary of $k_1$ , $E_A$ , and $T_{\max}$ for 2 m PZ/2 m K <sup>+</sup> /amino acids, and 2 m PZ/2 m ether amines with 0.2 mol CO <sub>2</sub> /mole alkalinity. ....	29
Table 3.1:	Comparison of measured $H_{\text{am}}$ at 40 °C to values estimated by Nguyen (2013) and by the updated model from this work.....	42
Table 3.1:	Comparison of measured $H_{\text{am}}$ at 40 °C to values estimated by Nguyen (2013) and by the updated model from this work (continued). ....	43
Table 3.2:	Model parameter values. ....	44
Table 3.3:	Volatility of 2.5 m PZ/2.5 m tertiary amines at normal loading range for coal-fired flue gas and 40 °C. ....	48
Table 3.3:	Volatility of 2.5 m PZ/2.5 m tertiary amines at normal loading range for coal-fired flue gas and 40 °C (continued). ....	49
Table 3.4:	Volatility of 2.5 m PZ/2.5 m hindered amines at normal loading range for coal-fired flue gas and 40 °C.....	50
Table 4.1:	Tertiary and hindered amines with their structures and pK <sub>a</sub> .....	58

Table 4.1:	Tertiary and hindered amines with their structures and pKa (continued).	59
Table 4.2:	Properties of 2.5 m PZ/2.5 m tertiary amines, compared to 7 m MEA, 2.5 m PZ, 5 m PZ, and 2.5 m PZ/2.5 m MDEA.	73
Table 4.2:	Properties of 2.5 m PZ/2.5 m tertiary amines, compared to 7 m MEA, 2.5 m PZ, 5 m PZ, and 2.5 m PZ/2.5 m MDEA (continued).	74
Table 5.1:	Nitrogen mass balance 2 m PZ/3 m HMPD with 0.26 mol CO <sub>2</sub> /mole alkalinity degraded at 150 °C for 30 weeks.	84
Table 5.2:	k <sub>2,f,c</sub> values for PZ/HMPD with variable total amine and PZ/HMPD at 0.24 mol CO <sub>2</sub> /mole alkalinity and 175 °C.	87
Table 6.1:	Properties of PZ/HMPD compared to 7 m MEA, 5 m PZ, and 8 m PZ.	112
Table 7.1:	Properties of DGA <sup>®</sup> /MAE/DMAEE solvents with variable concentration, compared to 7 m MEA, 10 m DGA <sup>®</sup> , and 5 m PZ.	133
Table A.1:	Thermal degradation of 2 m PZ/2 m imidazoles with 0.2 mol CO <sub>2</sub> /mole alkalinity.	144
Table A.2:	Thermal degradation of 2 m PZ/2 m diamines with 0.2 mol CO <sub>2</sub> /mole alkalinity.	145
Table A.3:	Thermal degradation of 2 m PZ/2 m tertiary amines with 0.2 mol CO <sub>2</sub> /mole alkalinity.	146
Table A.4:	Thermal degradation of 2 m PZ/2 m hindered amines with 0.2 mol CO <sub>2</sub> /mole alkalinity.	147
Table A.5:	Thermal degradation of 2 m PZ/2 m K <sup>+</sup> /amino acids, and 2 m PZ/2 m ether amines with 0.2 mol CO <sub>2</sub> /mole alkalinity.	148
Table B.1:	Detailed WWC data for 2.5 m PZ.	149

Table B.2:	Detailed WWC data for 2.5 m PZ / 2.5 m IMI.	150
Table B.3:	Detailed WWC data for 2.5 m PZ / 2.5 m HEMor.	151
Table B.4:	Detailed WWC data for 2.5 m PZ / 2.5 m 2E-IMI.	152
Table B.5:	Detailed WWC data for 2.5 m PZ / 2.5 m 2E-4M-IMI.	153
Table B.6:	Detailed WWC data for 2.5 m PZ / 2.5 m MDEA.	154
Table B.7:	Detailed WWC data for 2.5 m PZ / 2.5 m DMAEE.	155
Table B.8:	Detailed WWC data for 2.5 m PZ / 2.5 m HMPD.	156
Table B.9:	Detailed WWC data for 2.5 m PZ / 2.5 m BDMAEE.	157
Table B.10:	Detailed WWC data for 2.5 m PZ / 2.5 m HEPD.	158
Table B.11:	Detailed WWC data for 2.5 m PZ / 2.5 m DEA-PDL.	159
Table B.12:	Detailed WWC data for 2.5 m PZ / 2.5 m Tropine.	160
Table B.13:	Detailed WWC data for 1.07 m DGA <sup>®</sup> / 1.93 m MAE / 7 m DMAEE.	161
Table B.14:	Detailed WWC data for 2.5 m DGA <sup>®</sup> / 2.5 m MAE / 10 m DMAEE.	162
Table B.15:	Detailed WWC data for 0.75 m DGA <sup>®</sup> / 1.35 m MAE / 4.9 m DMAEE.	163
Table B.16:	Detailed WWC data for 2.1 m DGA <sup>®</sup> / 4.9 m DMAEE.	164
Table B.17:	Detailed WWC data for 1.75 m DGA <sup>®</sup> / 1.75 m MAE / 3.5 m DMAEE at 20 °C.	165
Table B.18:	Detailed WWC data for 1.75 m DGA <sup>®</sup> / 1.75 m MAE / 3.5 m DMAEE at 40 °C.	166
Table B.19:	Detailed WWC data for 1.75 m DGA <sup>®</sup> / 1.75 m MAE / 3.5 m DMAEE at 60 °C.	167
Table B.20:	Detailed WWC data for 2 m PZ / 3 m HMPD at 0.157 mol CO <sub>2</sub> /mol alkalinity.	168

Table B.21: Detailed WWC data for 2 m PZ / 3 m HMPD at 0.257 mol CO <sub>2</sub> /mol alkalinity. ....	169
Table B.22: Detailed WWC data for 2 m PZ / 3 m HMPD at 0.377 mol CO <sub>2</sub> /mol alkalinity. ....	170
Table B.23: Detailed WWC data for 2 m PZ / 3 m HMPD at 0.444 mol CO <sub>2</sub> /mol alkalinity. ....	171
Table B.24: Detailed WWC data for 2 m PZ / 3 m HMPD at 0.521 mol CO <sub>2</sub> /mol alkalinity. ....	172
Table C.1: Thermal degradation of 5 m DGA <sup>®</sup> with 0.2 mol H <sup>+</sup> /mole alkalinity at 150 °C. ....	173
Table C.2: Thermal degradation of 5 m DMAEE with 0.2 mol H <sup>+</sup> /mole alkalinity at 150 °C, along with the formation of MAEE and QUAT. ....	173
Table C.3: Degradation of 7 m DGA <sup>®</sup> with 0.3 mol CO <sub>2</sub> /mole alkalinity at 150 °C, along with the formation of morpholine. ....	174
Table C.4: Thermal degradation of 5 m DGA <sup>®</sup> /5 m DMAEE with 0.2 mol H <sup>+</sup> /mole alkalinity at 175 °C, along with the formation of MAEE. ....	174
Table C.5: Thermal degradation of 2.5 m DGA <sup>®</sup> /7.5 m DMAEE with 0.2 mol H <sup>+</sup> /mole alkalinity at 175 °C, along with the formation of MAEE. ....	174
Table C.6: Thermal degradation of 7.5 m DGA <sup>®</sup> /2.5 m DMAEE with 0.2 mol H <sup>+</sup> /mole alkalinity at 175 °C, along with the formation of MAEE. ....	175
Table C.7: Degradation of 5 m DGA <sup>®</sup> /5 m DMAEE with 0.4 mol CO <sub>2</sub> /mole alkalinity at 150 °C, along with the formation of MAEE and other minor products. ....	175

Table C.8: Degradation of 5 m DGA <sup>®</sup> /5 m DMAEE with 0.3 mol CO <sub>2</sub> /mole alkalinity at 150 °C, along with the formation of MAEE and other minor products.....	175
Table C.9: Degradation of 5 m DGA <sup>®</sup> /5 m DMAEE with 0.3 mol CO <sub>2</sub> /mole alkalinity at 135 °C, along with the formation of MAEE and other minor products.....	176

## List of Figures

Figure 1.1: Process flow diagram of an amine scrubbing process for CO <sub>2</sub> recovery from coal-fired power plant flue gas.....	2
Figure 2.1: PZ loss and equivalent NH <sub>3</sub> production in 2 m PZ/2 m imidazoles with 0.2 mol CO <sub>2</sub> /mole alkalinity after 2 weeks at 150 °C (solid bar: PZ; open bar: NH <sub>3</sub> ). .....	16
Figure 2.2: Effect of PZ, acidity, and CO <sub>2</sub> on NH <sub>3</sub> production for IMI at 175 °C after 1 week. ....	17
Figure 2.3: Effect of PZ, acidity, and CO <sub>2</sub> on HEP degradation at 175 °C.....	20
Figure 2.4: Degradation of 2 m PZ/2 m 2AM-PD, and 2 m PZ/2 m 1,3 DAP with 0.2 mol CO <sub>2</sub> /mole alkalinity at 175 °C for 1 week. ....	21
Figure 2.5: Degradation of DMG, L-Pro and HL-Pro in 2 m PZ/2 m K <sup>+</sup> /amino acids with 0.2 mol CO <sub>2</sub> /mole alkalinity at 150 °C.....	28
Figure 3.1: FTIR system for volatility measurement. Figure adapted by author from Nguyen (2013). ....	35
Figure 3.2: Schematic of Gasmeter Calibrator mechanics. From: Nguyen (2013).	37
Figure 3.3: Comparison of the Henry's law constant (H <sub>am</sub> ) from this work and Nguyen (2013). ....	39
Figure 3.4: P <sub>am</sub> at 40°C of tertiary amine in 2.5 m PZ/2.5 m tertiary amine with variable pK <sub>a</sub> .....	51
Figure 3.5: P <sub>am</sub> at 40°C of hindered amines in 2.5 m PZ/2.5 m hindered amine with variable pK <sub>a</sub> .....	52

Figure 3.6: Correlation between $H_{am}$ and $P_{am}$ of tertiary and hindered amines in 2.5 m PZ/2.5 m tertiary and hindered amines at nominal lean loading for coal-fired flue gas ( $\sim 0.5$ kPa $P^*_{CO_2}$ ) at 40 °C.....	53
Figure 4.1: Wetted wall column system.....	61
Figure 4.2: Plot of flux of $CO_2$ vs. driving force obtained from a set of measurements for 2.5 m piperazine/2.5 m 1-(2-hydroxyethyl)piperidine at 40 °C and the loading of 0.60 mol $CO_2$ /mol PZ in the WWC. ....	63
Figure 4.3: $CO_2$ solubility of 2.5 m PZ/2.5 m tertiary amine with similar volatility but variable $pK_a$ at 40 °C, compared to 2.5 m PZ (dashed line). ....	65
Figure 4.4: Effect of solution polarity on the $CO_2$ solubility of 2.5 m PZ/2.5 m tertiary amine at 40 °C.....	66
Figure 4.5: Lean ( $P_{CO_2}=0.5$ kPa at 40 °C) and rich loading ( $P_{CO_2}=5$ kPa at 40 °C) of 2.5 m PZ/2.5 m tertiary amine as a function of the $pK_a$ of tertiary amine at 25 °C; solid points: measured lean loadings; open points: measured rich loadings; lines: generic Aspen Plus® model prediction. ....	68
Figure 4.6: $\Delta\alpha_{CO_2}$ of 2.5 m PZ/2.5 m tertiary amines as a function of the $pK_a$ of tertiary amines at 25 °C; solid points: measured 2.5 m PZ/2.5 m mono-tertiary amines; open points: measured 2.5 m PZ/2.5 m di-tertiary amines; dashed line: $\Delta\alpha_{CO_2}$ of 2.5 m PZ; solid line: generic Aspen Plus® model prediction. ....	69
Figure 4.7: Lean ( $P_{CO_2}=0.5$ kPa at 40 °C) and rich loading ( $P_{CO_2}=5$ kPa at 40 °C) of 2.5 m PZ/2.5 m tertiary amines as a function of the $pK_a$ of tertiary amines at 25 °C; solid points: measured lean loadings; open points: measured rich loadings; lines: generic Aspen Plus® model prediction.	70

Figure 4.8: $k_g'$ of 2.5 m PZ/2.5 m tertiary amines at 40 °C as a function of the $pK_a$ of tertiary amines at 25 °C; solid points: 2.5 m PZ/2.5 m mono-tertiary amines; open point: 2.5 m PZ/2.5 m di-tertiary amine (BDMAEE); dotted lines: $k_g'$ of 7 m MEA and 2.5 m PZ. ....	72
Figure 5.1: Degradation of 2 m PZ/3 m HMPD with 0.26 mol CO <sub>2</sub> /mole alkalinity at 150 °C, along with the formation of the major degradation products. Solid lines indicate second-order rate models fit the data (Equation 5.3). ....	82
Figure 5.2: Formation of the minor degradation products for degradation of 2 m PZ/3 m HMPD with 0.26 mol CO <sub>2</sub> /mole alkalinity at 150 °C.....	83
Figure 5.3: Degradation of 2 m PZ/3 m HMPD loaded with CO <sub>2</sub> , or H <sub>2</sub> SO <sub>4</sub> at 175 °C. ....	86
Figure 5.4: Degradation of PZ and HMPD in 2 m PZ/3 m HMPD with 0.26 mol CO <sub>2</sub> /mole alkalinity at 150, 165, and 175 °C. Lines indicate second-order rate models fit the data (Equation 5.3). ....	88
Figure 5.5: The Arrhenius behavior of the second-order rate constant ( $k_{2,f,c}$ ) for thermal degradation of 2 m PZ/3 m HMPD with 0.26 mol CO <sub>2</sub> /mole alkalinity. ....	89
Figure 5.6: Degradation of 5 m PZ/5 m HMPD and 5 m PZ/5 m MDEA with 0.24 mol CO <sub>2</sub> /mole alkalinity at 175 °C. Lines indicate first-order rate models fit the data.....	90
Figure 5.7: Degradation of 2 m PZ/1 m HPD with 0.31 mol CO <sub>2</sub> /mole alkalinity at 150 °C, compared to 7 m PZ/2 m DEA with 0.31 mol CO <sub>2</sub> /mole alkalinity (Namjoshi, 2015). ....	91

Figure 5.8: Degradation of 5 m HMPD and 5 m MDEA with 0.2 mol H <sup>+</sup> /mole alkalinity at 175 °C. ....	92
Figure 5.9: Degradation of 2 m PZ/3 m HMPD and 2 m PZ/3 m MDEA with 0.26 mol H <sup>+</sup> /mole alkalinity at 175 °C. Lines indicate first-order rate models fit the data. ....	93
Figure 5.10: PZ, 1MPZ and 1,4 DMPZ in the degradation of 5 m PZ/5 m HMPD and 5 m PZ/5 m MDEA with 0.24 mol CO <sub>2</sub> /mole alkalinity at 175 °C. ....	95
Figure 5.11: K <sub>i</sub> for PZ/HMPD/1MPZ/HPD degraded at 150 °C (α=0.26). Labels indicate the concentrations of PZ, HMPD, 1-MPZ, and HPD in solution in molal (m). Lines indicate reversible second-order rate models fit the data (Equation 5.2). ....	96
Figure 6.1: Partial pressure of HMPD in PZ/HMPD at variable CO <sub>2</sub> loading at 40 °C, compared to AMP in 5 m PZ/2.3 m AMP, 8 m PZ, 7 m MEA, and 4.8 m AMP (Nguyen, 2013). ....	104
Figure 6.2: Viscosity of PZ/HMPD at variable CO <sub>2</sub> partial pressure and 40 °C, compared to 7 m MEA, 5 m PZ (Dugas, 2009), and 8 m PZ (Freeman, 2011). ....	105
Figure 6.3: CO <sub>2</sub> absorption rate (kg <sup>3</sup> ) by WWC in PZ/HMPD at 40 °C, compared to 7 m MEA, 5 m PZ, and 8 m PZ (Dugas, 2009). ....	106
Figure 6.4: CO <sub>2</sub> solubility by WWC in PZ/HMPD at 40 °C, compared to 7 m MEA (Plaza, 2011), 5 m PZ and 8 m PZ (Frailie, 2014). ....	107
Figure 6.5: Normalized CO <sub>2</sub> capacity and average absorption rate (kg <sup>3</sup> <sub>avg</sub> ) at 40 °C for PZ/HMPD with variable concentration, compared to 7 m MEA, 5 m PZ, and 8 m PZ. ....	109

Figure 6.6: Dissolution temperature ( $T_d$ ) for PZ/HMPD over a range of $\text{CO}_2$ concentration, compared to 5 m PZ and 8 m PZ (Freeman, 2011).	110
Figure 6.7: Dissolution temperature ( $T_d$ ) (solid points) and precipitation temperature ( $T_p$ ) (open points) for 2 m PZ/3 m HMPD over a range of $\text{CO}_2$ partial pressure at 40 °C, compared to 5 m PZ and 8 m PZ.	111
Figure 6.8: $\text{CO}_2$ solubility in 2 m PZ/3 m HMPD. Squares: volatility results; other solid points: WWC results; open points: total pressure results; lines: model prediction (Equation 6.4).	113
Figure 6.9: Amine loss for 2 m PZ/3 m HMPD at 70 °C with 98% $\text{O}_2$ /2% $\text{CO}_2$ , as well as 0.1 mM $\text{Mn}^{2+}$ , 0.4 mM $\text{Fe}^{2+}$ , 0.05 mM $\text{Cr}^{3+}$ , and 0.1 mM $\text{Ni}^{2+}$ , compared to 10 m MEA (Liu, 2015).	114
Figure 7.1: Degradation of 5 m DGA <sup>®</sup> and 5 m DMAEE with 0.2 mol $\text{H}^+$ /mole alkalinity at 150 °C, along with the formation of MAEE and QUAT for DMAEE degradation.	122
Figure 7.2: Degradation of 7 m DGA <sup>®</sup> with 0.3 mol $\text{CO}_2$ /mole alkalinity at 150 °C, compared to 5 m DGA <sup>®</sup> with 0.4 mol $\text{CO}_2$ /mole alkalinity measured by Hatchell (2015) at the same temperature.	123
Figure 7.3: Degradation of 5 m DGA <sup>®</sup> /5 m DMAEE with 0.3 mol $\text{H}^+$ /mole alkalinity at 175 °C, along with the formation of MAEE. Lines indicate second-order reversible rate models fit the data (Equation 7.4).	125
Figure 7.4: $K_t$ for DGA <sup>®</sup> /DMAEE/MAEE thermally degraded at 175 °C ( $\alpha_{\text{H}}=0.3$ ). points are experimental $K_t$ ; Lines indicate second-order reversible rate models fit the data (Equation 7.5).	127

Figure 7.5: Degradation of 5 m DGA<sup>®</sup>/5 m DMAEE with 0.4 mol CO<sub>2</sub>/mole alkalinity at 150 °C, along with the formation of MAEE and other minor products. Solid lines and dashed line indicate second-order reversible rate models fit the data (Equation 7.4).....128

Figure 7.6: Comparison of the loss of effective amine for 5 m DGA<sup>®</sup>/5 m DMAEE to 7 m MEA with 0.4 mol CO<sub>2</sub>/mole alkalinity at 150 °C (Davis and Rochelle, 2009). The solid line indicates a first-order rate model fit the data.....129

Figure 7.7: CO<sub>2</sub> cyclic capacity and average absorption rate (kg'avg) at 40 °C for DGA<sup>®</sup>/MAE/DMAEE with variable concentration, compared to 7 m MEA, 10 m DGA<sup>®</sup>, and 5 m PZ. Labels indicate the concentrations of DGA<sup>®</sup>, MAE, and DMAEE in solution in molal (m). .....132

Figure 7.8: CO<sub>2</sub> solubility in 1.75 m DGA<sup>®</sup>/1.75 m MAE (as a proxy for MAEE)/3.50 m DMAEE. Solid points: WWC results; open points: total pressure results; lines: model prediction (Equation 7.9).....135

## **Chapter 1: Introduction**

### **1.1 GLOBAL WARMING AND CO<sub>2</sub> EMISSION**

Anthropogenic greenhouse gas emissions are changing climates worldwide (IPCC, 2014). Mitigation of greenhouse gas emissions can substantially reduce risks of climate change in the second half of the 21st century (IPCC, 2014). CO<sub>2</sub> emissions from fossil fuel combustion and industrial processes contributed about 78 % of the total GHG emission increase from 1970 to 2010, and accounted for 65% of the total anthropogenic GHG emissions in 2010 (IPCC, 2014).

The coal fired power plant is the largest single source of carbon emissions, accounting for 29% of U.S. CO<sub>2</sub> emissions and 31% of world emissions (EPA, 2015a). In 2015, the U.S. Environmental Protection Agency (EPA) announced the new carbon emission standard for the new and existing coal-fired power plant, aiming to reduce carbon emissions 32% from 2005 levels by 2030 (EPA, 2015b). Under this regulation, the power sector may add the carbon capture and storage to the coal-fired power plants or shift to other carbon-free power generation.

### **1.2 AMINE SCRUBBING TECHNOLOGY FOR CO<sub>2</sub> CAPTURE**

Amine scrubbing has shown the most promise for effective capture of CO<sub>2</sub> from coal-fired flue gas (Rochelle, 2009). A typical amine scrubbing process for CO<sub>2</sub> capture is shown in Figure 1.1. Desulfurized flue gas from coal combustion with 12% CO<sub>2</sub> is contacted with the aqueous amine in the absorber where 90% of the CO<sub>2</sub> is removed. The rich solvent from the bottom of the absorber is sent to the stripper and heated for CO<sub>2</sub> regeneration. The hot lean solvent is cooled by the cold rich solvent in the cross exchanger before being recycled back to the absorber. The stripped CO<sub>2</sub> is then compressed to 150 bar for further storage and sequestration. Aqueous

monoethanolamine (MEA) with a concentration of 15–30 wt % has been previously used in similar applications such as CO<sub>2</sub> removal from natural gas and hydrogen, and is currently considered the benchmark solvent for flue gas CO<sub>2</sub> capture (Rochelle, 2009).

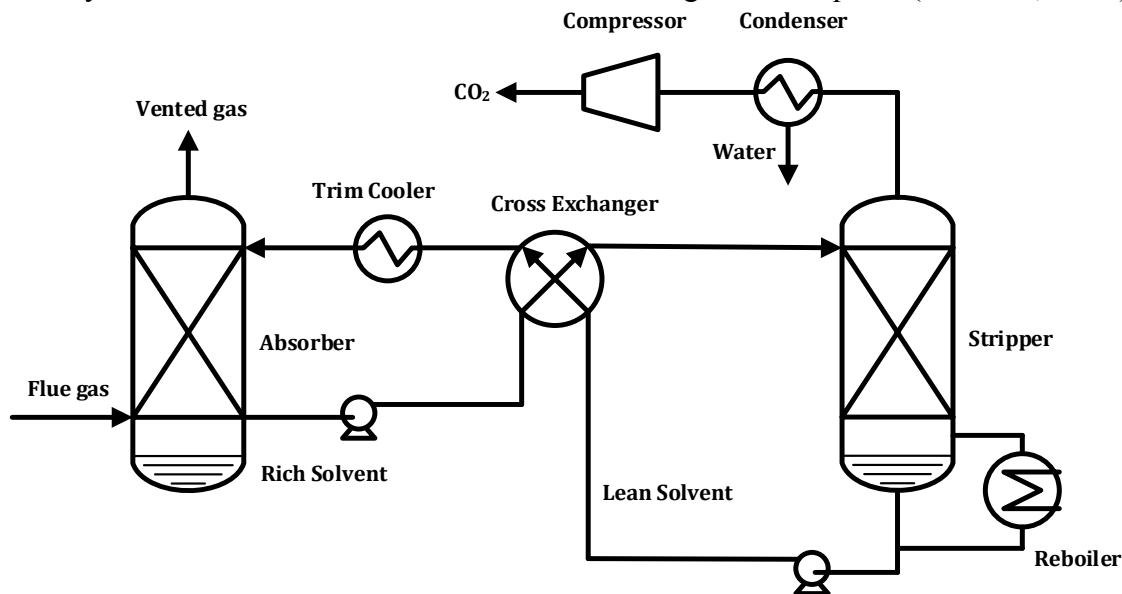


Figure 1.1: Process flow diagram of an amine scrubbing process for CO<sub>2</sub> recovery from coal-fired power plant flue gas.

### 1.3 SOLVENT DEVELOPMENT

Although amine scrubbing is a mature technology and has been used in the gas treating industry for around 100 years (Bottoms, 1933), the low CO<sub>2</sub> partial pressure in flue gas will lead to high capital and operating costs of the amine scrubbing unit. Current estimates suggest a 40–70% increase in cost of electricity to remove 90% CO<sub>2</sub> from a coal-fired power plant (Rubin et al., 2007). To minimize capital and operating costs, current research efforts focus on 1) finding new solvents with desirable chemical and physical properties at low costs; and 2) optimizing process design to improve efficiency (Rochelle, 2009). This work focuses on the first category by screening piperazine (PZ)-based amine blends and other amine solvents for their CO<sub>2</sub> capture

performance and potential environmental, health and safety (EHS) issues. Generally, a desired solvent should have the following properties:

1. High CO<sub>2</sub> cyclic capacity

CO<sub>2</sub> cyclic capacity represents the amount of CO<sub>2</sub> removed per unit mass of solvent. With higher capacity, less solvent is required to remove the same amount of CO<sub>2</sub>. The capacity value directly relates to the sensible heat requirement for stripping, pump work, and the size and cost of the cross-exchanger (L. Li et al., 2013b).

2. Fast absorption rate

The removal of CO<sub>2</sub> is a function of packing area, mass transfer coefficient ( $k_g'$ ) and driving force. With the same driving force, large  $k_g'$  reduces the amount of packing required for the same amount of CO<sub>2</sub> removal, which leads to smaller absorber size and thus lower capital cost. On the other hand, for an absorber with fixed amount of packing and CO<sub>2</sub> removal, larger  $k_g'$  allows smaller driving force to be used and thus less solvent circulate rate.

3. Resistance to thermal degradation

At high temperature, amines can degrade by different mechanisms, resulting in solvent makeup cost and potential EHS issues. While the rate of amine degradation increases with increase in temperature, the energy performance of the process generally improves with higher stripper operating temperature (Oyenekan and Rochelle, 2007).

4. Resistance to oxidation

Oxidation is the degradation of amine in response to the oxygen in the flue gas. Oxidation causes the major amine loss in CO<sub>2</sub> capture process for coal-fired flue gas (Nielsen et al., 2013; Strazisar et al., 2003). In addition, some

oxidative degradation products are corrosive or toxic (Shao and Stangeland, 2009).

5. Low volatility

Amine volatility is one of the key criteria used in screening an amine solvent for CO<sub>2</sub> capture: (1) amine losses up the stack can react in the atmosphere to form ozone and other toxic compounds; (2) high volatility losses can result in greater solvent make-up costs; (3) additionally high losses will require the use of larger water wash units, and more water, to capture fugitive amines prior to venting - these translate to higher capital and operating costs (Nguyen et al., 2010); (4) high amine volatility may enhance the growth of amine aerosols when aerosol nuclei such as H<sub>2</sub>SO<sub>4</sub> are present (Khakharia, 2015).

6. Low solvent cost

Due to the low CO<sub>2</sub> partial pressure and high flow rate of flue gas in coal-fired power plant, a large amount of solvent is required for CO<sub>2</sub> capture. For a 300 MW coal-fired power plant, around 3000 gal solvent is needed. Solvent cost generally accounts for 5% of total capital cost.

7. Others

High water solubility and low viscosity are also preferred, as they allow high amine concentration used in the solvent, and give better CO<sub>2</sub> absorption performance in general.

#### **1.4 REVIEW OF RELEVANT LITERATURE**

Most of previous solvent screening works outside the Rochelle group only focused on CO<sub>2</sub> capture performance (CO<sub>2</sub> capacity and CO<sub>2</sub> absorption rate) (Adeosun et al., 2013; Chowdhury et al., 2014; Conway et al., 2014; Goto et al., 2011; Hook, 1997; Li

et al., 2014a; Murai et al., 2013; Puxty et al., 2009; Robinson et al., 2011; Singh, 2011). Although several amines identified from these works shows better CO<sub>2</sub> capture performance than MEA, none of them has been proved applicable to commercial scale CO<sub>2</sub> capture, probably due to the high amine volatility, poor solvent stability, or high cost of production of these amines.

Piperazine (PZ) has been investigated extensively in the Rochelle group, due to its superior properties for CO<sub>2</sub> capture (Rochelle et al., 2011). Freeman et al. (2010) first identified the concentrated PZ (8 m or 40 wt % PZ) as a superior solvent for CO<sub>2</sub> capture. 8 m PZ has double the CO<sub>2</sub> absorption rate and capacity, remarkable resistance to oxidation and thermal degradation, and lower amine volatility than 30 wt % MEA. However, the low water solubility of PZ and its zwitterionic carbamate may cause precipitation under certain conditions in a process, limiting its industrial application (Freeman et al., 2010b; Ma et al., 2012). Effort has been made to find another useful amine to blend with less concentrated PZ in order not only to mitigate the precipitation issues, but also to maintain the desirable CO<sub>2</sub> capture properties of concentrated PZ (Chen and Rochelle, 2011; L. Li et al., 2013a, 2013b). Among these PZ-based amine blends, PZ/N-methyl-diethanolamine (MDEA) (Chen et al., 2011) and PZ/2-amino-2-methyl-1-propanol (AMP) (L. Li et al., 2013a) showed the best CO<sub>2</sub> capture performance for CO<sub>2</sub> capture. However, PZ/MDEA was found to be significantly less thermally stable than PZ alone (Closmann, 2011). Although PZ/AMP is more stable than PZ/MDEA, AMP was found to have high volatility (Nguyen et al., 2010), which is prohibitive for flue gas CO<sub>2</sub> capture.

## **1.5 RESEARCH OBJECTIVES**

The primary objective of this work is to find a useful amine to blend with less concentrated PZ, so that this blend maintains the desired properties of concentrated PZ for low partial pressure CO<sub>2</sub> capture but alleviates the precipitation issue.

The secondary objective of this work is to investigate the amine structure-property relationships for thermal stability, amine volatility, CO<sub>2</sub> capacity, and CO<sub>2</sub> absorption rate.

## **Chapter 2: Thermal Degradation of Novel Piperazine/Amine Blends for CO<sub>2</sub> Capture**

36 novel piperazine (PZ)-based amine blends were investigated for their thermal stability for CO<sub>2</sub> capture. These amines include 7 imidazoles, 8 cyclic and long-chain diamines, 12 tertiary amines, 4 hindered amines, 3 hindered and tertiary amino acids, and 2 ether amines that were selected based on known amine structure-property relationships and their potential for industrial application. 18 thermally stable PZ-based amine blends were identified based on their degradation rates in CO<sub>2</sub> loaded solutions at 150 and 175 °C. Degradation mechanisms were studied to understand the relationships between the structure and thermal stability of the blended amines of the blends.

### **2.1 INTRODUCTION**

Carbon capture and storage is a necessary tool for mitigating the impact of fossil fuel combustion on global climate change. Post-combustion capture of CO<sub>2</sub> by amine scrubbing is the most applicable technology for existing coal-fired power plants (Rochelle, 2009). Its commercial application, however, is impeded by the high capital and energy costs that result from the low CO<sub>2</sub> partial pressure and high flow rate of flue gas (Finkenrath, 2012). Using novel amines with superior CO<sub>2</sub> capture performance is a critical approach to reduce the cost. Most previous solvent screening studies focused on CO<sub>2</sub> capacity and CO<sub>2</sub> absorption rate (Chen and Rochelle, 2011; Chowdhury et al., 2014; Conway et al., 2014; Li et al., 2014b; Li, 2015; Puxty et al., 2009), as CO<sub>2</sub> capacity and CO<sub>2</sub> absorption rate are directly related to the CO<sub>2</sub> absorber cost and solvent regeneration cost. However, thermal stability should also be a crucial criterion for solvent selection for flue gas CO<sub>2</sub> capture. At high solvent regeneration temperature, amine solvents can degrade by different mechanisms (Lepaumier et al., 2009; Rochelle,

2012), resulting in solvent make-up cost and potential environmental issues (Mazari et al., 2015). In addition, Rochelle et al. (2011) identified the benefit of operating at high temperature for thermal swing regeneration. However, the regeneration temperature is limited by thermal degradation of the solvent.

Aqueous 30 wt % monoethanolamine (MEA) is currently considered the benchmark solvent for flue gas CO<sub>2</sub> capture due to its low production cost, and extensive prior use in high pressure CO<sub>2</sub> capture applications (Astarita et al., 1983), in spite of its moderate CO<sub>2</sub> absorption performance, and low thermal and oxidative stability. In recent years, some piperazine (PZ)-based amine blends, such as PZ/*n*-methyldiethanolamine (MDEA) (Chen and Rochelle, 2011) and PZ/2-amino-2-methyl-1-propanol (AMP) (H. Li et al., 2013), have been proposed as promising solvents for flue gas CO<sub>2</sub> capture. These PZ-based amines blends could mitigate the precipitation issues of concentrated PZ (Ma et al., 2012), while maintaining the high CO<sub>2</sub> capacity, and fast absorption rate of concentrated PZ (Rochelle et al., 2011). However, blending with other amines usually reduces the solvent stability relative to PZ, due to their interaction PZ with the other amine (Rochelle, 2012). For example, oxazolidone resulting from the degradation of MDEA and AMP could cause significant degradation of PZ (Closmann et al., 2009; H. Li et al., 2013).

In this work, 36 novel PZ-based amine blends have been screened for their thermal stability. These amines include 7 imidazoles, 8 cyclic and long-chain diamines, 12 tertiary amines, 4 hindered amines, 3 hindered and tertiary amino acids, and 2 ether amines. These amines were selected based on known amine structure-property relationships, and their potential for industrial application. Imidazole and its derivatives have been widely used as corrosion inhibitors (Mousavi et al., 2011) and catalysts for a variety of reactions (Jencks and Carriuolo, 1959). Due to the basicity of the tertiary

nitrogen of imidazoles, they were proposed as promising solvents for high pressure CO<sub>2</sub> removal (Tomizaki et al., 2010). The study of imidazole for low pressure CO<sub>2</sub> is limited. Shannon and Bara (2011) investigated the blend of n-functionalized imidazoles and MEA for flue gas CO<sub>2</sub> capture. They concluded that the 1-n-alkylimidazoles enable more efficient use of MEA and overcome stoichiometric limitations on MEA in non-aqueous solvents. Although the imidazole ring is generally resistant to fission (Hofmann, 1953), the thermal stability of imidazoles in the presence of other amines and CO<sub>2</sub> has not been studied yet. Cyclic and long-chain diamines in general have good thermal stability, as they are unlikely to form cyclic urea at normal solvent regeneration temperature (Namjoshi et al., 2013; Rochelle, 2012). Diamines usually also have high CO<sub>2</sub> capacity compared to monoamines, due to the additional amino group (Li, 2015; Zhou et al., 2010), and low volatility in CO<sub>2</sub> loaded solutions (Nguyen et al., 2010). The blend of PZ with some tertiary and sterically hindered amines could combine the fast absorption rate of PZ with the high CO<sub>2</sub> capacity of the tertiary and hindered amines (Bishnoi and Rochelle, 2002; Seo and Hong, 2000). 6-membered cyclic tertiary amines are expected to have good thermal stability (Freeman and Rochelle, 2011). Steric hindrance groups impede the adjacent amino group to be attacked, and thus could increase amine stability (Eide-Haugmo et al., 2011; Rochelle, 2012). Amino acids have been proposed as attractive solvents for CO<sub>2</sub> capture due to their negligible partial pressure and low toxicity (Song et al., 2012). Although most primary and secondary amino acids were found to be less stable than MEA (Huang et al., 2013), cyclic hindered amino acids and tertiary amino acids are expected to have better stability due to their steric hindrance and stable ring structure (Rochelle, 2012). Ether amines are expected to have better stability than their corresponding alkanolamines, because they are not likely to degrade by carbamate polymerization as alkanolamines do (Rochelle, 2012).

The major objective of this work is to identify several thermally stable PZ-based amine blends for further evaluation for CO<sub>2</sub> capture. Degradation rates of these blends will be compared to PZ/MDEA and PZ/AMP at the same amine concentration, CO<sub>2</sub> loading, and temperature. A secondary objective of this work is to investigate the effect of the structural features of blended amines on the thermal stability of the PZ-based amine blends.

## **2.2 EXPERIMENTAL METHODS**

### **2.2.1 Solution preparation**

All amines (reagent grade) studied in this work were obtained from commercial sources. Aqueous PZ-based amine blends were prepared by melting anhydrous PZ in mixtures of distilled de-ionized water and other blended amines. CO<sub>2</sub> loaded solutions were prepared by gravimetrically sparging CO<sub>2</sub> (99.5%, Matheson Tri Gas, Basking Ridge, NJ) in unloaded amine solutions in a gas-washing bottle. The CO<sub>2</sub> concentration was checked by total inorganic carbon (TIC) analysis, described by Freeman et al. (2010). Acid loaded solutions were prepared by adding 10 N sulfuric acid to unloaded aqueous amine.

### **2.2.2 Experimental Approach**

Thermal degradation of 2 m PZ/2 m other amine with 0.2 mol CO<sub>2</sub>/mole alkalinity was measured at 150 °C for 2 weeks and 175 °C for 1 week in 3/8-inch 316 stainless steel Swagelok® cylinders with a volume of 4.5 ml and diameter of 0.95 cm. Cylinders were filled with 4 mL of amine solution with about 0.5 mL of headspace, sealed with two Swagelok® end caps, and placed in forced convection ovens maintained at the target temperature. Individual cylinders were removed from the ovens at each

sampling time and then analyzed for the parent amines and degradation products present in solution.

### **2.2.3 Analytical Tools - Cation and Anion Chromatography**

A Dionex ICS-2100 cation ion chromatograph (Dionex Corporation) was used to quantify parent amines and determine the presence of other amine byproducts. A  $4 \times 50$  mm CG17 guard column and a  $4 \times 250$  mm CS17 analytical column were connected in series and used to carry out the separation. The eluent contained varying concentrations of methanesulfonic acid (MSA) in analytical grade water. A Dionex ICS-3000 chromatograph (Dionex Corporation) was used to determine anions in the samples, such as amino acids. A  $4 \times 50$  mm AS15 guard column and a  $4 \times 250$  mm AS15 analytical column were connected in series to carry out the separation. The mobile phase consisted of 18.2  $\mu\text{mho}$  analytical grade water spiked with a gradient of potassium hydroxide. Ion suppression was used for both cation and anion chromatography to improve the signal/noise ratio. Standard curves of parent amines and degradation products were prepared to quantify the amount of amine present. Samples were diluted by a factor of 2000 to 10000 (mass) in analytical grade water. Degradation products were identified by matching their retention-time with standard samples. The combined expected dilution, cylinder, and instrument error is assumed to be  $\pm 3.5$ . The details of the experimental apparatus, procedure, and analytical methods are described by Namjoshi (2015).

### **2.2.4 Thermal degradation model**

Thermal degradation was modeled using a rate model that assumes a first-order loss in amines as shown in Equation 2.1 where  $C_{Am}$  is the concentration of amines, and  $k_1$  is a first-order rate constant. The integrated form is shown in Equations 2.2 where  $C_{Am,0}$

is the initial amine concentration, and  $t$  is the experimental time in seconds. This model can represent thermal degradation well for various amine solvent systems (Freeman and Rochelle, 2012a; Namjoshi, 2015).

$$-\frac{dC_{Am}}{dt} = k_1 C_{Am} \quad (2.1)$$

$$C_{Am} = C_{Am,0} \cdot e^{-k_1 \cdot t} \quad (2.2)$$

By assuming  $k_1$  has an Arrhenius dependence on temperature, the activation energy ( $E_A$ ) for degradation can be calculated using the following equation where  $A$  is a pre-exponential constant,  $R$  is the gas constant, and  $T$  is the absolute temperature.

$$k_1 = A \cdot e^{\frac{-E_A}{RT}} \quad (2.3)$$

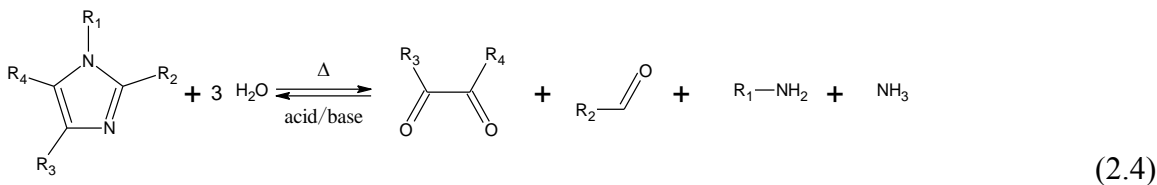
For a blend,  $E_A$  can be calculated for each amine species and for the total amine. To compare the thermal stability for different solvents, the maximum stripper operating temperature ( $T_{max}$ ) for each solvent was calculated.  $T_{max}$  is defined as the temperature at which a solvent will degrade at the same rate as 7 m MEA at 121 °C ( $2.9 \times 10^{-8} \text{ s}^{-1}$ ) (Freeman and Rochelle, 2012a).

## 2.3 RESULTS AND DISCUSSION

### 2.3.1 PZ/Imidazoles

Table 2.1 summarizes  $k_1$ ,  $E_A$ , and  $T_{max}$  for 2 m PZ/2 m imidazoles (IMIs) with 0.2 mol CO<sub>2</sub>/mole alkalinity. For amine that has amine loss less than 4% during the entire period, the degradation rate cannot be quantified sufficiently, and its activation energy is assumed to be the same as the one has similar structure (Namjoshi, 2015). The imidazole blends, except for PZ/IMI and PZ/4M-IMI, show remarkable resistance to thermal degradation, with  $T_{max}$  of both components much higher than MEA ( $T_{max} = 121$

°C) (Freeman and Rochelle, 2012a). Previous studies (Brookes and Lawley, 1961; Haines et al., 1962) found that imidazoles are subject to complete ring fission by alkali or OH radical attacking at C-2 under vigorous conditions (Equation 2.4). The mechanism for the ring-opening of imidazoles can be viewed as a reversal of the Debus-Radziszewski imidazole synthesis, producing glyoxal (or substituted glyoxal), aldehyde, and ammonia (or primary amine and ammonia if R<sub>1</sub> is not H) (Radziszewski, 1882).



R<sub>1</sub>, R<sub>2</sub>, R<sub>3</sub>, R<sub>4</sub> can be H or alkyl.

The enhanced thermal stability of PZ/imidazole derivatives in comparison with PZ/IMI is believed to result from the decreased electrophilicity of the C-2 in imidazole rings. The electron-donating substituents, such as CH<sub>3</sub> and C<sub>2</sub>H<sub>5</sub>, weaken the electrophilicity of the C-2 atom, and thus reduce the rate of ring opening (Kochetkov and Budovskii, 1972). The relatively low stability of PZ/4M-IMI in comparison with other PZ/imidazole derivatives is due to the fact that substituents at the C-4 position have less influence on the C-2 than those substituents at C-2 and N-1.

Figure 2.1 compares the loss of PZ and IMIs in 2 m PZ/2 m IMIs with 0.2 mol CO<sub>2</sub>/mole alkalinity at 150 °C after two weeks. As the signal of imidazoles with low pK<sub>a</sub> in cation chromatography is too weak to be sufficiently quantified, the major degradation product, NH<sub>3</sub>, from the fission of imidazole rings was chosen as an indicator of the loss of imidazoles. NH<sub>3</sub> produced from 2 m PZ with 0.2 mol CO<sub>2</sub>/mole alkalinity at 150 °C was found to be negligible within the first 2 weeks. In Figure 2.1, two moles

NH<sub>3</sub> are produced with the loss of one mole of imidazole. The loss of PZ was correlated with the equivalent production of NH<sub>3</sub>, indicating the interaction between PZ and imidazoles.

Table 2.1: Summary of  $k_1$ ,  $E_A$ , and  $T_{max}$  for 2 m PZ/2 m imidazoles with 0.2 mol  $CO_2$ /mole alkalinity.

Amine (blended with PZ)	Structure	$k_1$ ( $\times 10^{-7} s^{-1}$ )				$E_A$ (KJ/mol)		$T_{max}$ ( $^{\circ}C$ )	
		150 $^{\circ}C$		175 $^{\circ}C$		PZ	Am	PZ	Am
		PZ	Am	PZ	Am				
N-methyl-diethanolamine (MDEA)		6.5	2.2	33.0	10.8	103	100	110	122
2-Amino-2-methyl-1-propanol (AMP)		0.7	1.0	3.5	5.3	101	105	137	133
Imidazole (IMI)		1.5	— <sup>a</sup>	6.0	— <sup>a</sup>	87	—	124	—
1-Methylimidazole (1M-IMI)		0.4	0.3	1.9	1.0	108	76	148	150
2-Methylimidazole (2M-IMI)		<0.3 <sup>b</sup>	0.3	0.5	1.3	118 <sup>c</sup>	92	167	150
4(5)-Methylimidazole (4M-IMI)		0.4	1.3	2.5	5.0	118	85	147	125
2-Ethylimidazole (2E-IMI)		<0.3 <sup>b</sup>	0.3	0.7	1.3	118 <sup>c</sup>	92	164	150
1,2-Dimethylimidazole (1,2-DIMI)		<0.3 <sup>b</sup>	<0.3 <sup>b</sup>	0.9	<0.3 <sup>b</sup>	118 <sup>c</sup>	—	160	—
2-Ethyl 4-methylimidazole (2E-4M-IMI)		<0.3 <sup>b</sup>	<0.3 <sup>b</sup>	<0.3 <sup>b</sup>	0.7	—	85 <sup>c</sup>	—	158

a: the signal in cation chromatography is too weak to be sufficiently quantified

b: based on the assumption that the combined error is about  $\pm 3.5\%$  (Namjoshi, 2015)

c: assumed to be the same as PZ/4M-IMI

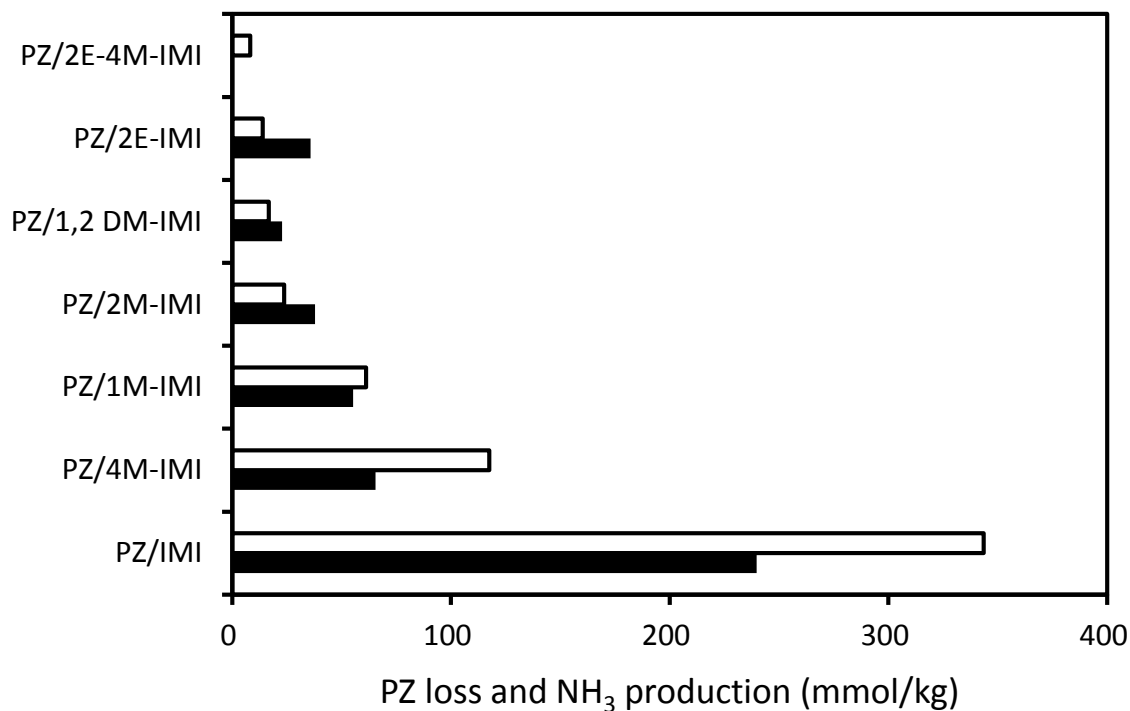


Figure 2.1: PZ loss and equivalent NH<sub>3</sub> production in 2 m PZ/2 m imidazoles with 0.2 mol CO<sub>2</sub>/mole alkalinity after 2 weeks at 150 °C (solid bar: PZ; open bar: NH<sub>3</sub>).

To better understand the effect of PZ, acidity, and CO<sub>2</sub> on the degradation of imidazoles, 2 m IMI, 2 m PZ/2 m IMI, and 2 m IMI with 0.2 mol H<sup>+</sup>/mol alkalinity (added as H<sub>2</sub>SO<sub>4</sub>) were tested at 175 °C for one week. NH<sub>3</sub> production was chosen as a surrogate for imidazole degradation (Figure 2.2). At these conditions, NH<sub>3</sub> from PZ was negligible within the first week (Freeman, 2011). No NH<sub>3</sub> was detected in degraded 2 m IMI, indicating the good thermal stability of imidazole. The addition of 0.2 mol H<sup>+</sup>/mol alkalinity in 2 m IMI increased NH<sub>3</sub> production. The protonation of imidazole rings increases the electrophilicity of the C-2, accelerating the rate of ring opening. The addition of 2 m PZ to 2 m IMI also induced NH<sub>3</sub> production. PZ could react with aldehyde to form polymerized products (Sandler and Delgado, 1969), and with glyoxal

(or substituted glyoxal) to form corresponding ethanone and ethanediol (Treybig, 1989), accelerating the degradation of imidazoles and PZ. A synergistic effect of the addition of PZ and  $H^+$  was observed in the production of  $NH_3$ . There was no significant difference in the production of  $NH_3$  between  $CO_2$  loaded and  $H^+$  loaded PZ/IMI.

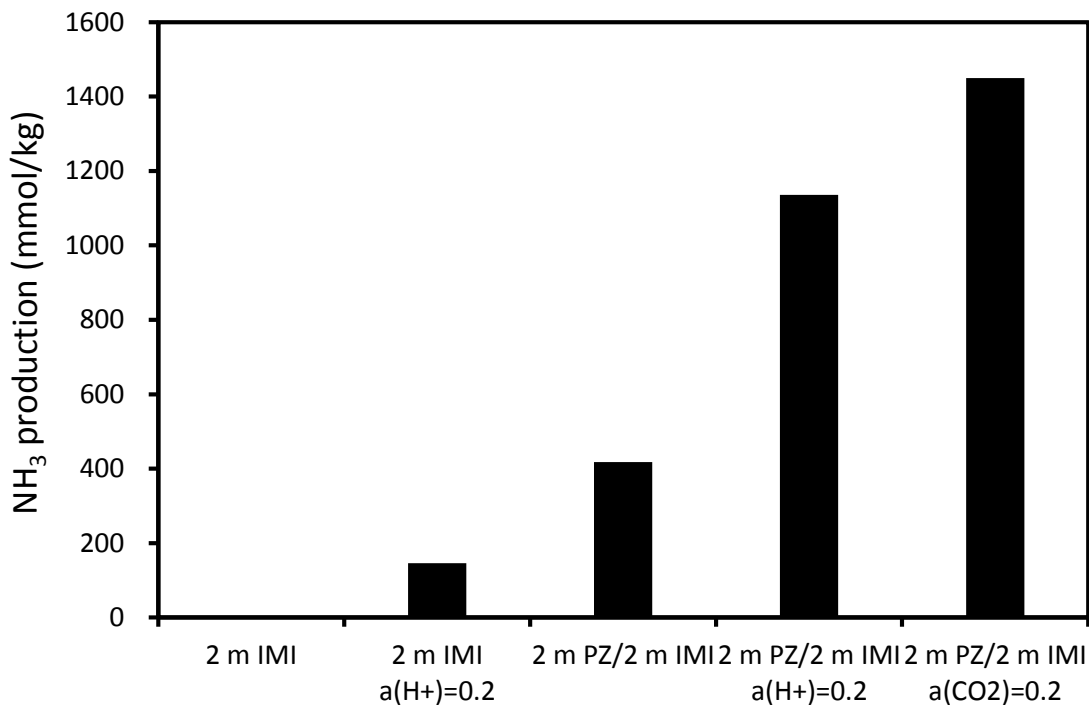
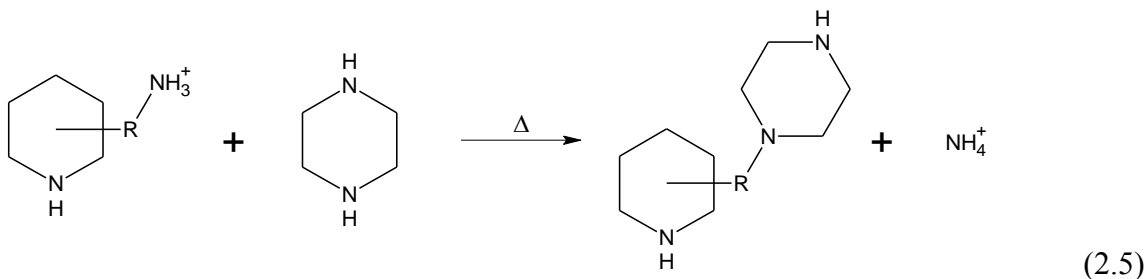


Figure 2.2: Effect of PZ, acidity, and  $CO_2$  on  $NH_3$  production for IMI at 175 °C after 1 week.

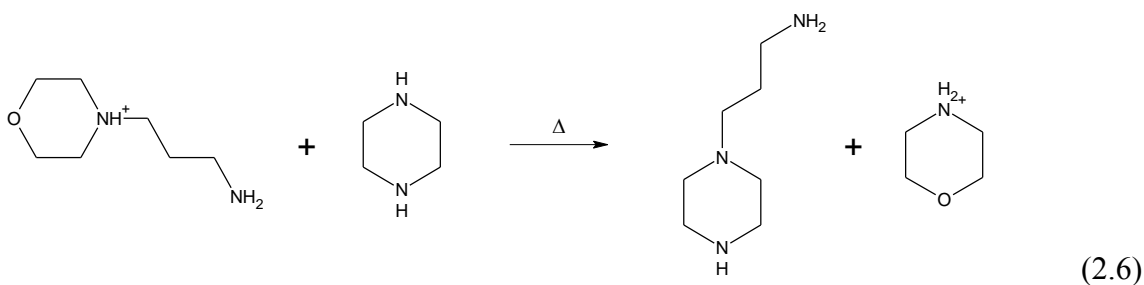
### 2.3.2 PZ/Diamines

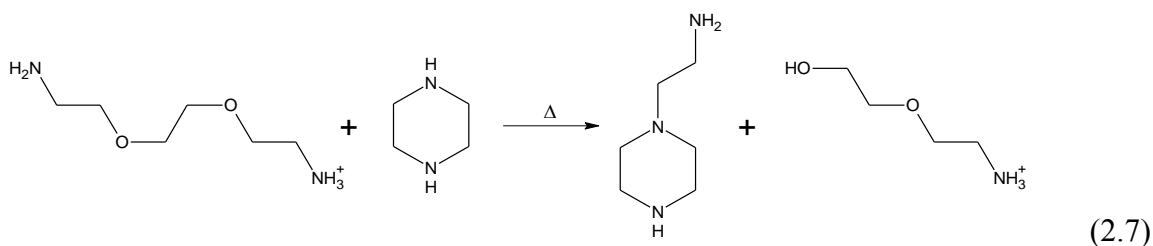
Table 2.2 summarizes  $k_1$ ,  $E_A$ , and  $T_{max}$  for 2 m PZ/2 m diamines with 0.2 mol  $CO_2$ /mole alkalinity. PZ/3AM-PD, PZ/4AM-PD, PZ/4A-PD, PZ/APMor, and PZ/BAEE show good thermal stability, due to their stable 6-membered ring structure, and/or the larger distance between two amino groups, which prevents the formation of cyclic urea (Hatchell et al., 2014; Rochelle, 2012). The primary degradation products

for PZ/3AM-PD, PZ/4AM-PD, and PZ/4A-PD are  $\text{NH}_3$  and a tri-amine, indicating the following mechanism (Equation 2.5):

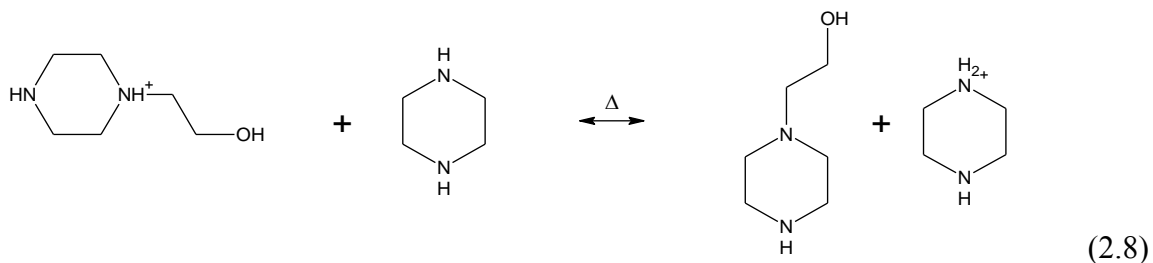


$\text{NH}_3$  was found to account for 12%, 18% and 24% of the total N loss for PZ/3AM-PD, PZ/4AM-PD, and PZ/4A-PD, respectively, at 175 °C after 1 week. With the proposed degradation mechanism (Equation 2.5), the production of  $\text{NH}_3$  should account for 25% of the total N loss with the tri-amine accounting for the other 75%, indicating some other degradation pathways that do not produce  $\text{NH}_3$  may occur in PZ/3AM-PD and PZ/4AM-PD. In degraded PZ/APMor and PZ/BAEE, morpholine and 2-(2-aminoethoxy)ethanol were also detected, in addition to  $\text{NH}_3$  and a tri-amine, by cation chromatography, respectively, indicating the following mechanisms (Equation 2.6 and 2.7):





HEP was reported to degrade through the formation of the HEP dimer, resulting in a degradation rate 40 times faster than PZ at 135 °C at a loading of 0.4 mol  $\text{CO}_2$ /mole alkalinity (Davis, 2009). However, the degradation rate for HEP in 2 m PZ/2 m HEP with 0.2 mol  $\text{CO}_2$ /mole alkalinity was found to be on the same scale as that of 8 m PZ at 175 °C (Freeman and Rochelle, 2012a) (Table 2). The faster rate reported by Davis probably results from the high  $\text{CO}_2$  loading, which accelerates the degradation. The degradation rate of 4 m HEP with 0.2 mol  $\text{CO}_2$ /mole alkalinity is similar to that of HEP in 2 m PZ/2 m HEP with the same loading, but greater than that of 4 m HEP with 0.2 mol  $\text{H}^+$ /mole alkalinity (Figure 2.3). Another reason for the good stability of PZ/HEP is the self-regeneration reaction between PZ and HEP at the high temperature used in this study (150 and 175 °C) (Equation 2.8):



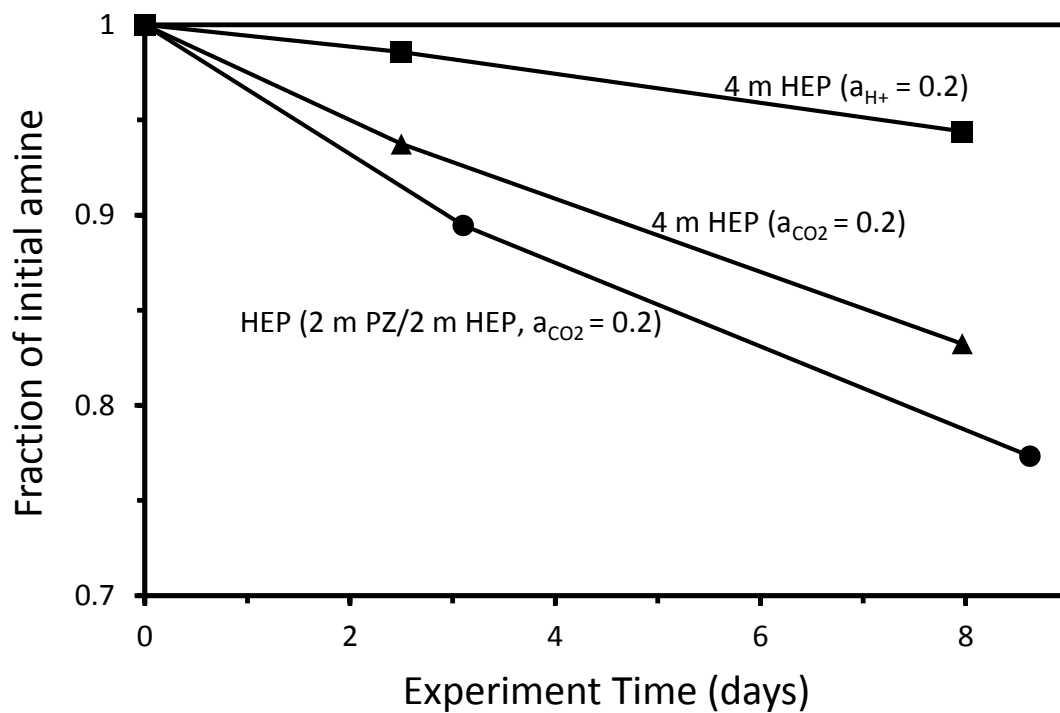


Figure 2.3: Effect of PZ, acidity, and CO<sub>2</sub> on HEP degradation at 175 °C.

In both PZ/2AM-PD and PZ/1,3-DAP solutions, although 2AM-PD and 1,3-DAP degraded rapidly due to cyclic urea formation (Rochelle, 2012), PZ degraded slowly, indicating no strong interaction between PZ and the other amines or their degradation products (Figure 2.4).

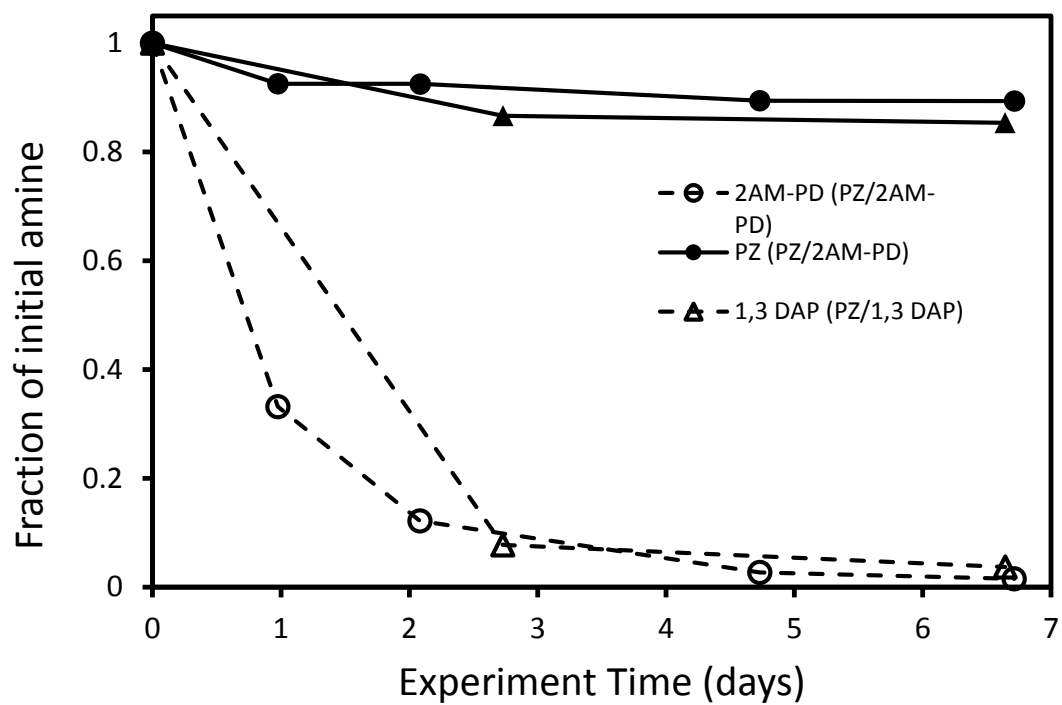


Figure 2.4: Degradation of 2 m PZ/2 m 2AM-PD, and 2 m PZ/2 m 1,3 DAP with 0.2 mol CO<sub>2</sub>/mole alkalinity at 175 °C for 1 week.

Table 2.2: Summary of  $k_1$ ,  $E_A$ , and  $T_{max}$  for 2 m PZ/2 m diamines with 0.2 mol  $\text{CO}_2$ /mole alkalinity.

Amine (blended with PZ)	Structure	$k_1 (\times 10^{-7} \text{ s}^{-1})$				$E_A (\text{KJ/mol})$		$T_{max} (^\circ\text{C})$	
		150 °C		175 °C		PZ	Am	PZ	Am
		PZ	Am	PZ	Am				
N-methyl-diethanolamine (MDEA)		6.5	2.2	33.0	10.8	103	100	110	122
2-Amino-2-methyl-1-propanol (AMP)		0.7	1.0	3.5	5.3	101	105	137	133
1,3-Diaminopentane (1,3-DAP)		0.8	12.6	3.2	64.7	90	103	134	102
2-(Aminomethyl)piperidine (2AM-PD)		0.7	12.7	2.4	80.9	80	117	135	107
3-(Aminomethyl)piperidine (3AM-PD)		<0.3 <sup>a</sup>		2.4 <sup>b</sup>		132 <sup>c</sup>		150	
4-Aminopiperidine (4A-PD)		0.3	0.4	2.9	3.1	145	132	150	147
4-(Aminomethyl)piperidine (4AM-PD)		<0.3 <sup>a</sup>		2.6 <sup>b</sup>		132 <sup>c</sup>		149	
4-(3-Aminopropyl)morpholine (APMor)		<0.3 <sup>a</sup>	<0.3 <sup>a</sup>	1.6	2.4	145 <sup>c</sup>	132 <sup>c</sup>	156	150
1-(2-Hydroxyethyl)piperazine (HEP)		<0.3	<0.3	2.8	3.6	145 <sup>c</sup>	132 <sup>c</sup>	151	145
1,2-Bis(2-aminoethoxy)ethane (BAEE)		<0.3		1.0		132 <sup>c</sup>		160	

a: based on the assumption that the combined error is about  $\pm 3.5\%$  (Namjoshi, 2015)

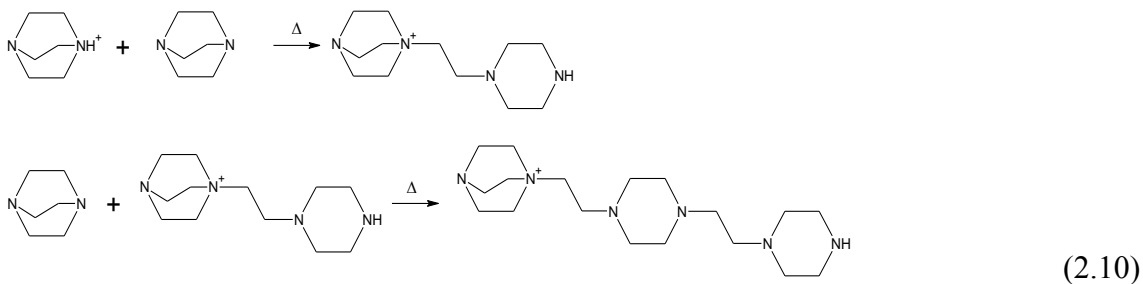
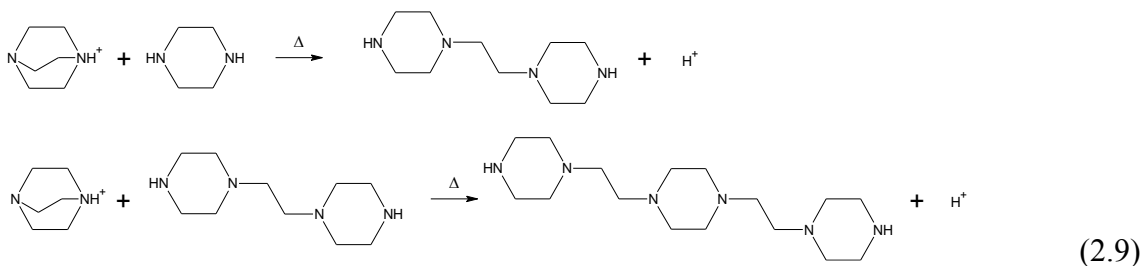
b: only average values shown due to peak overlap in cation chromatography

c: assumed to be the same as PZ/4A-PD

### 2.3.3 PZ/Tertiary amines

Table 2.3 summarizes  $k_1$ ,  $E_A$ , and  $T_{max}$  for 2 m PZ/2 m tertiary amines with 0.2 mol  $\text{CO}_2$ /mole alkalinity. All the PZ/cyclic tertiary amines, except for PZ/TEDA, are significantly more stable than PZ/MDEA because the initial degradation product is a stable cyclic secondary amine. For example, the thermal stability of the blend of PZ and 4-hydroxy-piperidine (HPD), which is the initial degradation product for HMPD, was

found to be significantly greater than the blend of PZ and diethanolamine (DEA), which is the initial degradation product for MDEA, in CO<sub>2</sub> loaded solutions (Du et al., 2016b). Although the degradation rate of PZ/TEDA is slower than PZ/MDEA at 150 °C, large amounts of solids were found in degraded PZ/TEDA. The precipitation was found to be accelerated by loading CO<sub>2</sub> or acid. Two tetra-amines (suspected to be the dimer of PZ-TEDA, and the dimer of TEDA-TEDA) were identified on cation ion chromatograph in degraded PZ/TEDA, while only one of them was identified in degraded TEDA. The precipitates are probably the polymerization of TEDA initiated by PZ (Equation 2.9), and initiated by itself (Equation 2.10) (Maraš et al., 2012).



All the  $\alpha$ -carbons and methyl groups in BDMAEE are subject to attack by PZ, resulting in fast degradation rate of PZ/BDMAEE. PZ/DMA-PDL shows thermal stability comparable to PZ/MDEA, which is lower than PZ/DEA-PDL and PZ/DEEA. This supports findings by Namjoshi (2015), who concluded that PZ/tertiary amines with methyl groups are less stable than PZ/tertiary amines with ethyl groups. It is also consistent with the data in the literature that suggest that SN<sub>2</sub> reactions with bulkier

substituent groups react slower than methyl substituent groups (Anslyn and Dougherty, 2006). The degradation rate of PZ/DMAEE was lower than that of PZ/MDEA, because the immediate degradation products of DMAEE cannot form oxazolidone as degraded MDEA does (Namjoshi, 2015). DIPAE is the only acyclic tertiary amine that is thermally stable when blended with PZ. This is probably due to the steric hindrance caused by the two isopropyl groups of DIPAE.

Table 2.3: Summary of  $k_1$ ,  $E_A$ , and  $T_{max}$  for 2 m PZ/2 m tertiary amines with 0.2 mol  $CO_2$ /mole alkalinity.

Amine (blended with PZ)	Structure	$k_1 (\times 10^{-7} s^{-1})$				$E_A$ (KJ/mol)		$T_{max}$ (°C)	
		150 °C		175 °C		PZ	Am	PZ	Am
		PZ	Am	PZ	Am				
N-methyl-diethanolamine (MDEA)		6.5	2.2	33.0	10.8	103	100	110	122
2-Amino-2-methyl-1-propanol (AMP)		0.7	1.0	3.5	5.3	101	105	137	133
Bis[2-(N,N-dimethylamino)ethyl] ether (BDMAEE)		5.3	7.4	33.9	35.4	117	99	116	106
3-(Dimethylamino)-1,2-propanediol (DMA-PDL)		2.8	2.5	22.7	16.5	132	119	126	125
Dimethylaminoethoxyethanol (DMAEE)		2.0	2.0	16.1	16.4	130	131	129	129
2-(Diethylamino)ethanol (DEEA)		2.6	2.1	28.0	31.8	151	172	130	134
3-(Diethylamino)-1,2-propanediol (DEA-PDL)		2.3	1.9	27.4	22.7	157	157	132	133
2-(Diisopropylamino)ethanol (DIPAE)		0.6	0.6	16.7	17.9	213	210	145	145
Triethylenediamine (TEDA)		1.1	2.4			— <sup>a</sup>			
3-Quinuclidinol (3-QD)		0.4	1.1	3.8	6.9	138	118	146	134
4-Hydroxy-1-methylpiperidine (HMPD)		0.7	0.6	4.5	3.1	120	111	140	142
1-(2-Hydroxyethyl)piperidine (HEPD)		0.5	0.3	3.6	2.0	124	111	144	148
4-(2-Hydroxyethyl)morpholine (HEMor)		<0.3 <sup>b</sup>	<0.3 <sup>b</sup>	2.1	1.5	124 <sup>c</sup>	111 <sup>c</sup>	150	152
Tropine		0.3	0.3	2.3	2.4	129	130	150	150

a: complete solidification occurred at 175 °C after 3 days

b: based on the assumption that the combined error is about  $\pm 3.5\%$  (Namjoshi, 2015)

c: assumed to be the same as PZ/HEPD

### 2.3.4 PZ/Hindered amines

Table 2.4 summarizes  $k_1$ ,  $E_A$ , and  $T_{max}$  for 2 m PZ/2 m hindered amines with 0.2 mol CO<sub>2</sub>/mole alkalinity. PZ/DIPA and PZ/2-AB degraded significantly faster than PZ/AMP, indicating the amino groups of DIPA and 2-AB were not sufficiently hindered to form carbamate. This is consistent to the experimental results by Davis (2009), and quantum chemical calculations by Gangarapu et al. (2013), both of which indicate single additional methyl group at  $\alpha$ -carbon, or substations at  $\beta$ -carbon only have mild effect on carbamate stability. PZ/AEPD degraded faster than PZ/AMP due to the additional –OH group of AEPD, making it more likely to form oxazolidone than AMP (Rochelle, 2012). PZ/IPAE degraded slight faster than PZ/AMP.

Table 2.4: Summary of  $k_1$ ,  $E_A$ , and  $T_{max}$  for 2 m PZ/2 m hindered amines with 0.2 mol CO<sub>2</sub>/mole alkalinity.

Amine (blended with PZ)	Structure	$k_1$ ( $\times 10^{-7} \text{ s}^{-1}$ )				$E_A$ (KJ/mol)		$T_{max}$ (°C)	
		150 °C		175 °C		PZ	Am	PZ	Am
		PZ	Am	PZ	Am				
N-methyl-diethanolamine (MDEA)		6.5	2.2	33.0	10.8	103	100	110	122
2-Amino-2-methyl-1-propanol (AMP)		0.7	1.0	3.5	5.3	101	105	137	133
Diisopropanolamine (DIPA)		6.2	9.4	23.9	26.6	85	66	102	84
2-Amino-1-butanol (2-AB)		5.2	9.0	15.5	45.3	68	102	95	106
2-Amino-2-ethyl-1,3-propanediol (AEPD)		2.4	3.2	10.2	14.0	92	93	119	115
2-(Isopropylamino)ethanol (IPAE)		2.4	2.6	14.2	17.5	113	120	124	125

### 2.3.5 PZ/Amino acids and PZ/Ether amines

Table 2.5 summarizes  $k_1$ ,  $E_A$ , and  $T_{max}$  for 2 m PZ/2 m  $K^+$ /amino acids, 2 m PZ/2 m BMEA, and 2 m PZ/2 m MOPA. PZ blended with  $K^+$ /L-Pro and  $K^+$ /HL-Pro was resistant to thermal degradation, indicating no interaction between PZ and the blended amino acids. PZ blended with  $K^+$ /DMG degraded rapidly due to the demethylation of DMG by PZ, forming 1-methyl-piperazine (1MPZ) and sarcosine. The formation of amide oligomers are the major pathway for the thermal degradation of primary and secondary amino acids in  $CO_2$  loaded solutions (Huang et al., 2013). Although DMG cannot form oligomers by itself, its degradation products in blend with PZ, sarcosine, was proved to form oligomers (Huang et al., 2013). The faster degradation of DMG in blend with PZ, compared to L-Pro and HL-Pro (Figure 2.5) results from the demethylation of DMG by PZ and its less steric hindrance.

Two PZ blended with ether amines, PZ/BMEA and PZ/MOPA, degraded much slower than most PZ/acyclic alkanolamines, because ether amines cannot form oxazolidone as easily as acyclic alkanolamines (Rochelle, 2012).

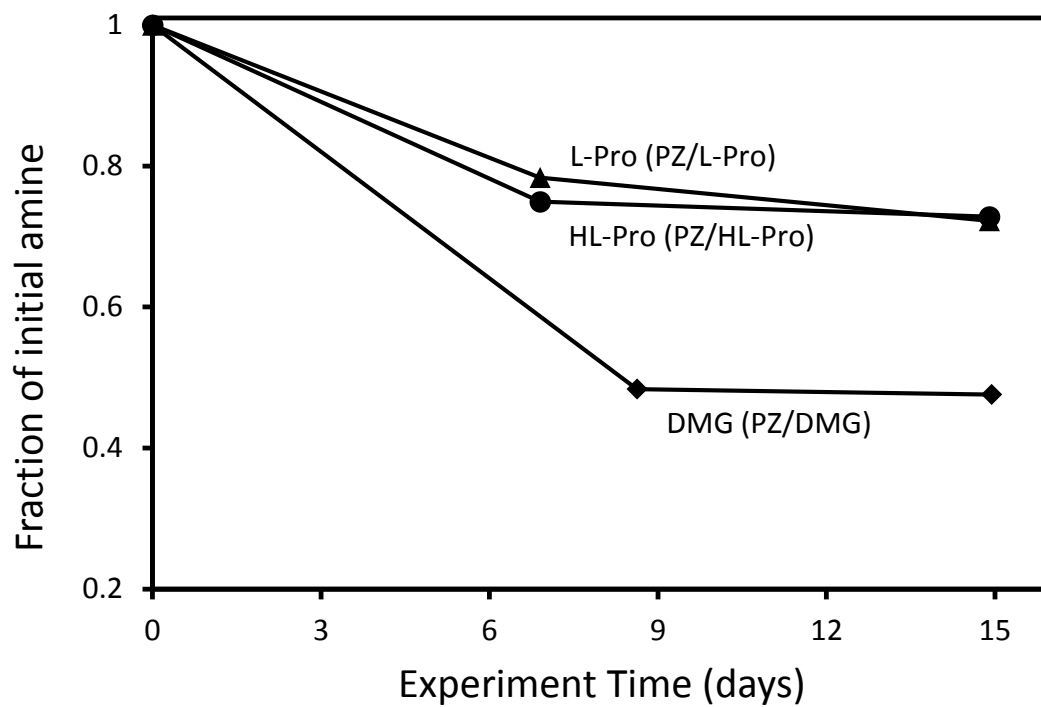


Figure 2.5: Degradation of DMG, L-Pro and HL-Pro in 2 m PZ/2 m K<sup>+</sup>/amino acids with 0.2 mol CO<sub>2</sub>/mole alkalinity at 150 °C.

Table 2.5: Summary of  $k_1$ ,  $E_A$ , and  $T_{max}$  for 2 m PZ/2 m  $K^+$ /amino acids, and 2 m PZ/2 m ether amines with 0.2 mol  $CO_2$ /mole alkalinity.

Amine (blended with PZ)	Structure	$k_1 (\times 10^{-7} s^{-1})$				$E_A$ (KJ/mol)		$T_{max}$ (°C)	
		150 °C		175 °C		PZ	Am	PZ	Am
		PZ	Am <sup>a</sup>	PZ	Am <sup>a</sup>				
N-methyl-diethanolamine (MDEA)		6.5	2.2	33.0	10.8	103	100	110	122
2-Amino-2-methyl-1-propanol (AMP)		0.7	1.0	3.5	5.3	101	105	137	133
N,N-Dimethylglycine (DMG)		4.0	6.7	21.4	25.0	106	83	116	100
L-Proline (L-Pro)		<0.3	2.8	1.8	8.1	106 <sup>b</sup>	67	148	105
4-Hydroxy-L-proline (HL-Pro)		<0.3	2.9	1.1	7.7	106 <sup>b</sup>	62	155	102
Bis(2-methoxyethyl)amine (BMEA)		<0.3	<0.3	3.2	1.6	145 <sup>c</sup>	132 <sup>c</sup>	149	154
3-Methoxypropylamine (MOPA)		<0.3	<0.3	1.4	0.6	145 <sup>c</sup>	132 <sup>c</sup>	158	165

a: degradation of amino acids in blends was not measured

b: assumed to be the same as PZ/ $K^+$ /DMG

c: assumed to be the same as PZ/4A-PD

## 2.4 CONCLUSIONS

In this study, 36 novel PZ-based amine blends were investigated for their thermal stability for  $CO_2$  capture. 18 of them were found to be resistant to thermal degradation with  $T_{max}$  greater than 140 °C. These included PZ blends with five imidazoles, six diamines, five tertiary amines, and two ether amines. Although imidazole itself is not stable in the presence of PZ,  $CO_2$ , or proton, imidazoles with electron-donating substituents at C-2 and N-1 positions are resistant to thermal degradation even in the presence of PZ and  $CO_2$ . The ring opening of imidazole can be catalyzed by either acid

or base. Diamines show high thermal stability in blends with PZ, unless they can form cyclic urea. 6-membered cyclic tertiary amines are resistant to thermal degradation, except for TEDA which goes through polymerization initiated by PZ and itself when protonated. DIPAE is the only acyclic tertiary amine that is thermally stable when blended with PZ. The thermal stability of DIPAE probably results from the steric hindrance caused by the two isopropyl groups. A single additional methyl group at  $\alpha$ -carbon, or substitutions at  $\beta$ -carbon are not sufficient to prevent the amine from carbamate formation. An additional  $-OH$  group decreases the thermal stability of the amine by making it more likely to form oxazolidone. PZ blended with  $K^+/L$ -Pro and  $K^+/HL$ -Pro was resistant to thermal degradation, while PZ blended with  $K^+/DMG$  degraded rapidly due to the demethylation of DMG by PZ. Ether amines are more stable than their alkanolamines counterparts, because ether amines cannot form oxazolidone as easily as alkanolamines.

## 2.5 RECOMMENDATIONS

Imidazole should be analyzed by Liquid Chromatography–Mass Spectrometry (LC/MS) to give a more accurate degradation rate. The suspected degradation products from PZ/imidazoles (aldehyde and glyoxal) should be analyzed by High Performance Liquid Chromatography (HPLC) to support the proposed degradation pathway (Equation 2.4). The solid produced from the degradation of PZ/triethylenediamine (TEDA) should be analyzed by X-ray Powder Diffraction (XRD) or other suitable tools to support the proposed degradation pathways (Equation 2.9 and 2.10). The products from the degradation of PZ/proline and PZ/4-hydroxy-L-proline should be analyzed by HPLC or LC/MS to understand the degradation pathway of this two amino acids in the presence of PZ.

## **2.6 ACKNOWLEDGEMENTS**

The author gratefully acknowledges Yukai Wang for helping measuring thermal degradation.

## Chapter 3: Volatility of Amines for CO<sub>2</sub> Capture

Volatility is a critical criterion for amine selection for CO<sub>2</sub> capture from low pressure gas streams, such as flue gas. The Henry's law constant ( $H_{am}$ ) of 24 novel amines, including 18 tertiary amines, 3 hindered amines, 2 ether amines, and 1 pyridine derivative was measured at 40 °C using a hot gas FTIR (Fourier Transform Infrared Spectroscopy). 14 of them show a  $H_{am}$  lower than 2-amino-2-methyl-1-propanol (AMP). A group contribution model that correlates  $H_{am}$  to molecular structure was developed based on the data from this work and data from literature. Non-cyclic groups and cyclic groups have significant effect on the volatility of the amine. The amine partial pressure ( $P_{am}$ ) of tertiary and hindered amines was also measured in a blend with PZ at 40 °C and their normal CO<sub>2</sub> loading range for flue gas CO<sub>2</sub> capture. With increased  $pK_a$ , the  $P_{am}$  of tertiary and hindered amines becomes a stronger function of CO<sub>2</sub> loading. These results at nominal lean loading were correlated with  $H_{am}$  of the amine.

### 3.1 INTRODUCTION

Carbon capture from flue gas using amine scrubbing is one of the most applicable technologies for mitigating the impact of fossil fuel combustion on global climate change (Rochelle, 2009). However, the low CO<sub>2</sub> partial pressure and high flow rate of flue gas lead to high capital and operating cost for amine scrubbing (Catalanotti et al., 2014; Clark and Herzog, 2014; Finkenrath, 2012). Amine scrubbing also has potential environmental issues due to amine volatilization, and degradation (Da Silva et al., 2013; Dai and Mitch, 2013; Eide-Haugmo et al., 2009; Mazari et al., 2015). Using novel amines with not only superior CO<sub>2</sub> capture performance, but also low amine volatility is a critical approach to improve this technology. Amine loss up the stack can react in the

atmosphere to form ozone and other toxic compounds and result in greater solvent make-up costs and other environmental issues. To capture excessive fugitive amines prior to venting, it is necessary to use bigger water wash units, and more water, resulting in higher capital and operating costs (Nguyen et al., 2010).

Tertiary and hindered amines activated by piperazine (PZ) or other primary and secondary amines have been proposed as promising solvents for flue gas CO<sub>2</sub> removal (Adeosun et al., 2013; Alvis et al., 2012; Bishnoi and Rochelle, 2002; Chen and Rochelle, 2011; Kumar and Kundu, 2012; H. Li et al., 2013; Seo and Hong, 2000). They combine the high CO<sub>2</sub> capacity of the tertiary and hindered amines with the fast rate of PZ. However, the volatility of tertiary and hindered amines is likely to be an issue as they are not converted to nonvolatile ions by CO<sub>2</sub> to the same extent as primary and secondary amines.

There are several publications on amine volatility in binary amine–H<sub>2</sub>O systems (Cai et al., 1996; Kim et al., 2008; Lenard et al., 1990; Pappa et al., 2006), but all the data are restricted to common amines, including monoethanolamine (MEA), n-methyldiethanolamine (MDEA), 2-amino-2-methyl-1-propanol (AMP), and methylaminopropanolamine (MAPA). The work by Nguyen (2013) is the largest source of volatility data available for amines used in CO<sub>2</sub> capture. However, only five of the amines in Nguyen (2013) are tertiary and hindered amines, and among them only MDEA and AMP were measured in both dilute unloaded solution and concentrated CO<sub>2</sub>-loaded solution.

The Henry's law constant ( $H_{am}$ ) of 24 novel amines, including 18 tertiary amines, 3 hindered amines, 2 ether amines, and 1 pyridine derivative has been measured in this work. These amines were selected for their potential viability for CO<sub>2</sub> capture (Du et al., 2016a, 2016c).  $H_{am}$  of these amines was obtained experimentally at the absorber

operating condition of 40 °C and 1 atm using a hot gas FTIR (Fourier Transform Infrared Spectroscopy). A group contribution model that correlates  $H_{am}$  of amines to their molecular structure has been developed based on the data from this work and data from literature (Nguyen, 2013). This model is updated from Nguyen (2013) which was regressed using the data for 20 alkanolamines and 16 alkylamines. The updated model includes 24 additional amines with more structural features including bi-cyclic ring, cyclic alcohol, imidazole ring, pyridine ring, and intramolecular hydrogen-bond.

The amine partial pressure ( $P_{am}$ ) of these tertiary and hindered amines was also measured in a blend with PZ at 40 °C at their normal CO<sub>2</sub> loading range for flue gas CO<sub>2</sub> capture. A correlation has been developed between the  $H_{am}$  of tertiary and hindered amines and their  $P_{am}$  in a blend with PZ at nominal lean CO<sub>2</sub> loading condition coal-fired flue gas (~0.5 kPa) and 40 °C, which are the standard operating conditions at the top of the absorber where volatility is of greatest concern.

## **3.2 EXPERIMENTAL METHODS**

### **3.2.1 Solution preparation**

All amines (reagent grade) studied in this work were obtained from commercial sources. Approximately 500g of solution was prepared for each experiment. The Henry's law constant ( $H_{am}$ ) was measured with amine at 0.1 – 1.0 molal (m) in water (< 1.0 mol% amine). Solutions were prepared by dissolving pure amine in water to achieve the desired molality. The amine partial pressure ( $P_{am}$ ) of those tertiary and hindered amines was measured in blends of 2.5 m PZ/2.5 other amine at their normal CO<sub>2</sub> loading range for flue gas CO<sub>2</sub> capture. Aqueous PZ-based amine blends were prepared by melting anhydrous PZ in mixtures of distilled de-ionized water and other blended amines. CO<sub>2</sub> loaded solutions were prepared by gravimetrically sparging CO<sub>2</sub> (99.5%,

Matheson Tri Gas, Basking Ridge, NJ) in unloaded amine solutions in a gas-washing bottle. The concentration was determined by total inorganic carbon (TIC) analysis, described in detail previously (Freeman et al., 2010b).

### 3.2.2 Amine volatility measurement

Amine partial pressure ( $P_{am}$ ) in aqueous solutions was measured at 40 °C in a stirred reactor coupled with a hot gas FTIR analyzer (Fourier Transform Infrared Spectroscopy, Temet Gasmet Dx-4000) as shown in Figure 3.1.

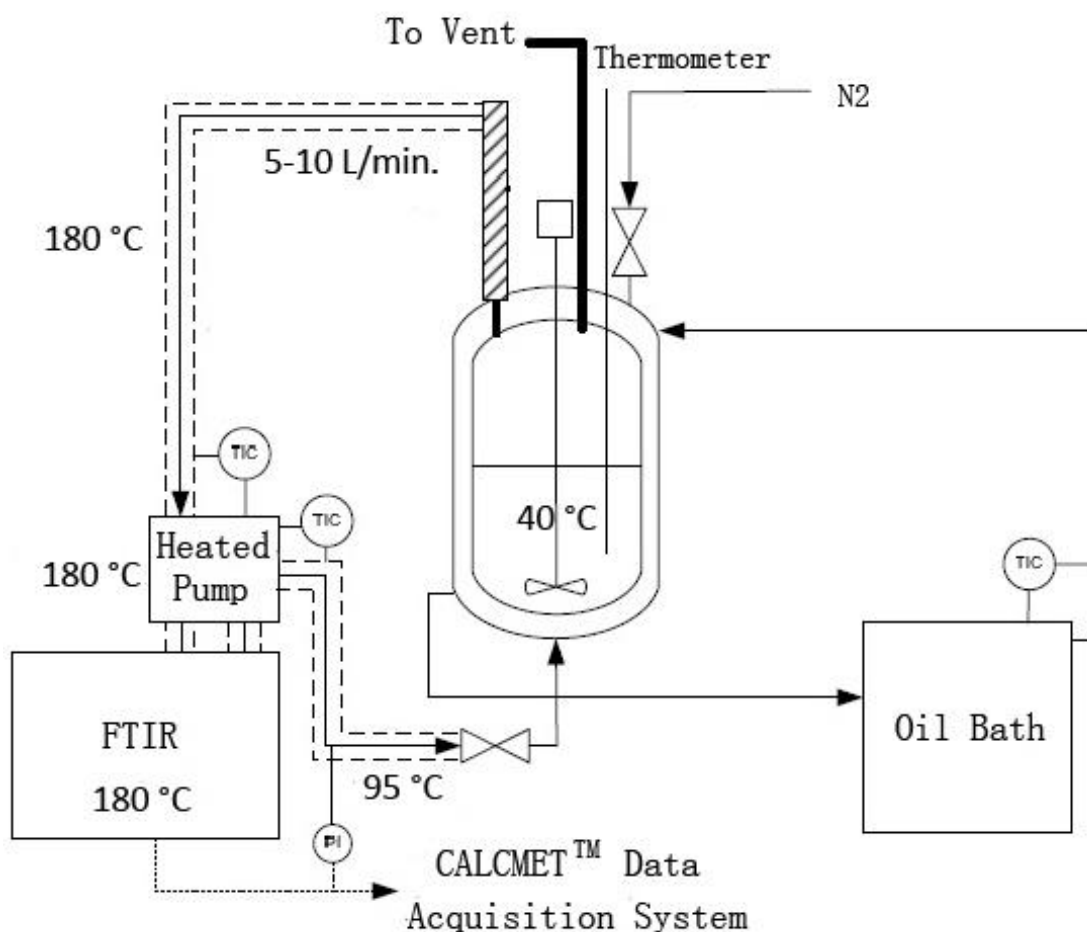


Figure 3.1: FTIR system for volatility measurement. Figure adapted by author from Nguyen (2013).

This was the same method and apparatus used by Nguyen (2013) to measure amine volatility. The 1 L glass reactor was filled with approximately 0.5 L of target amine solution and agitated at  $350 \text{ rpm} \pm 5 \text{ rpm}$ . Temperature in the reactor was controlled at  $40 \pm 0.1 \text{ }^\circ\text{C}$  by circulating heated dimethylsilicone oil in the outer reactor. The reactor was insulated with thick aluminum insulation material. The temperature inside the reactor was measured with a digital thermometer to within  $\pm 0.1 \text{ }^\circ\text{C}$ . Vapor from the headspace of the reactor was circulated at a rate of  $\sim 5\text{-}10 \text{ L/min}$ . by a heated sample pump to the FTIR through a heated Teflon line. The line, the pump cell, and FTIR analyzer were all maintained at  $180 \text{ }^\circ\text{C}$  to prevent the material in gas from condensation. After the gas passed through the FTIR, it was returned to the reactor through another heated line maintained at  $95 \text{ }^\circ\text{C}$  to maintain water balance and heat balance in the reactor. The concentration of amine,  $\text{CO}_2$ , and water in the gas were directly measured using the FTIR software (Calcmeter) with a measured calibration for each target component. The relative standard reproducibility for this measurement was estimated to be  $\pm 2\%$  in general, but can be up to  $\pm 10\%$  or greater for concentrations  $<10 \text{ ppm}$  (Nguyen, 2013).

FTIR calibration for each amine was performed using the Gasmeter Calibrator. Figure 3.2 displays the working mechanics of the Gasmeter Calibrator. The target amine is injected at a known flow rate by a syringe pump, and mixed with a  $\text{N}_2$  flow in a heated chamber kept at  $180 \text{ }^\circ\text{C}$ . The  $\text{N}_2$  is kept at a constant flow rate, typically between  $0.5\text{-}2.0 \text{ SLPM}$ , which produces a continual flow of a known concentration calibration gas that is introduced into the FTIR analyzer at  $180 \text{ }^\circ\text{C}$ . Calibration was performed at each concentration of interest by varying the flow rate of the target amine.

If the target amine is a solid at room temperature, it was dissolved in deionized water to form a homogeneous solution. The amine-water mixture with known

concentration was then injected into the heated chamber. The water component was subtracted from the overall spectra, leaving residual spectra as the reference spectra for the target amine. The following amines are solid at room temperature, and thus were calibrated by this way: piperazine, imidazole, 2-methylimidazole, 2-ethylimidazole, 1,2-dimethylimidazole, 2-ethyl-4-methylimidazole, triethylenediamine, 3-quinuclidinol, 4-hydroxy-1-methylpiperidine, tropine, 2-amino-2-ethyl-1,3-propanediol, 2-amino-2-methyl-1-propanol, 2-piperidineethanol. The details of the experimental apparatus, procedure, and calibration methods were described previously by Nguyen (2013).

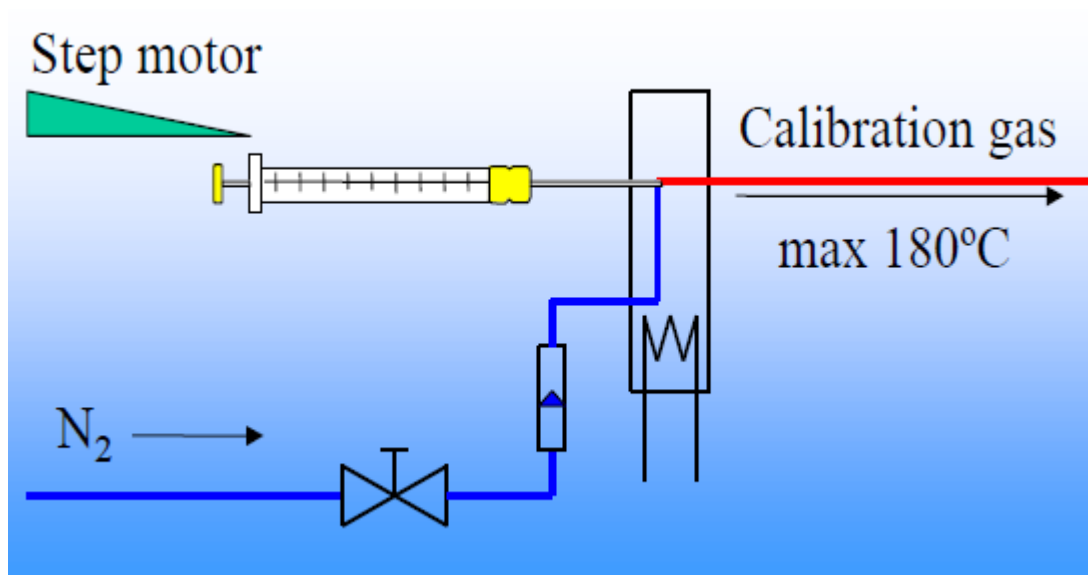


Figure 3.2: Schematic of Gasmet Calibrator mechanics. From: Nguyen (2013).

### 3.2.3 Henry's law constant

Amine volatility is expressed using the Henry's law constant ( $H_{am}$ ), as defined in Equation 3.1.

$$H_{am} = \frac{P_{amine}}{\gamma_{amine}^* x_{amine}} \quad (3.1)$$

where  $P_{\text{amine}}$  is the amine partial pressure (Pa);  $x_{\text{amine}}$  is the amine liquid phase mole fraction;  $\gamma^*_{\text{amine}}$  is the asymmetric amine activity coefficient defined at the reference state of infinite dilution of amine in water. At the dilute amine concentration used in this work ( $\sim 0.1 - 1.0$  m amine in  $\text{H}_2\text{O}$ ), the amine asymmetric activity coefficients are assumed to be 1 (Nguyen, 2013).

### **3.2.4 Experimental validation**

The FTIR method for amine volatility has been validated by Nguyen et al. (2010) by comparing the data measured by FTIR and measured by different techniques, such as gas chromatography. To validate the reproducibility of the FTIR method,  $H_{\text{am}}$  of 5 amines measured by Nguyen were measured again at  $40^\circ\text{C}$  in this work.  $H_{\text{am}}$  of the 5 amines from this work agrees well with that from Nguyen (2013), except for MDEA (Figure 3.3).  $H_{\text{am}}$  of MDEA at  $40^\circ\text{C}$  is close to the detection limit of the FTIR apparatus ( $\sim 1$  ppm), resulting in a high degree of uncertainty in the accuracy of the data.

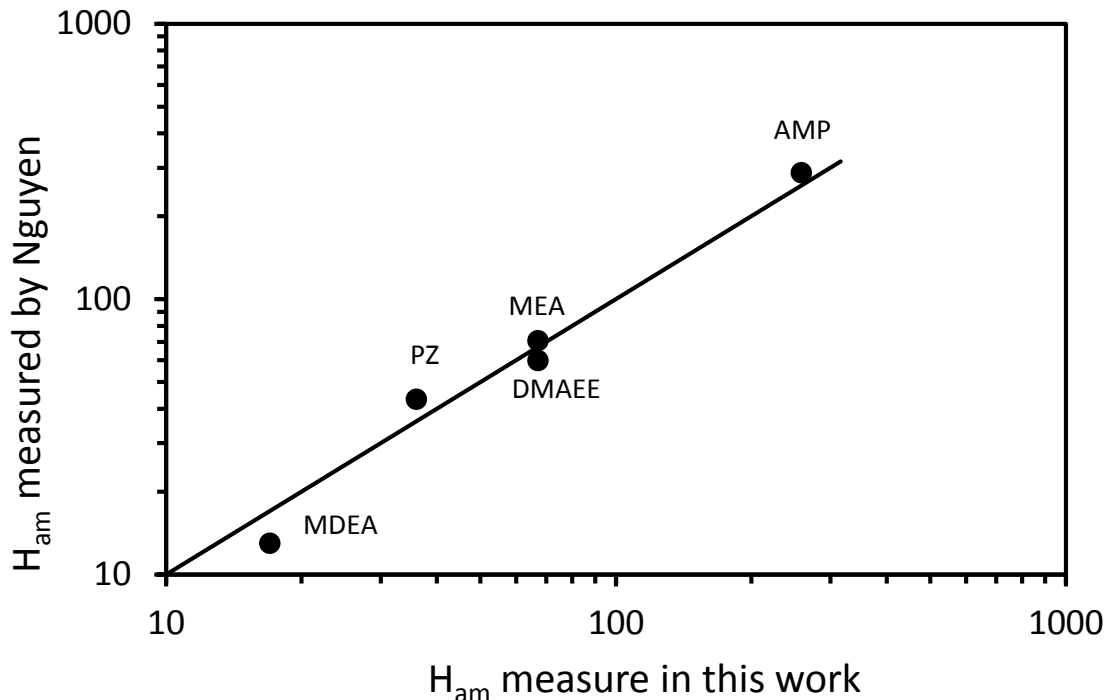


Figure 3.3: Comparison of the Henry's law constant ( $H_{am}$ ) from this work and Nguyen (2013).

### 3.3 RESULTS AND DISCUSSION

#### 3.3.1 Henry's law constant

Table 3.1 shows the structures and Henry's law constant ( $H_{am}$ ) at 40 °C for the 24 novel amines and 3 other common tertiary and hindered amines (MDEA, AMP, DMAEE). 14 of the novel amines show a  $H_{am}$  lower than AMP. The volatilities of amines are correlated with their molecular groups and structural shapes. In general, polar groups such as  $-NH_3$  and  $-OH$  reduce volatility; non-polar groups, such as  $-CH_3$  and  $-CH_2$ , increase the volatility. Volatility is increased by an intramolecular hydrogen bond, which impedes the formation of the hydrogen bond between water and the molecule. Most of the existing group contribution models for the prediction of amine volatility are regressed from alkylamine data, such as UNIFAC (Larsen et al., 1987) and

that of Hine and Mookerjee (1975), and thus cannot adequately predict the volatility of alkanolamines, which are more suitable for CO<sub>2</sub> capture. The group contribution model developed by Nguyen (2013) is the only one that was regressed mainly using the data for alkanolamines. However, due to the limited data (20 alkanolamines and 16 alkylamines) and structural features, the Nguyen model was unable to predict the volatility for half of the novel amines tested in this work (predictions are off by a factor of at least 3 for those amines) (Table 3.1). 2-Amino-2-ethyl-1,3-propanediol (AEPD), 4-(2-Hydroxyethyl)morpholine (HEMor), and 1-(2-Hydroxyethyl)piperidine (HEPD) show the greatest discrepancy by nearly two orders of magnitude between experimental  $H_{am}$  ( $H_{am-exp}$ ) and  $H_{am}$  predicted by Nguyen (2013) ( $H_{am-Nguyen}$ ). The under-prediction for AEPD results from the intramolecular hydrogen-bond, which was not considered in the model by Nguyen (2013). The over-prediction for HEMor and HEPD results from the large value assigned to the non-cyclic methylene group ( $-CH_2$ ) that is connected to a cyclic amino group in the model by Nguyen (2013) in order to match the  $H_{am-exp}$  of 2-Hydroxyethyl-piperazine (HEP) and 2,2-Dimorpholinodiethylether (DMORPH). The model by Nguyen (2013) was updated by regressing 24 additional amines from this work, along with the 20 alkanolamines and 16 alkylamines from Nguyen (2013). The data for HEP and DMORPH from Nguyen (2013) were excluded from regression. The  $H_{am-exp}$  of HEP from Nguyen (2013) is not reliable due to the low HEP concentration (0.13 m) used for  $H_{am-exp}$  measurement and the low volatility of HEP, resulting in a  $P_{am}$  of HEP that is lower than the detection limit of FTIR ( $\sim 1$  ppm). DMORPH has much larger molecular size than all the other amines tested in this work and in Nguyen (2013), and the molecular size is known to affect volatility (Müller-Schwarze and Silverstein, 1980).

Instead of considering a polar group (e.g.,  $-NH_2$  and  $-OH$ ) and the alkyl groups (e.g.,  $-CH_3$  and  $-CH_2$ ) connected to them as different parameters in Nguyen (2013), this

work considered them as a group parameter, which gives better comparison for the effect on amine volatility between different functional groups. The updated model is shown in Equation 3.2 with the regressed parameter values and their standard error shown in Table 3.2.

$$\ln H (Pa) = \text{Intercept} + \sum k_j * n_j \quad (3.2)$$

where  $k_j$  is the parameter value for functional group  $j$ ;  $n_j$  is the number of occurrences of group  $j$  in an amine structure.

Table 3.1: Comparison of measured  $H_{am}$  at 40 °C to values estimated by Nguyen (2013) and by the updated model from this work.

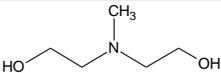
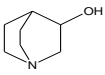
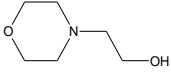
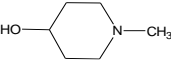
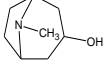
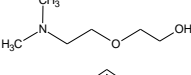
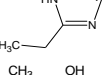
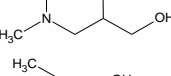
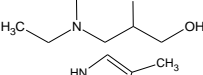
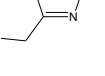
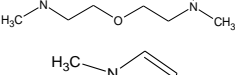
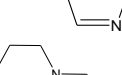
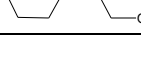
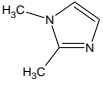
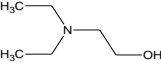
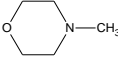
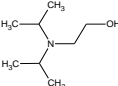
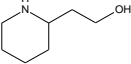
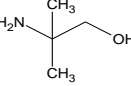
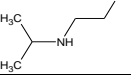
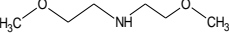
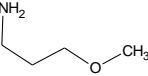
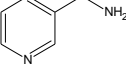
Name	Structure	Conc. <sup>a</sup> (m)	$H_{am-exp}$ <sup>b</sup> (Pa)	$H_{am-Nguyen}$ <sup>c</sup> (Pa)	$H_{am-pred}$ <sup>d</sup> (Pa)
Tertiary amine					
N-methyl-diethanolamine (MDEA)		1.0	17	23	29
Imidazole (IMI)		1.0	17	26 <sup>e</sup>	18
Triethylenediamine (TEDA)		1.0	18	62 <sup>e</sup>	25
3-Quinuclidinol (3-QD)		0.3	33	3 <sup>e</sup>	11
4-(2-Hydroxyethyl)morpholine (HEMor)		0.5	40	922	33
4-Hydroxy-1-methylpiperidine (HMPD)		0.5	41	12	52
Tropine		0.5	43	21	99
Dimethylaminoethoxyethanol (DMAEE)		0.5	67	99	90
2-Methylimidazole (2M-IMI)		0.5	68	30 <sup>e</sup>	48
2-Ethylimidazole (2E-IMI)		0.5	73	34 <sup>e</sup>	67
3-(Dimethylamino)-1,2-propanediol (DMA-PDL)		0.5	82	9	87
3-(Diethylamino)-1,2-propanediol (DEA-PDL)		0.5	103	79	211
2-Ethyl-4-methylimidazole (2E-4M-IMI)		0.3	196	40 <sup>e</sup>	180
Bis[2-(N,N-dimethylamino)ethyl] ether (BDMAEE)		0.3	697	235	707
1-Methylimidazole (1M-IMI)		0.3	805	163 <sup>e</sup>	622
1-(2-Hydroxyethyl)piperidine (HEPD)		0.3	1085	91126	1133

Table 3.1: Comparison of measured  $H_{am}$  at 40 °C to values estimated by Nguyen (2013) and by the updated model from this work (continued).

Name	Structure	Conc. <sup>a</sup> (m)	$H_{am-exp}$ <sup>b</sup> (Pa)	$H_{am-Nguyen}$ <sup>c</sup> (Pa)	$H_{am-pred}$ <sup>d</sup> (Pa)
1,2-Dimethylimidazole (1,2-DM-IMI)		0.3	1298	191 <sup>e</sup>	1681
2-(Diethylamino)ethanol (DEEA)		0.3	9436	17327	3153
N-Methylmorpholine (M-Morph)		0.1	10963	5745	15312
2-(Diisopropylamino)ethanol (DIPAE)		0.3	24672	23861	23050
Hindered amine					
2-Amino-2-ethyl-1,3-propanediol (AEPD)		0.5	78	1.4	20
2-Piperidineethanol (2-PE)		0.5	142	462	243
2-Amino-2-methyl-1-propanol (AMP)		0.3	258	311	595
2-(Isopropylamino)ethanol (IPAE)		0.3	498	3828	1028
Other amine					
Bis(2-methoxyethyl)amine (BMEA)		0.5	526	245	379
3-Methoxypropylamine (MOPA)		0.3	2682	1126	3989
3-(Aminomethyl)pyridine (3-AP)		0.5	128	111	149

a: the amine concentration used for volatility measurement (the activity coefficient is assumed to be 1 at this concentration); b: measured  $H_{am}$ ; c: predicted  $H_{am}$  from Nguyen (2013); d: predicted  $H_{am}$  from this work; e: to test the viability of the model from Nguyen (2013) for imidazoles, and bicyclic amines, it is assumed that an amino group on a bi-cyclic ring or an imidazole ring is the same as that on a mono-saturated ring.

Table 3.2: Model parameter values.

No.	Group j	Parameter Value	Standard error
1	$\text{CH}_2\text{-NCY-N}_{\text{NCY}}\text{-(CH}_3\text{-NCY)}_2$	-4.18	0.34
2	$\text{R}_{\text{NCY}}\text{-N}_{\text{NCY}}\text{-(CH}_2\text{-NCY)}_2$ $\text{R}_{\text{NCY}}\text{-N}_{\text{CY}}\text{-(CH}_2\text{-CY)}_2$	-5.29	0.33
3	$\text{R}_{\text{NCY}}\text{-N}_{\text{AR}}\text{-(R}_{\text{CY}})_2$	-3.60	0.50
4	$\text{N}_{\text{BCY}}\text{-(R}_{\text{CY}})_3$ $\text{(R}_{\text{CY}})\text{-N}_{\text{AR}}\text{=(R}_{\text{CY}})$ $\text{NH}_{\text{CY}}\text{-(R}_{\text{CY}})_2$ $\text{NH}_{\text{AR}}\text{-(R}_{\text{CY}})_2$	-7.15	0.27
5	$\text{R}_{\text{NCY}}\text{-NH}_{\text{NCY}}\text{-CH}_3\text{-NCY}$	-5.63	0.48
6	$\text{NH}_{\text{NCY}}\text{-(CH}_2\text{-NCY)}_2$	-6.41	0.52
7	$\text{R}_{\text{NCY}}\text{-NH}_2\text{-NCY}$	-6.96	0.28
8	$\text{R}_{\text{NCY}}\text{-O}_{\text{NCY}}\text{-R}_{\text{NCY}}$	-2.58	0.25
9	$\text{R}_{\text{CY}}\text{-O}_{\text{CY}}\text{-R}_{\text{CY}}$		
10	$\text{R}_{\text{NCY}}\text{-OH}$	-6.15	0.27
11	$\text{R}_{\text{CY}}\text{-OH}$	-8.90	0.41
12	$\text{-CH}_2\text{-}$	0.32	0.07
13	$\text{-CH}_3$	0.99	0.13
14	A	3.44	0.49
15	Intercept	17.50	0.49

NCY: non-cyclic; CY: cyclic; BCY: bi-cyclic; AR: aromatic; R: can be CH<sub>3</sub>, CH<sub>2</sub>, CH, and C; A: the intramolecular hydrogen-bond parameter for a molecule that has two -OH groups.

For example, PZ is considered as the sum of two  $\text{NH}_{\text{CY}}\text{-(R}_{\text{CY}})_2$ , MDEA is the sum of two  $\text{R}_{\text{NCY}}\text{-OH}$  and one  $\text{R}_{\text{NCY}}\text{-N}_{\text{NCY}}\text{-(CH}_2\text{-NCY)}_2$ , and 3-AP is the sum of one  $\text{(R}_{\text{CY}})\text{-N}_{\text{AR}}\text{=(R}_{\text{CY}})$ , one  $\text{R}_{\text{NCY}}\text{-NH}_2\text{-NCY}$ , and three  $\text{-CH}_2\text{-}$ . The updated model has the same number of parameters as that developed by Nguyen (2013), but accurately predicts the  $H_{\text{am-exp}}$  of the 24 novel amines from this work (Table 3.1), along with the amines from Nguyen (2013) (Figure 3.3). The four outliers (predictions are off by a factor of at least 3 for those amines) are diglycolamine<sup>®</sup> (DGA<sup>®</sup>), 3-QD, AEPD, and DEEA. This model only consider intramolecular hydrogen-bond between two hydroxyl groups. However,

intramolecular hydrogen-bond can also form in the molecule that has one amino group and one hydroxyl group, such as DGA<sup>®</sup> and 3-QD, although this kind of hydrogen-bond is generally weak. The majority of the parameter values are statistically significant with corresponding standard errors less than one order of magnitude. All of the group parameters used are independent with only one pair of groups having a correlation greater than 0.41. The correlated pair is, as expected, the non-cyclic hydroxyl group ( $R_{\text{NCY-OH}}$ ) and the intramolecular hydrogen-bond parameter for a molecule that has two  $\text{-OH}$  groups (A).

Among all the polar groups, the cyclic hydroxyl group ( $R_{\text{CY-OH}}$ ) shows the most significant effect on reducing the volatility, due to the strong hydrogen-bonding with water. Amines with linear hydroxyl groups ( $R_{\text{NCY-OH}}$ ) seem more volatile than amines with cyclic hydroxyl groups. It is probable that linear alcohols have stronger self-association compared to cyclic alcohols (Silvia Pérez-Casas et al., 1991), resulting in less hydrogen-bonding with water. Ether groups ( $R_{\text{NCY-ONCY-RNCY}}$  and  $R_{\text{CY-OCY-RCY}}$ ) are much less polar than hydroxyl and amino groups, resulting in much weaker hydrogen-bonding with water.

Primary amino groups ( $R_{\text{NCY-NH}_2\text{-NCY}}$ ) are more effective in reducing volatility than non-cyclic secondary amino groups ( $\text{NH}_{\text{NCY}}\text{-(CH}_2\text{-NCY)}_2$  and  $R_{\text{NCY-NH}_{\text{NCY}}\text{-CH}_3\text{-NCY}}$ ) and non-cyclic tertiary amino groups ( $\text{CH}_2\text{-NCY-N}_{\text{NCY}}\text{-(CH}_3\text{-NCY)}_2$  and  $R_{\text{NCY-N}_{\text{NCY}}\text{-(CH}_2\text{-NCY)}_2$ ), primarily due to the more H to form hydrogen-bond with water. Surprisingly, cyclic secondary amino groups ( $\text{NH}_{\text{CY}}\text{-(R}_{\text{CY}})_2$ ) and tertiary amino groups without a n-substitution ( $\text{N}_{\text{BCY}}\text{-(R}_{\text{CY}})_3$  and  $(\text{R}_{\text{CY}})\text{-N}_{\text{AR}}\text{=(R}_{\text{CY}})$ ) have an effect comparable to primary amino groups in reducing the amine volatility.

The noncyclic alkyl groups significantly reduce the polarity of the connected cyclic amino groups, comparing the value for  $\text{NH}_{\text{CY}}\text{-(R}_{\text{CY}})_2$  and  $\text{NH}_{\text{AR}}\text{-(R}_{\text{CY}})_2$  (-7.15) to

that for  $R_{NCY}-N_{AR}-(R_{CY})_2$  (-3.60) and  $R_{NCY}-N_{CY}-(CH_2-CY)_2$  (-5.29). Methyl groups (-CH<sub>3</sub>) are more nonpolar than methylene groups (-CH<sub>2</sub>-) when they are not connected to any polar group. The intramolecular hydrogen-bond parameter (A) was assigned to all molecules that have two hydroxyl groups without considering the distance between them.

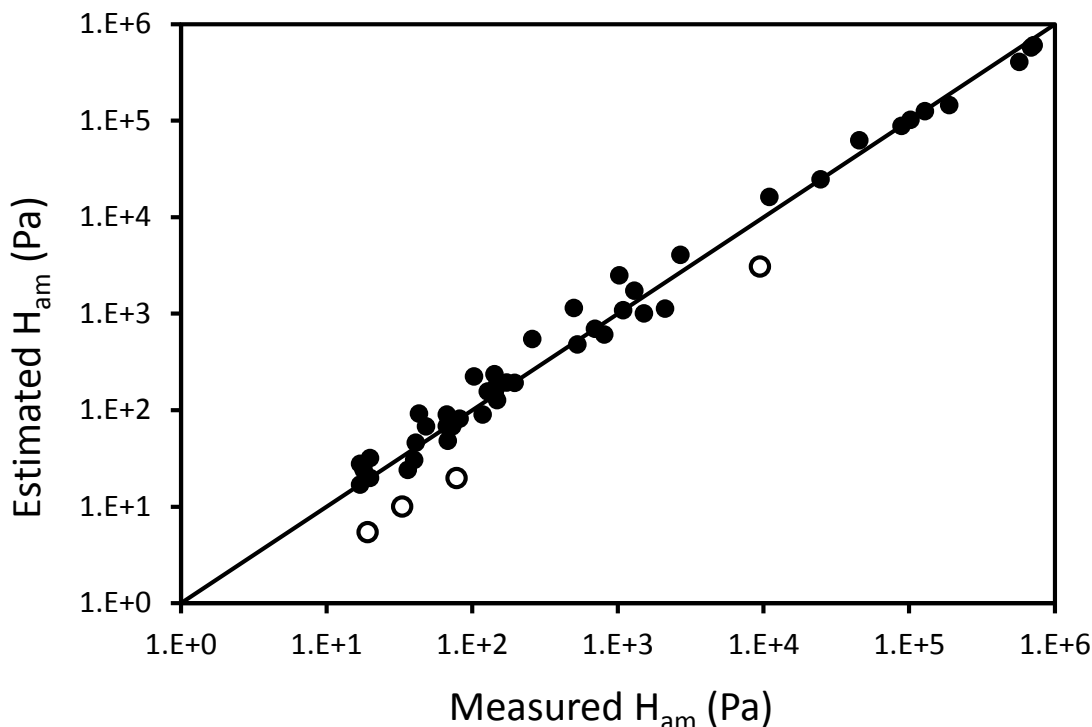


Figure 3.3: Evaluation of the updated model for  $H_{am}$  prediction at 40 °C.

### 3.3.2 Amine partial pressure ( $P_{am}$ ) of tertiary and hindered amines

Table 3.3 and Table 3.4 show the amine partial pressure ( $P_{am}$ ) at 40 °C in CO<sub>2</sub>-loaded PZ/tertiary amines and PZ/hindered amines, respectively, along with the partial pressure of CO<sub>2</sub> ( $P_{CO_2}$ ) and partial pressure of H<sub>2</sub>O ( $P_{H_2O}$ ).  $P_{am}$  of some PZ/tertiary amines was found to be difficult to quantify using FTIR, due to their severe peak overlap, including PZ/IMI, PZ/2M-IMI, PZ/DMA-PDL, and PZ/DEA-PDL, or due to phase separation, such as PZ/DIPAE. As expected,  $P_{am}$  of PZ in PZ/tertiary amines and

PZ/hindered amines is significantly decreased with the increase of CO<sub>2</sub> loading, as a result of carbamate formation. In general, the P<sub>am</sub> of tertiary and hindered amines is not significantly affected by the CO<sub>2</sub> loading, as they either cannot or are unable to form stable carbamates which result in limited speciation. However, with increased pK<sub>a</sub>, the P<sub>am</sub> of tertiary and hindered amines become a stronger function of CO<sub>2</sub> loading (represented as P\*<sub>CO2</sub>, the equilibrium CO<sub>2</sub> partial pressure, at 40°C), as a result of protonation (Figure 3.4 and 3.5).

Table 3.3: Volatility of 2.5 m PZ/2.5 m tertiary amines at normal loading range for coal-fired flue gas and 40 °C.

Tertiary amines in blend	pK <sub>a</sub> <sup>1</sup>	Ldg (mol CO <sub>2</sub> /mol PZ)	P <sub>H2O</sub> (kPa)	P <sub>CO2</sub> (kPa)	P <sub>PZ</sub> (Pa)	P <sub>am</sub> (Pa)
4-(2-Hydroxyethyl)morpholine (HEMor)	7.01 <sup>a</sup>	0.45	6.79	0.15	1.34	2.31
		0.69	6.81	1.84	0.67	2.18
		0.84	6.77	6.62	0.45	2.15
1-Methylimidazole (1M-IMI)	7.06 <sup>b</sup>	0.45	6.92	0.11	1.21	9.62
		0.75	6.96	2.70	0.64	10.18
		0.87	6.97	8.73	0.44	9.62
N-Methylmorpholine (M-Morph)	7.40 <sup>a</sup>	0.45	6.73	0.13	— <sup>2</sup>	731
		0.60	6.69	0.63	— <sup>2</sup>	769
		0.75	6.71	2.58	— <sup>2</sup>	794
		0.87	6.71	6.62	— <sup>2</sup>	793
2-Ethylimidazole (2E-IMI)	7.97 <sup>c</sup>	0.45	7.08	0.13	1.37	0.97
		0.69	7.01	1.12	0.48	0.70
		0.93	7.16	8.03	0.55	1.09
1,2-Dimethylimidazole (1,2-DM-IMI)	7.76 <sup>c</sup>	0.53	7.06	0.21	1.03	7.45
		0.69	6.93	0.99	1.02	6.61
		0.93	6.99	6.79	0.84	6.09
2-Ethyl-4-methylimidazole (2E-4M-IMI)	8.42 <sup>c</sup>	0.51	7.25	0.18	1.47	2.88
		0.70	7.29	0.90	1.30	2.65
		1.01	7.20	6.92	1.06	4.03
N-methyl-diethanolamine (MDEA)	8.56 <sup>d</sup>	0.51	6.89	0.21	1.19	0.72
		0.87	6.84	1.92	1.38	0.71
		1.14	6.86	7.18	1.11	0.70
Triethylenediamine (TEDA)	8.77/2.24 <sup>e,3</sup>	0.60	6.76	0.16	0.51	1.84
		0.88	6.58	0.87	0.17	1.40
		1.08	6.67	2.58	0.11	1.12
		1.24	6.72	5.69	0.11	0.87
Dimethylaminoethoxyethanol (DMAEE)	9.09 <sup>f</sup>	0.60	6.63	0.24	0.65	2.74
		0.78	6.67	0.54	0.43	2.60
		1.14	6.81	3.00	0.36	2.25
		1.26	6.82	5.80	0.37	1.90
4-Hydroxy-1-methylpiperidine (HMPD)	9.12	0.60	7.01	0.16	0.84	2.72
		0.81	6.85	0.56	1.06	2.95
		1.13	7.03	2.67	0.86	2.54
		1.30	6.92	6.53	0.34	1.03
Bis[2-(N,N-dimethylamino)ethyl] ether (BDMAEE)	9.80/8.21 <sup>g</sup>	0.60	6.47	0.10	— <sup>2</sup>	26.1
		0.98	6.64	0.64	— <sup>2</sup>	28.8
		1.50	6.43	4.04	— <sup>2</sup>	22.2
		1.65	6.60	6.52	— <sup>2</sup>	20.8
1-(2-Hydroxyethyl)piperidine (HEPD)	9.63 <sup>a</sup>	0.75	6.88	0.31	— <sup>2</sup>	32.1
		0.93	6.82	0.64	— <sup>2</sup>	31.7
		1.20	6.89	2.56	— <sup>2</sup>	21.8
		1.35	6.92	5.97	— <sup>2</sup>	15.7

Table 3.3: Volatility of 2.5 m PZ/2.5 m tertiary amines at normal loading range for coal-fired flue gas and 40 °C (continued).

Tertiary amines in blend	pK <sub>a</sub> <sup>1</sup>	Ldg (mol CO <sub>2</sub> /mol PZ)	P <sub>H<sub>2</sub>O</sub> (kPa)	P <sub>CO<sub>2</sub></sub> (kPa)	P <sub>PZ</sub> (Pa)	P <sub>am</sub> (Pa)
2-(Diethylamino)ethanol (DEEA)	9.75 <sup>h</sup>	0.66	6.81	0.09		153
		0.93	6.85	0.25	— <sup>2</sup>	147
		1.20	6.79	0.81		113
		1.53	6.85	4.34		58.9
3-Quinuclidinol (3-QD)	9.86 <sup>i,3</sup>	0.76	6.78	0.11	0.51	6.14
		0.97	6.74	0.34	0.24	2.24
		1.17	6.80	0.92	0.13	0.91
		1.35	6.79	3.05	0.10	0.32
		1.47	6.86	7.26	0.08	0.11
Tropine	10.48 <sup>a</sup>	0.88	7.01	0.09	2.63	1.19
		1.05	6.93	0.27	2.60	1.15
		1.20	6.88	0.70	1.45	0.71
		1.32	6.98	1.84	0.81	0.28
		1.44	6.98	5.23	1.00	0.09

1: Thermodynamic values at 25 °C and zero ionic strength

2: P<sub>am</sub> of PZ is not able to be measured due to the overlap of PZ peak by the much larger peak of these volatile tertiary amines.

3: The value is extrapolated to zero ionic strength according to a simplified version of the Debye-Huckel equation (Nozaki et al., 1957).

a: (Xu et al., 1993); b: (Nozaki et al., 1957); c: calculated by means of computer program ACD/pK<sub>a</sub> DB (Advanced Chemistry Development Inc.-Canada); d: (Hamborg et al., 2007); e: (Paoletti et al., 1965); f: (Simond et al., 2012); g: (Fakstorp et al., 1958); h: (Hamborg and Versteeg, 2009); i: (Grob, 1985)

Table 3.4: Volatility of 2.5 m PZ/2.5 m hindered amines at normal loading range for coal-fired flue gas and 40 °C.

Hindered amines in blend	pK <sub>a</sub>	Ldg (mol CO <sub>2</sub> /mol PZ)	P <sub>H2O</sub> (kPa)	P <sub>CO2</sub> (kPa)	P <sub>PZ</sub> (Pa)	P <sub>am</sub> (Pa)
2-Amino-2-ethyl-1,3- propanediol (AEPD)	8.82 <sup>h</sup>	0.60	6.97	0.14	0.71	1.81
		0.84	6.89	0.61	0.52	1.52
		1.09	6.93	2.49	0.29	1.29
		1.32	6.88	8.65	0.20	1.20
2-Amino-2-methyl-1-propanol (AMP)	9.64 <sup>i</sup>	0.69	6.92	0.08	1.03	11.4
		0.93	6.93	0.33	0.51	7.50
		1.20	6.87	1.24	0.41	4.21
		1.44	6.96	6.95	0.22	2.48
2-(Isopropylamino)ethanol (IPAE)	9.93 <sup>k</sup>	0.77	6.68	0.11	1.54	15.9
		1.05	6.64	0.46	1.08	11.6
		1.32	6.69	1.50	0.91	8.13
		1.56	6.74	6.76	0.71	5.29
2-Piperidineethanol (2-PE)	10.14 <sup>j</sup>	0.87	6.77	0.07	2.25	5.32
		1.2	6.80	0.66	1.39	2.44
		1.38	6.91	2.48	0.64	1.47
		1.47	6.92	5.32	0.55	1.08

f: (Simond et al., 2012); h: (Hamborg and Versteeg, 2009); i: (Grob, 1985); j: (Xu et al., 1992); k: (Yamada et al., 2010)

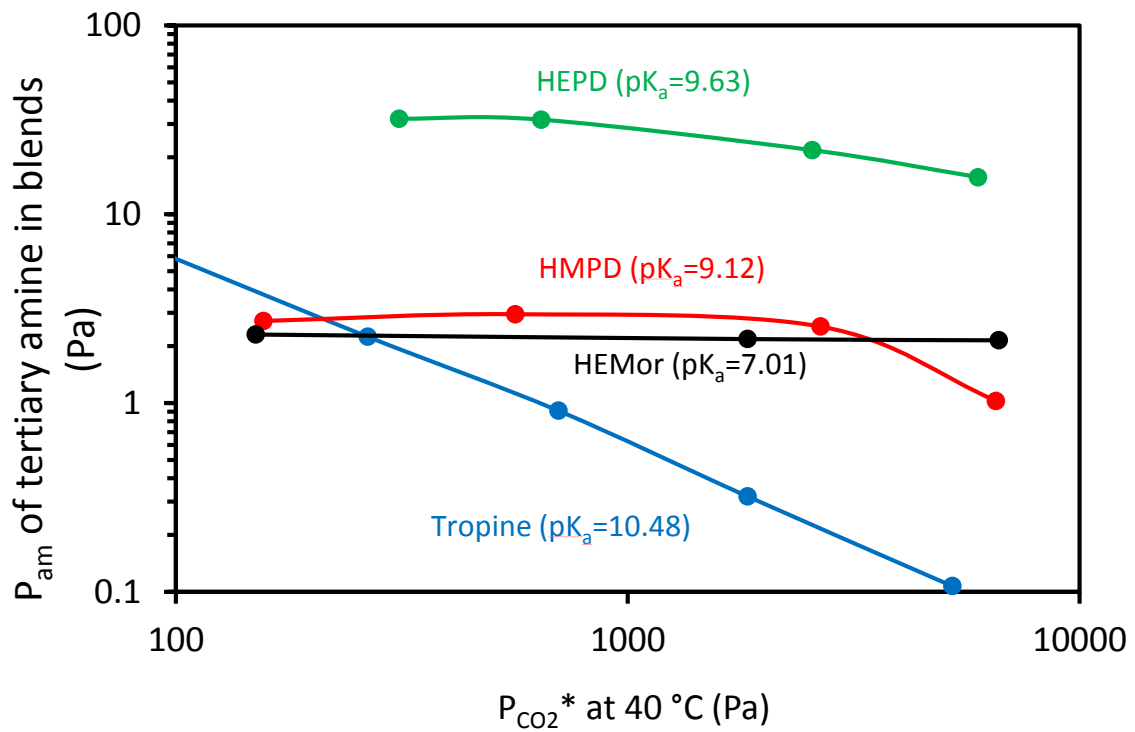


Figure 3.4:  $P_{am}$  at 40°C of tertiary amine in 2.5 m PZ/2.5 m tertiary amine with variable  $pK_a$ .

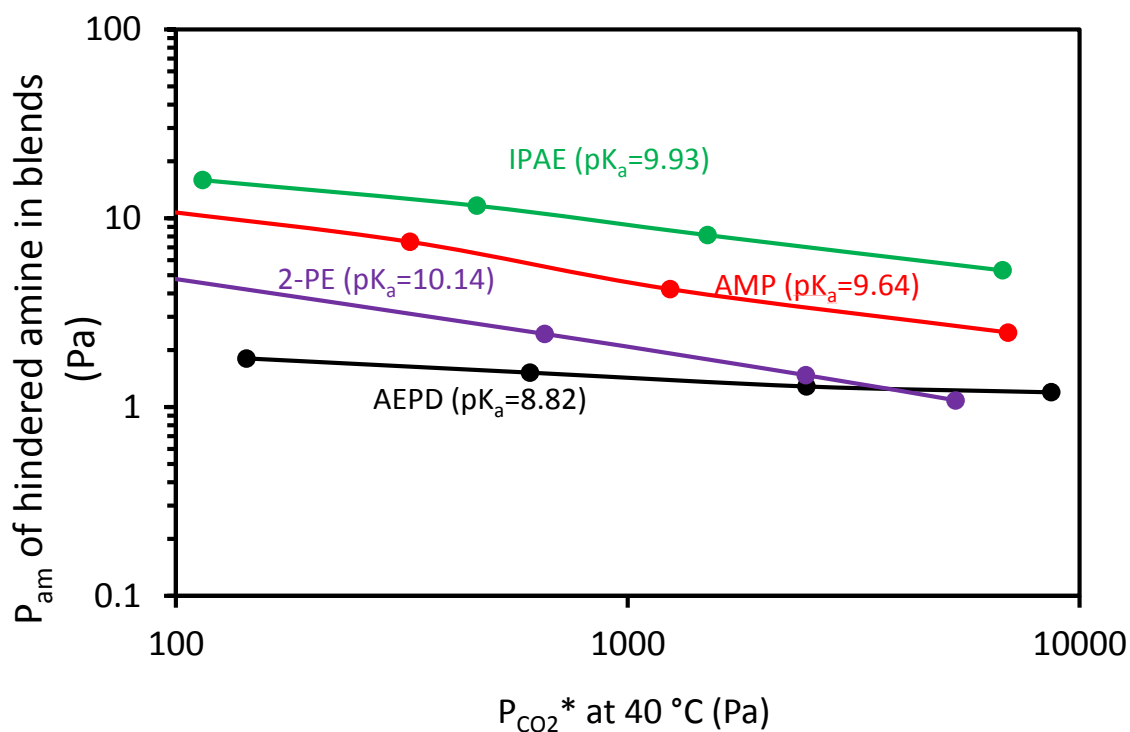


Figure 3.5:  $P_{am}$  at 40°C of hindered amines in 2.5 m PZ/2.5 m hindered amine with variable  $pK_a$ .

### 3.3.3 Correlation between $H_{am}$ and $P_{am}$ of tertiary and hindered amines at nominal lean loading for coal-fired flue gas

Although tertiary and hindered amines with high  $pK_a$  can be substantially protonated at rich  $CO_2$  loading, they are mostly free amine at lean loading where the pH of the solution is still high.  $H_{am}$  of tertiary and hindered amines can still be used as an indicator of their amine volatility at lean loading where volatility is of greatest concern. A correlation has been found between the  $H_{am}$  of tertiary and hindered amines and their  $P_{am}$  in a blend with PZ at nominal lean  $CO_2$  loading condition coal-fired flue gas (~ 0.5 kPa) and 40 °C (Figure 3.6).

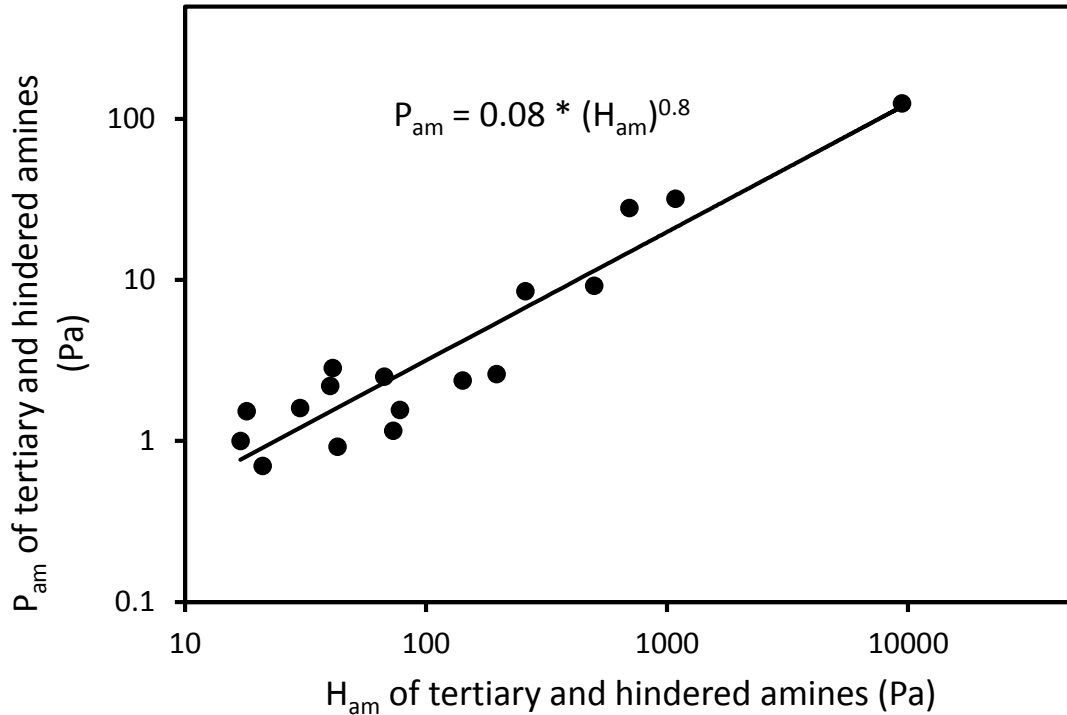


Figure 3.6: Correlation between  $H_{am}$  and  $P_{am}$  of tertiary and hindered amines in 2.5 m PZ/2.5 m tertiary and hindered amines at nominal lean loading for coal-fired flue gas ( $\sim 0.5$  kPa  $P^*_{CO_2}$ ) at 40 °C.

### 3.4 CONCLUSIONS

The Henry's law constant ( $H_{am}$ ) of 24 novel amines, including 18 tertiary amines, 3 hindered amines, 2 ether amines, and 1 pyridine derivative was measured at 40 °C using a hot gas FTIR. 14 have  $H_{am}$  lower than 2-amino-2-methyl-1-propanol (AMP).

A group contribution model that correlates  $H_{am}$  to molecular structure was developed based on the data from this work and data from literature. Non-cyclic groups and cyclic groups show a significant effect on the amine volatility.

The amine partial pressure ( $P_{am}$ ) of 2.5 m tertiary and hindered amines was also measured in a blend with 2.5 m PZ at 40 °C and their normal  $CO_2$  loading range for flue gas  $CO_2$  capture. With increased  $pK_a$ , the  $P_{am}$  of tertiary and hindered amines becomes a

stronger function of CO<sub>2</sub> loading. A correlation has been found between the H<sub>am</sub> of tertiary and hindered amines and their P<sub>am</sub> in a blend with PZ at nominal lean CO<sub>2</sub> loading condition coal-fired flue gas (~ 0.5 kPa) and 40 °C, which are the standard operating conditions at the top of the absorber where volatility is of greatest concern.

### **3.5 ACKNOWLEDGEMENTS**

The author gratefully acknowledges Ye Yuan for doing the statistical analysis for the updated model for H<sub>am</sub> prediction.

## **Chapter 4: CO<sub>2</sub> Capacity and Absorption Rate of Novel Piperazine/Amine Blends**

CO<sub>2</sub> cyclic capacity and CO<sub>2</sub> absorption rate are the two most important parameters that determine the capital cost and energy cost for a solvent for CO<sub>2</sub> capture. With higher CO<sub>2</sub> cyclic capacity, less solvent is required to remove the same amount of CO<sub>2</sub>, reducing sensible heat requirement for solvent regeneration and the size of the cross heat exchanger. Greater absorption rate reduces the amount of packing required for the same CO<sub>2</sub> removal, which leads to a lower absorber cost. Piperazine (PZ) in blend with a tertiary amine usually combines the high CO<sub>2</sub> capacity of the tertiary amine with the fast rate of PZ.

In a PZ/tertiary amine blend, the tertiary amine acts as a buffer to reduce the protonation of PZ. In the normal operating CO<sub>2</sub> loading range for flue gas CO<sub>2</sub> capture, a tertiary amine with pK<sub>a</sub> lower than 8.0 or higher than 10.0 cannot effectively buffer the solution. The optimum pK<sub>a</sub> of a tertiary amine blended with PZ is 9.1 to give the greatest CO<sub>2</sub> cyclic capacity.

A generic Aspen Plus<sup>®</sup> model for PZ/tertiary amine was developed based on a rigorous Aspen Plus<sup>®</sup> model for PZ/MDEA with electrolyte Nonrandom Two-Liquid (e-NRTL) as the thermodynamic framework. This generic model can reasonably predict the CO<sub>2</sub> vapor-liquid-equilibrium (VLE) in PZ/tertiary amine based on the pK<sub>a</sub> of the tertiary amine.

To a lesser degree than pK<sub>a</sub>, the polarity of the tertiary amine also affects the CO<sub>2</sub> solubility of the PZ/tertiary amine.

Hindered amines that form little carbamate mainly act as pH buffers in PZ/hindered amines, showing similar CO<sub>2</sub> VLE to PZ/tertiary amine with the same pK<sub>a</sub>.

CO<sub>2</sub> absorption rate of most 2.5 m PZ/2.5 m tertiary amines was found to be slightly slower than 2.5 m PZ itself, probably due to the higher viscosity of the blend. 2.5 m PZ/2.5 m tertiary amines still absorb CO<sub>2</sub> much faster than 7 m MEA.

2.5 m PZ/2.5 m HMPD shows the best overall performance for flue gas CO<sub>2</sub> capture, high thermal stability, low amine volatility, large  $\Delta C_{\mu}$ , and high  $k_g'_{avg}$ .

#### 4.1 INTRODUCTION

Chemical absorption using aqueous amine is the most applicable technology for flue gas CO<sub>2</sub> capture from fossil fuel combustion, due to its maturity proved in other industrial gas treating processes (Astarita et al., 1983), and its high energy efficiency compared to other alternative technologies, such as oxy-combustion, physical adsorption, and membrane separation (Rochelle, 2009). Its commercial application is impeded by the high capital and energy costs that result from the low CO<sub>2</sub> partial pressure and high flow rate of flue gas (Catalanotti et al., 2014; Clark and Herzog, 2014; Finkenrath, 2012).

CO<sub>2</sub> cyclic capacity and CO<sub>2</sub> absorption rate are the two most important parameters that determine the capital cost and energy cost for an amine solvent for CO<sub>2</sub> capture. With higher CO<sub>2</sub> cyclic capacity, less solvent is required to remove the same amount of CO<sub>2</sub>, reducing sensible heat requirement for solvent regeneration and the size of the cross heat exchanger. Greater absorption rate reduces the amount of packing required for the same CO<sub>2</sub> removal, which leads to a lower absorber cost.

Concentrated piperazine (PZ) has been proposed as a new standard for amine scrubbing (Rochelle et al., 2011). 8 molal (m) PZ (40 wt % PZ) has double the CO<sub>2</sub> absorption rate and capacity, and much better thermal stability than the benchmark solvent, 30 wt % monoethanolamine (MEA) (Rochelle et al., 2011). However, PZ and its zwitterionic carbamate have limited water solubility so solid precipitation may occur

(Freeman et al., 2010b; Ma et al., 2012), which may limit its application for CO<sub>2</sub> capture. Blending other useful amines with less concentrated PZ (2 – 3 m PZ) is a way to address the solid precipitation of PZ, while maintaining the good CO<sub>2</sub> capture performance of concentrated PZ. PZ blended with a tertiary or hindered amine, such as PZ/*n*-methyldiethanolamine (MDEA) and PZ/2-amino-2-methyl-1-propanol (AMP), usually combines the high CO<sub>2</sub> capacity of tertiary and hindered amines with the fast rate of PZ (Adeosun et al., 2013; Alvis et al., 2012; Bishnoi and Rochelle, 2002; Chen and Rochelle, 2011; Kumar and Kundu, 2012; H. Li et al., 2013; Seo and Hong, 2000).

In this work, 21 novel tertiary and hindered amines (Table 4.1) blended with PZ have been studied for their CO<sub>2</sub> capacity and CO<sub>2</sub> absorption rate, and compared to PZ/MDEA and PZ/AMP. The effect of the structural features of tertiary and hindered amines on the CO<sub>2</sub> capacity and absorption rate of the blends has also been investigated.

Table 4.1: Tertiary and hindered amines with their structures and pK<sub>a</sub>.

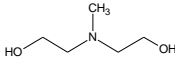
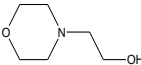
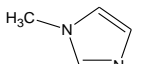
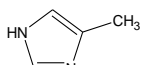
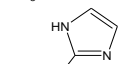
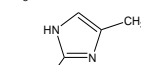
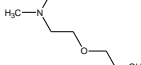
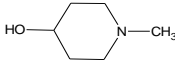
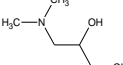
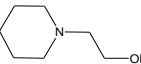
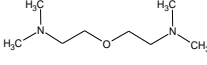
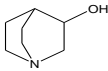
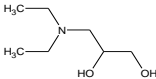
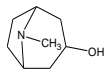
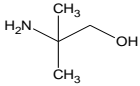
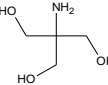
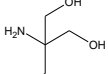
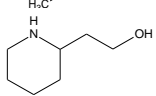
No.	Name	CAS number	Structure	pK <sub>a</sub> <sup>a</sup>	Ref.
R1	N-methyl-diethanolamine (MDEA)	105-59-9		8.56	(Hamborg et al., 2007)
1	N-Methyl-2-pyridone (NMP)	694-85-9		0.30	ACD/pK <sub>a</sub> DB <sup>b</sup>
2	Imidazole (IMI)	288-32-4		6.95	(Nozaki et al., 1957)
3	4-(2-Hydroxyethyl)morpholine (HEMor)	622-40-2		7.01	(Xu et al., 1993)
4	1-Methylimidazole (1M-IMI)	616-47-7		7.06	(Nozaki et al., 1957)
5	4(5)-Methylimidazole (4M-IMI)	822-36-6		7.52	(Nozaki et al., 1957)
6	1,2-Dimethylimidazole (1,2-DM-IMI)	1739-84-0		7.76	ACD/pK <sub>a</sub> DB <sup>b</sup>
7	2-Methylimidazole (2M-IMI)	693-98-1		7.86	(Nozaki et al., 1957)
8	2-Ethylimidazole (2E-IMI)	1072-62-4		7.97	ACD/pK <sub>a</sub> DB <sup>b</sup>
9	2-Ethyl 4-methylimidazole (2E-4M-IMI)	931-36-2		8.42	ACD/pK <sub>a</sub> DB <sup>b</sup>
10	Triethylenediamine (TEDA)	280-57-9		8.77/2.24 <sup>c</sup>	(Paoletti et al., 1965)
11	Dimethylaminoethoxyethanol (DMAEE)	1704-62-7		9.09	(Simond et al., 2012)
12	4-Hydroxy-1-methylpiperidine (HMPD)	106-52-5		9.12	This work
13	3-(Dimethylamino)-1,2-propanediol (DMA-PDL)	623-57-4		9.14	(Chowdhury et al., 2013)
14	1-(2-Hydroxyethyl)piperidine (HEPD)	3040-44-6		9.63	(Xu et al., 1993)
15	Bis[2-(N,N-dimethylamino)ethyl] ether (BDMAEE)	3033-62-3		9.80/8.21	(Fakstorp et al., 1958)

Table 4.1: Tertiary and hindered amines with their structures and pKa (continued).

No.	Name	CAS number	Structure	pK <sub>a</sub>	Ref.
16	3-Quinuclidinol (3-QD)	1619-34-7		9.86 <sup>c</sup>	(Grob, 1985)
17	3-(Diethylamino)-1,2-propanediol (DEA-PDL)	621-56-7		9.89	(Chowdhury et al., 2013)
18	Tropine	120-29-6		10.48	(Xu et al., 1993)
R2	2-Amino-2-methyl-1-propanol (AMP)	124-68-5		9.64	(Grob, 1985)
19	Tris(hydroxymethyl)aminomethane (TRIS)	77-86-1		8.08	(Simond et al., 2012)
20	2-Amino-2-ethyl-1,3-propanediol (AEPD)	115-70-8		8.82	(Hamborg and Versteeg, 2009)
21	2-Piperidineethanol (2-PE)	1484-84-0		10.14	(Grob, 1985)

a: Thermodynamic values at 25 °C and zero ionic strength; b: calculated by means of computer program ACD/pK<sub>a</sub> DB (Advanced Chemistry Development Inc.-Canada); c: The value is extrapolated to zero ionic strength according to a simplified version of the Debye-Huckel equation (Nozaki et al., 1957).

## 4.2 EXPERIMENT METHODS

### 4.2.1 Solution preparation

All amines studied in this work were reagent grade chemicals from commercial sources. Aqueous PZ/tertiary amines and PZ/hindered amines were prepared by melting anhydrous PZ in mixtures of distilled de-ionized water and tertiary amines or hindered amines, and gravimetrically sparging CO<sub>2</sub> (99.5%, Matheson Tri Gas, Basking Ridge, NJ) to achieve the desired CO<sub>2</sub> concentration. The CO<sub>2</sub> was determined by total inorganic carbon (TIC) analysis, described in detail previously (Freeman et al., 2010b).

#### **4.2.2 Viscosity measurement**

Viscosity of some of the PZ/tertiary amines with variable CO<sub>2</sub> loading was measured at 40 °C using a Physica MCR 300 cone-and-plate rheometer (Anton Paar GmbH, Graz, Austria). The method was described in detail previously (Freeman et al., 2010b).

#### **4.2.3 CO<sub>2</sub> solubility by FTIR**

CO<sub>2</sub> solubility in PZ/tertiary amines and PZ/hindered amines were measured at 40 °C and normal CO<sub>2</sub> loading range in a stirred reactor coupled with a hot gas FTIR analyzer (Fourier Transform Infrared Spectroscopy, Temet Gasmeter Dx-4000). The details of the experimental apparatus, and procedure were described in the Chapter 3.

#### **4.2.4 CO<sub>2</sub> solubility and absorption rate by WWC**

The CO<sub>2</sub> solubility and CO<sub>2</sub> absorption rate in some of the PZ/tertiary amines were measured at 40 °C and normal CO<sub>2</sub> loading range using a wetted wall column (WWC) (Figure 4.1), which counter currently contacted an aqueous amine solution with a saturated N<sub>2</sub>/CO<sub>2</sub> stream on the surface of a stainless steel rod with a known surface area to simulate the situation of CO<sub>2</sub> absorption in an absorber.

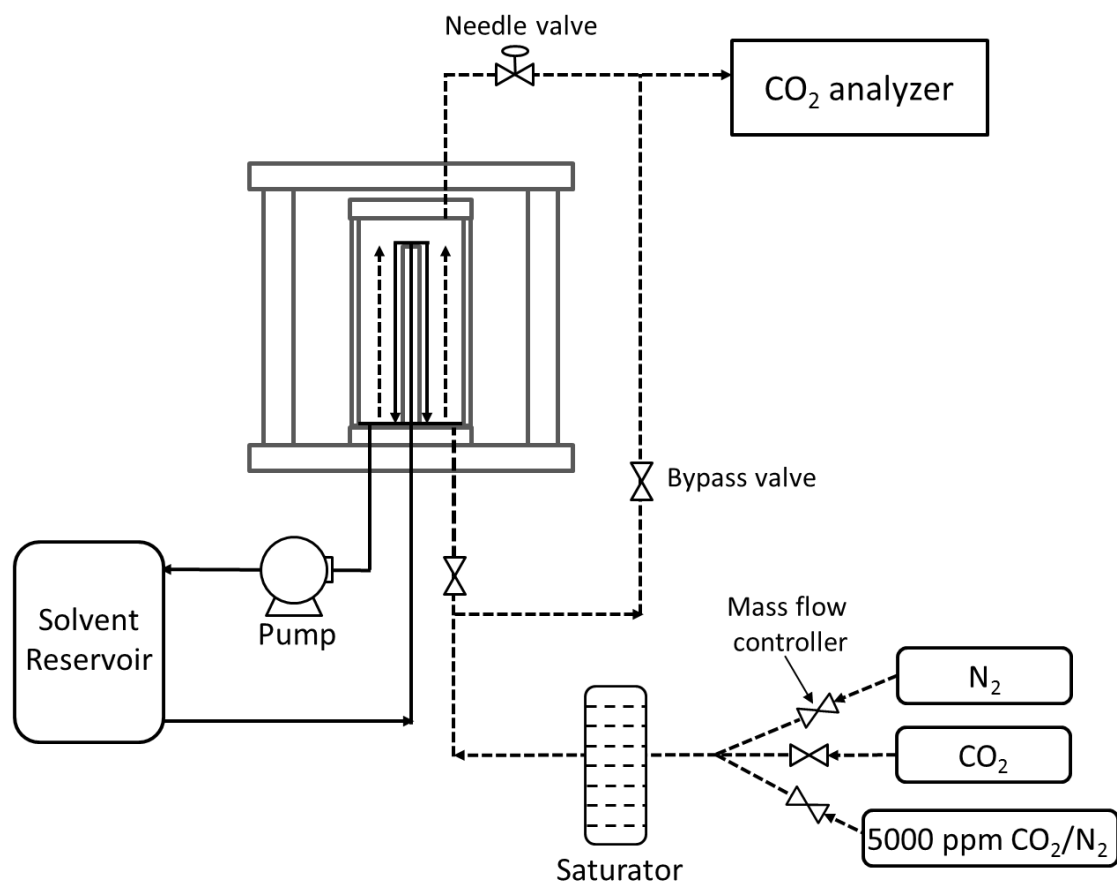


Figure 4.1: Wetted wall column system.

The amine solution circulated through the WWC at ( $Q_{\text{liquid}}$ ) approximately 4 ml/s. The total flow rate of the gas ( $Q_{\text{gas}}$ ) was 5 standard liter (STL)/min. Variable  $\text{CO}_2$  partial pressure in the gas mixture was achieved by mixing  $\text{N}_2$  with pure  $\text{CO}_2$  or diluted  $\text{CO}_2$  in  $\text{N}_2$  ( $\sim 5000$  ppm). The pressure in the chamber ( $P_{\text{tot}}$ ) was controlled using a needle valve directly downstream of the WWC chamber. In this work, the WWC was operated with  $P_{\text{tot}}$  at 20 or 40 psig. The temperature of the amine solution and gas was controlled at 40 °C using oil baths. The  $\text{CO}_2$  in the gas ( $P_{\text{CO}_2,\text{out}}$ ) exiting from top of the WWC chamber was measured continuously by an infrared  $\text{CO}_2$  analyzer (Horiba 2000). The inlet  $\text{CO}_2$  ( $P_{\text{CO}_2,\text{in}}$ ) was measured by bypassing the WWC chamber to the  $\text{CO}_2$  analyzer.

The difference in gas phase CO<sub>2</sub> before and after the WWC chamber was used to calculate the CO<sub>2</sub> flux of absorption/desorption (N<sub>CO<sub>2</sub></sub>), as described in Equation 4.1.

$$N_{CO_2} = \frac{(P_{CO_2,in} - P_{CO_2,out})}{P_{tot}} \cdot Q_{gas,sat} \cdot \frac{1}{V_M \cdot A} \quad (4.1)$$

In Equation 4.1, Q<sub>gas,sat</sub> is the total flow rate of the saturated gas; V<sub>M</sub> is the molar volume of an ideal gas; A is the total gas-liquid contact area.

Typically, four to six measurements with different P<sub>CO<sub>2</sub>,in</sub> were made for one CO<sub>2</sub> loading with half for absorption and the other half for desorption. The calculated N<sub>CO<sub>2</sub></sub> from Equation 4.1 should form a straight line when plotted against the logarithmic mean of the driving force at the top and the bottom of the column (Figure 4.2), as described by Equation 4.2 and 4.3.

$$N_{CO_2} = K_G (P_{CO_2} - P_{CO_2}^*)_{LM} \quad (4.2)$$

$$(P_{CO_2} - P_{CO_2}^*)_{LM} = \frac{(P_{CO_2,out} - P_{CO_2}^*) - (P_{CO_2,in} - P_{CO_2}^*)}{\ln\left(\frac{P_{CO_2,out} - P_{CO_2}^*}{P_{CO_2,in} - P_{CO_2}^*}\right)} \quad (4.3)$$

In Equation 4.2, P<sub>CO<sub>2</sub>\*</sub> is the equilibrium CO<sub>2</sub> partial pressure of the solution; K<sub>G</sub> is the overall gas side mass transfer coefficient. P<sub>CO<sub>2</sub>\*</sub> can be obtained by trial and error until the linear fit of these flux points passes through the origin, which means that N<sub>CO<sub>2</sub></sub> is zero when the driving force is zero with the correct P<sub>CO<sub>2</sub>\*</sub>. The slope of the linear fit is the K<sub>G</sub>. The liquid mass transfer coefficient (k<sub>g</sub>') can be calculated by subtracting the gas film resistance (1/k<sub>g</sub>) from the overall resistance (1/K<sub>G</sub>) (Equation 4.4).

$$\frac{1}{k_g'} = \frac{1}{K_G} - \frac{1}{k_g} \quad (4.4)$$

The gas film mass transfer coefficient ( $k_g$ ) was calculated using a pre-determined correlation for this wetted wall column (Bishnoi and Rochelle, 2000). The wetted wall column measurement was described in detail previously (Li, 2015).

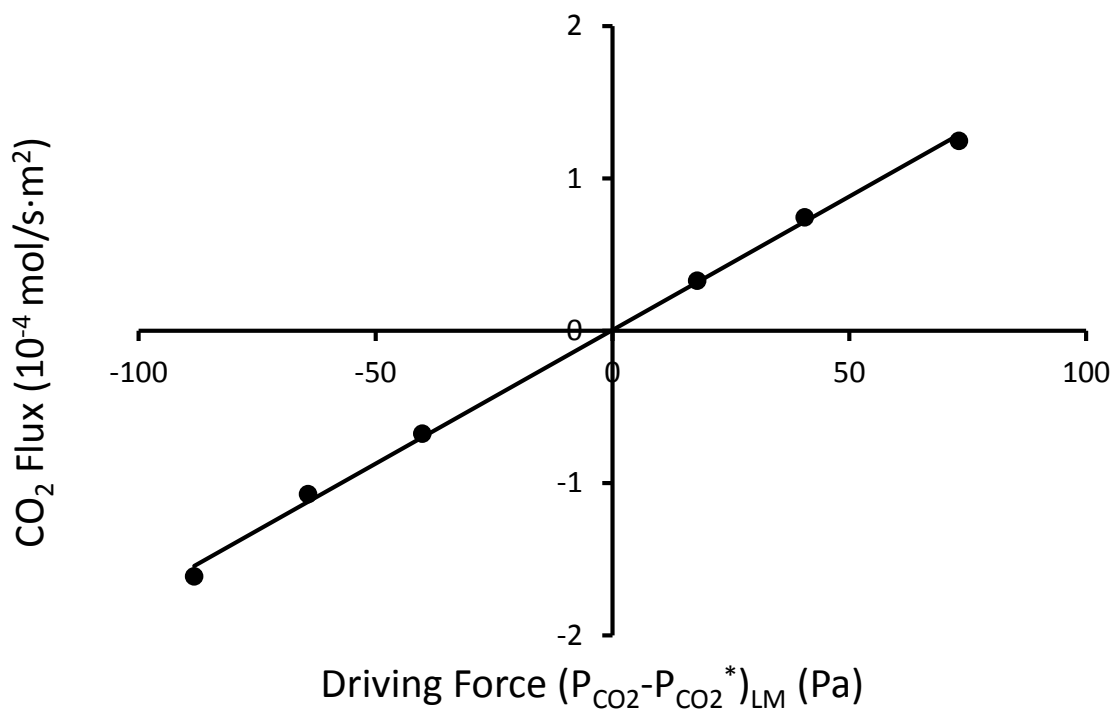


Figure 4.2: Plot of flux of CO<sub>2</sub> vs. driving force obtained from a set of measurements for 2.5 m piperazine/2.5 m 1-(2-hydroxyethyl)piperidine at 40 °C and the loading of 0.60 mol CO<sub>2</sub>/mol PZ in the WWC.

### 4.3 RESULTS AND DISCUSSION

#### 4.3.1 CO<sub>2</sub> solubility of PZ/tertiary amines

##### 4.3.1.1 Effect of $pK_a$ of tertiary amines

Figure 4.3 shows the CO<sub>2</sub> solubility of 2.5 m PZ/2.5 m tertiary amine with variable  $pK_a$  at 40 °C, compared to 2.5 m PZ. These tertiary amines have similar values of the Henry's law constant at 40 °C ( $H_{am} = 20 - 100$  Pa) (Du et al., 2016d), which

minimizes the effect of solution polarity on CO<sub>2</sub> solubility. The CO<sub>2</sub> solubility was found to be a strong function of the pK<sub>a</sub> of the tertiary amine. PZ blends with low pK<sub>a</sub> tertiary amines tend to have similar lean loading but different rich loading. In PZ/tertiary amine, the tertiary amine generally acts as a buffer and prevents PZ from protonation, resulting in increased CO<sub>2</sub> solubility. However, as CO<sub>2</sub> loaded amine normally has pH between 9 and 11 for flue gas CO<sub>2</sub> capture, a tertiary amine with low pK<sub>a</sub> (e.g., HEMor with pK<sub>a</sub>=7.01 and 2E-IMI with pK<sub>a</sub>=7.97) provides negligible buffering at lean loading where pH of the solution is much higher than the pK<sub>a</sub> of the tertiary amine.

Surprisingly, the addition of low pK<sub>a</sub> tertiary amines (e.g. HEMor and 2E-IMI) to 2.5 m PZ was found to decrease the CO<sub>2</sub> solubility at lean loading. It is probable that the tertiary amines reduced the overall polarity of the solution, resulting in increased activity coefficient of the PZ carbamate ion, which is the major form of CO<sub>2</sub> in the solution. The effect of solution polarity on CO<sub>2</sub> solubility will be discussed more in the next section.

With increased CO<sub>2</sub> loading, the pH of the solution drops, and these tertiary amines start to work as a pH buffer. The higher the pK<sub>a</sub> of the tertiary amines, the lower the CO<sub>2</sub> loading at which the buffer effect of tertiary amine starts to outweigh the salting-out effect of reduced polarity. The higher pK<sub>a</sub> of the tertiary amine also leads to a stronger buffering effect, resulting in a richer CO<sub>2</sub> loading at the same P<sub>CO<sub>2</sub></sub>.

On the other hand, PZ with high pK<sub>a</sub> tertiary amine tends to have different lean loading, but similar rich loading. A high pK<sub>a</sub> tertiary amine (e.g., tropine with pK<sub>a</sub>=10.48) would be substantially protonated at lean loading, leaving little free tertiary amine to buffer proton at normal rich loading.

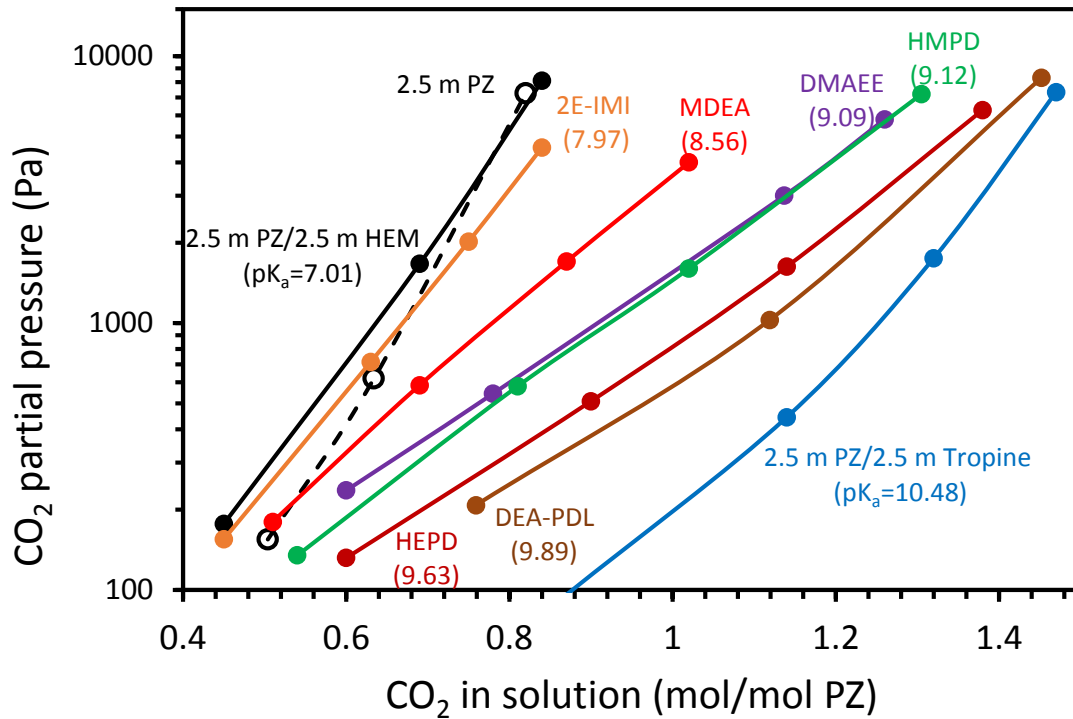


Figure 4.3: CO<sub>2</sub> solubility of 2.5 m PZ/2.5 m tertiary amine with similar volatility but variable pK<sub>a</sub> at 40 °C, compared to 2.5 m PZ (dashed line).

The CO<sub>2</sub> cyclic capacity of a solvent ( $\Delta C_{solv}$ ) is defined as the difference in CO<sub>2</sub> concentration between the lean and rich solvent (Equation 4.5).

$$\Delta C_{solv} = (\Delta \alpha_{CO_2} \cdot mol\ PZ) / kg\ (amine + H_2O)$$

$$\Delta \alpha_{CO_2} = (\alpha_{rich} - \alpha_{lean}) \quad (4.5)$$

$\alpha_{lean}$  and  $\alpha_{rich}$  are the CO<sub>2</sub> loading of lean and rich solvents (mol CO<sub>2</sub>/mol PZ).  $\Delta \alpha_{CO_2}$  is the difference of  $\alpha_{lean}$  and  $\alpha_{rich}$ . For coal-fired flue gas, the normal operating lean and rich solvents correspond to P<sub>CO<sub>2</sub>\*</sub> of 0.5 kPa and 5 kPa at 40 °C, respectively, in order to maintain enough driving force for CO<sub>2</sub> absorption throughout the absorber. The tertiary amine that is ineffective at lean loading but effective at rich loading (e.g., DMAEE and

HMPD with  $pK_a=9.12$ ) gives the flattest vapor liquid equilibrium (VLE) curve, and thus the highest  $\text{CO}_2$  cyclic capacity.

#### 4.3.1.2 Effect of solution polarity

Figure 4.4 shows the effect of solution polarity on the  $\text{CO}_2$  solubility of 2.5 m PZ at 40 °C. NMP with  $H_{am}$  of 92 Pa at 40 °C (Yuan et al., 2016) is expected to have a comparable polarity to those tertiary amines shown in Figure 4.3, which is much lower than water. The addition of 2.5 m NMP salted out  $\text{CO}_2$  from 2.5 m PZ significantly in the normal loading range. On the other hand, the addition of 2.5 m NaCl to 2.5 m PZ salted in  $\text{CO}_2$ , especially at lean loading, which resulted from the increased polarity of the solution.

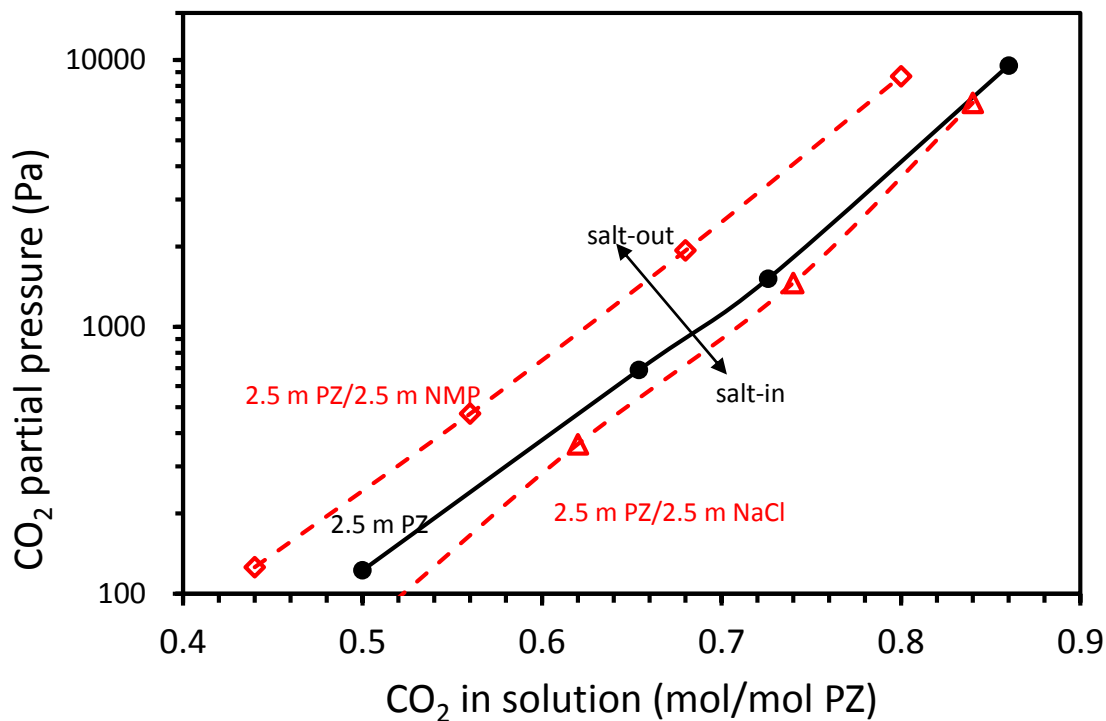


Figure 4.4: Effect of solution polarity on the  $\text{CO}_2$  solubility of 2.5 m PZ/2.5 m tertiary amine at 40 °C.

### 4.3.2 Generic Aspen Plus® model

Solvent screening for CO<sub>2</sub> capacity is time and effort consuming. It is desirable to have a generic model that can predict the CO<sub>2</sub> capacity with limited data on the solvent. In this work, a generic Aspen Plus® model for PZ/tertiary amine was developed based on the rigorous Aspen Plus® model for PZ/MDEA developed by Frailie (2014) using the electrolyte-Nonrandom Two-Liquid (e-NRTL) activity coefficient model. This generic model assumes that CO<sub>2</sub> solubility of PZ/tertiary amine is mainly a function of the pK<sub>a</sub> of the tertiary amine, and all tertiary amine related parameters for activity coefficient are the same as the corresponding MDEA related parameters.

Figure 4.5 shows the predicted lean and rich loading for all PZ/mono-tertiary amines tested in this work, compared to measured values. This generic model predicts both lean and rich loading well, which validates the assumption that CO<sub>2</sub> solubility of PZ/tertiary amine is mainly a function of the pK<sub>a</sub> of the tertiary amine. The small discrepancy between model prediction and measured values are mainly from two sources: 1) the error of pK<sub>a</sub> measurement (an error of ±0.1 is expected for pK<sub>a</sub> values from literature); 2) different polarity of these tertiary amines (the tertiary amines measured in this work have H<sub>am</sub> from 10 to 1300 Pa at 40 °C (Du et al., 2016d)).

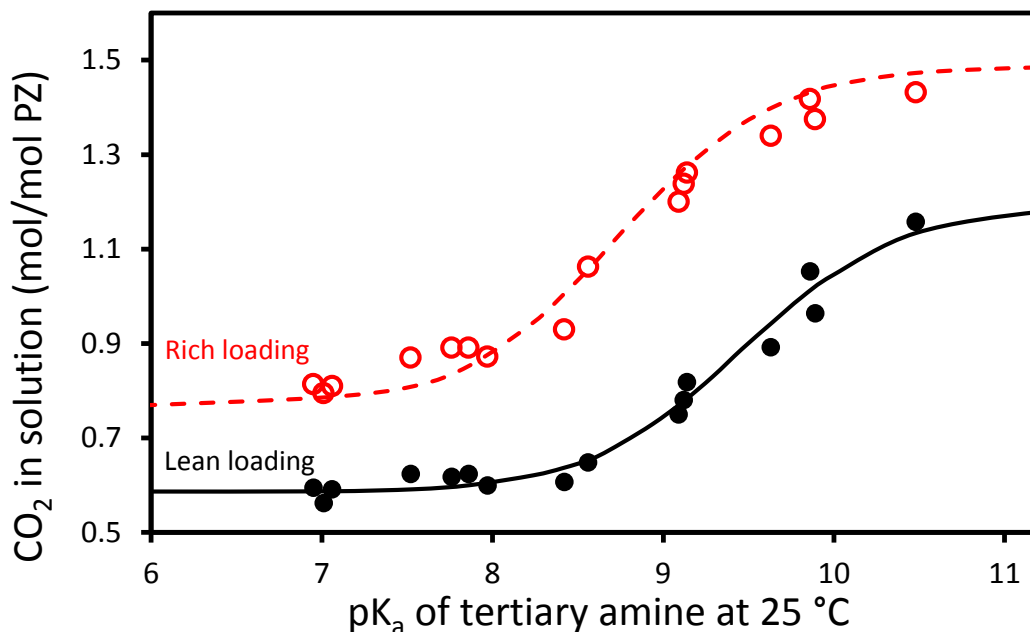


Figure 4.5: Lean ( $P_{\text{CO}_2}=0.5$  kPa at 40 °C) and rich loading ( $P_{\text{CO}_2}=5$  kPa at 40 °C) of 2.5 m PZ/2.5 m tertiary amine as a function of the  $pK_a$  of tertiary amine at 25 °C; solid points: measured lean loadings; open points: measured rich loadings; lines: generic Aspen Plus® model prediction.

Figure 4.6 shows the predicted  $\Delta\alpha_{\text{CO}_2}$  for all 2.5 m PZ/2.5 m tertiary amines tested in this work, compared to measured values. This generic model predicts the  $\Delta\alpha_{\text{CO}_2}$  of 2.5 m PZ/2.5 m mono-tertiary amines reasonably well. The optimum  $pK_a$  of a mono-tertiary amine blended with PZ is around 9.1 to give the greatest  $\Delta\alpha_{\text{CO}_2}$ . Two 2.5 m PZ/2.5 m di-tertiary amines were also tested. TEDA acts like a mono-tertiary amine, as the second  $pK_a$  of TEDA (2.24) is too low to have buffering effect. However, as the two N on BDMAEE are apart from each other, both of them can effectively buffer the solution, resulting in significant larger  $\Delta\alpha_{\text{CO}_2}$  than PZ/mono-tertiary amines.

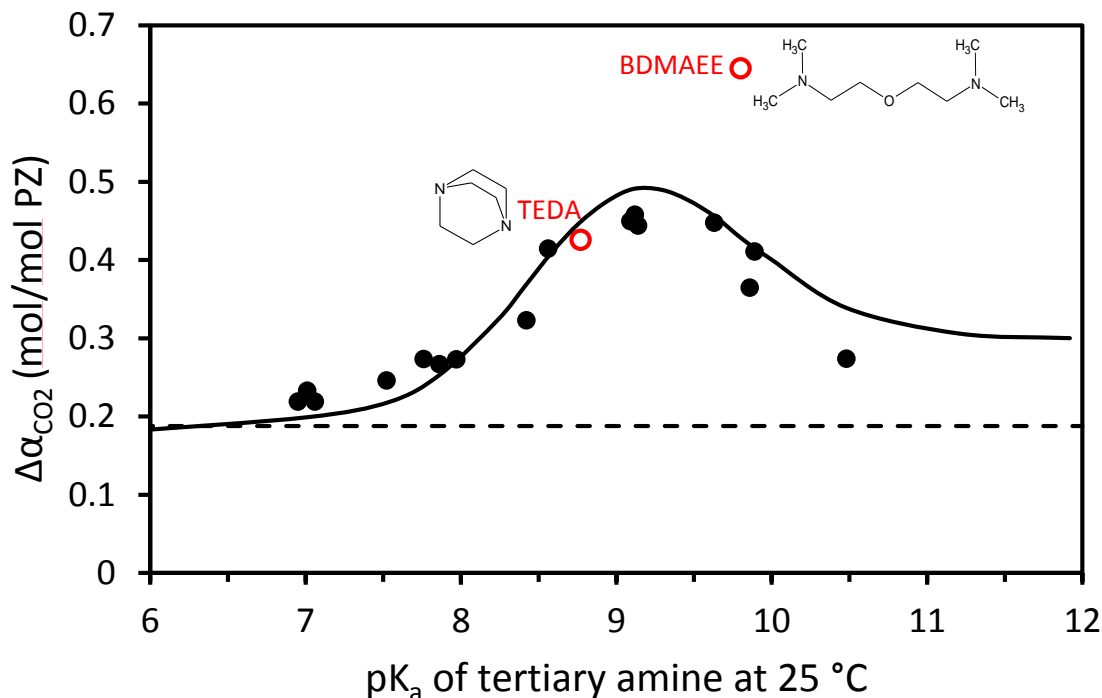


Figure 4.6:  $\Delta\alpha_{CO_2}$  of 2.5 m PZ/2.5 m tertiary amines as a function of the  $pK_a$  of tertiary amines at 25 °C; solid points: measured 2.5 m PZ/2.5 m mono-tertiary amines; open points: measured 2.5 m PZ/2.5 m di-tertiary amines; dashed line:  $\Delta\alpha_{CO_2}$  of 2.5 m PZ; solid line: generic Aspen Plus<sup>®</sup> model prediction.

#### 4.3.3 Comparison between PZ/tertiary amine and PZ/hindered amine

Figure 4.7 shows the measured lean and rich loading for four 2.5 m PZ/2.5 m hindered amines tested in this work, compared to the generic model prediction for PZ/tertiary amine. All four PZ/hindered amines show a higher lean loading than model prediction. As AEPD, AMP, and 2-PE have similar amine volatility to most of the tertiary amines tested in this work, indicating similar polarity of these amines, the shift of lean loading is probably due to the small amount of carbamate formed by these hindered amines. The larger lean loading shift for PZ/2-PE was due to the higher carbamate stability of 2-PE than AMP (Sherman et al., 2016). The shift of both lean and rich

loading for PZ/Tris may also result from the extremely high hydrogen bonding ability and low  $pK_a$  of Tris, which make it salt in PZ carbamate in the whole loading range.

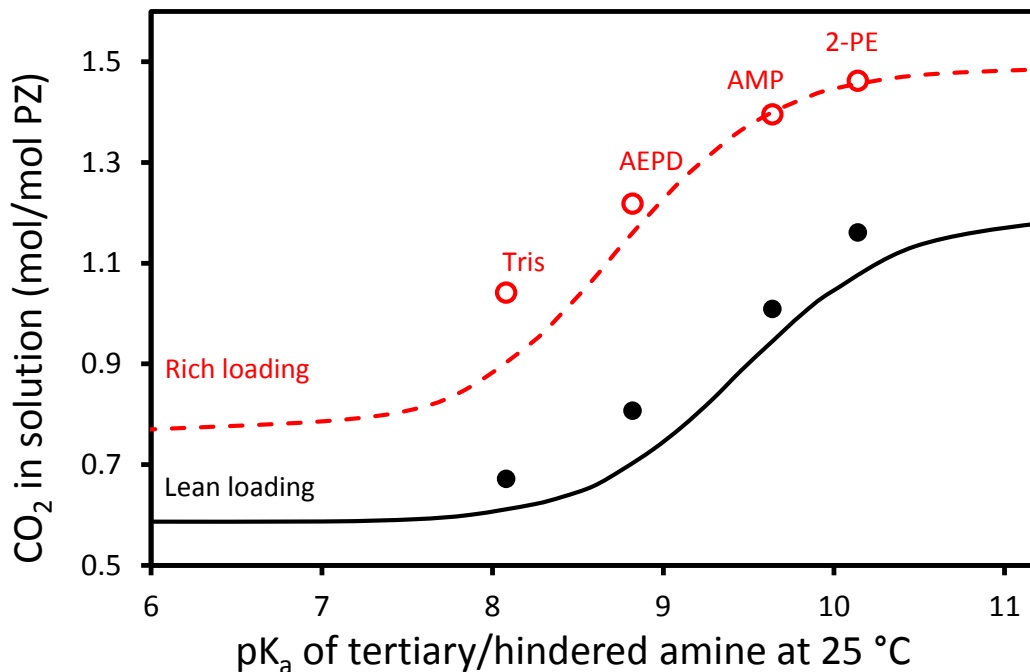


Figure 4.7: Lean ( $P_{CO_2}=0.5$  kPa at 40 °C) and rich loading ( $P_{CO_2}=5$  kPa at 40 °C) of 2.5 m PZ/2.5 m tertiary amines as a function of the  $pK_a$  of tertiary amines at 25 °C; solid points: measured lean loadings; open points: measured rich loadings; lines: generic Aspen Plus® model prediction.

#### 4.3.4 CO<sub>2</sub> absorption rate of PZ/tertiary amines

The average CO<sub>2</sub> absorption rate ( $k_g'_{avg}$ ) in ten novel 2.5 m PZ/2.5 m tertiary amines at 40 °C is compared to 7 m MEA, 2.5 m PZ, and 2.5 m PZ/2.5 m MDEA in Figure 4.8. For each solvent,  $k_g'_{avg}$  is calculated for an isothermal absorber at 40 °C for coal flue gas and 90% CO<sub>2</sub> removal (Equation 4.6), assuming a linear concentration

profile and equilibrium curve in the absorber, and negligible gas film resistance (L. Li et al., 2013b).

$$k'_g \text{ avg} = \frac{Flux_{CO_2,LM}}{(P_{CO_2} - P_{CO_2}^*)_{LM}} = \frac{(Flux_{CO_2,top} - Flux_{CO_2,bottom}) / \ln(Flux_{CO_2,top} / Flux_{CO_2,bottom})}{(P_{CO_2,top} - P_{CO_2,lean}^*) - (P_{CO_2,bottom} - P_{CO_2,rich}^*) / \ln\left(\frac{P_{CO_2,top} - P_{CO_2,lean}^*}{P_{CO_2,bottom} - P_{CO_2,rich}^*}\right)} \quad (4.6)$$

The  $P_{CO_2}$  at the bottom and top of the absorber are 12 and 1.2 kPa; the rich and lean  $P_{CO_2}^*$  are 5 and 0.5 kPa. Experimental values at 40 °C are used to interpolate  $k'_g$  that corresponds to  $P_{CO_2}^*$  at 5 and 0.5 kPa, which are then used to calculate the corresponding flux.  $CO_2$  absorption by aqueous amine solutions is controlled by diffusion with fast reaction in the liquid boundary layer (Rochelle et al., 2011). At most practical absorber conditions, the pseudo first order (PFO) approximation can be applied to the kinetics of  $CO_2$  and amine reaction, which assumes the free amine concentration is constant through the reaction boundary layer and equal to the liquid bulk (Li, 2015). With this approximation,  $k'_g$  depends on the reaction rate constant ( $k_2$ ), free amine concentration in the bulk solution ( $[Amine]_b$ ), diffusivity of  $CO_2$  ( $D_{CO_2}$ ), and Henry's law constant of  $CO_2$  ( $H_{CO_2}$ ) (Li, 2015), as described in Equation 4.7.

$$k'_g \approx \frac{\sqrt{D_{CO_2} k_2 [Amine]_b}}{H_{CO_2}} \quad (4.7)$$

The addition of 2.5 m tertiary amines to 2.5 m PZ, expect for IMI, caused a marked decrease of  $k'_g \text{ avg}$ . The decrease of  $k'_g \text{ avg}$  mainly results from the increase of viscosity, which reduces  $D_{CO_2}$  (Table 4.2). The viscosity of 2.5 m PZ/2.5 m IMI is only 10% higher than 2.5 m PZ, while the viscosity of other 2.5 m PZ/2.5 m tertiary amine is two to three times higher than 2.5 m PZ. The high  $k'_g$  of PZ/IMI may also result from its high physical solubility of  $CO_2$  (low  $H_{CO_2}$ ) (Yuan et al., 2016). The low  $k'_g$  of

PZ/DEA-PDL and PZ/Tropine, compared to other PZ/tertiary amines, resulted from their high  $pK_a$  (Table 4.2). The addition of high  $pK_a$  tertiary amines shifts the operating loading range to the richer side, resulting in both higher viscosity and less free PZ for  $CO_2$  absorption. 2.5 m PZ/2.5 m BDMAEE showed a relatively high  $k_g'$  in spite of its high  $pK_a$  and viscosity. This is because that BDMAEE has two effective amino groups to bind proton, resulting in more free PZ for  $CO_2$  absorption.

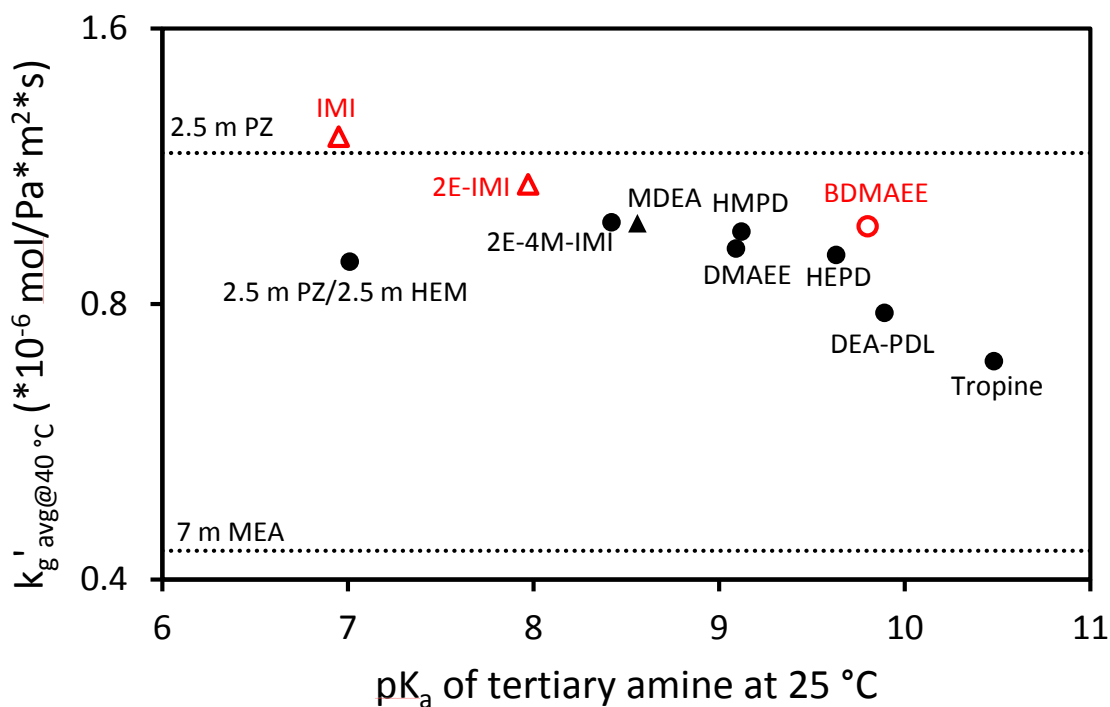


Figure 4.8:  $k_g'$  of 2.5 m PZ/2.5 m tertiary amines at 40 °C as a function of the  $pK_a$  of tertiary amines at 25 °C; solid points: 2.5 m PZ/2.5 m mono-tertiary amines; open point: 2.5 m PZ/2.5 m di-tertiary amine (BDMAEE); dotted lines:  $k_g'$  of 7 m MEA and 2.5 m PZ.

### 4.3.5 Proposed PZ/tertiary amines for CO<sub>2</sub> capture from flue gas

Table 4.2 shows the viscosity ( $\mu$ ), CO<sub>2</sub> cyclic capacity ( $\Delta C_{\text{solv}}$ ), and average absorption rate ( $k_g'_{\text{avg}}$ ) for ten novel 2.5 m PZ/2.5 tertiary amines, along with their other important properties. Data for 7 m MEA, 2.5 m PZ, 5 m PZ, and 2.5 m PZ/2.5 m MDEA are shown for comparison.  $\Delta C_{\mu}$  is the normalized CO<sub>2</sub> cyclic capacity, as defined in Equation 4.8.

$$\Delta C_{\mu} = \Delta C_{\text{solv}} / (\mu_{\text{mid}} / \mu_{5 \text{ m PZ}})^{0.175} \quad (4.8)$$

$\Delta C_{\text{solv}}$  is normalized by the viscosity of the solvent to consider the effect of viscosity on the optimized heat exchanger cost (L. Li et al., 2013b), based on the observation that the heat transfer coefficient generally depends on solvent viscosity to about -0.35 power (Ayub, 2003).  $\mu_{\text{mid}}$  and  $\mu_{5 \text{ m PZ}}$  are the viscosities of the studied amine and 5 m PZ, respectively, at mid-loading ( $P_{\text{CO}_2^*} = 2.0$  kPa) and 40 °C.  $T_{\text{max}}$  is defined as the temperature at which a solvent will degrade at the same rate as 7 m MEA at 121 °C.  $P_{\text{am}}$  is the partial pressure of the tertiary amine blended with PZ at lean loading ( $P_{\text{CO}_2^*} = 0.5$  kPa) and 40 °C.

Table 4.2: Properties of 2.5 m PZ/2.5 m tertiary amines, compared to 7 m MEA, 2.5 m PZ, 5 m PZ, and 2.5 m PZ/2.5 m MDEA.

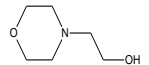
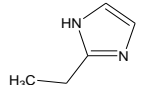
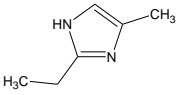
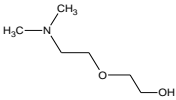
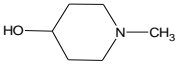
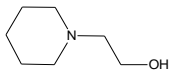
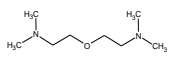
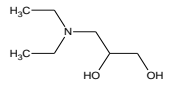
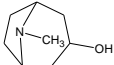
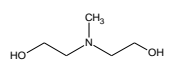
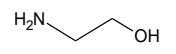
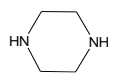
Amine (blended with PZ)	Structure	pK <sub>a</sub> <sup>a</sup>	T <sub>max</sub> (°C) <sup>b</sup>	P <sub>Am</sub> (Pa) <sup>c</sup>	$\mu_{\text{mid}}$ (cP) <sup>d</sup>	$\Delta C_{\text{solv}}$ (mol/kg)	$\Delta C_{\mu}$ (mol/kg)	$k_g'_{\text{avg-40 °C}}$ (10 <sup>-6</sup> mol/Pa*s)
IMI		6.95 <sup>1</sup>	124	0.5	1.9	0.41	0.47	1.22
HEMor		7.01 <sup>2</sup>	151	2.2	3.4	0.39	0.40	0.89
2E-IMI		7.97 <sup>3</sup>	157	1.2	3.1	0.47	0.49	1.08

Table 4.2: Properties of 2.5 m PZ/2.5 m tertiary amines, compared to 7 m MEA, 2.5 m PZ, 5 m PZ, and 2.5 m PZ/2.5 m MDEA (continued).

Amine (blended with PZ)	Structure	pK <sub>a</sub> <sup>a</sup>	T <sub>max</sub> (°C) <sup>b</sup>	P <sub>Am</sub> (Pa) <sup>c</sup>	μ <sub>mid</sub> (cP) <sup>d</sup>	ΔC <sub>solv</sub> (mol/kg)	ΔC <sub>μ</sub> (mol/kg)	kg' avg-40 °C (10 <sup>-6</sup> mol/Pa*m <sup>2</sup> *s)
2E-4M-IMI		8.42 <sup>3</sup>	158	2.6	3.4	0.57	0.59	0.98
DMAEE		9.09 <sup>4</sup>	129	2.5	4.2	0.76	0.76	0.92
HMPD		9.12 <sup>5</sup>	141	2.8	4.2	0.77	0.77	0.96
HEPD		9.63 <sup>2</sup>	146	32	4.3	0.73	0.72	0.91
BDMAEE		9.80/ 8.21 <sup>6</sup>	110	28	6.4	0.99	0.92	0.97
DEA-PDL		9.89 <sup>7</sup>	133	—	5.3	0.58	0.55	0.78
Tropine		10.48 <sup>2</sup>	150	0.9	5.3	0.45	0.44	0.69
2.5 m PZ/2.5 m MDEA		8.56 <sup>8</sup>	116	0.7	3.7	0.68	0.71	0.98
7 m MEA		9.44 <sup>9</sup>	122	3.1 <sup>10</sup>	2.7 <sup>12</sup>	0.35 <sup>12</sup>	0.38	0.43 <sup>12</sup>
2.5 m PZ		9.71 <sup>9</sup>	164	0.3 <sup>11</sup>	1.7	0.39	0.46	1.17
5 m PZ				0.5 <sup>11</sup>	4.2 <sup>12</sup>	0.57 <sup>12</sup>	0.57	1.13 <sup>12</sup>

a: Thermodynamic values at 25 °C and zero ionic strength; 1: (Nozaki et al., 1957); 2: (Xu et al., 1993); 3: calculated by means of computer program ACD/pK<sub>a</sub> DB (Advanced Chemistry Development Inc.-Canada); 4: (Simond et al., 2012); 5: (Arlinda Fejzo Ciftja, 2015); 6: (Fakstorp et al., 1958); 7: (Chowdhury et al., 2013); 8: (Hamborg et al., 2007); 9: (Hamborg and Versteeg, 2009);

b: T<sub>max</sub> is the maximum stripper operating temperature for the solvent, which is defined as the temperature at which a solvent will degrade at the same rate as 7 m MEA at 121 °C; values are from Du et al. (2016a);

c: P<sub>Am</sub> is the partial pressure of the tertiary amine blended with PZ at lean loading (P<sub>CO<sub>2</sub>\*</sub> = 0.5 kPa) and 40 °C; 10: (Nguyen et al., 2010); 11: estimated from the P<sub>Am</sub> of 8 m PZ (Nguyen et al., 2010);

d: Viscosity of the solvent at mid-loading (P<sub>CO<sub>2</sub>\*</sub> = 2.0 kPa) and 40 °C; 12: (Dugas, 2009)

Among these ten novel 2.5 m PZ/2.5 m tertiary amines, 2.5 m PZ/2.5 m IMI, 2.5 m PZ/2.5 m HEMor, 2.5 m PZ/2.5 m Tropine, 2.5 m PZ/2.5 m 2E-IMI, and 2.5 m PZ/2.5

m DEA-PDL show lower  $\Delta C_{\mu}$  than 5 m PZ, due to their suboptimal  $pK_a$ . Although PZ/HEPD and PZ/BDMAEE show great  $\Delta C_{\mu}$  and  $k_g'$ , their high volatility would impede their application in low pressure CO<sub>2</sub> capture. PZ/HEPD and PZ/BDMAEE can be considered for high pressure CO<sub>2</sub> capture applications, such as the purification of liquefied natural gas (LNG). 2.5 m PZ/2.5 m DMAEE has low amine volatility, great  $\Delta C_{\mu}$  and  $k_g'$ , but relatively low  $T_{max}$ . PZ/DMAEE may be considered as an alternative to PZ/MDEA for CO<sub>2</sub> capture when the solvent regeneration temperature is below 130 °C. 2.5 m PZ/2.5 m 2E-4M-IMI and 2.5 m PZ/2.5 m HMPD show good overall performance: high thermal stability, low amine volatility, and great CO<sub>2</sub> capacity and rate. As 2.5 m PZ/2.5 m HMPD has 30% higher  $\Delta C_{\mu}$ , but similar  $k_g'_{avg}$  to 2.5 m PZ/2.5 m 2E-4M-IMI, it will be evaluated further in the next two chapters.

#### 4.4 CONCLUSIONS

The optimum  $pK_a$  of the 2.5 m tertiary amine with 2.5 m PZ was found to be around 9.1 to give the greatest CO<sub>2</sub> cyclic capacity.

A generic Aspen Plus model for PZ/tertiary amine was developed based on a rigorous Aspen Plus<sup>®</sup> model for PZ/MDEA with electrolyte-Nonrandom Two-Liquid (e-NRTL) as the thermodynamic framework. This generic model can reasonably predict the CO<sub>2</sub> vapor-liquid-equilibrium (VLE) in PZ/tertiary amine based on the  $pK_a$  of the tertiary amine.

To a lesser degree than  $pK_a$ , the polarity of the tertiary amine also affects the CO<sub>2</sub> solubility of the PZ/tertiary amine.

Hindered amines that form little carbamate mainly act as pH buffers in PZ/hindered amine, giving similar CO<sub>2</sub> VLE to PZ/tertiary amine with the same  $pK_a$  and similar polarity.

CO<sub>2</sub> absorption rate of most 2.5 m PZ/2.5 m tertiary amine was found to be slightly slower than 2.5 m PZ itself, probably due to the higher viscosity of the blend. 2.5 m PZ/2.5 m tertiary amine still absorb CO<sub>2</sub> much faster than 7 m MEA.

2.5 m PZ/2.5 m HMPD shows the best overall performance for flue gas CO<sub>2</sub> capture, high thermal stability, low amine volatility, large  $\Delta C_{\mu}$ , and high  $k_g'_{avg}$ .

#### **4.5 ACKNOWLEDGEMENTS**

The author gratefully acknowledges Ye Yuan for measuring the CO<sub>2</sub> capacity and absorption rate of PZ/MDEA, PZ/HMPD, PZ/2E-4M-IMI, and PZ/DMAEE using WWC.

The author gratefully acknowledges Arlinda Fejzo Ciftja for measuring the pK<sub>a</sub> of HMPD.

## **Chapter 5: Thermal Degradation of Piperazine/4-Hydroxy-1-methylpiperidine**

The thermal degradation of aqueous piperazine (PZ)/4-hydroxy-1-methylpiperidine (HMPD) for CO<sub>2</sub> capture was rigorously evaluated and compared to PZ/N-methyldiethanolamine (MDEA). The degradation mechanism for PZ/HMPD was investigated by performing measurements under various conditions, and identifying degradation products. Over 81% of the nitrogen lost in degraded PZ/HMPD was recovered in seven quantified degradation products, with 1-methyl-piperazine (1MPZ) and 4-hydroxy-piperidine (HPD) accounting for 54% of the nitrogen lost. The “arm switching” reaction between PZ and HMPD is the major degradation pathway. A second-order rate model consistent with proposed degradation pathways can model initial degradation reasonably well. The concentration-based second-order rate constant,  $k_{2,f,c}$ , depends on the total amine concentration and, to a lesser extent, the PZ to HMPD ratio. CO<sub>2</sub> loading and temperature accelerate the degradation of PZ/HMPD. The significantly greater stability of PZ/HMPD compared to PZ/MDEA is due to the remarkable thermal stability of HPD which prevents PZ from further degradation, the smaller initial degradation rate of PZ/HMPD, and the greater thermal stability of HMPD compared to MDEA. The potential environmental issues caused by the volatility of one minor degradation product, 1,4-dimethyl-piperazine (1,4 DMPZ), need to be addressed for commercial application of this solvent.

### **5.1 INTRODUCTION**

CO<sub>2</sub> capture from flue gas is a critical technology in the tool box to mitigate global warming. Amine scrubbing is the most applicable technology for this application (Rochelle, 2009). However, the low CO<sub>2</sub> partial pressure and high flow rate of flue gas

result in high capital and energy costs for CO<sub>2</sub> capture using amine scrubbing (Catalanotti et al., 2014; Clark and Herzog, 2014; Finkenrath, 2012). Using novel amines with large CO<sub>2</sub> cyclic capacity, fast absorption rate, and high thermal stability is a critical approach to reduce the cost (Rochelle et al., 2011). High capacity solvents result in lower solvent regeneration cost, while solvents with faster absorption rate reduce the packing cost for the CO<sub>2</sub> absorber. The benefit of operating at high temperature for thermal swing regeneration was identified by Rochelle et al. (2011), but the regeneration temperature is limited by thermal stability of the solvent.

8 molal (m) piperazine (PZ) (40 wt % PZ) is one of the most effective solvents for flue gas CO<sub>2</sub> capture, with double the CO<sub>2</sub> absorption rate and capacity, and much better thermal stability than the benchmark solvent, 30 wt % monoethanolamine (MEA) (Rochelle et al., 2011). However, PZ and its zwitterionic carbamate have limited water solubility so solid precipitation may occur (Freeman et al., 2010b; Ma et al., 2012). The precipitation risk may limit the application of concentrated PZ for CO<sub>2</sub> capture. Blending a tertiary amine with less concentrated PZ is a way to mitigate the solid precipitation issue of PZ, while maintaining the good CO<sub>2</sub> capture performance of concentrated PZ. PZ/N-methyldiethanolamine (MDEA) has been proposed as a promising solvent with CO<sub>2</sub> capacity and absorption rate comparable to concentrated PZ (Chen et al., 2011). However, PZ/MDEA was found to be significantly less thermally stable than PZ alone, due to the interaction between PZ and MDEA (Closmann et al., 2009; Closmann, 2011; Namjoshi, 2015). Du et al. (2016b, 2016c) recently identified PZ/4-hydroxy-1-methylpiperidine (HMPD) as a superior solvent, showing not only better CO<sub>2</sub> absorption performance than PZ/MDEA, but also significantly greater thermal stability.

The objective of this work is to rigorously evaluate the thermal degradation of PZ/HMPD. The thermal degradation mechanism for PZ/HMPD has been investigated by performing degradation measurements under various conditions, and identifying degradation products. The reasons for the greater thermal stability of PZ/HMPD compared to PZ/MDEA have been explored. The potential environmental issues of degradation products from PZ/HMPD have also been evaluated.

## **5.2 EXPERIMENT METHODS**

### **5.2.1 Solution preparation**

Aqueous PZ/HMPD solutions were prepared by melting anhydrous PZ (99%, Sigma Aldrich, USA) in mixtures of distilled de-ionized water and HMPD (98%, Acros Organics). CO<sub>2</sub> loaded solutions were prepared by gravimetrically sparging CO<sub>2</sub> (99.5%, Matheson Tri Gas, Basking Ridge, NJ) in unloaded amine solutions in a gas-washing bottle. The concentration of CO<sub>2</sub> was checked by total inorganic carbon (TIC) analysis, described in detail previously.(Freeman et al., 2010a) Acid loaded solutions were prepared by adding 10 N sulfuric acid to unloaded aqueous amine solutions.

### **5.2.2 Experimental Approach**

Thermal degradation of PZ/HMPD under various conditions was measured in 3/8-inch 316 stainless steel Swagelok<sup>®</sup> cylinders with a volume of 4.5 ml and diameter of 0.95 cm. Cylinders were filled with 4 mL of amine solution with 0.5 mL of headspace, sealed with two Swagelok<sup>®</sup> end caps, and placed in forced convection ovens maintained at the target temperature. Individual cylinders were removed from the ovens at each sampling time and then analyzed for the parent amines and degradation products present in solution. The details of the experimental apparatus and procedure were described in detail previously (Namjoshi, 2015).

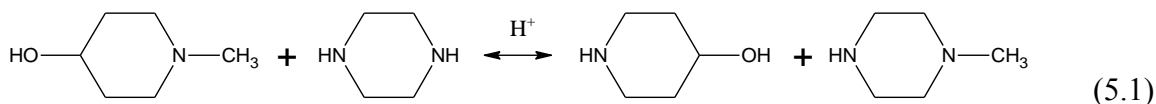
### 5.2.3 Analytical Tools - Cation Chromatography

A Dionex ICS-2100 cation ion chromatograph (Dionex Corporation) was used to quantify parent amines and determine the presence of other amine byproducts. A 4 × 50 mm CG17 guard column and a 4 × 250 mm CS17 analytical column were connected in series and used to carry out the separation. The eluent contained varying concentrations of methanesulfonic acid (MSA) in analytical grade water. Ion suppression was used to improve the signal/noise ratio. Standard curves of parent amines and degradation products were prepared to quantify the amount of amine present. Samples were diluted by a factor of 10000 (mass) in analytical grade water. Degradation products were identified by matching their retention-time with standard samples. Due to the lack of a commercial source for 1-methyl-4-ethyl-piperazine (1M-4EPZ), 1-methyl-piperazine (1MPZ) was reacted with 1-ethyl-piperazine (1EPZ) to identify the retention-time of 1M-4EPZ. The standard curve of 1,4-dimethyl-piperazine (1,4 DMPZ) was used for the quantification of 1M-4EPZ, based on their similar structures.(Namjoshi, 2015) The details of the analytical methods were described in detail previously (Namjoshi, 2015).

## 5.3 RESULTS AND DISCUSSION

### 5.3.1 Degradation Mechanism and Products

Thermal degradation of PZ/HMPD was investigated at 150 to 175 °C, with the intention to accelerate degradation. Figure 5.1 shows the degradation of 2 m PZ/3 m HMPD with 0.26 mol CO<sub>2</sub>/mole alkalinity at 175 °C, along with the formation of its major degradation products, 1-methyl-piperazine (1MPZ) and 4-hydroxy-piperidine (HPD). PZ and HMPD initially appear to reach equilibrium with 1MPZ and HPD (Equation 5.1).



This mechanism is supported by prior work by Namjoshi at high temperature where PZ, as a strong nucleophile, reacted with a protonated tertiary amine, forming a substituted PZ and a secondary amine (Namjoshi, 2015). This  $\text{S}_{\text{N}}2$  substitution reaction is commonly referred to as “arm switching” (Bedell et al., 2010; Freeman, 2011). Based on the initial degradation pathway shown in Equation 5.1, a second-order rate model was used to fit the degradation for PZ/HMPD (Equation 5.2).

$$-\frac{dC_{\text{PZ}}}{dt} = -\frac{dC_{\text{HMPD}}}{dt} = \frac{dC_{\text{HPD}}}{dt} = \frac{dC_{\text{1MPZ}}}{dt} = k_{2,f,c} * C_{\text{PZ}} * C_{\text{HMPD}} - k_{2,r,c} * C_{\text{1MPZ}} * C_{\text{HPD}} \quad (5.2)$$

where  $C_{\text{PZ}}$ ,  $C_{\text{HMPD}}$ ,  $C_{\text{1MPZ}}$ , and  $C_{\text{HPD}}$  are the concentration of amines;  $k_{2,f,c}$  and  $k_{2,r,c}$  are concentration-based second-order forward and reverse rate constants, respectively;  $t$  is the experimental time in seconds. When the initial concentration of 1MPZ and HPD is 0, or very small compared to parent amines, the reverse rate can be neglected for the initial degradation (Equation 5.3).

$$-\frac{dC_{\text{PZ}}}{dt} = -\frac{dC_{\text{HMPD}}}{dt} = \frac{dC_{\text{HPD}}}{dt} = \frac{dC_{\text{1MPZ}}}{dt} = k_{2,f,c} * C_{\text{PZ}} * C_{\text{HMPD}} \quad (5.3)$$

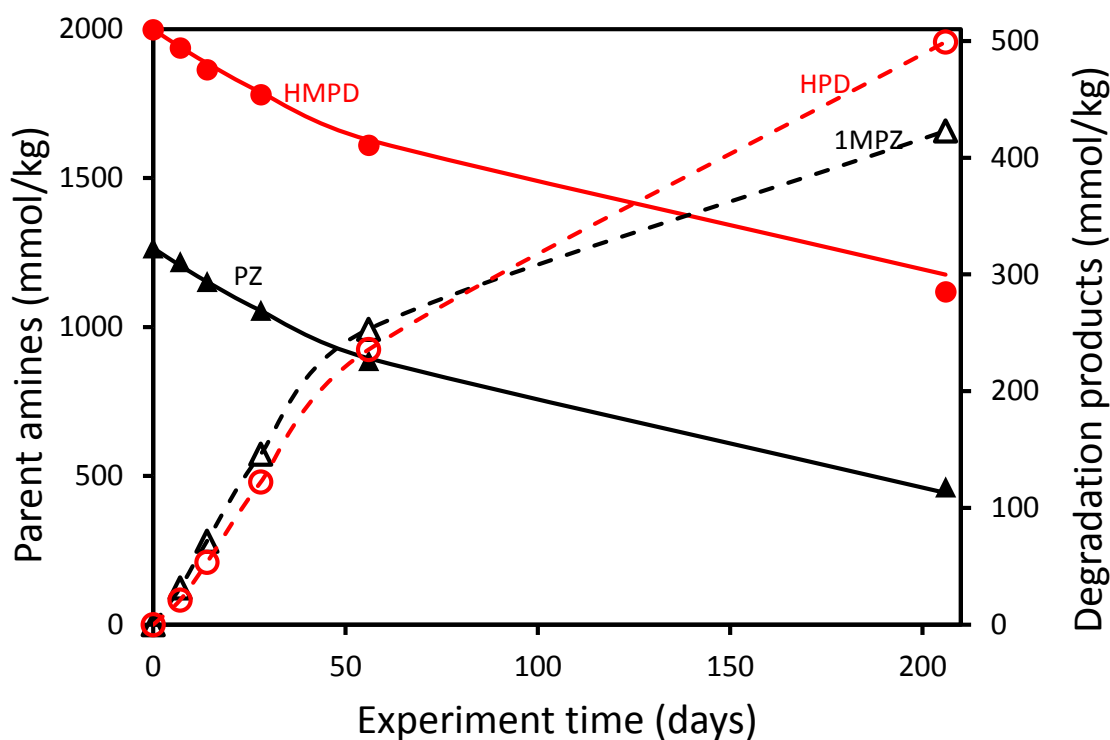
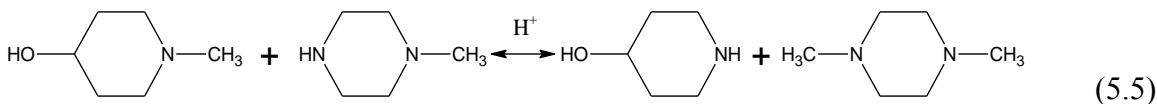
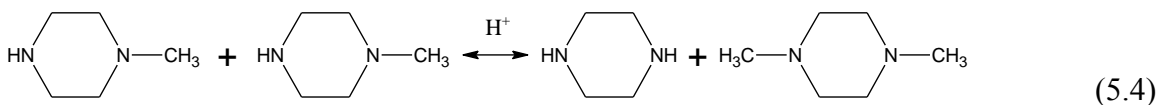


Figure 5.1: Degradation of 2 m PZ/3 m HMPD with 0.26 mol CO<sub>2</sub>/mole alkalinity at 150 °C, along with the formation of the major degradation products. Solid lines indicate second-order rate models fit the data (Equation 5.3).

With the formation of 1MPZ, other “arm switching” reactions may occur to produce 1,4-dimethyl-piperazine (1,4 DMPZ) (Freeman, 2011).



Besides 1,4 DMPZ, another four minor products appeared in degraded PZ/HMPD (Figure 5.2). NH<sub>4</sub><sup>+</sup> and 1-ethyl-piperazine (1EPZ) are common thermal degradation products for PZ, although the pathway for the production of 1EPZ is not clear (Freeman and Rochelle,

2012b). 1-Methyl-4-ethyl-piperazine (1M-4EPZ) can be produced by the reactions between 1MPZ and 1EPZ (Equation 5.6), and between HMPD and 1EPZ (Equation 5.7). Another minor product is suspected to be MEA based on its retention-time on the cation chromatograph.

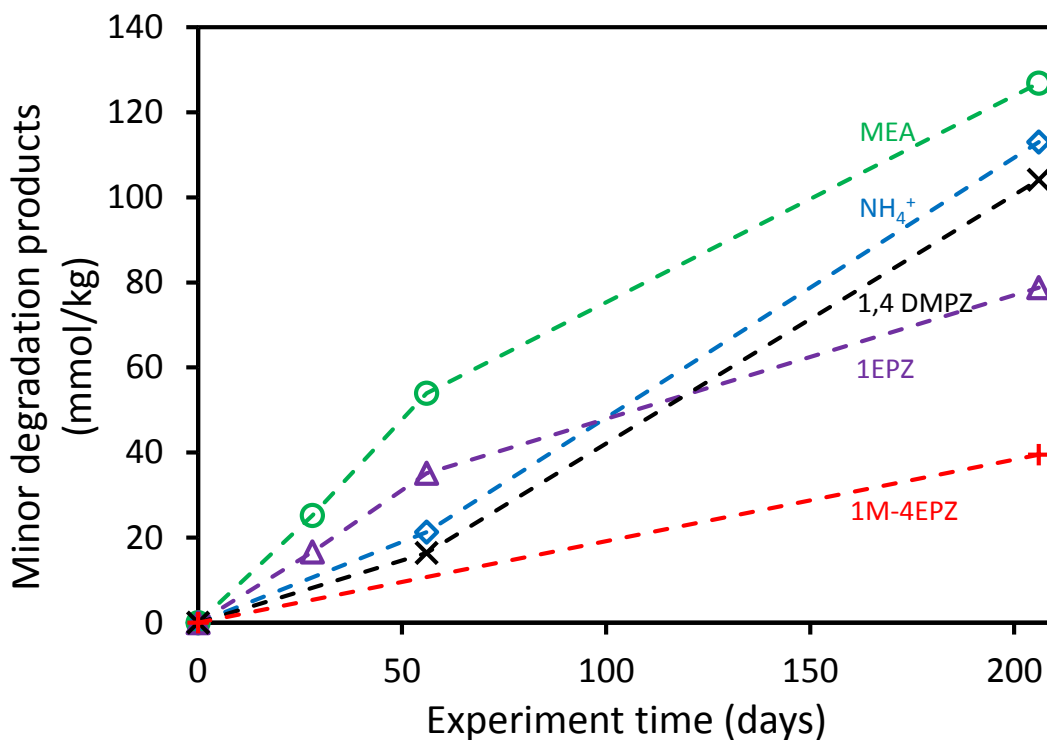
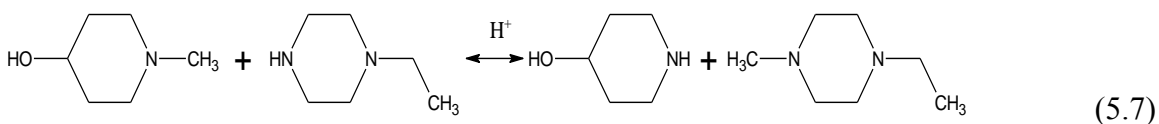
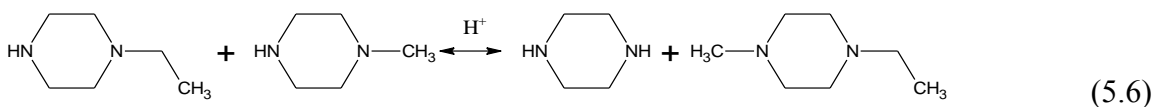


Figure 5.2: Formation of the minor degradation products for degradation of 2 m PZ/3 m HMPD with 0.26 mol CO<sub>2</sub>/mole alkalinity at 150 °C.

The nitrogen mass balance achieved after 30 weeks at 150 °C is presented in Table 5.1 to demonstrate the products achieved and the relative concentration or

importance of each product. The mass balance is presented as the percent that each product represents in terms of the lost nitrogen from PZ and HMPD disappearance. Over 81% of nitrogen lost in degraded PZ/HMPD was recovered in the seven quantified degradation products, with HPD and 1MPZ accounting for 54% of nitrogen lost.

Table 5.1: Nitrogen mass balance 2 m PZ/3 m HMPD with 0.26 mol CO<sub>2</sub>/mole alkalinity degraded at 150 °C for 30 weeks.

	Conc. (mmol/kg)	Nitrogen balance	
		N (mmol/kg)	Lost N (%)
PZ lost	803	1606	—
HMPD lost	880	880	—
Total N lost	—	2486	—
HPD	499	499	20.1
1MPZ	423	846	34.0
14DMPZ	104	208	8.4
1EPZ	79	158	6.3
MEA	127	127	5.1
NH <sub>4</sub> <sup>+</sup>	113	113	4.5
1M-4EPZ	39	79	3.2
Total recovery	—	2030	81.6

### 5.3.2 Effect of Process Conditions

The effect of CO<sub>2</sub> loading, total amine concentration, PZ to HMPD ratio, and temperature on the thermal degradation of aqueous PZ/HMPD was studied using thermal cylinders under various conditions. The basis for comparison between conditions is a comparison of the  $k_{2,f,c}$  value extracted from the PZ and HMPD concentration data over the experimental time.

### ***5.3.2.1 Effect of CO<sub>2</sub> loading***

The effect of CO<sub>2</sub> loading on the degradation of 2 m PZ/3 m HMPD at 175 °C is shown in Figure 5.3. PZ/HMPD does not significantly degrade in the absence of CO<sub>2</sub>, while the increase of CO<sub>2</sub> loading from 0 to 0.26 mol CO<sub>2</sub>/mol alkalinity accelerated the degradation by a factor of 36. This can be ascribed to the increased protonated PZ/HMPD species present in solution, which are likely to be more reactive in thermal degradation (Freeman and Rochelle, 2012a). 2 m PZ/3 m HMPD acidified with sulfuric acid was degraded in the absence of CO<sub>2</sub> to confirm the effect of protonation on degradation rate. The initial H<sup>+</sup> concentration was calculated to be 0.017 mol/mol alkalinity based on the pK<sub>a</sub> of PZ and HMPD. The addition of sulfuric acid created reactive protonated amine species such as H<sup>+</sup>PZ and H<sup>+</sup>HMPD in the absence of CO<sub>2</sub>. The increase of sulfuric acid to 0.26 mol H<sup>+</sup>/mol alkalinity also accelerated the degradation of 2 m PZ/3 m HMPD significantly. However, with further increase of H<sup>+</sup>, the degradation of PZ/HMPD became slower, indicating free PZ and HMPD are also necessary for the degradation to occur.

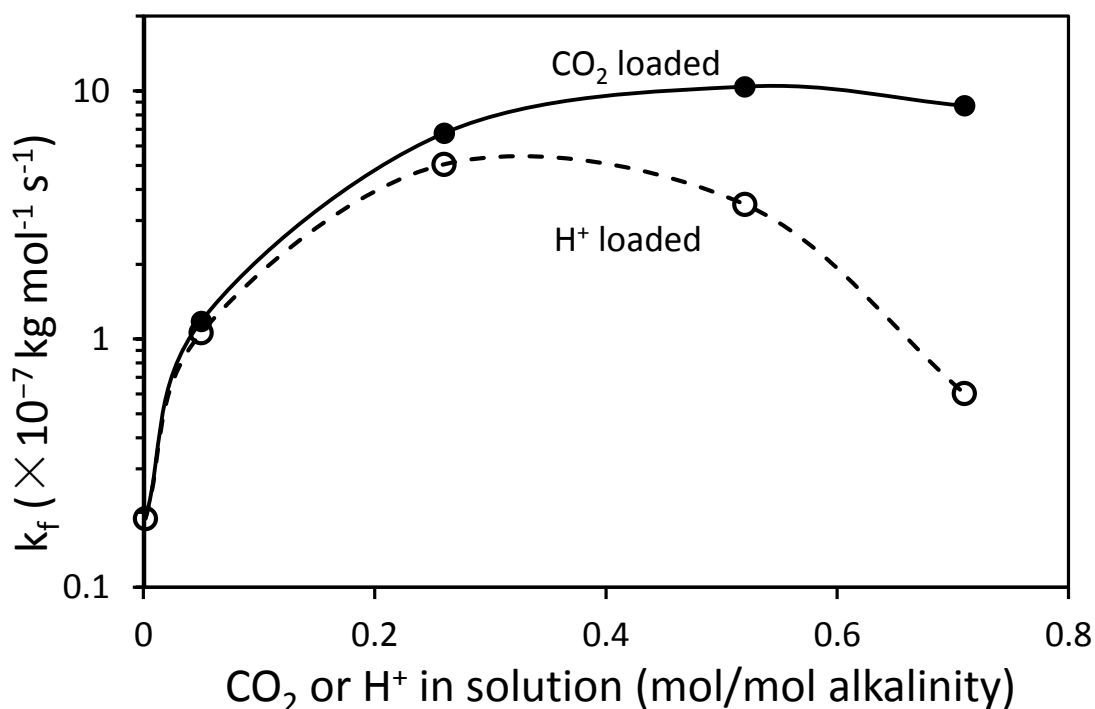


Figure 5.3: Degradation of 2 m PZ/3 m HMPD loaded with CO<sub>2</sub>, or H<sub>2</sub>SO<sub>4</sub> at 175 °C.

### 5.3.2.2 Effect of solvent composition

The effect of solvent composition on the degradation of PZ/HMPD with 0.24 mol CO<sub>2</sub>/mole alkalinity at 175 °C is shown in Table 5.2. The concentration-based second-order rate constant,  $k_{2,f,c}$ , depends on the total amine concentration and, to a lesser extent, the PZ to HMPD ratio. For many concentrated reaction systems it is known that the activity-based rate constant is independent of solvent composition, while the concentration-based rate “constant” depends both on the ionic strength, and type of ions in solution.(Haubrock et al., 2007; Knuutila et al., 2010) With the increase of total concentration of PZ/HMPD from 2 m to 10 m, the activity coefficients of reactive species can be very different. The calculation of the activity-based rate constant requires a

reliable activity-based thermodynamic model for all related species, and is out of the scope of this study.

Table 5.2:  $k_{2,f,c}$  values for PZ/HMPD with variable total amine and PZ/HMPD at 0.24 mol CO<sub>2</sub>/mole alkalinity and 175 °C.

<b>PZ (m)</b>	<b>HMPD (m)</b>	<b><math>k_{2,f,c}</math> (<math>\times 10^{-7}</math> kg mol<sup>-1</sup> s<sup>-1</sup>)</b>
1	1	7.84
3	3	4.12
5	5	3.54
2	4	4.17
3	3	4.12
4	2	3.39

### 5.3.2.3 Effect of temperature

The degradation of 2 m PZ/3 m HMPD with 0.26 mol CO<sub>2</sub>/mole alkalinity at 150, 165, and 175 °C is represented using the second-order rate model (Equation 5.3) and is given in Figure 5.4. The  $k_{2,f,c}$  for 2 m PZ/3 m HMPD has an Arrhenius dependence on temperature (Figure 5.5) with an activation energy ( $E_A$ ) of 162 kJ/mol, using the following equation where  $A$  is a pre-exponential constant,  $R$  is the gas constant, and  $T$  is the absolute temperature (Equation 5.8). This  $E_A$  is higher than that for PZ/MDEA (140 kJ/mol), but smaller than PZ (180 kJ/mol) (Namjoshi, 2015).

$$\ln(k_{2,f,c}) = \ln(A) - \frac{E_A}{R} * \frac{1}{T} \quad (5.8)$$

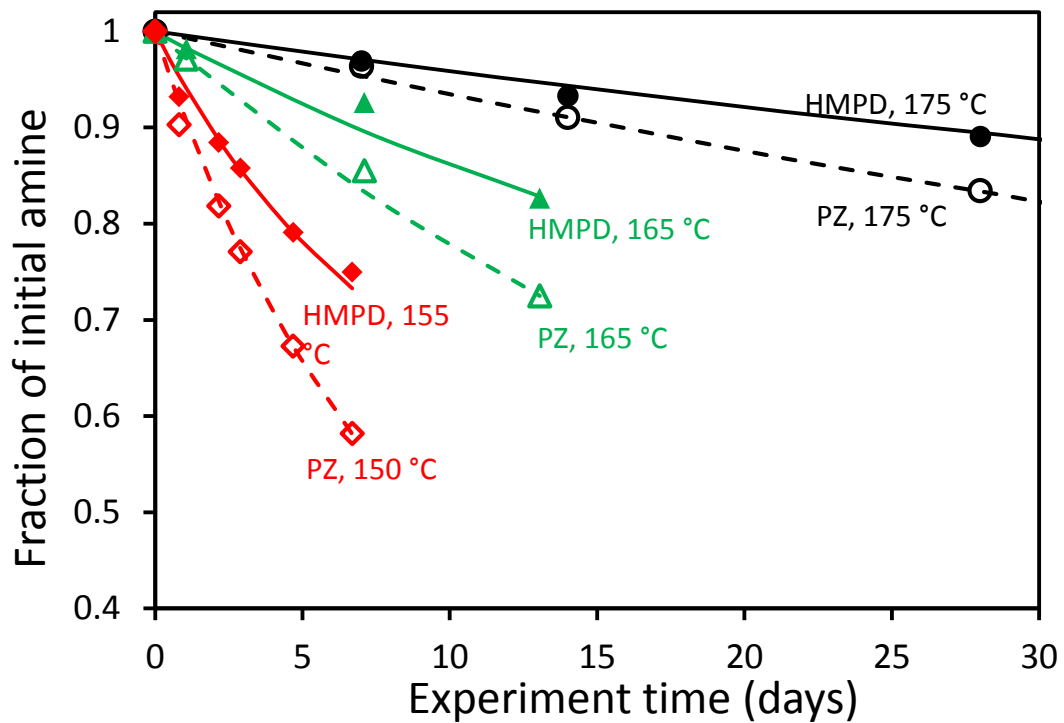


Figure 5.4: Degradation of PZ and HMPD in 2 m PZ/3 m HMPD with 0.26 mol CO<sub>2</sub>/mole alkalinity at 150, 165, and 175 °C. Lines indicate second-order rate models fit the data (Equation 5.3).

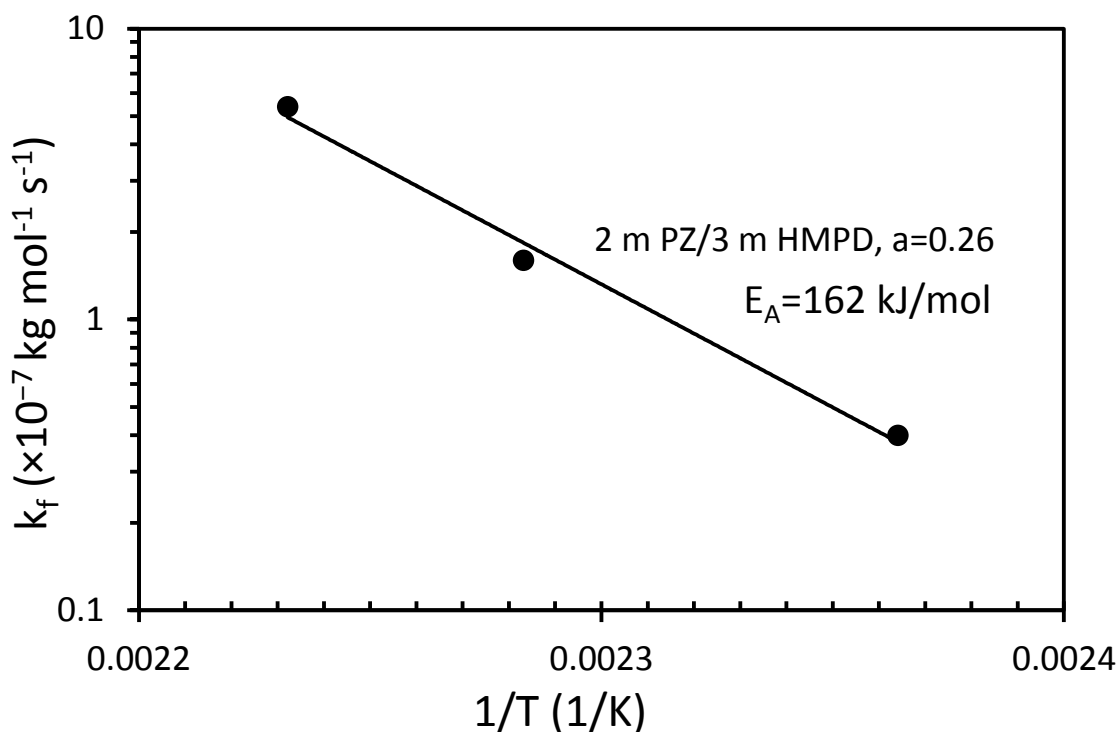


Figure 5.5: The Arrhenius behavior of the second-order rate constant ( $k_{2,f,c}$ ) for thermal degradation of 2 m PZ/3 m HMPD with 0.26 mol CO<sub>2</sub>/mole alkalinity.

### 5.3.3 Comparison between PZ/HMPD and PZ/MDEA

Figure 5.6 compares the amine loss for 5 m PZ/5 m HMPD to 5 m PZ/5 m MDEA at 0.24 mol CO<sub>2</sub>/mole alkalinity and 175 °C. The thermal degradation of PZ/MDEA in the presence of CO<sub>2</sub> was found to be first-order in amine concentration (Namjoshi, 2015). In order to compare the thermal degradation rate of PZ/HMPD to PZ/MDEA, the amine loss in 5 m PZ/5 m HMPD was also represented using the first-order rate model as shown in Equation 5.9 where  $C_{Am}$  is the concentration of amines, and  $k_1$  is a first-order rate constant. The integrated form is given in Equation 5.10 where  $C_{Am,0}$  is the initial amine concentration, and  $t$  is the experimental time in seconds.

$$\frac{C_{Am}}{dt} = k_1 C_{Am} \quad (5.9)$$

$$C_{Am} = C_{Am,0} \cdot e^{-k_1 \cdot t} \quad (5.10)$$

5 m PZ/5 m HMPD is significantly more stable than 5 m PZ/5 m MDEA in the presence of CO<sub>2</sub>. The first-order rate constants for PZ and tertiary amine degradation in 5 m PZ/5 m HMPD are 7 and 3.5 times smaller than that in 5 m PZ/5 m MDEA, respectively.

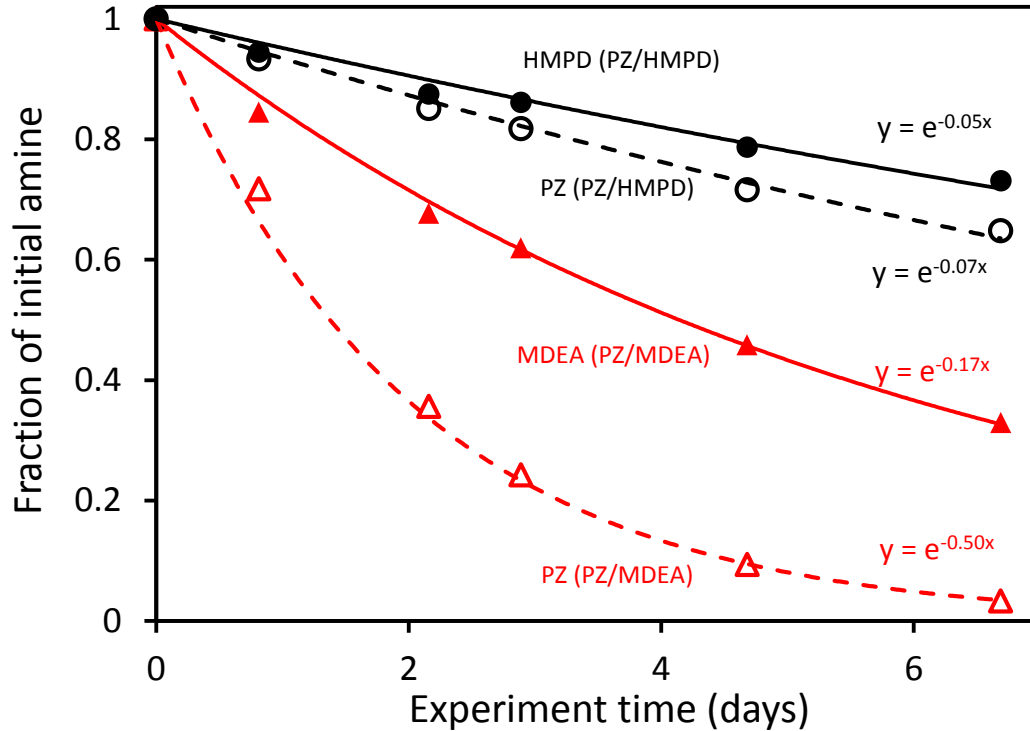


Figure 5.6: Degradation of 5 m PZ/5 m HMPD and 5 m PZ/5 m MDEA with 0.24 mol CO<sub>2</sub>/mole alkalinity at 175 °C. Lines indicate first-order rate models fit the data.

The rapid degradation of PZ in PZ/MDEA was ascribed to the rapid reaction between PZ and oxazolidinone produced from the degradation of diethanolamine (DEA), which is the immediate product of MDEA degradation. (Namjoshi, 2015) Unlike DEA, HPD, the immediate product of HMPD degradation, cannot form oxazolidinone in CO<sub>2</sub> loaded solutions. HPD is also expected to be resistant to other common thermal

degradation mechanisms due to its stable 6-membered ring structure and absence of any substituent group on the amino group.(Freeman and Rochelle, 2011; Lepaumier et al., 2009; Rochelle, 2012) The thermal stability of PZ/HPD in CO<sub>2</sub> loaded solutions was found to be significantly greater than PZ/DEA under similar conditions (Figure 5.7).

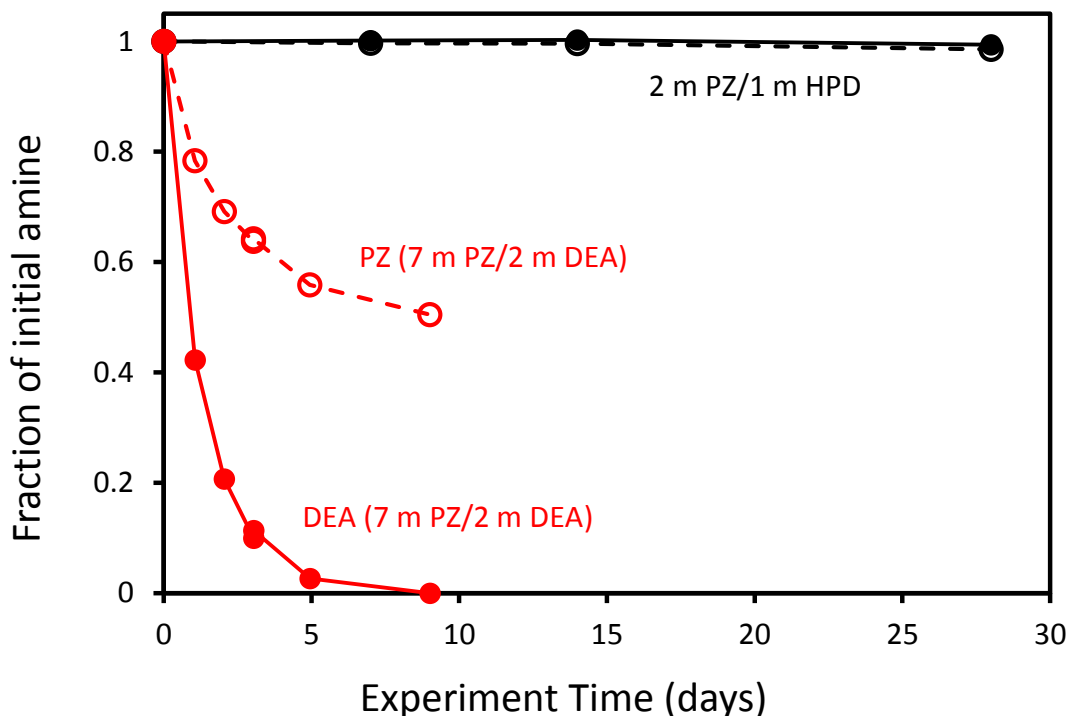


Figure 5.7: Degradation of 2 m PZ/1 m HPD with 0.31 mol CO<sub>2</sub>/mole alkalinity at 150 °C, compared to 7 m PZ/2 m DEA with 0.31 mol CO<sub>2</sub>/mole alkalinity (Namjoshi, 2015).

The thermal stability of HMPD is compared to MDEA in acidified solutions (0.2 mol H<sup>+</sup>/mole alkalinity) at 175 °C (Figure 5.8). In acidified solutions both HMPD and MDEA showed a fast degradation in the first 2 days, and reached steady state afterwards. The degradation mechanism for HMPD in acidified solutions should be similar to other tertiary amines.(Bedell et al., 2010; Namjoshi, 2015) Free HMPD attacks protonated HMPD (H<sup>+</sup>HMPD), and reaches equilibrium with HPD and 4-hydroxy-

dimethylpiperidine (HDMPD), a quaternary amine (Equation 5.11). The equilibrium constant for HMPD system is smaller than that for MDEA system as indicated by less amine loss for acidified HMPD at equilibrium (Figure 5.8).

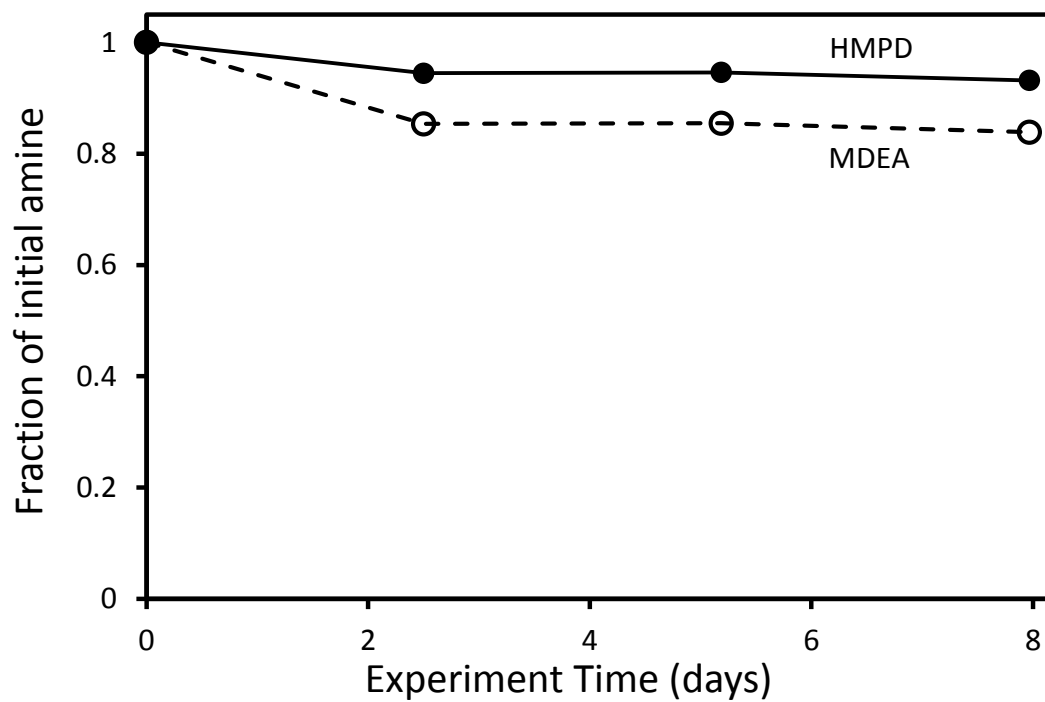
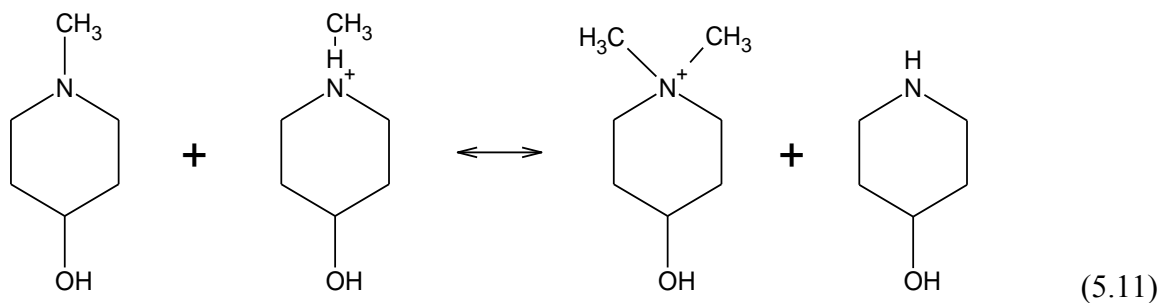


Figure 5.8: Degradation of 5 m HMPD and 5 m MDEA with 0.2 mol H<sup>+</sup>/mole alkalinity at 175 °C.

The thermal stability of 2 m PZ/3 m HMPD is compared to 2 m PZ/3 m MDEA in acidified solutions (0.26 mol H<sup>+</sup>/mole alkalinity) at 175 °C (Figure 5.9). In acidified solutions, the “arm-switching” mechanism is the major route for the degradation of both PZ/HMPD and PZ/MDEA. The slower degradation of PZ/HMPD compared to PZ/MDEA in acidified solutions suggests a slower initial degradation of PZ/HMPD in CO<sub>2</sub>-loaded solutions.

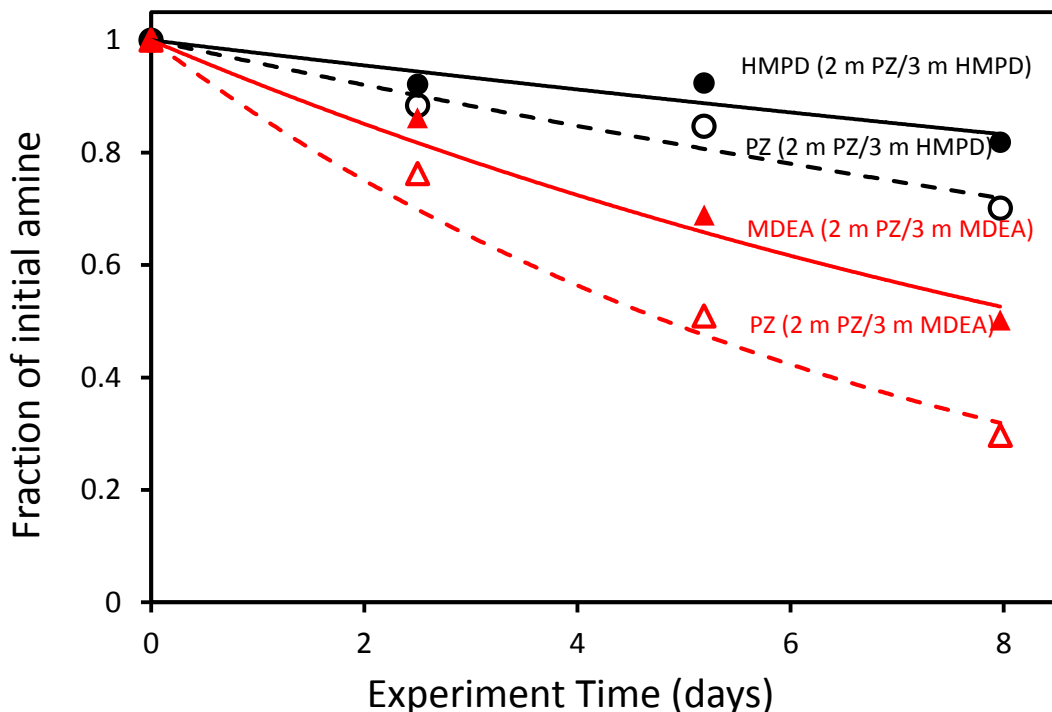


Figure 5.9: Degradation of 2 m PZ/3 m HMPD and 2 m PZ/3 m MDEA with 0.26 mol H<sup>+</sup>/mole alkalinity at 175 °C. Lines indicate first-order rate models fit the data.

From these results it can be concluded that the significantly greater stability of PZ/HMPD in comparison with PZ/MDEA is due to the remarkable thermal stability of HMPD which prevents PZ from further degradation, the smaller initial degradation rate of PZ/HMPD, and the greater thermal stability of HMPD compared to MDEA.

### 5.3.4 Potential environmental issues of 1,4 DMPZ

Although 1,4 DMPZ is only a minor product of thermal degradation of PZ/HMPD, the high volatility of 1,4 DMPZ may require an expensive water wash system to meet emission limits.(Nguyen, 2013) 1,4 DMPZ is expected to be produced in any PZ promoted tertiary amine at high temperature if the tertiary amine has at least one methyl group.(Namjoshi, 2015) Prior work by Freeman suggested that any system containing 1MPZ will tend toward a  $K_{eq1}$  of 0.29 for PZ/1-MPZ/1,4 DMPZ at 150 °C.(Freeman, 2011)

$$K_{eq1} = \frac{[PZ] * [1,4 DMPZ]}{[1MPZ]^2} \quad (5.12)$$

Figure 5.10 shows the concentration of PZ and 1,4 DMPZ in the degradation of PZ/HMPD and PZ/MDEA at 175 °C.  $K_{eq1}$  for both PZ/HMPD and PZ/MDEA was determined to be 0.25–0.30, which is consistent with Freeman.(Freeman, 2011) After the same period of time, PZ/MDEA produced four times more 1,4 DMPZ than PZ/HMPD, due to the rapid loss of PZ by other degradation mechanisms in PZ/MDEA which accelerated the production of 1,4 DMPZ. However, for the same PZ loss, the yield of 1,4 DMPZ from PZ/HMPD is comparable to that from PZ/MDEA.

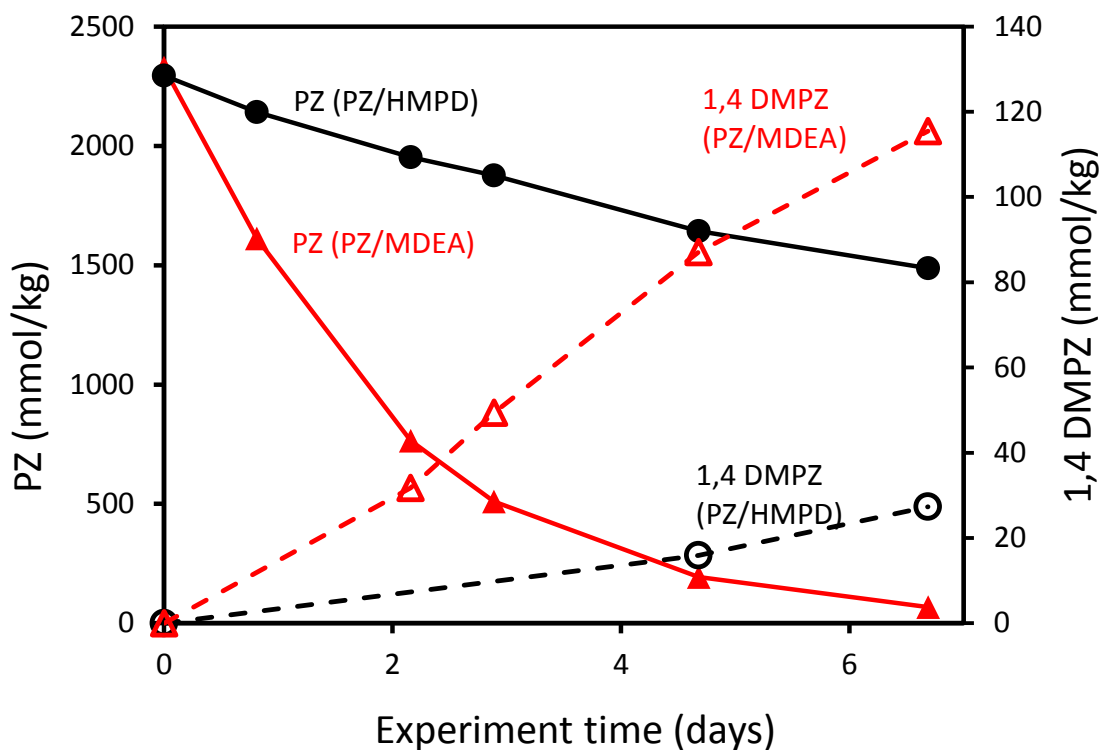


Figure 5.10: PZ, 1MPZ and 1,4 DMPZ in the degradation of 5 m PZ/5 m HMPD and 5 m PZ/5 m MDEA with 0.24 mol CO<sub>2</sub>/mole alkalinity at 175 °C.

To calculate the equilibrium concentration of 1,4 DMPZ in the thermal degradation of PZ/HMPD, which is considered to be the worst case scenario, solutions with variable composition of PZ/HMPD/1MPZ/HPD with 0.26 mol CO<sub>2</sub>/mole alkalinity were thermally degraded at 150 °C for 7 months (Figure 5.11). The interconversion of PZ, HMPD, 1MPZ, and HPD at this temperature (Equation 5.1) is assumed to occur more rapidly than other side reactions. The reversible second-order rate model shown in Equation 5.2 was used to fit the experimental  $K_t$  values (the ratio of products to reactants at time  $t$ ) (Equation 5.13). As seen from Figure 5.11,  $K_t$  for PZ/HMPD/1MPZ/HPD tends toward a value of 2.1 at equilibrium at 150 °C (when  $K_t = K_{eq2}$ , the equilibrium constant for the reaction).

$$K_t = \frac{[1MPZ] * [HPD]}{[PZ] * [HMPD]} \quad (5.13)$$

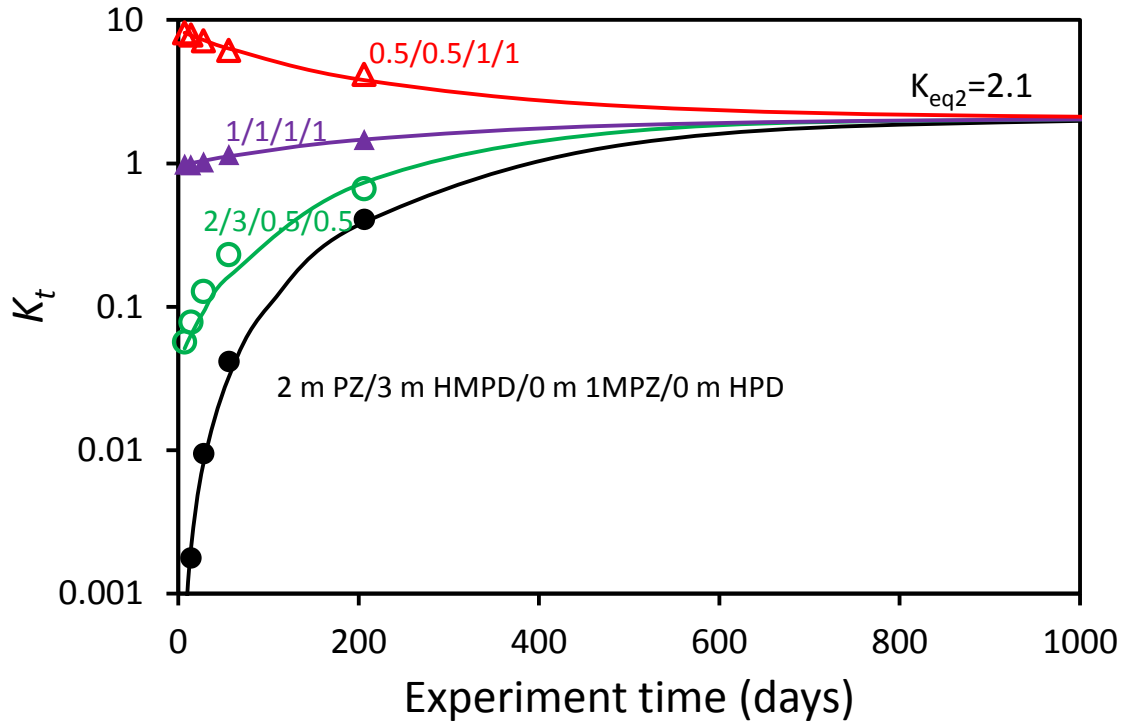


Figure 5.11:  $K_t$  for PZ/HMPD/1MPZ/HPD degraded at 150 °C ( $\alpha=0.26$ ). Labels indicate the concentrations of PZ, HMPD, 1-MPZ, and HPD in solution in molal (m). Lines indicate reversible second-order rate models fit the data (Equation 5.2).

Based on  $K_{eq1}$  and  $K_{eq2}$ , the equilibrium concentration of 1,4 DMPZ from 2 m PZ/3 m HMPD at 150 °C is determined to be 0.4 molal (m) leading to a partial pressure of 10 Pa at 40 °C in unloaded ideal solutions based on the Henry's law constant of 1,4 DMPZ in water (Nguyen, 2013). This partial pressure of 1,4 DMPZ is three times higher than 7 m MEA at the same temperature and nominal lean loading (the partial pressure of CO<sub>2</sub> is about 0.5 kPa at 40 °C), but similar to 5 m AMP (Nguyen, 2013).

## 5.4 CONCLUSIONS

1. At high temperature PZ and HMPD reach equilibrium with the major degradation products, 1MPZ and HPD, by “arm switching”.  $K_{eq2}$  for PZ/HMPD/1MPZ/HPD tends toward a value of 2.1 at 150 °C.
2. Over 81% of nitrogen lost in degraded PZ/HMPD was recovered in seven quantified degradation products, with 1MPZ and HPD accounting for 54% of nitrogen lost.
3. A second-order rate model consistent with proposed degradation pathways can model initial degradation reasonably well. The concentration-based second-order rate constant,  $k_{2,f,c}$ , depends on the total amine concentration and, to a lesser extent, the PZ to HMPD ratio. The increase of CO<sub>2</sub> loading and temperature accelerate the degradation of PZ/HMPD. The activation energy of PZ/HMPD degradation is 162 kJ/mol.
4. 5 m PZ/5 m HMPD is significantly more stable than 5 m PZ/5 m MDEA in the presence of CO<sub>2</sub>. The first-order rate constants for PZ and tertiary amine degradation in 5 m PZ/5 m HMPD are 7 and 3.5 times smaller than that in 5 m PZ/5 m MDEA, respectively.
5. The significantly greater stability of PZ/HMPD in comparison with PZ/MDEA is due to the remarkable thermal stability of HPD which prevents PZ from further degradation, the smaller initial degradation rate of PZ/HMPD, and the greater thermal stability of HMPD compared to MDEA.

## 5.5 ACKNOWLEDGEMENTS

The author gratefully acknowledges Yukai Wang for helping measuring the thermal degradation of PZ/HMPD.

## **Chapter 6: Piperazine/4-Hydroxy-1-methylpiperidine for CO<sub>2</sub> Capture**

Aqueous piperazine (PZ)/4-hydroxy-1-methylpiperidine (HMPD) was rigorously evaluated for CO<sub>2</sub> capture from flue gas. CO<sub>2</sub> cyclic capacity, CO<sub>2</sub> absorption rate, solvent viscosity, solvent volatility, and solid solubility were investigated as a function of the solvent composition. 2 m PZ/3 m HMPD is the composition that offers the best overall performance with more than twice the CO<sub>2</sub> cyclic capacity and CO<sub>2</sub> absorption rate of 7 m MEA. This blend also shows much greater resistance to oxidative degradation than MEA at the same condition, as well as lower amine volatility. When compared to 5 m PZ, 2 m PZ/3 m HMPD has 40% greater CO<sub>2</sub> cyclic capacity, 10% lower rate and 10% higher viscosity. 2 m PZ/3 m HMPD also has a much better solid solubility than 5 m PZ, showing no precipitation down to -10 °C at normal CO<sub>2</sub> loading range. The cost of production for HMPD in large scale was also investigated based on current synthesis routes. The capital and energy cost for flue gas CO<sub>2</sub> capture using 2 m PZ/3 m HMPD is expected to be much lower than that using 7 m MEA, while comparable to that using 5 m PZ.

### **6.1 INTRODUCTION**

CO<sub>2</sub> capture from flue gas has gained considerable attention due to concern about global warming. Amine scrubbing is the most applicable technology for effective capture of CO<sub>2</sub> from flue gas, and has been used in other industrial gas treating processes for nearly a century (Astarita et al., 1983). Amine scrubbing has higher energy efficiency than other advanced technologies for flue gas CO<sub>2</sub> capture (Rochelle, 2009). However, the low CO<sub>2</sub> partial pressure and high flow rate of flue gas lead to high capital and operating costs for amine scrubbing (Finkenrath, 2012). Amine scrubbing also has

potential environmental issues due to amine volatilization and degradation (Eide-Haugmo et al., 2009; Mazari et al., 2015). Using novel amines with desirable chemical and physical properties, including high CO<sub>2</sub> capacity, fast absorption rate, high resistance to degradation, low amine volatility, low viscosity, low corrosivity and low cost of production, is a critical approach to reduce the cost and mitigate environmental issues.

Aqueous 30 wt % monoethanolamine (MEA) is currently the benchmark solvent for CO<sub>2</sub> capture from flue gas due to its success in high pressure applications, and low cost of production. However aqueous MEA has moderate CO<sub>2</sub> absorption rate, and low thermal and oxidative stability. Rochelle et al. (2011) proposed 8 m piperazine (PZ) (40 wt % PZ) as a new standard solvent. 8 m PZ has double the CO<sub>2</sub> absorption rate and capacity, remarkable resistance to oxidation and thermal degradation, and lower amine volatility than 30 wt % MEA (Rochelle et al., 2011). The low water solubility of PZ and its zwitterionic carbamate may limit its industrial application (Freeman et al., 2010b; Ma et al., 2012). Effort has been made to blend other useful amines with less concentrated PZ in order not only to mitigate its precipitation issues, but also to maintain the desirable CO<sub>2</sub> capture properties of concentrated PZ (Chen and Rochelle, 2011; Du et al., 2013; Li et al., 2014b; L. Li et al., 2013b; Namjoshi et al., 2013). Recently, Du et al. (2016b, 2016c) identified PZ/4-Hydroxy-1-methylpiperidine (HMPD) as a promising solvent. It has a CO<sub>2</sub> absorption rate and CO<sub>2</sub> cyclic capacity comparable to concentrated PZ, as well as good thermal stability.

The main objective of this work is to find a composition for PZ/HMPD that offers the best overall performance. In general, a higher amine concentration leads to higher CO<sub>2</sub> cyclic capacity, but also higher viscosity. The high viscosity of a solvent reduces mass transfer and heat transfer, resulting in increased cost for CO<sub>2</sub> absorption and solvent regeneration (L. Li et al., 2013a). Increased HMPD in the blend causes more solvent

loss and potential environmental issues due to amine volatilization (Du et al., 2016d). Amine volatilization is particularly important for CO<sub>2</sub> capture from flue gas which is normally at ambient pressure. The solvent volatility is evaluated in CO<sub>2</sub>-loaded solutions, because the partial pressure of an amine in a CO<sub>2</sub>-loaded solution depends not only on its physical solubility in water (Henry's law volatility constant), but also on its ability to be speciated by CO<sub>2</sub> (Nguyen et al., 2010). Increased PZ decreases the solid solubility of the blend, increasing the risk of precipitation when process upsets occur (Freeman et al., 2010b; Ma et al., 2012).

A secondary objective of this work is to evaluate other important properties of PZ/HMPD at operating conditions, such as oxidative stability and heat of CO<sub>2</sub> absorption. Oxidation is the primary cause of amine loss in CO<sub>2</sub> capture from flue gas (Nielsen et al., 2013; Silva et al., 2012; Strazisar et al., 2003). In addition, some oxidative degradation products are corrosive or toxic (Mazari et al., 2015). For CO<sub>2</sub> capture with thermal swing solvent regeneration, higher heat of absorption is desirable for a solvent, as it leads to higher stripper pressure at constant stripper temperature, reducing compression cost downstream (Oexmann and Kather, 2010; Oyenekan and Rochelle, 2007).

## **6.2 EXPERIMENTAL METHODS**

### **6.2.1 Solution preparation**

Aqueous PZ/HMPD was prepared by melting anhydrous PZ (99%, Sigma Aldrich, USA) in mixtures of distilled de-ionized water and HMPD (98%, Acros Organics), and gravimetrically sparging CO<sub>2</sub> (99.5%, Matheson Tri Gas, Basking Ridge, NJ) to achieve the desired CO<sub>2</sub> concentration. The concentration was determined by total inorganic carbon (TIC) analysis, described in detail previously (Freeman et al., 2010b).

### **6.2.2 Viscosity measurement**

Viscosity of PZ/HMPD with variable concentration and CO<sub>2</sub> loading was measured using a Physica MCR 300 cone-and-plate rheometer (Anton Paar GmbH, Graz, Austria). The method was described in detail previously (Freeman et al., 2010b).

### **6.2.3 Amine volatility**

Amine volatility and CO<sub>2</sub> solubility in aqueous solutions was measured at 40–60 °C in a stirred reactor coupled with a hot gas FTIR analyzer (Fourier Transform Infrared Spectroscopy, Temet Gasetm Dx-4000). The details of the experimental apparatus, and procedure were described in detail in Chapter 3.

### **6.2.4 CO<sub>2</sub> solubility and absorption rate**

CO<sub>2</sub> equilibrium partial pressure ( $P_{\text{CO}_2^*}$ ) and absorption rate in PZ/HMPD were measured at 20–100 °C using a wetted wall column (WWC), which counter-currently contacted an aqueous amine solution with a saturated N<sub>2</sub>/CO<sub>2</sub> stream on the surface of a stainless steel rod with a known surface area to simulate CO<sub>2</sub> absorption in an absorber. A detailed description of wetted wall column was given previously (Chen and Rochelle, 2011).

The total pressure of CO<sub>2</sub>-loaded PZ/HMPD at high temperature (100–160 °C) was measured using a sealed autoclave.  $P_{\text{CO}_2^*}$  was calculated by subtracting the partial pressure of N<sub>2</sub> and water from the measured total pressure. The pressure of water was assumed to follow Raoult's Law and the pressure of the amine was neglected. The experimental method and calculation of CO<sub>2</sub> partial pressure were described in detail previously (Xu and Rochelle, 2011).

CO<sub>2</sub> solubility in PZ/HMPD at 40–60 °C was also obtained along with the volatility for PZ/HMPD in CO<sub>2</sub> loaded solutions.

### 6.2.5 Solid Solubility

The solid solubility of PZ/HMPD was measured in a water bath over a range of CO<sub>2</sub> loading (from 0 to 0.3 mol CO<sub>2</sub>/mol alkalinity), solvent composition, and temperature (from -10 to 50 °C). The solid solubility measurements were based on visual observations and the method was described in detail previously (Freeman, 2011). Solutions with desired properties were heated to 50 °C in a water bath to dissolve precipitates with lean CO<sub>2</sub> loading. The solution was then cooled to -10 °C slowly, and the temperature at which the solution first began to precipitate was regarded as the precipitation temperature. The solidified sample was heated again to carefully observe the temperature when the precipitates fully dissolve and this was noted as the dissolution temperature. The difference between precipitation and dissolution temperature (which is also called hysteresis), mainly caused by the free energy barrier for phase transitions (Hu et al., 2002; Luo et al., 2004), was minimized by giving enough equilibrium time and repeating the precipitation-dissolution process. The approximate temperature ramp near transitions was 1 °C or less every 5 hours.

### 6.2.6 Oxidative Degradation

Oxidative degradation experiments for PZ/HMPD spiked with 0.05 mM Cr<sup>3+</sup>, 0.1 mM Ni<sup>2+</sup>, 0.4 mM Fe<sup>2+</sup> and 0.1 mM Mn<sup>2+</sup> were conducted at 70 °C in a low gas flow agitated reactor with 100 mL/min of a saturated 98%/2% O<sub>2</sub>/CO<sub>2</sub> gas mixture fed into the reactor headspace. The duration of the experiment was 8 days. 3 ml samples were taken every two to three days and water was added periodically to maintain the water balance of the reactor contents. The liquid samples were analyzed for PZ, HMPD, and degradation products using ion chromatography. The details of the experimental apparatus, procedure, and analytical methods were described in detail previously (Liu et al., 2014).

## 6.3 RESULTS AND DISCUSSION

### 6.3.1 Amine volatility

Figure 6.1 shows the volatility of HMPD in PZ/HMPD at variable CO<sub>2</sub> loading at 40 °C, compared to AMP in 5 m PZ/2.3 m AMP, 8 m PZ, 7 m MEA, and 4.8 m AMP (Nguyen, 2013). At nominal lean loading for coal-fired flue gas ( $P_{\text{CO}_2} = 500 \text{ Pa}$ ), HMPD partial pressure in loaded 2 m PZ/3 m HMPD and 3 m PZ/3 m HMPD is greater than 8 m PZ, but is only 50% of 7 m MEA, 35% of AMP in 5 m PZ/2.3 m AMP, and 10% of 4.8 m AMP. With increasing CO<sub>2</sub> loading, HMPD is gradually protonated, resulting in decreased partial pressure of HMPD in both 2 m PZ/3 m HMPD and 3 m PZ/3 m HMPD. Although HMPD has a lower Henry's law constant than MEA (Du et al., 2016d), the partial pressure of HMPD in loaded 5 m PZ/5 m HMPD is expected to be twice as high as 7 m MEA at similar conditions, because HMPD, as a tertiary amine, cannot be effectively speciated by CO<sub>2</sub> to form carbamate in solution.

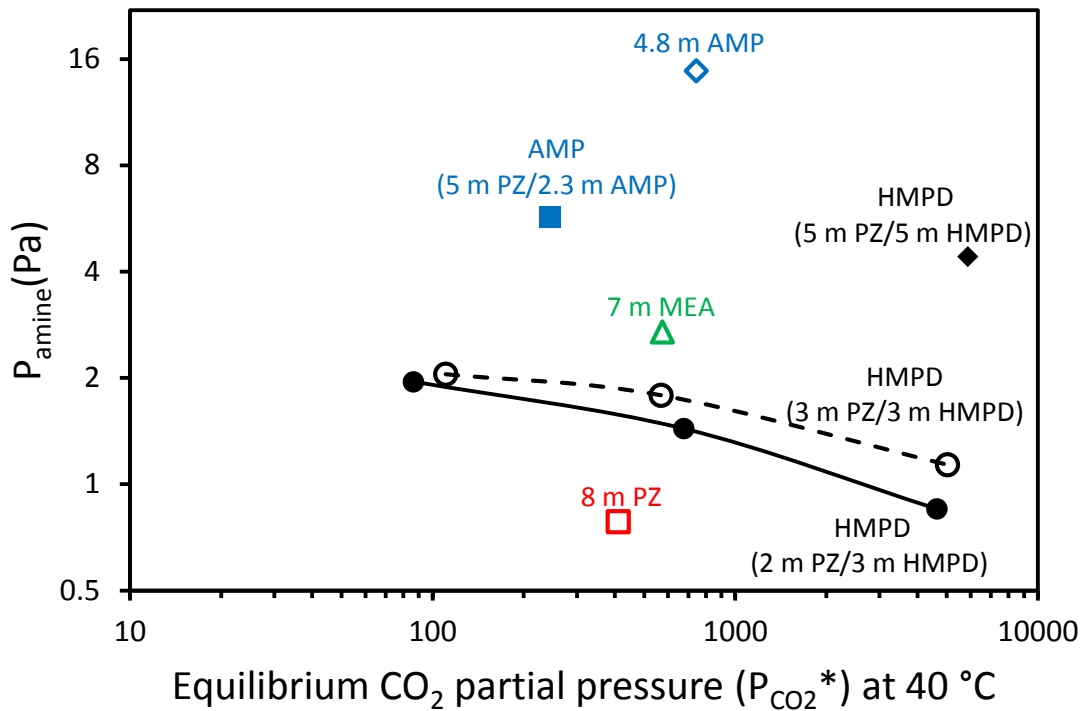


Figure 6.1: Partial pressure of HMPD in PZ/HMPD at variable  $CO_2$  loading at 40 °C, compared to AMP in 5 m PZ/2.3 m AMP, 8 m PZ, 7 m MEA, and 4.8 m AMP (Nguyen, 2013).

### 6.3.2 Viscosity

Figure 6.2 shows the viscosity of loaded PZ/HMPD at 40 °C, compared to 7 m MEA, 5 m PZ (Dugas, 2009), and 8 m PZ (Freeman, 2011) within a similar  $CO_2$  partial pressure range. 2 m PZ/3 m HMPD has a viscosity that is 10% higher than 5 m PZ, and 70% higher than 7 m MEA. 3 m PZ/3 m HMPD has a 50% higher viscosity than 5 m PZ, but it is still significantly less viscous than 8 m PZ. 5 m PZ/5 m HMPD has an even higher viscosity than 8 m PZ at the same conditions.

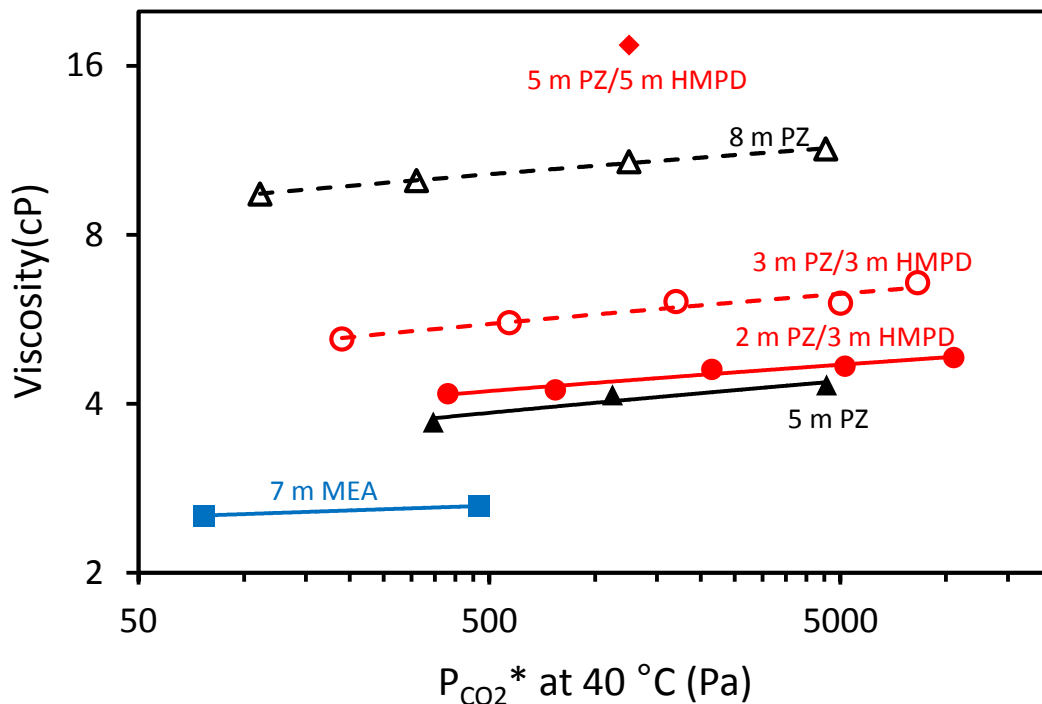


Figure 6.2: Viscosity of PZ/HMPD at variable CO<sub>2</sub> partial pressure and 40 °C, compared to 7 m MEA, 5 m PZ (Dugas, 2009), and 8 m PZ (Freeman, 2011).

### 6.3.3 CO<sub>2</sub> capacity and absorption rate

The CO<sub>2</sub> absorption rate (kg') in loaded PZ/HMPD solutions at 40 °C is compared to 7 m MEA, 5 m PZ, and 8 m PZ (Dugas, 2009) in Figure 3. kg' is defined as the liquid film mass transfer coefficient on a partial pressure basis, and is calculated as the ratio of CO<sub>2</sub> flux to the liquid film partial pressure driving force. To compare kg' on the same basis, the rate data are plotted against equilibrium partial pressure of CO<sub>2</sub> instead of CO<sub>2</sub> loading. At most practical absorption conditions, kg' depends on the reaction rate constant of CO<sub>2</sub> and the amine, the amount of free amine in solution, and the viscosity of the solution (L. Li et al., 2013b). Viscosity in general has a more significant effect on the absorption rate at rich loading where the absorption is likely to be limited by the

diffusion of reactants and products in the liquid phase. At lean loading, 2 m PZ/3 m HMPD and 3 m PZ/3 m HMPD have similar absorption rate to 5 m and 8 m PZ, while at rich loading, they absorb CO<sub>2</sub> faster than 8 m PZ, at a rate comparable to 5 m PZ, as a result of their relatively low viscosity. Although 5 m PZ/5 m HMPD has a lower kg' than 2 m PZ/3 m HMPD and 3 m PZ/3 m HMPD as a result of its high viscosity, it absorbs CO<sub>2</sub> twice as fast as 7 m MEA.

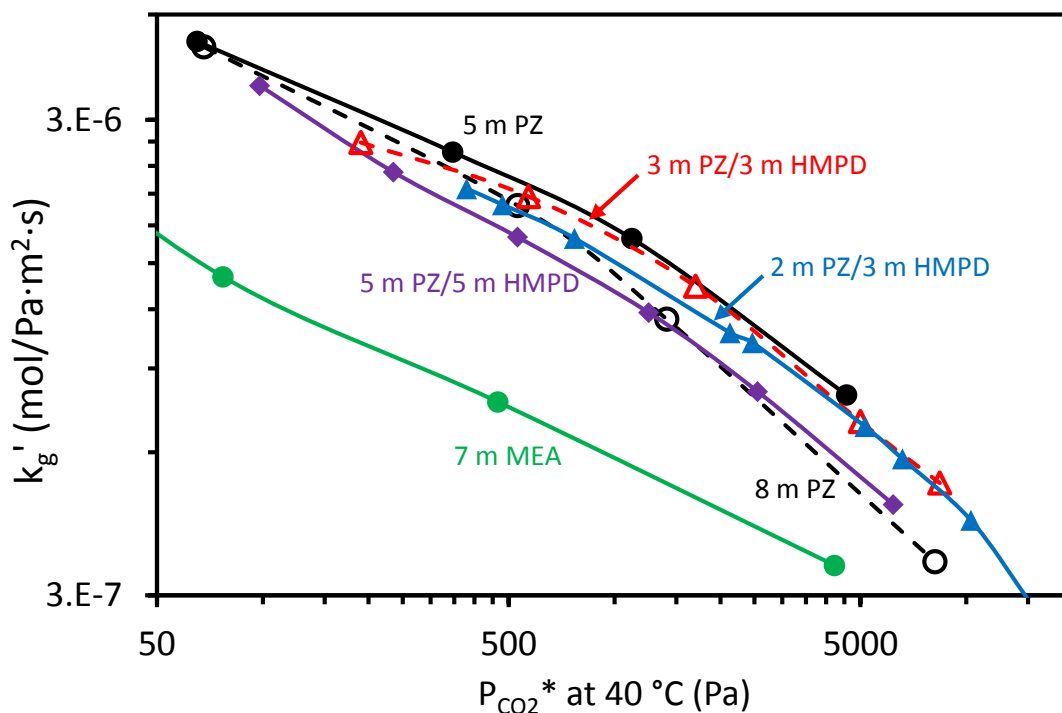


Figure 6.3: CO<sub>2</sub> absorption rate (kg') by WWC in PZ/HMPD at 40 °C, compared to 7 m MEA, 5 m PZ, and 8 m PZ (Dugas, 2009).

Figure 6.4 shows the CO<sub>2</sub> solubility for PZ/HMPD with variable blend composition, compared to 7 m MEA (Plaza, 2011), 5 m PZ and 8 m PZ (Frailie, 2014). To compare CO<sub>2</sub> cyclic capacity directly, the CO<sub>2</sub> partial pressure is plotted against total CO<sub>2</sub> concentration (mol CO<sub>2</sub>/kg amine + water). The CO<sub>2</sub> cyclic capacity of a solvent

$(\Delta C_{solv})$  is defined as the difference in CO<sub>2</sub> concentration between the lean and rich solvents (Equation 6.1).

$$\Delta C_{solv}(\text{mol CO}_2/\text{kg}) = (C_{rich} - C_{lean})/(\text{kg amine} + \text{water}) \quad (6.1)$$

$C_{lean}$  and  $C_{rich}$  are the CO<sub>2</sub> concentration of lean and rich solvents. For coal-fired flue gas, the normal operational lean and rich solvents correspond to  $P_{CO_2^*}$  of 0.5 kPa and 5 kPa at 40 °C, respectively, in order to maintain enough driving force for CO<sub>2</sub> absorption throughout the absorber. As the slopes of the vapor liquid equilibrium (VLE) curves indicate, the cyclic capacities of solvents increase as follows: 7 m MEA < 5 m PZ < 2 m PZ/3 m HMPD < 3 m PZ/3 m HMPD  $\approx$  8 m PZ < 5 m PZ/5 m HMPD.

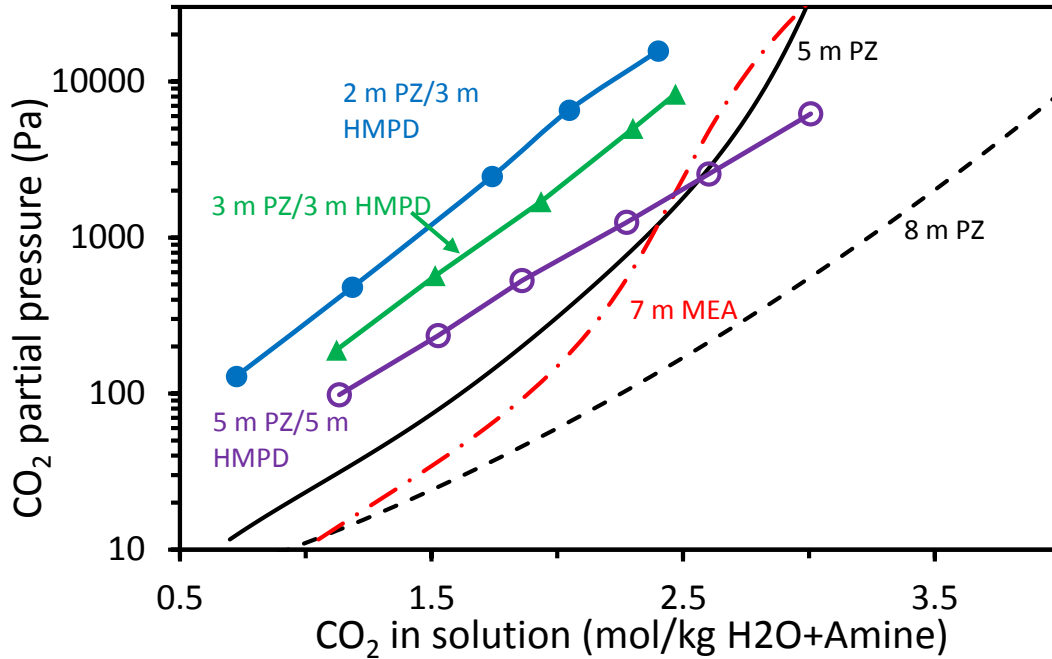


Figure 6.4: CO<sub>2</sub> solubility by WWC in PZ/HMPD at 40 °C, compared to 7 m MEA (Plaza, 2011), 5 m PZ and 8 m PZ (Frailie, 2014).

As shown in Figure 6.2 and 6.4, higher PZ/HMPD leads to greater capacity but also higher viscosity. With increasing CO<sub>2</sub> cyclic capacity, less solvent is required to remove the same amount of CO<sub>2</sub>, resulting in less sensible heat requirement for stripping. The heat transfer coefficient generally depends on solvent viscosity to about -0.35 power (Ayub, 2003). To consider the effect of viscosity on the optimized heat exchanger cost, CO<sub>2</sub> cyclic capacity is normalized by the viscosity of the solvent as Equation 6.2 (L. Li et al., 2013b).

$$\Delta C_{\mu} = \Delta C_{solv} / (\mu_{mid} / \mu_{8\text{ m PZ}})^{0.175} \quad (6.2)$$

$\Delta C_{\mu}$  is the normalized CO<sub>2</sub> capacity, while  $\mu_{mid}$  and  $\mu_{8\text{ m PZ}}$  are the viscosities of the studied amine and 8 m PZ, respectively, at mid-loading ( $P_{CO_2}^* = 2.0$  kPa) and 40 °C. Figure 6.5 shows the normalized CO<sub>2</sub> cyclic capacity and average absorption rate at 40 °C for PZ/HMPD at variable concentration, compared to 7 m MEA, 5 m PZ, and 8 m PZ. The average absorption rate ( $k_g'_{avg}$ ) is defined in Equation 6.3, assuming a linear concentration profile and equilibrium curve in the absorber (L. Li et al., 2013b).

$$k_g'_{avg} = \frac{Flux_{CO_2,LM}}{(P_{CO_2} - P_{CO_2}^*)_{LM}} = \frac{(Flux_{CO_2,top} - Flux_{CO_2,bottom}) / \ln(Flux_{CO_2,top} / Flux_{CO_2,bottom})}{(P_{CO_2,top} - P_{CO_2,lean}^*) - (P_{CO_2,bottom} - P_{CO_2,rich}^*) / \ln\left(\frac{P_{CO_2,top} - P_{CO_2,lean}^*}{P_{CO_2,bottom} - P_{CO_2,rich}^*}\right)} \quad (6.3)$$

Normalized CO<sub>2</sub> capacity of solvents increases as follows: 7 m MEA < 5 m PZ < 8 m PZ < 2 m PZ/3 m HMPD < 3 m PZ/3 m HMPD < 5 m PZ/5 m HMPD. Assuming normalized CO<sub>2</sub> cyclic capacity and average absorption rate equally affect the overall CO<sub>2</sub> capture cost, 2 m PZ/3 m HMPD, 3 m PZ/3 m HMPD and 5 m PZ/5 m HMPD are comparable to 5 m PZ and 8 m PZ, but much better than 7 m MEA.

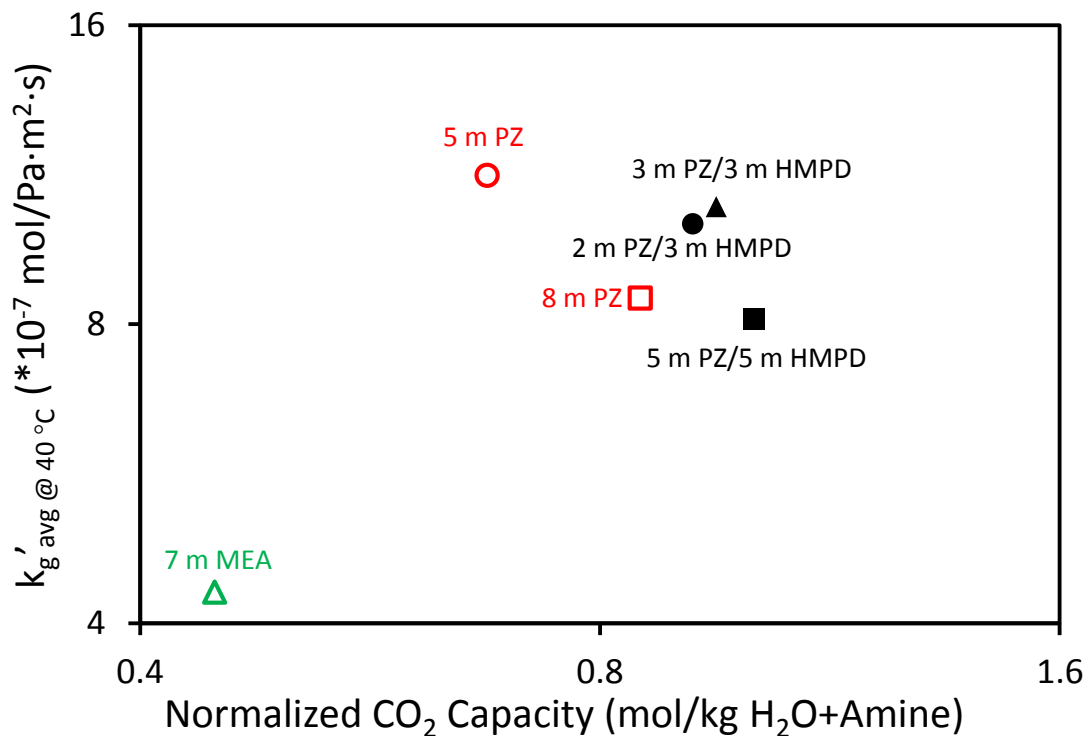


Figure 6.5: Normalized CO<sub>2</sub> capacity and average absorption rate ( $\text{kg}'_{\text{avg}}$ ) at 40 °C for PZ/HMPD with variable concentration, compared to 7 m MEA, 5 m PZ, and 8 m PZ.

### 6.3.4 Solid solubility

The dissolution temperature ( $T_d$ ) for 2 m PZ/3 m HMPD, 3 m PZ/3 m HMPD, and 5 m PZ/5 m HMPD over a range of CO<sub>2</sub> concentration is shown in Figure 6.6, and compared to that for 5 m PZ and 8 m PZ (Freeman, 2011). Solid solubility of 2 m PZ/3 m HMPD and 3 m PZ/3 m HMPD are significantly better than 5 m PZ and 8 m PZ, due to the low concentration of PZ in blends. The addition of 5 m HMPD to 5 m PZ enhances PZ solid solubility, probably because of the interaction between PZ and HMPD (Long and McDevit, 1952). With increasing CO<sub>2</sub> concentration, the  $T_d$  decreases in all the three PZ/HMPD compositions as a result of the speciation of PZ by CO<sub>2</sub> to form

carbamate. Unlike 8 m PZ, no zwitterionic carbamate precipitation was observed for the three different PZ/HMPD solvents at rich CO<sub>2</sub> loading.

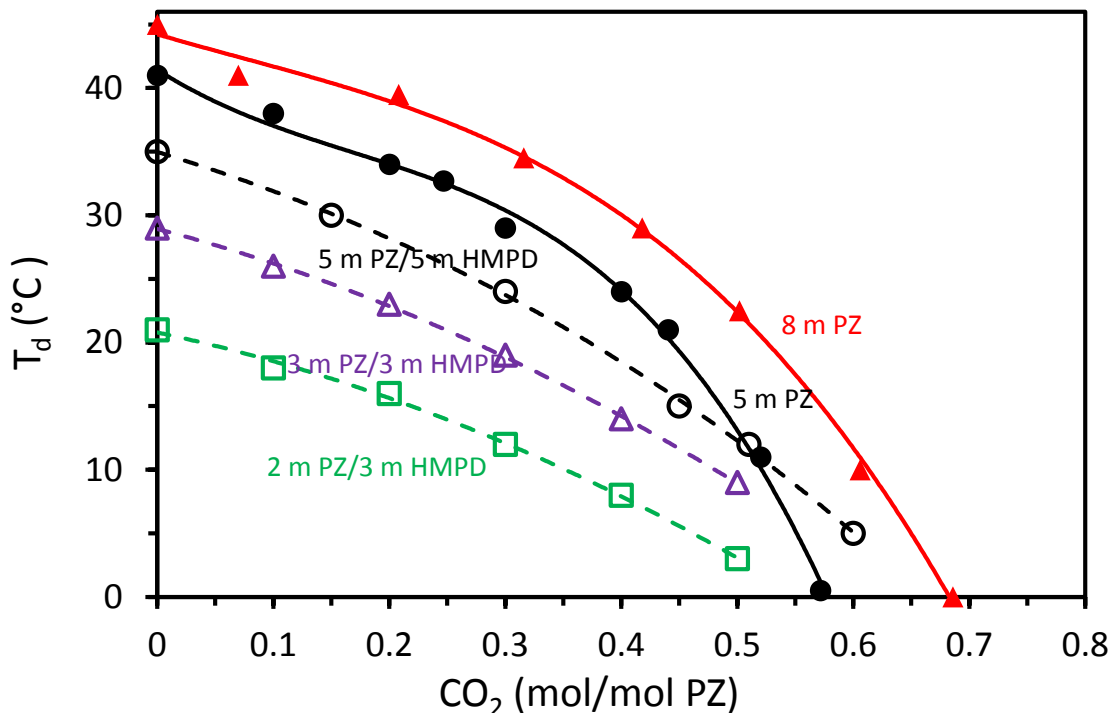


Figure 6.6: Dissolution temperature ( $T_d$ ) for PZ/HMPD over a range of CO<sub>2</sub> concentration, compared to 5 m PZ and 8 m PZ (Freeman, 2011).

In practice, solid solubility for different solvents should be compared at the same CO<sub>2</sub> partial pressure instead of at the same CO<sub>2</sub> concentration, because different solvents tend to have different lean loadings at operational conditions. In Figure 6.7, the  $T_d$  and precipitation temperature ( $T_p$ ) for 2 m PZ/3 m HMPD are plotted against CO<sub>2</sub> partial pressure at 40 °C and compared to that of 5 m PZ and 8 m PZ. If the process is operating at the lean loading corresponding to CO<sub>2</sub> partial pressure of 100 Pa at 40 °C, the  $T_d$  is 23 °C for 8 m PZ, 18 °C for 5 m PZ, while only 4 °C for 2 m PZ/3 m HMPD. Although precipitation is the most likely concern in practice, it is difficult to get  $T_p$  with good precision due to the complicated nucleation process which can be largely affected

by impurities in the solution, and the contacting surface (Mullin, 2001). On the other hand, a solid will almost always dissolve at the same temperature for a given pressure (Spencer et al., 2010). For all the solvents tested in this study, hysteresis effects become more pronounced at low transition temperature, which is likely caused by the slow kinetics of phase change (Mullin, 2001).

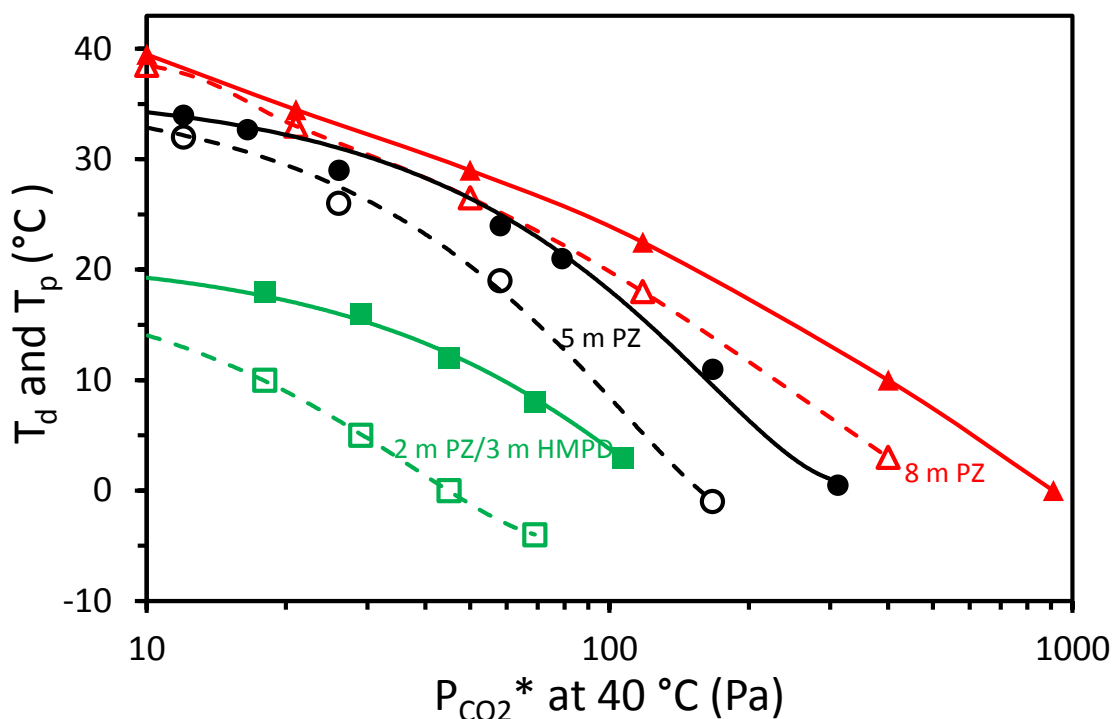


Figure 6.7: Dissolution temperature ( $T_d$ ) (solid points) and precipitation temperature ( $T_p$ ) (open points) for 2 m PZ/3 m HMPD over a range of  $CO_2$  partial pressure at 40 °C, compared to 5 m PZ and 8 m PZ (Freeman, 2011).

Table 6.1 compares the important properties of the three PZ/HMPD blends. Data for 7 m MEA, 5 m PZ, and 8 m PZ are shown for comparison. 2 m PZ/3 m HMPD is the best composition giving the lowest  $P_{HMPD}$  and best solid solubility, as well as  $CO_2$  absorption performance comparable to the other two PZ/HMPD blends.

Table 6.1: Properties of PZ/HMPD compared to 7 m MEA, 5 m PZ, and 8 m PZ.

Amine	$P_{\text{HMPD}}^a$ (Pa)	$\mu_{\text{mid}}^b$ (cP)	$\Delta C_{\text{solv}}^b$ (mol/kg)	$\Delta C_{\mu}^b$ (mol/kg)	$k_{\text{g}}^{\text{avg}^b}$ (*10 <sup>-7</sup> mol/Pa m <sup>2</sup> s)	$T_p^c$ (°C)
2 m PZ/3 m HMPD	1.4	4.5	0.79	0.92	10.1	<-10
3 m PZ/3 m HMPD	1.8	6.0	0.86	0.95	10.5	-1
5 m PZ/5 m HMPD	4.4	17.7	1.10	1.01	8.1	3
7 m MEA	2.7	2.7	0.35	0.45	4.3	—
5 m PZ	—	4.2	0.57	0.67	11.3	8
8 m PZ	0.8	11.0	0.85	0.85	8.5	18

<sup>a</sup> Measured at solvent lean loading ( $P_{\text{CO}_2^*} = 0.5$  kPa) and 40 °C

<sup>b</sup> Measured at solvent mid-loading ( $P_{\text{CO}_2^*} = 2.0$  kPa) and 40 °C

<sup>c</sup> Measured at  $P_{\text{CO}_2^*} = 0.1$  kPa

### 6.3.5 CO<sub>2</sub> solubility in 2 m PZ/3 m HMPD at 20 – 160 °C

Figure 6.8 shows the vapor liquid equilibrium (VLE) of CO<sub>2</sub> in 2 m PZ/3 m HMPD at 20–160 °C. CO<sub>2</sub> equilibrium partial pressure,  $P_{\text{CO}_2^*}$  (Pa), was regressed using the following semi-empirical model (Equation 6.4) as a function of temperature,  $T$  (K), and CO<sub>2</sub> loading,  $\alpha$  (mol CO<sub>2</sub>/mol/mol alkalinity), in the liquid phase.

$$\ln P_{\text{CO}_2^*} = 34 - 9741 \cdot \frac{1}{T} + 4050 \cdot \frac{\alpha}{T} \quad (6.4)$$

The heat of CO<sub>2</sub> absorption ( $\Delta H_{\text{abs}}$ ) for 2 m PZ/3 m HMPD can be extracted from the equilibrium data by applying the fundamental thermodynamic relationship to the semi-empirical model (Equation 6.5):

$$-\Delta H_{\text{abs}} = R \cdot \left( \frac{\partial \ln(P_{\text{CO}_2^*})}{\partial (1/T)} \right)_{P,x} = -9741 + 4050 \cdot \alpha \quad (6.5)$$

$\Delta H_{\text{abs}}$  for 2 m PZ/3 m HMPD at CO<sub>2</sub> loading corresponding to a  $P_{\text{CO}_2^*}$  of 1.5 kPa at 40 °C is 69 kJ/mol, which is higher than 8 m PZ (64 kJ/mol) but slightly lower than 7 m MEA (71 kJ/mol) (L. Li et al., 2013b).

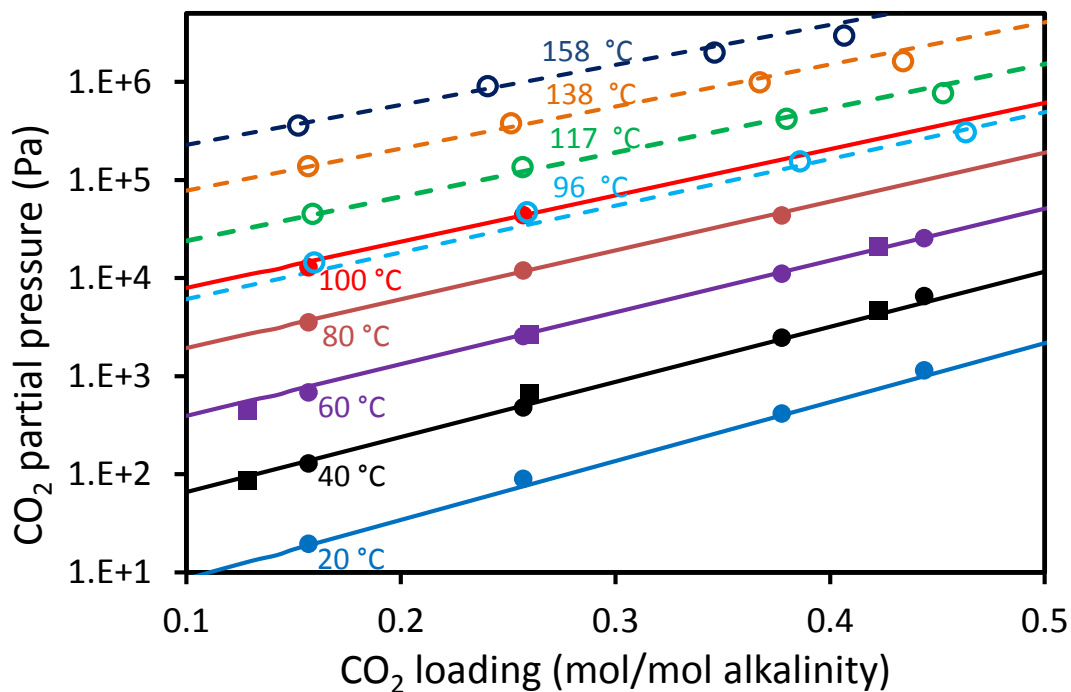


Figure 6.8: CO<sub>2</sub> solubility in 2 m PZ/3 m HMPD. Squares: volatility results; other solid points: WWC results; open points: total pressure results; lines: model prediction (Equation 6.4).

### 6.3.6 Oxidative stability and thermal stability

The oxidation for 2 m PZ/3 m HMPD at 70 °C in the presence of 0.1 mM Mn<sup>2+</sup> and a typical SSM mixture (0.4 mM Fe<sup>2+</sup>, 0.05 mM Cr<sup>3+</sup>, and 0.1 mM Ni<sup>2+</sup>) is shown in Figure 6.9, along with the oxidation for 10 m MEA at the same condition (Liu, 2015). 2 m PZ/3 m HMPD shows no detectable degradation after 8 days at this condition, while the amine loss of 10 m MEA is more than 70% for the same period of time at the same condition. This observation is consistent with the previous work by Voice (Voice, 2013) who found that both tertiary amines and PZ are resistant to oxidative degradation at low temperatures.

The thermal stability of this solvent has been studied previously (Du et al., 2016a, 2016b). PZ/HMPD was found to be significantly more stable than PZ/ MDEA in the presence of CO<sub>2</sub> at high temperatures, with a T<sub>max</sub> (the maximum stripper operating temperature) 25 °C higher than PZ.MDEA.

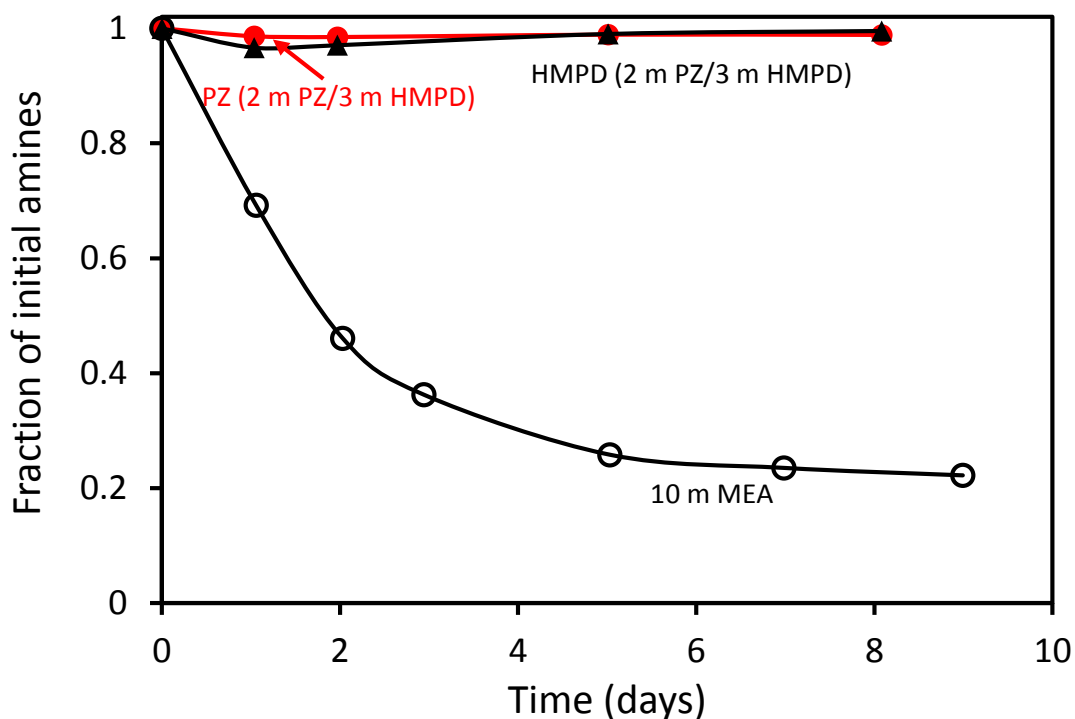


Figure 6.9: Amine loss for 2 m PZ/3 m HMPD at 70 °C with 98% O<sub>2</sub>/2% CO<sub>2</sub>, as well as 0.1 mM Mn<sup>2+</sup>, 0.4 mM Fe<sup>2+</sup>, 0.05 mM Cr<sup>3+</sup>, and 0.1 mM Ni<sup>2+</sup>, compared to 10 m MEA (Liu, 2015).

### 6.3.7 Synthesis and cost of HMPD

The cost of production for HMPD is the major challenge for commercial application of this solvent for CO<sub>2</sub> capture. Currently, HMPD is used as an intermediate for the preparation of several pharmaceutical products (Chang et al., 2002), and mainly obtained by the reduction of n-methyl-4-piperidone (MPD) (McElvain and McMahon, 1949). Due to the high cost of MPD, which results from its complicated synthesis route

with low overall yield (HOWTON, 1945), the cost of HMPD is expected to be more than twice that of PZ for industrial grade (Matton, R. Eastman Chemical Company, personal communication, 2015). However, as some byproducts of HMPD may also be effective for CO<sub>2</sub> capture, and thus do not need to be separated, the cost of HMPD for CO<sub>2</sub> capture can be significantly reduced by choosing proper synthesis routes. For example, hydroxylation of n-methylpiperidine gives a mixture of 3-hydroxy-1-methylpiperidine, and 4-hydroxy-1-methylpiperidine (Kato et al., 2002; Li et al., 2004). 3-Hydroxy-1-methylpiperidine is expected to behave similar to 4-hydroxy-1-methylpiperidine for CO<sub>2</sub> capture, based on their similar structure and pKa (Du et al., 2016a, 2016c, 2016d).

#### **6.4 CONCLUSIONS**

2 m PZ/3 m HMPD is a superior solvent for CO<sub>2</sub> capture from flue gas. Its CO<sub>2</sub> cyclic capacity and CO<sub>2</sub> absorption rate are more than twice that of 7 m MEA. This blend also shows much greater resistance to oxidative degradation than MEA at the same condition, as well as lower amine volatility. When compared to 5 m PZ, 2 m PZ/3 m HMPD has a 40% higher CO<sub>2</sub> cyclic capacity, while 10% lower rate and 10% higher viscosity. 2 m PZ/3 m HMPD also has a much better solid solubility than 5 m PZ, showing no precipitation down to -10 °C at normal CO<sub>2</sub> loading range. The heat of CO<sub>2</sub> absorption for 2 m PZ/3 m HMPD is 69 kJ/mol, which is higher than 5 m PZ (64 kJ/mol) but slightly lower than 7 m MEA (71 kJ/mol). The capital and energy cost for flue gas CO<sub>2</sub> capture using 2 m PZ/3 m HMPD is expected to be much lower than that using 7 m MEA, while comparable to that using 5 m PZ. Although the cost of production for HMPD is currently too high for commercial application of this solvent for CO<sub>2</sub> capture, it can be significantly reduced by choosing proper synthesis routes.

## **Chapter 7: Thermally Degraded Diglycolamine<sup>®</sup>/Dimethylaminoethoxyethanol for CO<sub>2</sub> Capture**

Thermally degraded diglycolamine<sup>®</sup> (DGA<sup>®</sup>)/dimethylaminoethoxyethanol (DMAEE) was found to have a better performance for CO<sub>2</sub> capture than the original solvent. At high temperature, DGA<sup>®</sup>/DMAEE reaches equilibrium with its major degradation product, methylaminoethoxyethanol (MAEE). The production of MAEE enhances the CO<sub>2</sub> absorption rate, while maintaining the CO<sub>2</sub> capacity of the original solvent. The normalized CO<sub>2</sub> cyclic capacity of DGA<sup>®</sup>/MAEE/DMAEE is substantially greater than that of 7 m MEA and 10 m DGA<sup>®</sup>, and comparable to 5 m PZ. The average CO<sub>2</sub> absorption rate of DGA<sup>®</sup>/MAEE/DMAEE is 30-70% higher than 7 m MEA, although it is still much lower than 5 m PZ. The heat of CO<sub>2</sub> absorption ( $\Delta H_{\text{abs}}$ ) for 1.75 m DGA<sup>®</sup>/1.75 m MAEE/3.50 m DMAEE at CO<sub>2</sub> loading corresponding to a  $P_{\text{CO}_2^*}$  of 1.5 kPa at 40 °C is 72 kJ/mol, which is comparable to 7 m MEA, and greater than 5 m PZ. The capital and energy cost for flue gas CO<sub>2</sub> capture using thermally degraded DGA<sup>®</sup>/DMAEE is expected to be much lower than that using 7 m MEA, while still higher than that using 5 m PZ.

### **7.1 INTRODUCTION**

Amine scrubbing has shown the most promise for effective capture of CO<sub>2</sub> from coal-fired flue gas (Rochelle, 2009). Aqueous monoethanolamine (MEA) with a concentration between 15–30% has been previously used in similar applications such as CO<sub>2</sub> removal from natural gas and hydrogen, and is currently considered the state-of-the-art technology for CO<sub>2</sub> absorption/stripping because of its effectiveness for CO<sub>2</sub> capture and low cost of production. However, the low resistance to degradation, and low CO<sub>2</sub>

capacity and CO<sub>2</sub> absorption rates of MEA lead to high capital and energy cost, as well as some environmental issues (Mazari et al., 2015).

Diglycolamine<sup>®</sup> (DGA<sup>®</sup>) has been traditionally used as an alternative to MEA for many natural gas sweetening plants, due to its ability to partially remove COS, low volatility, and reversible thermal degradation pathway (Kohl and Nielsen, 1997). DGA<sup>®</sup> has been investigated for flue gas CO<sub>2</sub> capture recent years (Al-Juaied and Rochelle, 2006; Chen et al., 2011; Hatchell et al., 2014; Liu et al., 2014; Salkuyeh and Mofarahi, 2012). Although DGA<sup>®</sup> has greater thermal stability than MEA (Hatchell et al., 2014), it still oxidatively degrades (Liu et al., 2014). The CO<sub>2</sub> capacity and absorption rate of 10 m DGA is lower than 7 m MEA by ~ 20% for flue gas CO<sub>2</sub> capture (Chen et al., 2011).

Using novel amines with desirable chemical and physical properties is a critical approach to reduce the cost and mitigate environmental issues. An ideal amine solvent would feature high CO<sub>2</sub> cyclic capacity, fast absorption rate, high resistance to degradation, low amine volatility, low viscosity, and high heat of CO<sub>2</sub> absorption. However, it is not likely to find a single solvent that has all the desired features. Primary amines, such as MEA and DGA<sup>®</sup>, feature high heat of CO<sub>2</sub> absorption, but have disadvantages of low CO<sub>2</sub> cyclic capacity due to the high carbamate stability. Tertiary amines, which cannot form carbamate, show much higher CO<sub>2</sub> cyclic capacity than primary amines, but substantially lower CO<sub>2</sub> absorption rate and heat of CO<sub>2</sub> absorption. Secondary amines generally have fast CO<sub>2</sub> absorption rate, but moderate CO<sub>2</sub> cyclic capacity and heat of CO<sub>2</sub> absorption. Blending different solvents is one approach to combine desirable characteristics.

Thermal degradation of amine solvents is in general unfavorable, as it causes the loss of original amines, and some of the degradation products may cause environmental

and health issues (Mazari et al., 2015). However, some degradation products may have better properties than the original amine solvent for CO<sub>2</sub> capture.

A unique blend of DGA<sup>®</sup> and dimethylaminoethoxyethanol (DMAEE) was identified in this work. As a tertiary amine, DMAEE can increase the CO<sub>2</sub> cyclic capacity of DGA<sup>®</sup>. At high temperature, DGA<sup>®</sup>/DMAEE reaches equilibrium with its major degradation product, methylaminoethoxyethanol (MAEE), a secondary amine. The production of MAEE enhances the CO<sub>2</sub> absorption rate, while maintaining the CO<sub>2</sub> capacity of the original solvent. Due to the high cost of production, MAEE is not able to be directly used for CO<sub>2</sub> capture. Thermally degraded DGA<sup>®</sup>/DMAEE was found to have a better performance for CO<sub>2</sub> capture than the original solvent and the benchmark solvent, 7 m MEA. The thermal degradation of DGA<sup>®</sup>/DMAEE has been evaluated at normal operating conditions to calculate the equilibrium constant for DGA<sup>®</sup>/MAEE/DMAEE. The degraded DGA<sup>®</sup>/DMAEE at equilibrium with variable composition has been evaluated for CO<sub>2</sub> cyclic capacity, CO<sub>2</sub> absorption rate, viscosity, and heat of CO<sub>2</sub> absorption.

## **7.2 EXPERIMENTAL METHODS**

### **7.2.1 Solution preparation**

All amines studied in this work were reagent grade chemicals from commercial sources. Aqueous DGA<sup>®</sup>/DMAEE solutions were prepared by mixing DGA<sup>®</sup> and DMAEE in distilled de-ionized water. CO<sub>2</sub> loaded solutions were prepared by gravimetrically sparging CO<sub>2</sub> (99.5%, Matheson Tri Gas, Basking Ridge, NJ) in unloaded amine solutions in a gas-washing bottle. The concentration of CO<sub>2</sub> was checked by total inorganic carbon (TIC) analysis, described in detail previously (Freeman et al., 2010a).

Acid loaded solutions were prepared by adding 10 N sulfuric acid to unloaded aqueous amine.

Due to the lack of a commercial source for large quantity of MAEE, 2-(methylamino)ethanol (MAE), which is a secondary amine with similar structure and  $pK_a$  to MAEE, was used as a proxy for MAEE for evaluation.

### **7.2.2 Thermal degradation**

Thermal degradation of DGA<sup>®</sup>/DMAEE under various conditions was measured in 3/8-inch 316 stainless steel Swagelok<sup>®</sup> cylinders with a volume of 4.5 ml and diameter of 0.95 cm. A number of cylinders were filled with 4 mL target amine solution. The cylinders were then sealed with two Swagelok<sup>®</sup> end caps, and placed in forced convection ovens maintained at the target temperature. Individual cylinders were removed from the ovens at each sampling time. The parent amines and degradation products in the solutions were analyzed using cation chromatography. The details of the experimental apparatus and procedure were described in detail previously (Namjoshi, 2015).

### **7.2.3 Analytical Tools - Cation Chromatography**

A Dionex ICS-2100 cation ion chromatograph (Dionex Corporation) was used to quantify parent amines and identify degradation products. A 4 × 50 mm CG17 guard column connected with a 4 × 250 mm CS17 analytical column were used for separation. The eluent contained varying concentrations of methanesulfonic acid (MSA) in analytical grade water. Ion suppression was used to improve the signal/noise ratio. Standard curves of parent amines and degradation products were prepared to quantify the amount of amine present. Due to the lack of a commercial source for methylaminoethoxyethanol (MAEE) and 2-[2-(methylamino)ethoxy]ethanol, a quaternary amine (QUAT), the standard curves for DGA<sup>®</sup> and DMAEE<sup>®</sup> were used to

quantify MAEE and QUAT, respectively. Samples were diluted by a factor of 10000 (mass) in analytical grade water. Degradation products were identified by matching their retention-time with standard samples. The details of the analytical methods were described in detail previously (Namjoshi, 2015).

#### **7.2.4 Viscosity measurement**

Viscosity of DGA<sup>®</sup>/DMAEE/MAEE with variable concentration and CO<sub>2</sub> loading was measured using a Physica MCR 300 cone-and-plate rheometer (Anton Paar GmbH, Graz, Austria). The method was described in detail previously (Freeman et al., 2010b).

#### **7.2.5 CO<sub>2</sub> solubility and absorption rate**

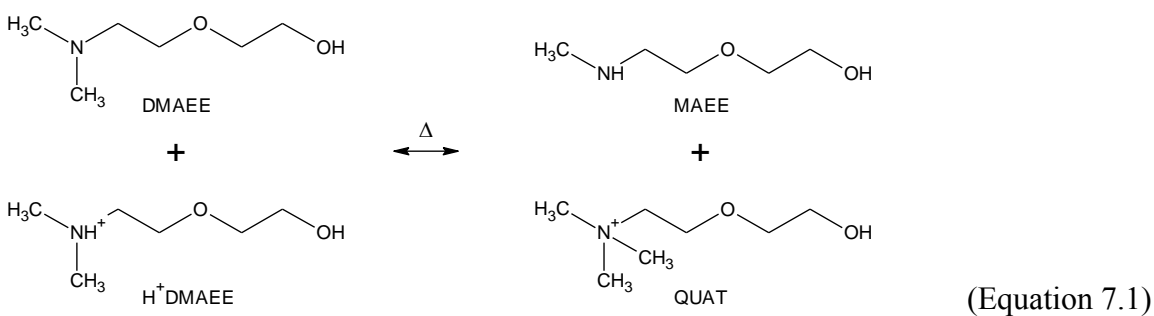
CO<sub>2</sub> equilibrium partial pressure ( $P_{CO_2^*}$ ) and absorption rate in DGA<sup>®</sup>/DMAEE/MAEE with variable concentration and CO<sub>2</sub> loading were measured at 40 °C using a wetted wall column (WWC), which counter-currently contacted an aqueous amine solution with a saturated N<sub>2</sub>/CO<sub>2</sub> stream on the surface of a stainless steel rod with a known surface area to simulate CO<sub>2</sub> absorption in an absorber. A detailed description of the wetted wall column is given in Chapter 4.

The equilibrium partial pressure ( $P_{CO_2^*}$ ) of 1.75 m DGA<sup>®</sup>/3.5 m DMAEE/1.75 m MAEE was also measured at 20, 40, and 60 °C using WWC and at high temperature (100–160 °C) using a sealed autoclave.  $P_{CO_2^*}$  measured by autoclave was calculated by subtracting the partial pressure of N<sub>2</sub> and water from the measured total pressure. The pressure of water was assumed to follow Raoult's Law and the pressure of the amine was neglected. The experimental method and calculation of CO<sub>2</sub> partial pressure were described in detail previously (Xu and Rochelle, 2011).

## 7.3 RESULTS AND DISCUSSION

### 7.3.1 Degradation of DGA<sup>®</sup> and DMAEE in Acidified Solution

Degradation in solution acidified by sulfuric acid instead of CO<sub>2</sub>, which has protonated amine but no amine carbamate, was performed to develop understanding of the mechanism for the initial degradation reaction between a free amine species and a protonated amine species. Figure 7.1 shows the degradation of 5 m DGA<sup>®</sup> and 5 m DMAEE with 0.20 mol H<sup>+</sup>/mole alkalinity (added as H<sub>2</sub>SO<sub>4</sub>) at 150 °C, along with the formation of the degradation product for 5 m DMAEE. No degradation of DGA<sup>®</sup> was observed at this condition for 2 weeks, indicating the good thermal stability of DGA<sup>®</sup>. DMAEE appears to reach equilibrium with its two degradation products. The degradation products are suspected to be MAEE and 2-[2-(methylamino)ethoxy]ethanol, a quaternary amine (QUAT), based on their retention-time on the cation chromatograph and the proposed degradation mechanism. The degradation mechanism for DMAEE in acidified solutions should be similar to other tertiary amines (Bedell et al., 2010; Namjoshi, 2015). Free DMAEE attacks protonated DMAEE (H<sup>+</sup>DMAEE), and reaches equilibrium with MAEE and QUAT (Equation 7.1).



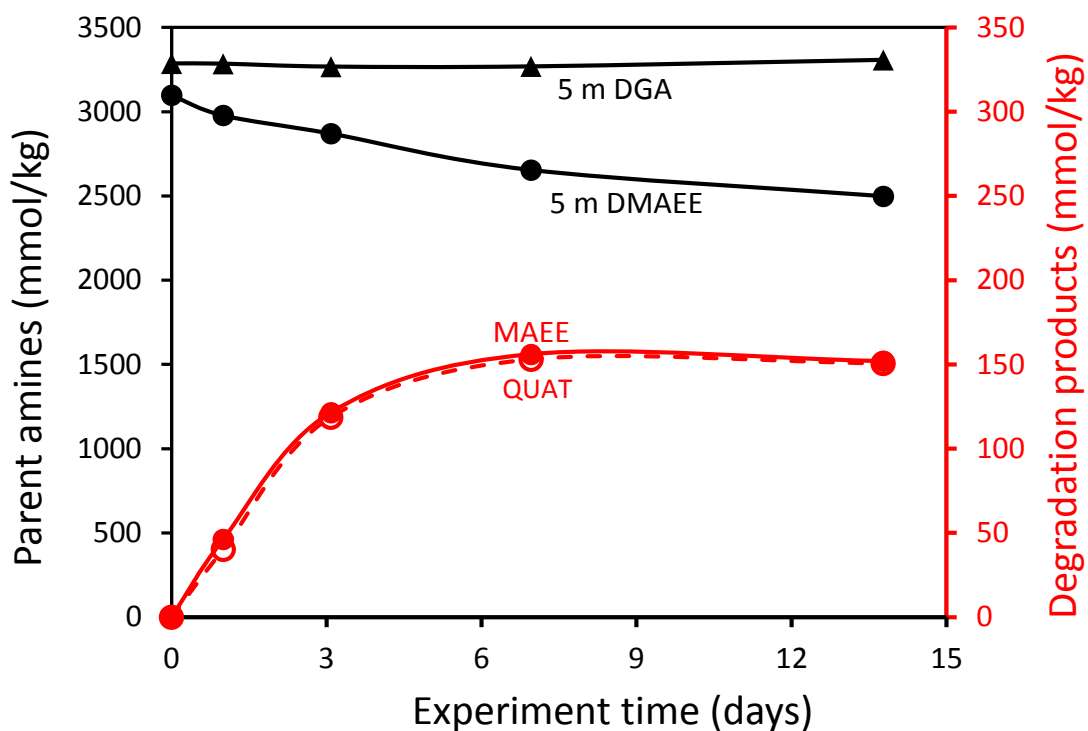


Figure 7.1: Degradation of 5 m DGA<sup>®</sup> and 5 m DMAEE with 0.2 mol H<sup>+</sup>/mole alkalinity at 150 °C, along with the formation of MAEE and QUAT for DMAEE degradation.

### 7.3.2 Degradation of DGA<sup>®</sup> in CO<sub>2</sub> Loaded Solution

Although the acid-loaded experiments are useful in understanding the initial degradation pathway of DGA<sup>®</sup>, the degradation of DGA<sup>®</sup> was also investigated in CO<sub>2</sub> loaded solutions to evaluate its thermal stability in a real CO<sub>2</sub> capture application with other side reactions caused by the formation of amine carbamate. Figure 7.2 shows the degradation of 7 m DGA<sup>®</sup> with 0.3 mol CO<sub>2</sub>/mole alkalinity at 150 °C, compared to 5 m DGA<sup>®</sup> with 0.4 mol CO<sub>2</sub>/mole alkalinity measured by Hatchell (2015) at the same temperature.

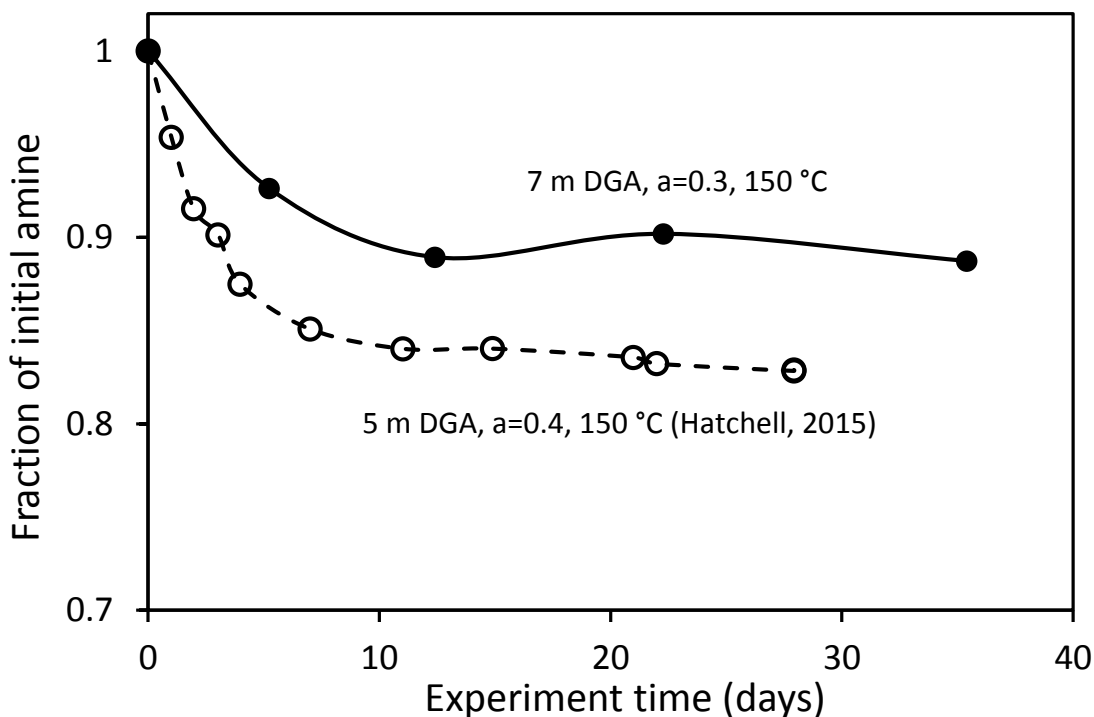
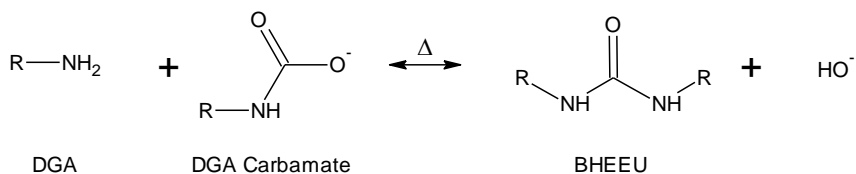
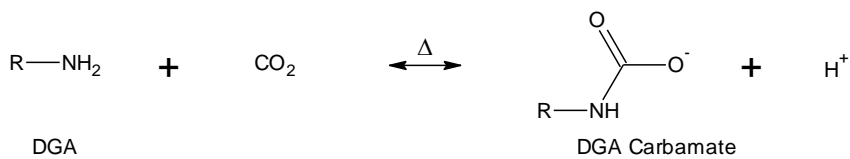


Figure 7.2: Degradation of 7 m DGA<sup>®</sup> with 0.3 mol CO<sub>2</sub>/mole alkalinity at 150 °C, compared to 5 m DGA<sup>®</sup> with 0.4 mol CO<sub>2</sub>/mole alkalinity measured by Hatchell (2015) at the same temperature.

In both cases, DGA<sup>®</sup> appears to reach equilibrium with the degradation products. Morpholine was identified as the only degradation product on cation chromatography for the degradation of 7 m DGA with 0.3 mol CO<sub>2</sub>/mole alkalinity at 150 °C. The production of morpholine only accounted for ~ 10% of the DGA loss. The majority of the lost DGA<sup>®</sup> was probably converted to N,N-bis(hydroxyethoxyethyl)urea (BHEEU), which is the predominant degradation product for CO<sub>2</sub> loaded DGA<sup>®</sup> solution (Equation 7.2) (Kohl and Nielsen, 1997).

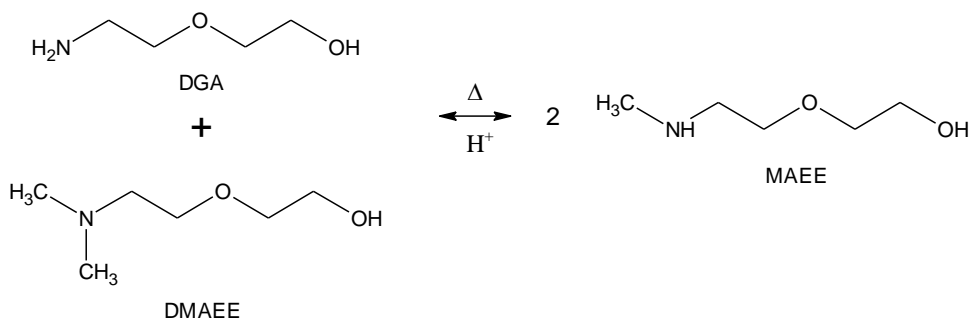


(Equation 7.2)

R in Equation 7.2 denotes HOCH<sub>2</sub>CH<sub>2</sub>OCH<sub>2</sub>CH<sub>2</sub>-.

### 7.3.3 Degradation of DGA<sup>®</sup>/DMAEE in Acidified Solution

Thermal degradation of DGA<sup>®</sup>/DMAEE with variable composition was investigated in acidified solution up to 175 °C, above expected operating conditions, to accelerate degradation in order to more easily quantify the reactions occurring. Figure 7.3 shows the degradation of 5 m DGA<sup>®</sup>/5 m DMAEE with 0.30 mol H<sup>+</sup>/mole alkalinity at 175 °C, along with the formation of the only degradation product, MAEE. DGA<sup>®</sup> and DMAEE appear to reach equilibrium with MAEE (Equation 7.3).



(7.3)

This S<sub>N</sub>2 substitution reaction is commonly referred to as “arm switching” (Bedell et al., 2010; Freeman, 2011). Based on the initial degradation pathway shown in Equation 7.3, a second-order rate model was used to fit the degradation for DGA<sup>®</sup>/DMAEE (Equation 7.4).

$$-\frac{dC_{DGA}}{dt} = -\frac{dC_{DMAEE}}{dt} = 2 * \frac{dC_{MAEE}}{dt} = k_{2,f,c} * C_{DGA} * C_{DMAEE} - k_{2,r,c} * (C_{MAEE})^2 \quad (7.4)$$

where C<sub>DGA</sub>, C<sub>DMAEE</sub>, and C<sub>MAEE</sub> are the concentration of amines; k<sub>2,f,c</sub> and k<sub>2,r,c</sub> are concentration-based second-order forward and reverse rate constants, respectively; t is the experimental time in seconds.

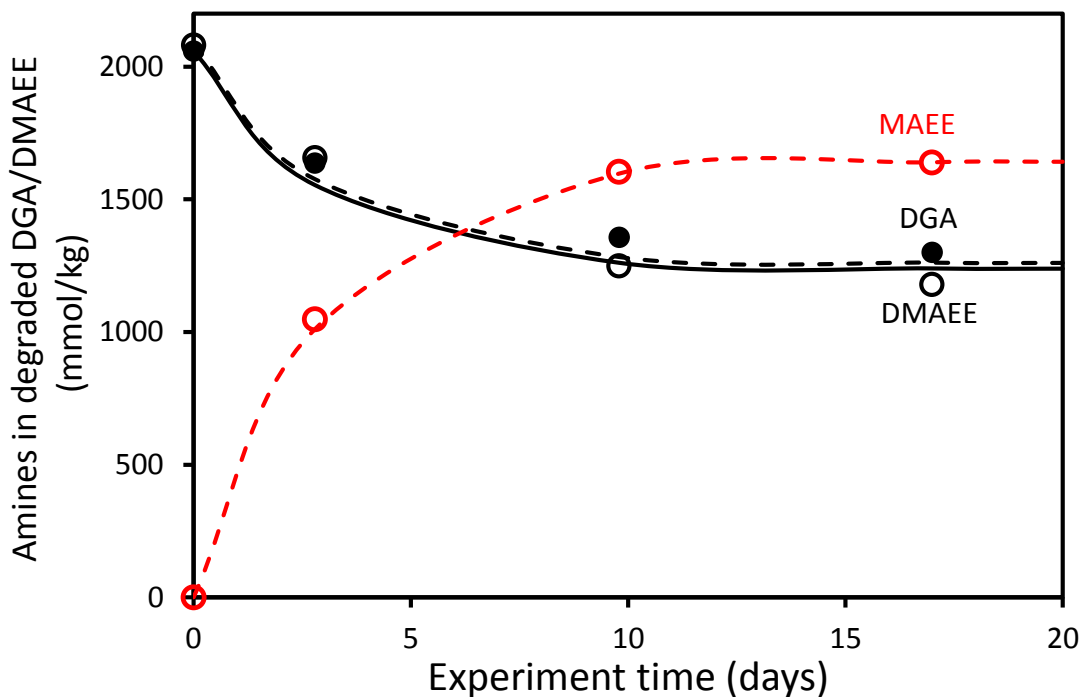


Figure 7.3: Degradation of 5 m DGA<sup>®</sup>/5 m DMAEE with 0.3 mol H<sup>+</sup>/mole alkalinity at 175 °C, along with the formation of MAEE. Lines indicate second-order reversible rate models fit the data (Equation 7.4).

Figure 7.4 shows the effect of initial DGA<sup>®</sup> to DMAEE ratio on the interconversion of DGA<sup>®</sup>, DMAEE, and MAEE (Equation 7.5) with 0.30 mol H<sup>+</sup>/mole alkalinity at 175 °C.

$$K_t = \frac{[MAEE]^2}{[DGA] * [DMAEE]} \quad (7.5)$$

K<sub>t</sub> is the ratio of products to reactants at time t. K<sub>t</sub> for 2.5 m DGA<sup>®</sup>/7.5 m DMAEE and 5 m DGA<sup>®</sup>/5 m DMAEE tend toward a value of 1.7 at equilibrium (when K<sub>t</sub>= K<sub>eq</sub>, the equilibrium constant), while K<sub>t</sub> for 7.5 m DGA<sup>®</sup>/2.5 m DMAEE tends toward a value of 1.1. The lower K<sub>eq</sub> in 7.5 m DGA<sup>®</sup>/2.5 m DMAEE may result from the degradation of DGA<sup>®</sup> to morpholine.

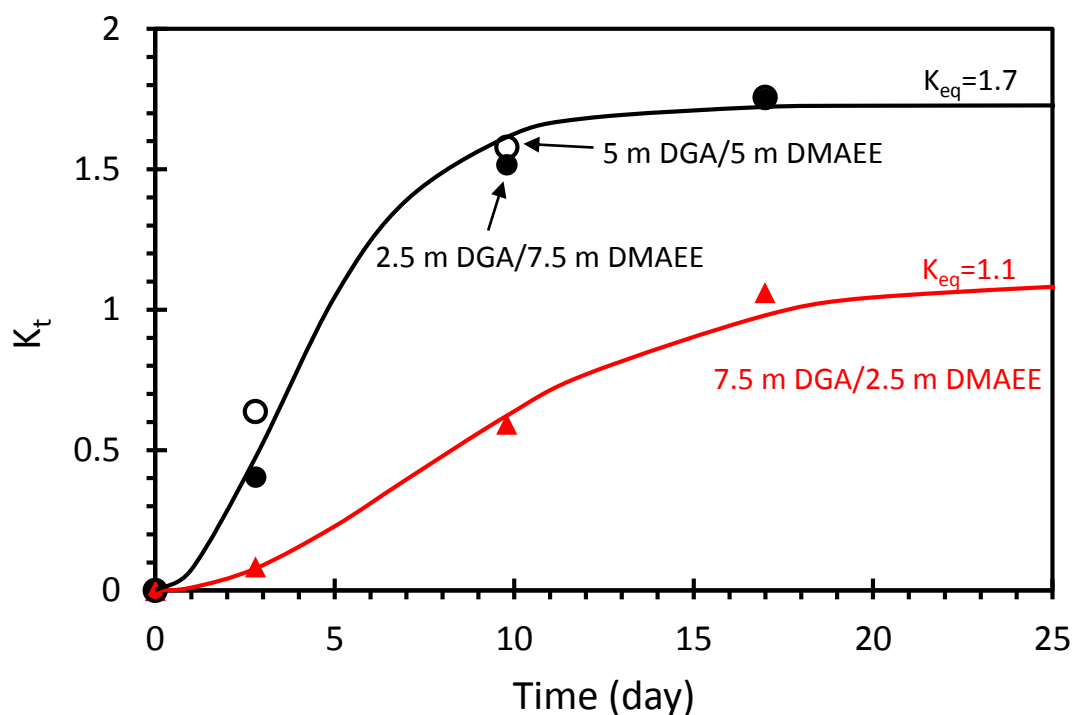


Figure 7.4:  $K_t$  for DGA<sup>®</sup>/DMAEE/MAEE thermally degraded at 175 °C ( $\alpha_H=0.3$ ). points are experimental  $K_t$ ; Lines indicate second-order reversible rate models fit the data (Equation 7.5).

### 7.3.4 Degradation of DGA<sup>®</sup>/DMAEE in CO<sub>2</sub>-loaded solution

Figure 7.5 shows the degradation of 5 m DGA<sup>®</sup>/5 m DMAEE with 0.4 mol CO<sub>2</sub>/mole alkalinity at 150 °C, along with the formation of the degradation products. Similar to that in acidified solution, DGA<sup>®</sup> and DMAEE in CO<sub>2</sub> loaded solution also reach equilibrium with its major degradation product, MAEE (Equation 7.3). Two minor products, which were not identified in acidified solution, were present in the CO<sub>2</sub>-loaded DGA<sup>®</sup>/DMAEE. One of them was identified as 1-methylmorpholine (1M-Morph), and the other one was QUAT. BHEEU, as the major degradation product for DGA in CO<sub>2</sub> loaded solution (Kohl and Nielsen, 1997), should also be present in the solution.

The second-order reversible rate model (Equation 7.4) under-predicted the loss of DGA<sup>®</sup> and DMAEE, while over-predicted the production of MAEE, as a result of the formation of BHEEU, 1M-Morph and QAUT.  $K_{eq}$  for 5 m DGA<sup>®</sup>/5 m DMAEE (Equation 7.4) in CO<sub>2</sub> loaded solutions was found to be from 0.4 to 1.0, depending on the CO<sub>2</sub> loading and temperature, which is significantly smaller than that in acidified solutions.

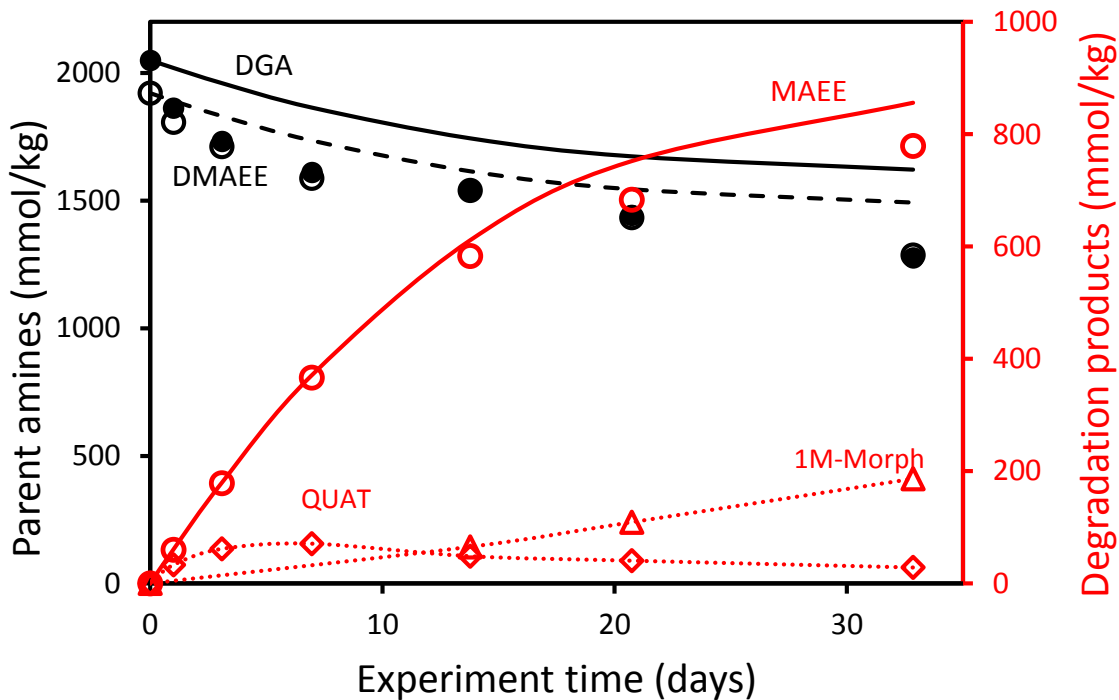


Figure 7.5: Degradation of 5 m DGA<sup>®</sup>/5 m DMAEE with 0.4 mol CO<sub>2</sub>/mole alkalinity at 150 °C, along with the formation of MAEE and other minor products. Solid lines and dashed line indicate second-order reversible rate models fit the data (Equation 7.4).

### 7.3.5 Loss of effective amine in degraded DGA<sup>®</sup>/DMAEE

Figure 7.6 compares the loss of effective amine for 5 m DGA<sup>®</sup>/5 m DMAEE (MAEE is considered an effective amine for CO<sub>2</sub> absorption) to 7 m MEA with 0.4 mol CO<sub>2</sub>/mole alkalinity at 150 °C (Davis and Rochelle, 2009). The sum of DGA<sup>®</sup>,

DMAEE, and MAEE decreased by 6% within one day and then maintained a constant value for the next 3 weeks. 1M-Morph and QAUT accounted for ~ 35% of the loss of the effective amine, while BHEEU may accounted for the rest. However, the degradation of MEA followed a first order rate model, and lost 60% of its initial amine within 2 weeks.

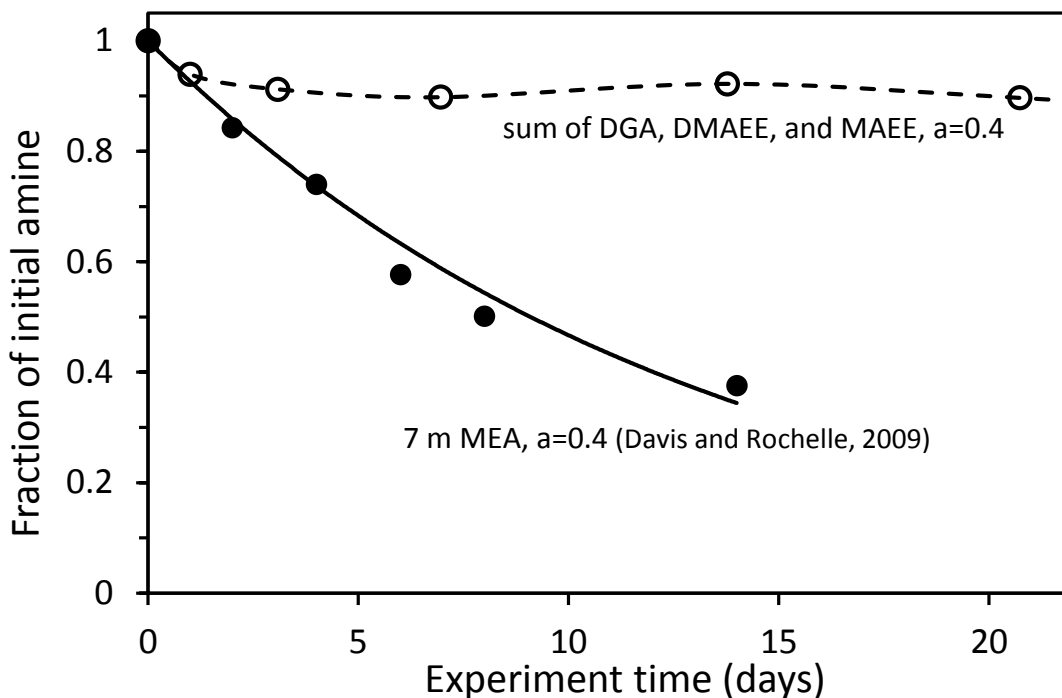


Figure 7.6: Comparison of the loss of effective amine for 5 m DGA<sup>®</sup>/5 m DMAEE to 7 m MEA with 0.4 mol CO<sub>2</sub>/mole alkalinity at 150 °C (Davis and Rochelle, 2009). The solid line indicates a first-order rate model fit the data.

### 7.3.6 CO<sub>2</sub> Cyclic Capacity and Absorption Rate

Based on the thermal degradation of DGA<sup>®</sup>/DMAEE in CO<sub>2</sub> loaded solutions, a  $K_{eq}$  of 0.5 was chose to to evaluate the CO<sub>2</sub> cyclic capacity and absorption rate for DGA<sup>®</sup>/DMAEE/MAEE. CO<sub>2</sub> equilibrium partial pressure ( $P_{CO_2^*}$ ) and absorption rate in DGA<sup>®</sup>/DMAEE/MAEE with five different compositions were measured at 40 °C using a wetted wall column (WWC). Due to the lack of a commercial source for a large

quantity of MAEE, 2-(methylamino)ethanol (MAE), which is a secondary amine with similar structure and pKa to MAEE, was used as a proxy for MAEE for evaluation.

The CO<sub>2</sub> cyclic capacity of a solvent ( $\Delta C_{solv}$ ) is defined as the difference in CO<sub>2</sub> concentration between the lean and rich solvents (Equation 7.6).

$$\Delta C_{solv} = \frac{C_{rich} - C_{lean}}{kg (amine + water)} = \frac{mol CO_2}{kg} \quad (7.6)$$

$C_{lean}$  and  $C_{rich}$  are the CO<sub>2</sub> concentration of lean and rich solvents. For coal-fired flue gas, the normal operational lean and rich solvents correspond to  $P_{CO_2}^*$  of 0.5 kPa and 5 kPa at 40 °C, respectively, in order to maintain enough driving force for CO<sub>2</sub> absorption throughout the absorber.  $\Delta C_{solv}$  is normalized by the viscosity of the solvent to consider the effect of viscosity on the optimized heat exchanger cost (Equation 7.7) (L. Li et al., 2013b), based on the observation that the heat transfer coefficient generally depends on solvent viscosity to about -0.35 power (Ayub, 2003).

$$\Delta C_{\mu} = \Delta C_{solv} / (\mu_{mid} / \mu_{7m MEA})^{0.175} \quad (7.7)$$

$\mu_{mid}$  and  $\mu_{7m MEA}$  are the viscosities of the studied amine and 7 m MEA, respectively, at mid-loading ( $P_{CO_2}^* = 2.0$  kPa) and 40 °C.

$k_g'$  is defined as the liquid film mass transfer coefficient on a partial pressure basis, and is calculated as the ratio of CO<sub>2</sub> flux to the liquid film partial pressure driving force. For each solvent,  $k_g'_{avg}$  is calculated for an isothermal absorber at 40 °C for coal flue gas and 90% CO<sub>2</sub> removal (Equation 7.8), assuming a linear concentration profile and equilibrium curve in the absorber, and negligible gas film resistance (L. Li et al., 2013b).

$$k_g'_{avg} = \frac{Flux_{CO_2, LM}}{(P_{CO_2} - P_{CO_2}^*)_{LM}} = \frac{(Flux_{CO_2, top} - Flux_{CO_2, bottom}) / \ln(Flux_{CO_2, top} / Flux_{CO_2, bottom})}{(P_{CO_2, top} - P_{CO_2, lean}^*) - (P_{CO_2, bottom} - P_{CO_2, rich}^*) / \ln\left(\frac{P_{CO_2, top} - P_{CO_2, lean}^*}{P_{CO_2, bottom} - P_{CO_2, rich}^*}\right)} \quad (7.8)$$

The  $P_{CO_2}$  at the bottom and top of the absorber are 12 and 1.2 kPa, the rich and lean  $P_{CO_2}^*$  are 5 and 0.5 kPa. Experimental values at 40 °C are used to interpolate  $k_g'$  that corresponds to  $P_{CO_2}^*$  at 5 and 0.5 kPa, which are then used to calculate the corresponding flux.

Figure 7.7 and Table 7.1 show the normalized  $CO_2$  cyclic capacity ( $\Delta C_\mu$ ) and average  $CO_2$  absorption rate ( $k_g'_{avg}$ ) at 40 °C for DGA<sup>®</sup>/DMAEE/MAE at variable composition, compared to 7 m MEA, 10 m DGA<sup>®</sup>, and 5 m PZ. 2.1 m DGA<sup>®</sup>/4.9 m DMAEE shows a comparable  $\Delta C_\mu$  to 5 m PZ, which is substantially larger than that of 7 m MEA and 10 m DGA<sup>®</sup>. However, the  $k_g'_{avg}$  of 2.1 m DGA<sup>®</sup>/4.9 m DMAEE is slightly lower than 7 m MEA. Replacing some DGA<sup>®</sup> and DMAEE with MAE increases the  $k_g'_{avg}$  significantly.  $k_g'_{avg}$  of the four DGA<sup>®</sup>/DMAEE/MAE solvents tested in this work is 30-70% higher than that of 7 m MEA, but it is still much lower than that of 5 m PZ. Although 2.5 m DGA<sup>®</sup>/2.5 m MAE/5.0 m DMAEE and 1.07 m DGA<sup>®</sup>/1.93 m MAE/7 m DMAEE absorb  $CO_2$  faster than the other DGA<sup>®</sup>/MAE/DMAEE with total alkalinity of 7 m, as a result of the higher concentration of MAE, their  $\Delta C_\mu$  are smaller, due to higher viscosity.

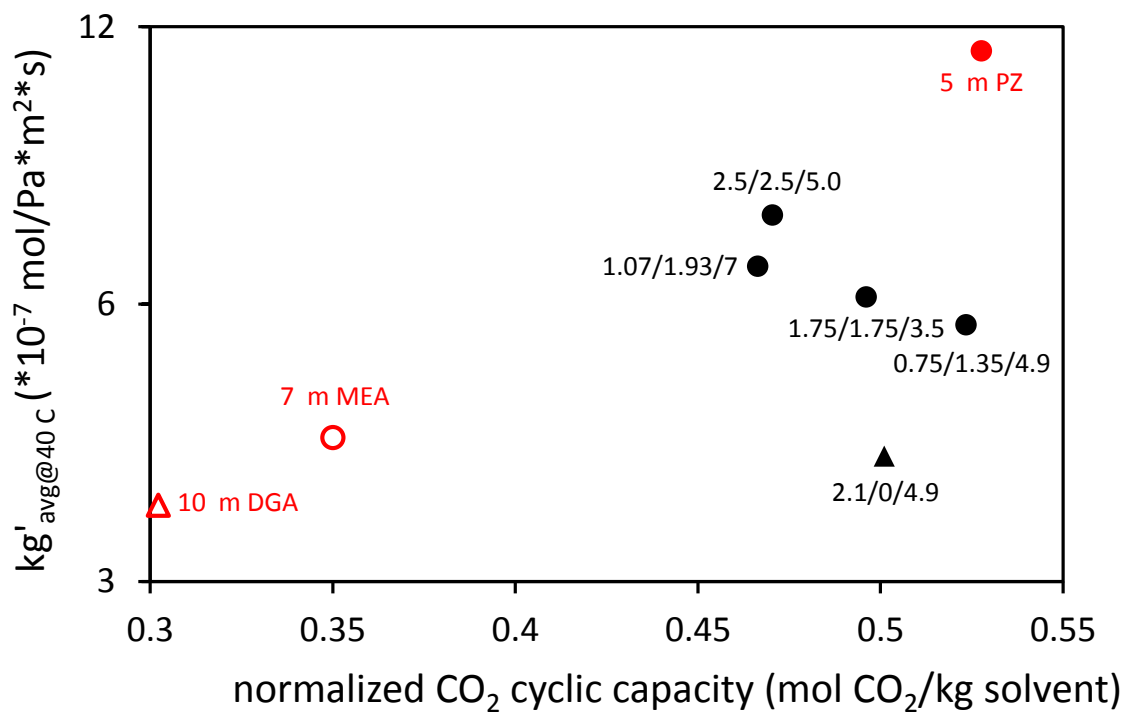


Figure 7.7: CO<sub>2</sub> cyclic capacity and average absorption rate (kg'avg) at 40 °C for DGA<sup>®</sup>/MAE/DMAEE with variable concentration, compared to 7 m MEA, 10 m DGA<sup>®</sup>, and 5 m PZ. Labels indicate the concentrations of DGA<sup>®</sup>, MAE, and DMAEE in solution in molal (m).

Table 7.1: Properties of DGA<sup>®</sup>/MAE/DMAEE solvents with variable concentration, compared to 7 m MEA, 10 m DGA<sup>®</sup>, and 5 m PZ.

Amine (m)			$\mu_{mid}$ (cP)	$\Delta C_{solv}$ (mol/kg)	$\Delta C_{\mu}^b$ (mol/kg)	$k_g'_{avg-40\text{ }^\circ\text{C}}$ ( $10^{-6}$ mol/Pa*m <sup>2</sup> *s)
DGA <sup>®</sup>	MAE <sup>a</sup>	DMAEE				
2.50	2.50	5.00	7.3	0.56	0.47	0.66
1.07	1.93	7.00	8.1	0.57	0.47	0.75
1.75	1.75	3.50	5.4	0.56	0.50	0.61
0.75	1.35	4.90	5.1	0.59	0.52	0.57
2.10		4.90	5.1	0.56	0.50	0.41
10 <sup>c</sup>			10.0	0.38	0.30	0.36
	7 m MEA <sup>d</sup>		2.7	0.35	0.35	0.43
	5 m PZ <sup>d</sup>		4.2	0.57	0.53	1.13

a: MAE was used as a proxy for MAEE

b:  $\Delta C_{\mu} = \Delta C_{solv} / (\mu_{mid} / \mu_{7\text{ m MEA}})^{0.175}$

c: from (Li, 2015)

d: from (Dugas, 2009)

### 7.3.7 CO<sub>2</sub> Solubility in 1.75 m DGA<sup>®</sup>/1.75 m MAEE/3.50 m DMAEE at 20 – 160 °C

Figure 7.8 shows the vapor liquid equilibrium (VLE) of CO<sub>2</sub> in 1.75 m DGA<sup>®</sup>/1.75 m MAE (as a proxy for MAEE)/3.50 m DMAEE at 20–160 °C. CO<sub>2</sub> equilibrium partial pressure, P<sub>CO<sub>2</sub>\*</sub> (Pa), was regressed using the following semi-empirical model (Equation 7.9) as a function of temperature, T (K), and CO<sub>2</sub> loading,  $\alpha$  (mol CO<sub>2</sub>/mol alkalinity), in the liquid phase.

$$\ln P_{CO_2}^* = 35 - 10212 \cdot \frac{1}{T} + 4777 \cdot \frac{\alpha}{T} \quad (7.9)$$

The heat of CO<sub>2</sub> absorption ( $\Delta H_{abs}$ ) for 1.75 m DGA<sup>®</sup>/1.75 m MAE/3.50 m DMAEE can be extracted from the equilibrium data by applying the fundamental thermodynamic relationship to the semi-empirical model (Equation 7.10):

$$-\Delta H_{abs} = R \cdot \left( \frac{\partial \ln(P_{CO_2}^*)}{\partial (1/T)} \right)_{P,x} = -10212 + 4777 \cdot \alpha \quad (7.10)$$

$\Delta H_{abs}$  for 1.75 m DGA<sup>®</sup>/1.75 m MAE/3.50 m DMAEE at CO<sub>2</sub> loading corresponding to a  $P_{CO_2}^*$  of 1.5 kPa at 40 °C is 72 kJ/mol, which is comparable to 7 m MEA (71 kJ/mol), and higher than 5 m PZ (64 kJ/mol) (L. Li et al., 2013b).

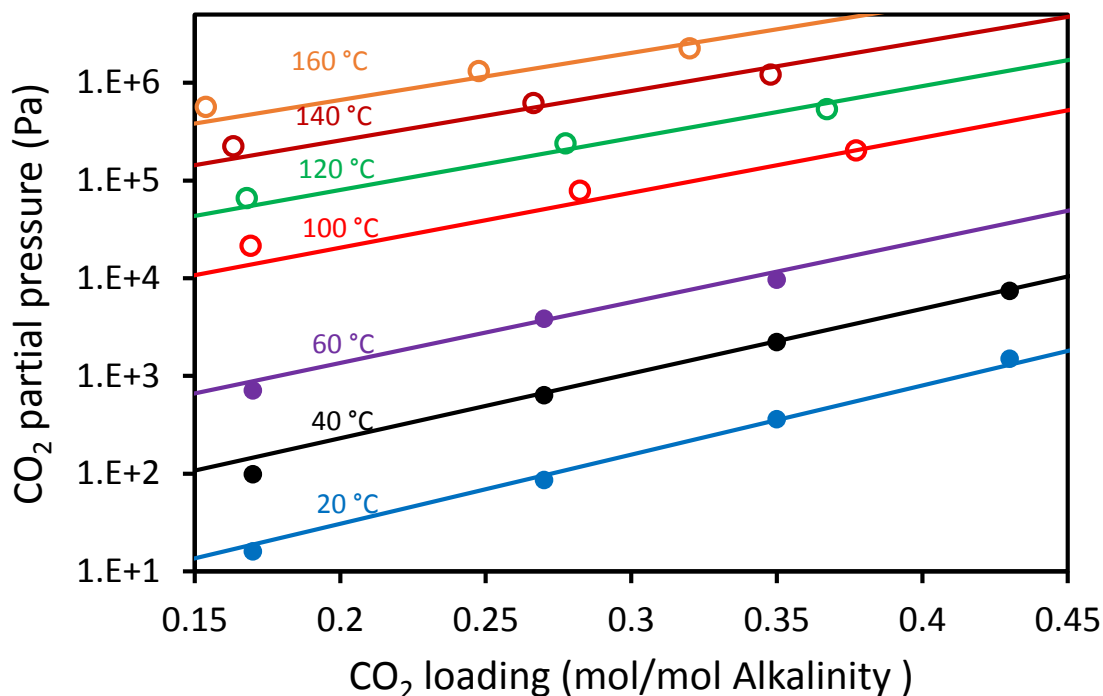


Figure 7.8: CO<sub>2</sub> solubility in 1.75 m DGA<sup>®</sup>/1.75 m MAE (as a proxy for MAEE)/3.50 m DMAEE. Solid points: WWC results; open points: total pressure results; lines: model prediction (Equation 7.9).

#### 7.4 CONCLUSIONS

Thermally degraded DGA<sup>®</sup>/DMAEE is a superior solvent for CO<sub>2</sub> capture from flue gas. At high temperature, DGA<sup>®</sup>/DMAEE reaches equilibrium with its major degradation product, MAEE. When starting with 5 m DGA<sup>®</sup>/5 m DMAEE with 0.4 mol CO<sub>2</sub>/mole alkalinity, the sum of DGA<sup>®</sup>, DMAEE, and MAEE decreased by 6% within one day at 150 °C, and then maintained a constant value for the next 3 weeks. At the same condition, MEA lost 60% of its initial amine within 2 weeks.

The production of MAEE from the thermal degradation of DGA<sup>®</sup>/DMAEE enhances the CO<sub>2</sub> absorption rate, while maintaining the CO<sub>2</sub> capacity of the original solvent. The normalized CO<sub>2</sub> cyclic capacity ( $\Delta C_{\mu}$ ) of DGA<sup>®</sup>/MAEE/DMAEE is

substantially larger than that of 7 m MEA and 10 m DGA<sup>®</sup>, and comparable to 5 m PZ. The average CO<sub>2</sub> absorption rate ( $k_g'_{avg}$ ) of DGA<sup>®</sup>/MAEE/DMAEE is 30-70% higher than 7 m MEA, although it is still much lower than 5 m PZ.

The heat of CO<sub>2</sub> absorption ( $\Delta H_{abs}$ ) for 1.75 m DGA<sup>®</sup>/1.75 m MAEE/3.50 m DMAEE at CO<sub>2</sub> loading corresponding to a  $P_{CO_2^*}$  of 1.5 kPa at 40 °C is 72 kJ/mol, which is comparable to 7 m MEA, and greater than 5 m PZ.

The capital and energy cost for flue gas CO<sub>2</sub> capture using thermally degraded DGA<sup>®</sup>/DMAEE is expected to be much lower than that using 7 m MEA, while still higher than that using 5 m PZ.

## **7.5 RECOMMENDATIONS**

A better way to evaluate this solvent is to synthesis MAEE from DGA<sup>®</sup>/DMAEE, instead of using MAE as a proxy for MAEE. M-Morph, which is a minor degradation product for DGA<sup>®</sup>/DMAEE, has high volatility (Chapter 3). The emission of M-Morph should be addressed before application. The oxidative stability of DGA<sup>®</sup>/DMAEE should be evaluated. Although DGA<sup>®</sup> itself oxidatively degrades, DMAEE, as a tertiary amine is expected to inhibit oxidation. Other properties for CO<sub>2</sub> capture should be measured for this solvent, such as corrosivity and foam formation. As DGA<sup>®</sup> is widely used in commercial gas treating plants, it is convenient to directly add DMAEE to validate the enhanced absorption capacity and rate.

## **7.6 ACKNOWLEDGEMENTS**

The author gratefully acknowledges Ye Yuan for measuring the CO<sub>2</sub> solubility in 1.75 m DGA<sup>®</sup>/1.75 m MAEE/3.50 m DMAEE at 20 - 160 °C.

The author gratefully acknowledges Yukai Wang for helping measuring thermal degradation of DGA<sup>®</sup>/DMAEE.

## Chapter 8: Conclusions and Recommendations

### 8.1 CONCLUSIONS

#### Amine Screening for Thermal Degradation

In this study, 36 novel piperazine (PZ)-based amine blends were investigated for their thermal stability for CO<sub>2</sub> capture. 18 of them were found to be resistant to thermal degradation with  $T_{\max}$  greater than 140 °C. These included PZ blends with five imidazoles, six diamines, five tertiary amines, and two ether amines. Although imidazole itself is not stable in the presence of PZ, CO<sub>2</sub>, or proton, imidazoles with electron-donating substituents at C-2 and N-1 positions are resistant to thermal degradation even in the presence of PZ and CO<sub>2</sub>. The ring opening of imidazole can be catalyzed by either acid or base. Diamines show high thermal stability in blends with PZ, unless they can form cyclic urea. 6-membered cyclic tertiary amines are resistant to thermal degradation, except for triethylenediamine (TEDA) which goes through polymerization initiated by PZ and itself when protonated. 2-(Diisopropylamino)ethanol (DIPAE) is the only acyclic tertiary amine that is thermally stable when blended with PZ. The thermal stability of DIPAE probably results from the steric hindrance caused by the two isopropyl groups. A single additional methyl group at  $\alpha$ -carbon, or substitutions at  $\beta$ -carbon are not sufficient to prevent the amine from carbamate formation. An additional –OH group decreases the thermal stability of the amine by making it more likely to form oxazolidone. PZ blended with K<sup>+</sup>/ L-proline and K<sup>+</sup>/4-hydroxy-L-proline was resistant to thermal degradation, while PZ blended with K<sup>+</sup>/ N,N-dimethylglycine degraded rapidly due to the demethylation of N,N-dimethylglycine by PZ. Ether amines are more stable than their alkanolamines counterparts, because ether amines cannot form oxazolidone as easily as alkanolamines.

#### Amine Screening for Volatility

The Henry's law constant ( $H_{am}$ ) of 24 novel amines, including 18 tertiary amines, 3 hindered amines, 2 ether amines, and 1 pyridine derivative was measured at 40 °C using a hot gas FTIR. 14 have  $H_{am}$  lower than 2-amino-2-methyl-1-propanol (AMP).

A group contribution model that correlates  $H_{am}$  to molecular structure was developed based on the data from this work and data from literature. Non-cyclic groups and cyclic groups show a significant effect on the amine volatility.

The amine partial pressure ( $P_{am}$ ) of 2.5 m tertiary and hindered amines was also measured in a blend with 2.5 m PZ at 40 °C and their normal CO<sub>2</sub> loading range for flue gas CO<sub>2</sub> capture. With increased  $pK_a$ , the  $P_{am}$  of tertiary and hindered amines becomes a stronger function of CO<sub>2</sub> loading. A correlation has been found between the  $H_{am}$  of tertiary and hindered amines and their  $P_{am}$  in a blend with PZ at nominal lean CO<sub>2</sub> loading condition coal-fired flue gas (~ 0.5 kPa) and 40 °C, which are the standard operating conditions at the top of the absorber where volatility is of greatest concern.

#### **Amine Screening for CO<sub>2</sub> Capacity and Absorption Rate**

The optimum  $pK_a$  of the 2.5 m tertiary amine with 2.5 m PZ was found to be around 9.1 to give the greatest CO<sub>2</sub> cyclic capacity.

A generic Aspen Plus model for PZ/tertiary amine was developed based on a rigorous Aspen Plus® model for PZ/MDEA with electrolyte-Nonrandom Two-Liquid (e-NRTL) as the thermodynamic framework. This generic model can reasonably predict the CO<sub>2</sub> vapor-liquid-equilibrium (VLE) in PZ/tertiary amine based on the  $pK_a$  of the tertiary amine.

To a lesser degree than  $pK_a$ , the polarity of the tertiary amine also affects the CO<sub>2</sub> solubility of the PZ/tertiary amine.

Hindered amines that form little carbamate mainly act as pH buffers in PZ/hindered amine, giving similar CO<sub>2</sub> VLE to PZ/tertiary amine with the same pK<sub>a</sub> and similar polarity.

CO<sub>2</sub> absorption rate of most 2.5 m PZ/2.5 m tertiary amine was found to be slightly slower than 2.5 m PZ itself, probably due to the higher viscosity of the blend. 2.5 m PZ/2.5 m tertiary amine still absorb CO<sub>2</sub> much faster than 7 m MEA.

2.5 m PZ/2.5 m HMPD shows the best overall performance for flue gas CO<sub>2</sub> capture, high thermal stability, low amine volatility, large  $\Delta C_{\mu}$ , and high  $k_g'_{avg}$ .

### **Thermal Degradation of Piperazine/4-Hydroxy-1-methylpiperidine**

At high temperature PZ and HMPD reach equilibrium with the major degradation products, 1MPZ and HPD, by “arm switching”.  $K_{eq2}$  for PZ/HMPD/1MPZ/HPD tends toward a value of 2.1 at 150 °C.

Over 81% of nitrogen lost in degraded PZ/HMPD was recovered in seven quantified degradation products, with 1MPZ and HPD accounting for 54% of nitrogen lost.

A second-order rate model consistent with proposed degradation pathways can model initial degradation reasonably well. The concentration-based second-order rate constant,  $k_{2,f,c}$ , depends on the total amine concentration and, to a lesser extent, the PZ to HMPD ratio. The increase of CO<sub>2</sub> loading and temperature accelerate the degradation of PZ/HMPD. The activation energy of PZ/HMPD degradation is 162 kJ/mol.

5 m PZ/5 m HMPD is significantly more stable than 5 m PZ/5 m MDEA in the presence of CO<sub>2</sub>. The first-order rate constants for PZ and tertiary amine degradation in 5 m PZ/5 m HMPD are 7 and 3.5 times smaller than that in 5 m PZ/5 m MDEA, respectively.

The significantly greater stability of PZ/HMPD in comparison with PZ/MDEA is due to the remarkable thermal stability of HMPD which prevents PZ from further degradation, the smaller initial degradation rate of PZ/HMPD, and the greater thermal stability of HMPD compared to MDEA.

The equilibrium concentration of 1,4 DMPZ in degraded 2 m PZ/3 m HMPD at 150 °C is estimated to be 0.4 molal (m) leading to a partial pressure of 100 ppm at 40 °C. The potential environmental issues caused by the volatile 1,4 DMPZ need to be addressed for commercial application of this solvent.

#### **Piperazine/4-Hydroxy-1-methylpiperidine for CO<sub>2</sub> Capture**

2 m PZ/3 m HMPD is a superior solvent for CO<sub>2</sub> capture from flue gas. Its CO<sub>2</sub> cyclic capacity and CO<sub>2</sub> absorption rate are more than twice that of 7 m MEA. This blend also shows much greater resistance to oxidative degradation than MEA at the same condition, as well as lower amine volatility. When compared to 5 m PZ, 2 m PZ/3 m HMPD has a 40% higher CO<sub>2</sub> cyclic capacity, while 10% lower rate and 10% higher viscosity. 2 m PZ/3 m HMPD also has a much better solid solubility than 5 m PZ, showing no precipitation down to -10 °C at normal CO<sub>2</sub> loading range. The heat of CO<sub>2</sub> absorption for 2 m PZ/3 m HMPD is 69 kJ/mol, which is higher than 5 m PZ (64 kJ/mol) but slightly lower than 7 m MEA (71 kJ/mol). The capital and energy cost for flue gas CO<sub>2</sub> capture using 2 m PZ/3 m HMPD is expected to be much lower than that using 7 m MEA, while comparable to that using 5 m PZ. Although the cost of production for HMPD is currently too high for commercial application of this solvent for CO<sub>2</sub> capture, it can be significantly reduced by choosing proper synthesis routes.

#### **Thermally Degraded Diglycolamine<sup>®</sup>/Dimethylaminoethoxyethanol for CO<sub>2</sub> Capture**

Thermally degraded DGA<sup>®</sup>/DMAEE is a superior solvent for CO<sub>2</sub> capture from flue gas. At high temperature, DGA<sup>®</sup>/DMAEE reaches equilibrium with its major degradation product, MAEE. When starting with 5 m DGA<sup>®</sup>/5 m DMAEE with 0.4 mol CO<sub>2</sub>/mole alkalinity, the sum of DGA<sup>®</sup>, DMAEE, and MAEE decreased by 6% within one day at 150 °C, and then maintained a constant value for the next 3 weeks. At the same condition, MEA lost 60% of its initial amine within 2 weeks.

The production of MAEE from the thermal degradation of DGA<sup>®</sup>/DMAEE enhances the CO<sub>2</sub> absorption rate, while maintaining the CO<sub>2</sub> capacity of the original solvent. The normalized CO<sub>2</sub> cyclic capacity ( $\Delta C_{\mu}$ ) of DGA<sup>®</sup>/MAEE/DMAEE is substantially larger than that of 7 m MEA and 10 m DGA<sup>®</sup>, and comparable to 5 m PZ. The average CO<sub>2</sub> absorption rate ( $k_g'_{avg}$ ) of DGA<sup>®</sup>/MAEE/DMAEE is 30-70% higher than 7 m MEA, although it is still much lower than 5 m PZ.

The heat of CO<sub>2</sub> absorption ( $\Delta H_{abs}$ ) for 1.75 m DGA<sup>®</sup>/1.75 m MAEE/3.50 m DMAEE at CO<sub>2</sub> loading corresponding to a  $P_{CO_2^*}$  of 1.5 kPa at 40 °C is 72 kJ/mol, which is comparable to 7 m MEA, and greater than 5 m PZ.

The capital and energy cost for flue gas CO<sub>2</sub> capture using thermally degraded DGA<sup>®</sup>/DMAEE is expected to be much lower than that using 7 m MEA, while still higher than that using 5 m PZ.

## **8.2 RECOMMENDATIONS**

### **Amine Screening for Thermal Degradation**

Imidazole should be analyzed by Liquid Chromatography–Mass Spectrometry (LC/MS) to give a more accurate degradation rate. The suspected degradation products from PZ/imidazoles (aldehyde and glyoxal) should be analyzed by High Performance Liquid Chromatography (HPLC) to support the proposed degradation pathway (Equation

2.4). The solid produced from the degradation of PZ/triethylenediamine (TEDA) should be analyzed by X-ray Powder Diffraction (XRD) or other suitable tools to support the proposed degradation pathways (Equation 2.9 and 2.10). The products from the degradation of PZ/proline and PZ/4-hydroxy-L-proline should be analyzed by HPLC or LC/MS to understand the degradation pathway of these two amino acids in the presence of PZ. Ureas should be determined in solvents such as diglycolamine<sup>®</sup> (DGA<sup>®</sup>) where they are known to be important.

#### **Amine Screening for Volatility**

More amines with aromatic structure and intramolecular hydrogen-bonding should be measured. The different ability to form intramolecular hydrogen-bond should be considered to improve the reliability of the updated group contribution for volatility prediction.

#### **Amine Screening for CO<sub>2</sub> Capacity and Absorption Rate**

The effect of polarity and viscosity on CO<sub>2</sub> absorption rate should be further investigated.

#### **Thermal Degradation of Piperazine/4-Hydroxy-1-methylpiperidine**

The suspected minor degradation products should be analysed by LC/MS or IC/MS to support the proposed degradation pathways. The degradation pathway to produce MEA and 1-EPZ from PZ/ HMPD need to be explored.

#### **Piperazine/4-Hydroxy-1-methylpiperidine for CO<sub>2</sub> Capture**

Other properties for CO<sub>2</sub> capture should be measured for this solvent, such as corrosivity and foam formation. The synthesis method for HMPD should be investigated to lower the cost of production for HMPD. The solvent needs to be tested in a pilot plant to validate its properties measured at lab scale.

## **Thermally Degraded Diglycolamine<sup>®</sup>/Dimethylaminoethoxyethanol for CO<sub>2</sub> Capture**

A better way to evaluate this solvent is to synthesis MAEE from DGA<sup>®</sup>/DMAEE, instead of using MAE as a proxy for MAEE. M-Morph, which is a minor degradation product for DGA<sup>®</sup>/DMAEE, has high volatility. The emission of M-Morph should be addressed before application. The oxidative stability of DGA<sup>®</sup>/DMAEE should be evaluated. Although DGA<sup>®</sup> itself oxidatively degrades, DMAEE, as a tertiary amine is expected to inhibit oxidation. Other properties for CO<sub>2</sub> capture should be measured for this solvent, such as corrosivity and foam formation. As DGA<sup>®</sup> is widely used in commercial gas treating plants, it is convenient to directly add DMAEE to validate the enhanced absorption capacity and rate.

## Appendix A: Thermal Degradation Data for Chapter 2

The following tables give the detailed thermal degradation data for 2 m PZ/2 m other amines with 0.2 mol CO<sub>2</sub>/mole alkalinity at 150 and 175 °C.

Table A.1: Thermal degradation of 2 m PZ/2 m imidazoles with 0.2 mol CO<sub>2</sub>/mole alkalinity.

Amine (blended with PZ)	Structure	Amine left (Initial Conc.=1.00)							
		150 °C				175 °C			
		PZ		Am		PZ		Am	
		7 d	14 d	7 d	14 d	3 d	7 d	3 d	7 d
Imidazole (IMI)		0.91	0.84	— <sup>a</sup>		0.81	0.65	— <sup>a</sup>	
1-Methylimidazole (1M-IMI)		0.97	0.97	0.93	0.95	0.94	0.90	0.93	0.94
2-Methylimidazole (2M-IMI)		— <sup>b</sup>		0.97	0.96	— <sup>b</sup>	0.97	0.96	0.93
4(5)-Methylimidazole (4M-IMI)		0.96	0.96	0.90	0.87	0.92	0.88	0.83	0.77
2-Ethylimidazole (2E-IMI)			— <sup>b</sup>		0.96	0.97	0.97	— <sup>b</sup>	0.92
1,2-Dimethylimidazole (1,2-DIMI)				— <sup>b</sup>		0.96	0.96	— <sup>b</sup>	
2-Ethyl 4-methylimidazole (2E-4M-IMI)					— <sup>b</sup>				0.94

a: the signal in cation chromatography is too weak to be sufficiently quantified

b: amine loss is too small to be sufficiently quantified, based on the assumption that the combined error is about ±3.5% (Namjoshi, 2015)

Table A.2: Thermal degradation of 2 m PZ/2 m diamines with 0.2 mol CO<sub>2</sub>/mole alkalinity.

Amine (blended with PZ)	Structure	Amine left (Initial Conc.=1.00)							
		150 °C				175 °C			
		PZ		Am		PZ		Am	
		7 d	14 d	7 d	14 d	3 d	7 d	3 d	7 d
1,3-Diaminopentane (1,3-DAP)		0.99	0.89	0.49	0.22	0.87	0.85	0.08	0.04
2-(Aminomethyl)piperidine (2AM-PD)		0.91	0.95	0.40	0.24	0.91	0.89	0.07	0.01
3-(Aminomethyl)piperidine (3AM-PD)		— <sup>a</sup>	0.96 <sup>b</sup>	— <sup>a</sup>	0.96 <sup>b</sup>	0.94 <sup>b</sup>	0.90 <sup>b</sup>	0.94 <sup>b</sup>	0.90 <sup>b</sup>
4-Aminopiperidine (4A-PD)		— <sup>a</sup>	0.97	0.97	0.96	0.93	0.84	0.91	0.83
4-(Aminomethyl)piperidine (4AM-PD)			— <sup>a</sup>			0.94 <sup>b</sup>		0.88 <sup>b</sup>	
4-(3-Aminopropyl)morpholine (APMor)			— <sup>a</sup>			0.95	0.91	0.91	0.88
1-(2-Hydroxyethyl)piperazine (HEP)			— <sup>a</sup>			0.92	0.82	0.89	0.77
1,2-Bis(2-aminoethoxy)ethane (BAEE)			— <sup>a</sup>		0.95	— <sup>a</sup>	0.90	0.89	

a: amine loss is too small to be sufficiently quantified, based on the assumption that the combined error is about ±3.5% (Namjoshi, 2015)

b: only average values shown due to peak overlap in cation chromatography

Table A.3: Thermal degradation of 2 m PZ/2 m tertiary amines with 0.2 mol CO<sub>2</sub>/mole alkalinity.

Amine (blended with PZ)	Structure	Amine left (Initial Conc.=1.00)							
		150 °C				175 °C			
		PZ		Am		PZ		Am	
		7 d	14 d	7 d	14 d	3 d	7 d	3 d	7 d
N-methyl-diethanolamine (MDEA)		0.63	0.42	0.85	0.75	0.50	0.08	0.77	0.44
Bis[2-(N,N-dimethylamino)ethyl] ether (BDMAEE)		0.67	0.56	0.56	0.44	0.40	0.15	0.38	0.16
3-(Dimethylamino)-1,2-propanediol (DMA-PDL)		0.87	0.71	0.85	0.75	0.49	0.29	0.58	0.41
Dimethylaminoethoxyethanol (DMAEE)		0.87	0.79	0.86	0.80	0.64	0.41	0.64	0.40
2-(Diethylamino)ethanol (DEEA)		0.83	0.75	0.85	0.80	0.41	0.17	0.49	0.21
3-(Diethylamino)-1,2-propanediol (DEA-PDL)		0.86	0.77	0.87	0.81	0.52	0.29	0.61	0.20
2-(Diisopropylamino)ethanol (DIPAE)		0.96	0.94	0.92	0.95	0.61	0.40	0.55	0.38
Triethylenediamine (TEDA)		0.93	0.87	0.87	0.75			— <sup>a</sup>	
3-Quinuclidinol (3-QD)		0.96	0.95	0.94	0.88	0.88	0.82	0.79	0.69
4-Hydroxy-1-methylpiperidine (HMPD)		0.96	0.92	0.96	0.94	0.85	0.79	0.89	0.85
1-(2-Hydroxyethyl)piperidine (HEPD)		— <sup>b</sup>	0.94	0.99	0.96	0.86	0.85	0.90	0.91
4-(2-Hydroxyethyl)morpholine (HEMor)		— <sup>b</sup>	0.92	1.00	0.93	0.93	0.89	0.96	0.92
Tropine		— <sup>b</sup>	0.96	— <sup>b</sup>	0.95	0.90	0.90	0.90	0.89

a: complete solidification occurred at 175 °C after 3 days

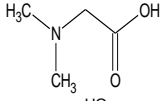
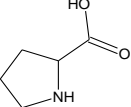
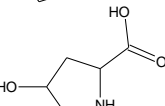
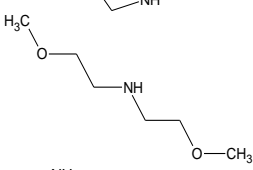
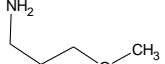
b: amine loss is too small to be sufficiently quantified, based on the assumption that the combined error is about ±3.5% (Namjoshi, 2015)

Table A.4: Thermal degradation of 2 m PZ/2 m hindered amines with 0.2 mol CO<sub>2</sub>/mole alkalinity.

Amine (blended with PZ)	Structure	Amine left (Initial Conc.=1.00)							
		150 °C				175 °C			
		PZ		Am		PZ		Am	
		7 d	14 d	7 d	14 d	3 d	7 d	3 d	7 d
2-Amino-2-methyl-1-propanol (AMP)		0.63	0.42	0.85	0.75	0.50	0.08	0.77	0.44
Diisopropanolamine (DIPA)		0.77	0.45	0.58	0.32	0.49	0.17	0.34	0.16
2-Amino-1-butanol (2-AB)		0.79	0.51	0.75	0.30	0.51	0.34	0.28	0.04
2-Amino-2-ethyl-1,3-propanediol (AEPD)		0.89	0.74	0.85	0.67	0.69	0.49	0.57	0.38
2-(Isopropylamino)ethanol (IPAE)		0.89	0.74	0.89	0.72	— <sup>a</sup>	0.37	— <sup>a</sup>	0.40

a: data are lost

Table A.5: Thermal degradation of 2 m PZ/2 m K<sup>+</sup>/amino acids, and 2 m PZ/2 m ether amines with 0.2 mol CO<sub>2</sub>/mole alkalinity.

Amine (blended with PZ)	Structure	Amine left (Initial Conc.=1.00)							
		150 °C				175 °C			
		PZ		Am		PZ		Am	
		7 d	14 d	7 d	14 d	3 d	7 d	3 d	7 d
N,N-Dimethylglycine (DMG)		0.71	0.61	0.48	0.48	0.40	0.23	0.34	0.18
L-Proline (L-Pro)		— <sup>a</sup>		0.78	0.72	0.94	0.88	0.66	0.67
4-Hydroxy-L-proline (HL-Pro)		— <sup>a</sup>		0.75	0.73	0.97	0.92	0.70	0.68
Bis(2-methoxyethyl)amine (BMEA)		— <sup>a</sup>	0.97	— <sup>a</sup>		0.92	0.83	0.96	0.91
3-Methoxypropylamine (MOPA)				— <sup>a</sup>		0.93		— <sup>a</sup>	

<sup>a</sup>: amine loss is too small to be sufficiently quantified, based on the assumption that the combined error is about ±3.5% (Namjoshi, 2015)

## Appendix B: Detailed WWC data

Table B.1: Detailed WWC data for 2.5 m PZ.

CO <sub>2</sub> Loading	T	P <sub>tot</sub>	Q <sub>liquid</sub>	Q <sub>gas</sub>	Q <sub>gas,wet</sub>	P <sub>CO<sub>2</sub>,in,dry</sub>	P <sub>CO<sub>2</sub>,in,wet</sub>	P <sub>CO<sub>2</sub>,out,dry</sub>	P <sub>CO<sub>2</sub>,out,wet</sub>	P <sub>CO<sub>2</sub>*</sub>	(P <sub>CO<sub>2</sub>-P<sub>CO<sub>2</sub>*</sub>)<sub>LM</sub></sub>	N <sub>CO<sub>2</sub></sub>	k <sub>g</sub>	K <sub>g</sub>	k <sub>g</sub> '	K <sub>g</sub> /k <sub>g</sub> '
mol CO <sub>2</sub> /mol PZ	°C	psig	ml/s	StdL/min	StdL/min	Pa	Pa	Pa	Pa	Pa	Pa	mol/s m <sup>2</sup>	mol/s Pa m <sup>2</sup>	mol/s Pa m <sup>2</sup>	mol/s Pa m <sup>2</sup>	%
0.504	40	20	4	5.0	5.2	0	0	45	44	155	-99	-1.82E-4	4.57E-6	1.74E-6	3.18E-6	62%
						50	48	77	75		-60	-1.09E-4				
						100	97	107	104		-22	-2.83E-5				
						200	194	171	166		57	1.17E-4				
						250	242	207	201		98	1.74E-4				
						300	291	244	236		140	2.26E-4				
0.634	40	20	4	5.0	5.2	0	0	155	150	620	-884	-6.26E-4	4.57E-6	7.44E-7	2.12E-6	84%
						300	291	420	407		-610	-4.84E-4				
						600	581	670	649		-344	-2.83E-4				
						1200	1163	1160	1124		182	1.61E-4				
						1500	1454	1415	1371		450	3.43E-4				
						1800	1744	1670	1618		719	5.25E-4				
0.82	40	40	4	5.0	5.1	0	0	585	574	7250	-4439	-1.50E-3	2.87E-6	3.28E-7	6.76E-7	89%
						1000	980	1480	1451		-3511	-1.23E-3				
						2000	1961	2300	2255		-2621	-7.68E-4				
						6000	5883	5800	5686		1049	5.12E-4				
						7000	6863	6750	6618		2006	6.40E-4				
						8000	7843	7670	7520		2947	8.45E-4				

Table B.2: Detailed WWC data for 2.5 m PZ / 2.5 m IMI.

CO <sub>2</sub> Loading	T	P <sub>tot</sub>	Q <sub>liquid</sub>	Q <sub>gas</sub>	Q <sub>gas,wet</sub>	P <sub>CO<sub>2</sub>,in,dry</sub>	P <sub>CO<sub>2</sub>,in,wet</sub>	P <sub>CO<sub>2</sub>,out,dry</sub>	P <sub>CO<sub>2</sub>,out,wet</sub>	P <sub>CO<sub>2</sub>*</sub>	(P <sub>CO<sub>2</sub>-P<sub>CO<sub>2</sub>*</sub>)<sub>LM</sub></sub>	N <sub>CO<sub>2</sub></sub>	k <sub>g</sub>	K <sub>g</sub>	k <sub>g</sub> '	K <sub>g</sub> /k <sub>g</sub> '
mol CO <sub>2</sub> /mol PZ	°C	psig	ml/s	StdL/min	StdL/min	Pa	Pa	Pa	Pa	Pa	Pa	mol/s m <sup>2</sup>	mol/s Pa m <sup>2</sup>	mol/s Pa m <sup>2</sup>	mol/s Pa m <sup>2</sup>	%
0.450	40	20	4	5.0	5.2	28	28	69	67	122	-73	-1.65E-4	4.57E-6	2.17E-6	4.14E-6	53%
						55	53	84	81		-54	-1.16E-4				
						80	78	98	95		-35	-7.14E-5				
						157	152	143	139		23	5.60E-5				
						181	175	159	154		42	8.88E-5				
						206	200	175	169		61	1.27E-4				
0.570	40	20	4	5.0	5.2	153	148	238	230	387	-195	-3.42E-4	4.57E-6	1.71E-6	2.74E-6	63%
						252	244	300	291		-118	-1.96E-4				
						345	335	362	351		-44	-6.85E-5				
						630	611	553	535		183	3.13E-4				
						773	749	647	627		297	5.07E-4				
						486	471	457	443		69	1.16E-4				
0.720	40	40	4	5.0	5.1	756	741	1089	1068	1756	-841	-8.53E-4	2.87E-6	9.94E-7	1.52E-6	65%
						317	311	788	773		-1199	-1.20E-3				
						982	963	1229	1205		-665	-6.32E-4				
						2202	2159	2066	2026		332	3.48E-4				
						2903	2846	2556	2506		910	8.88E-4				
						2556	2506	2315	2270		625	6.18E-4				
0.843	40	40	4	5.0	5.1	2492	2443	3359	3294	6922	-4039	-2.22E-3	2.87E-6	5.34E-7	6.56E-7	81%
						3265	3201	3978	3900		-3359	-1.82E-3				
						4819	4724	5199	5098		-2005	-9.75E-4				
						7805	7652	7654	7504		653	3.86E-4				
						9237	9057	8823	8650		1924	1.06E-3				
						10670	10461	10029	9833		3215	1.64E-3				

Table B.3: Detailed WWC data for 2.5 m PZ / 2.5 m HEMor.

CO <sub>2</sub> Loading	T	P <sub>tot</sub>	Q <sub>liquid</sub>	Q <sub>gas</sub>	Q <sub>gas,wet</sub>	P <sub>CO2,in,dry</sub>	P <sub>CO2,in,wet</sub>	P <sub>CO2,out,dry</sub>	P <sub>CO2,out,wet</sub>	P <sub>CO2</sub> *	(P <sub>CO2</sub> -P <sub>CO2</sub> ) <sub>LM</sub>	N <sub>CO2</sub>	k <sub>g</sub>	K <sub>g</sub>	k <sub>g</sub> '	K <sub>g</sub> /k <sub>g</sub> '
mol CO <sub>2</sub> /mol PZ	°C	psig	ml/s	StdL/min	StdL/min	Pa	Pa	Pa	Pa	Pa	Pa	mol/s·m <sup>2</sup>	mol/s·Pa·m <sup>2</sup>	mol/s·Pa·m <sup>2</sup>	mol/s·Pa·m <sup>2</sup>	%
0.450	40	20	4	5.0	5.2	46	44	94	91	177	-108	-1.93E-4	4.57E-6	1.76E-6	2.86E-6	62%
						27	26	83	80		-122	-2.23E-4				
						79	77	113	110		-83	-1.37E-4				
						311	301	269	261		103	1.70E-4				
						252	244	228	221		55	9.65E-5				
						214	207	200	194		23	5.41E-5				
0.690	40	40	4	5.0	5.1	222	218	622	610	1668	-1244	-1.02E-3	2.87E-6	8.01E-7	1.11E-6	72%
						733	719	999	980		-812	-6.81E-4				
						1180	1157	1297	1272		-451	-2.99E-4				
						2202	2159	2062	2022		419	3.57E-4				
						2888	2832	2575	2525		1002	8.01E-4				
						3571	3501	3084	3024		1582	1.25E-3				
0.840	40	40	4	5.0	5.1	2477	2429	3314	3249	8085	-5235	-2.14E-3	2.87E-6	3.76E-7	4.33E-7	87%
						4049	3970	4623	4532		-3827	-1.47E-3				
						5599	5489	5889	5774		-2451	-7.43E-4				
						9275	9094	9087	8909		913	4.83E-4				
						11424	11201	10972	10757		2888	1.16E-3				
						13536	13271	12895	12642		4865	1.64E-3				

Table B.4: Detailed WWC data for 2.5 m PZ / 2.5 m 2E-IMI.

CO <sub>2</sub> Loading	T	P <sub>tot</sub>	Q <sub>liquid</sub>	Q <sub>gas</sub>	Q <sub>gas,wet</sub>	P <sub>CO<sub>2</sub>,in,dry</sub>	P <sub>CO<sub>2</sub>,in,wet</sub>	P <sub>CO<sub>2</sub>,out,dry</sub>	P <sub>CO<sub>2</sub>,out,wet</sub>	P <sub>CO<sub>2</sub>*</sub>	(P <sub>CO<sub>2</sub>-P<sub>CO<sub>2</sub>*</sub>)<sub>LM</sub></sub>	N <sub>CO<sub>2</sub></sub>	k <sub>g</sub>	K <sub>g</sub>	k <sub>g</sub> '	K <sub>g</sub> /k <sub>g</sub> '
mol CO <sub>2</sub> / mol PZ	°C	psig	ml/s	StdL/min	StdL/min	Pa	Pa	Pa	Pa	Pa	Pa	mol/s m <sup>2</sup>	mol/s Pa m <sup>2</sup>	mol/s Pa m <sup>2</sup>	mol/s Pa m <sup>2</sup>	%
0.450	40	20	4	5.0	5.2	39	39	83	81	155	-93	-1.77E-4	4.57E-6	1.89E-6	3.22E-6	59%
						58	57	94	93		-79	-1.47E-4				
						270	264	228	223		87	1.70E-4				
						313	307	257	252		123	2.30E-4				
0.630	40	20	4	5.0	5.2	112	110	294	288	715	-511	-7.45E-4	4.57E-6	1.44E-6	2.10E-6	69%
						217	213	367	359		-424	-6.09E-4				
						317	310	436	427		-343	-4.86E-4				
						1076	1055	976	957		288	4.10E-4				
						1253	1229	1100	1079		434	6.25E-4				
0.750	40	40	4	5.0	5.1	988	969	1287	1262	2060	-937	-7.66E-4	2.87E-6	8.18E-7	1.14E-6	72%
						1465	1436	1656	1624		-524	-4.90E-4				
						871	854	1191	1168		-1041	-8.21E-4				
						3035	2976	2771	2717		779	6.76E-4				
						3276	3212	2948	2891		983	8.40E-4				
						3703	3630	3288	3223		1357	1.06E-3				
0.840	40	40	4	5.0	5.1	2409	2362	2892	2835	4550	-1942	-1.24E-3	2.87E-6	5.89E-7	7.41E-7	80%
						2854	2798	3205	3142		-1574	-8.98E-4				
						3318	3253	3537	3467		-1187	-5.60E-4				
						5946	5830	5674	5563		1141	6.95E-4				
						6979	6842	6500	6373		2049	1.23E-3				
						8559	8391	7767	7615		3439	2.03E-3				

Table B.5: Detailed WWC data for 2.5 m PZ / 2.5 m 2E-4M-IMI.

<b>CO<sub>2</sub> Loading</b>	<b>T</b>	<b>P<sub>tot</sub></b>	<b>Q<sub>liquid</sub></b>	<b>Q<sub>gas</sub></b>	<b>Q<sub>gas,wet</sub></b>	<b>P<sub>CO2,in,dry</sub></b>	<b>P<sub>CO2,in,wet</sub></b>	<b>P<sub>CO2,out,dry</sub></b>	<b>P<sub>CO2,out,wet</sub></b>	<b>P<sub>CO2</sub>*</b>	<b>(P<sub>CO2</sub>-P<sub>CO2</sub>*)<sub>LM</sub></b>	<b>N<sub>CO2</sub></b>	<b>k<sub>g</sub></b>	<b>K<sub>g</sub></b>	<b>k<sub>g</sub>'</b>	<b>K<sub>g</sub>/k<sub>g</sub>'</b>
mol CO <sub>2</sub> /mol PZ	°C	psig	ml/s	StdL/min	StdL/min	Pa	Pa	Pa	Pa	Pa	Pa	mol/s·m <sup>2</sup>	mol/s·Pa·m <sup>2</sup>	mol/s·Pa·m <sup>2</sup>	mol/s·Pa·m <sup>2</sup>	%
0.450	40	20	4	5.0	5.2	24	24	66	64	135	-90	-1.67E-4	4.57E-6	1.79E-6	2.93E-6	61%
						48	46	80	78		-72	-1.31E-4				
						68	66	93	90		-56	-1.02E-4				
						214	207	188	182		59	1.03E-4				
						242	235	207	201		82	1.41E-4				
						273	264	227	220		106	1.84E-4				
0.637	40	20	4	5.0	5.2	217	210	330	319	628	-360	-4.55E-4	4.57E-6	1.25E-6	1.73E-6	73%
						310	301	399	387		-282	-3.60E-4				
						408	395	468	454		-202	-2.43E-4				
						782	758	748	725		113	1.38E-4				
						973	943	890	863		273	3.35E-4				
						1165	1129	1030	998		432	5.46E-4				
0.975	40	40	4	5.0	5.1	2896	2839	3612	3541	6900	-3699	-1.83E-3	2.87E-6	4.89E-7	5.89E-7	83%
						4004	3926	4540	4451		-2703	-1.37E-3				
						10029	9833	9501	9315		2666	1.35E-3				
						12065	11829	11236	11016		4510	2.12E-3				

Table B.6: Detailed WWC data for 2.5 m PZ / 2.5 m MDEA.

CO <sub>2</sub> Loading	T	P <sub>tot</sub>	Q <sub>liquid</sub>	Q <sub>gas</sub>	Q <sub>gas,wet</sub>	P <sub>CO<sub>2</sub>,in,dry</sub>	P <sub>CO<sub>2</sub>,in,wet</sub>	P <sub>CO<sub>2</sub>,out,dry</sub>	P <sub>CO<sub>2</sub>,out,wet</sub>	P <sub>CO<sub>2</sub>*</sub>	(P <sub>CO<sub>2</sub>-P<sub>CO<sub>2</sub>*</sub>)<sub>LM</sub></sub>	N <sub>CO<sub>2</sub></sub>	k <sub>g</sub>	K <sub>g</sub>	k <sub>g</sub> '	K <sub>g</sub> /k <sub>g</sub> '
mol CO <sub>2</sub> /mol PZ	°C	psig	ml/s	StdL/min	StdL/min	Pa	Pa	Pa	Pa	Pa	Pa	mol/s m <sup>2</sup>	mol/s Pa m <sup>2</sup>	mol/s Pa m <sup>2</sup>	mol/s Pa m <sup>2</sup>	%
0.510	40	20	4	5.0	5.2	38	37	93	90	183	-118	-2.21E-4	4.57E-6	1.808E-6	2.99E-6	61%
						111	107	136	132		-63	-1.02E-4				
						80	78	118	114		-86	-1.52E-4				
						359	348	297	288		133	2.51E-4				
						311	301	269	261		97	1.67E-4				
						283	274	252	244		75	1.26E-4				
0.690	40	20	4	5.0	5.2	214	207	318	308	595	-335	-4.18E-4	4.57E-6	1.20E-6	1.63E-6	74%
						310	300	386	374		-256	-3.09E-4				
						487	472	515	500		-109	-1.16E-4				
						776	752	731	708		134	1.83E-4				
						962	932	873	846		292	3.57E-4				
						1150	1115	1020	989		454	5.26E-4				
0.870	40	40	4	5.0	5.1	954	935	1186	1163	1733	-678	-5.94E-4	2.87E-6	8.76E-7	1.26E-6	70%
						1448	1419	1532	1502		-270	-2.14E-4				
						786	771	1074	1053		-813	-7.37E-4				
						2549	2499	2311	2266		642	6.08E-4				
						2820	2765	2530	2480		882	7.43E-4				
						3265	3201	2843	2787		1250	1.08E-3				
1.020	40	40	4	5.0	5.1	1434	1406	1979	1941	3925	-2241	-1.40E-3	2.87E-6	6.02E-7	7.61E-7	79%
						1895	1858	2319	2273		-1852	-1.09E-3				
						2345	2299	2658	2606		-1467	-8.01E-4				
						5369	5264	5132	5031		1219	6.08E-4				
						6474	6347	5969	5852		2165	1.29E-3				
						7918	7763	7088	6950		3415	2.12E-3				
1.110	40	40	4	5.0	5.1	1900	1863	2734	2680	5910	-3623	-2.13E-3	2.87E-6	5.77E-7	7.22E-7	80%
						2835	2780	3431	3364		-2828	-1.53E-3				
						3555	3486	4076	3996		-2159	-1.33E-3				
						7013	6876	6824	6691		870	4.83E-4				
						7578	7430	7239	7097		1347	8.69E-4				
						9162	8983	8559	8391		2766	1.54E-3				

Table B.7: Detailed WWC data for 2.5 m PZ / 2.5 m DMAEE.

CO <sub>2</sub> Loading	T	P <sub>tot</sub>	Q <sub>liquid</sub>	Q <sub>gas</sub>	Q <sub>gas,wet</sub>	P <sub>CO<sub>2</sub>,in,dry</sub>	P <sub>CO<sub>2</sub>,in,wet</sub>	P <sub>CO<sub>2</sub>,out,dry</sub>	P <sub>CO<sub>2</sub>,out,wet</sub>	P <sub>CO<sub>2</sub>*</sub>	(P <sub>CO<sub>2</sub>-P<sub>CO<sub>2</sub>*</sub>)<sub>LM</sub></sub>	N <sub>CO<sub>2</sub></sub>	k <sub>g</sub>	K <sub>g</sub>	k <sub>g</sub> '	K <sub>g</sub> /k <sub>g</sub> '
mol CO <sub>2</sub> /mol PZ	°C	psig	ml/s	StdL/min	StdL/min	Pa	Pa	Pa	Pa	Pa	Pa	mol/s m <sup>2</sup>	mol/s Pa m <sup>2</sup>	mol/s Pa m <sup>2</sup>	mol/s Pa m <sup>2</sup>	%
0.660	40	20	4	5.0	5.2	130	126	191	185	315	-158	-2.48E-4	4.57E-6	1.55E-6	2.33E-6	66%
						164	159	212	205		-132	-1.95E-4				
						506	490	449	435		146	2.30E-4				
						557	540	486	471		188	2.90E-4				
0.900	40	20	4	5.0	5.2	387	376	554	537	1070	-610	-6.74E-4	4.57E-6	1.09E-6	1.42E-6	76%
						578	560	697	676		-449	-4.81E-4				
						1311	1270	1260	1222		175	2.03E-4				
						1842	1785	1674	1623		630	6.76E-4				
1.050	40	40	4	5.0	5.1	965	946	1280	1255	2113	-1004	-8.06E-4	2.87E-6	7.96E-7	1.10E-7	72%
						1437	1408	1621	1590		-610	-4.73E-4				
						2816	2761	2647	2595		561	4.34E-4				
						3684	3612	3280	3216		1291	1.03E-3				
1.200	40	40	4	5.0	5.1	965	946	1746	1712	5082	-3740	-2.00E-7	2.87E-6	4.94E-7	5.97E-7	83%
						1897	1859	2436	2388		-2950	-1.38E-7				
						2341	2296	2794	2739		-2558	-1.16E-7				
						6478	6351	6263	6140		1160	5.50E-8				
						7616	7467	7201	7060		2175	1.06E-7				

Table B.8: Detailed WWC data for 2.5 m PZ / 2.5 m HMPD.

CO <sub>2</sub> Loading	T	P <sub>tot</sub>	Q <sub>liquid</sub>	Q <sub>gas</sub>	Q <sub>gas,wet</sub>	P <sub>CO<sub>2</sub>,in,dry</sub>	P <sub>CO<sub>2</sub>,in,wet</sub>	P <sub>CO<sub>2</sub>,out,dry</sub>	P <sub>CO<sub>2</sub>,out,wet</sub>	P <sub>CO<sub>2</sub>*</sub>	(P <sub>CO<sub>2</sub>-P<sub>CO<sub>2</sub>*</sub>)<sub>LM</sub></sub>	N <sub>CO<sub>2</sub></sub>	k <sub>g</sub>	K <sub>g</sub>	k <sub>g</sub> '	K <sub>g</sub> /k <sub>g</sub> '
mol CO <sub>2</sub> /mol PZ	°C	psig	ml/s	StdL/min	StdL/min	Pa	Pa	Pa	Pa	Pa	Pa	mol/s m <sup>2</sup>	mol/s Pa m <sup>2</sup>	mol/s Pa m <sup>2</sup>	mol/s Pa m <sup>2</sup>	%
0.540	40	20	4	5.0	5.2	56	54	87	85	135	-64	-1.26E-4	4.57E-6	1.83E-6	3.04E-6	60%
						30	29	69	67		-86	-1.58E-4				
						63	61	89	86		-61	-1.04E-4				
						170	165	160	155		24	4.25E-5				
						191	185	173	167		40	7.24E-5				
						223	216	193	188		66	1.18E-4				
0.810	40	20	4	5.0	5.2	488	473	515	499	580	-93	-1.09E-4	4.57E-6	1.16E-6	1.56E-6	75%
						284	275	362	350		-265	-3.13E-4				
						385	373	437	424		-180	-2.12E-4				
						723	701	694	672		106	1.19E-4				
						823	797	771	747		191	2.09E-4				
						928	899	847	821		278	3.28E-4				
1.020	40	40	4	5.0	5.1	1043	1022	1210	1187	1620	-511	-4.30E-4	2.87E-6	8.96E-7	1.30E-6	69%
						539	529	871	854		-919	-8.50E-4				
						3997	3918	3318	3253		1947	1.74E-3				
						3024	2965	2624	2573		1138	1.02E-3				
1.350	40	40	4	5.0	5.1	2010	1970	2975	2917	7200	-4741	-2.47E-3	2.87E-6	4.90E-7	5.91E-7	83%
						3005	2946	3736	3663		-3884	-1.87E-3				
						5000	4902	5339	5234		-2128	-8.69E-4				
						8634	8465	8370	8206		1131	6.76E-4				
						9275	9094	8974	8798		1742	7.72E-4				
						9954	9759	9539	9352		2350	1.06E-3				

Table B.9: Detailed WWC data for 2.5 m PZ / 2.5 m BDMAEE.

CO <sub>2</sub> Loading	T	P <sub>tot</sub>	Q <sub>liquid</sub>	Q <sub>gas</sub>	Q <sub>gas,wet</sub>	PCO <sub>2,in,dry</sub>	PCO <sub>2,in,wet</sub>	PCO <sub>2,out,dry</sub>	PCO <sub>2,out,wet</sub>	PCO <sub>2</sub> *	(PCO <sub>2</sub> -PCO <sub>2</sub> <sup>†</sup> ) <sub>LM</sub>	Nco <sub>2</sub>	k <sub>g</sub>	K <sub>g</sub>	k <sub>g</sub> '	K <sub>g</sub> /k <sub>g</sub> '
mol CO <sub>2</sub> /mol PZ	°C	psig	ml/s	StdL/min	StdL/min	Pa	Pa	Pa	Pa	Pa	Pa	mol/s m <sup>2</sup>	mol/s Pa m <sup>2</sup>	mol/s Pa m <sup>2</sup>	mol/s Pa m <sup>2</sup>	%
0.693	40	20	4	5.0	5.2	156	151	176	170	215	-54	-8.01E-5	4.57E-6	1.58E-6	2.41E-6	66%
						347	336	306	297		100	1.63E-4				
						54	52	108	104		-135	-2.18E-4				
						105	101	140	136		-95	-1.45E-4				
						252	244	242	235		24	3.96E-5				
						300	291	277	268		64	9.36E-5				
0.960	40	40	4	5.0	5.1	152	149	326	320	630	-389	-4.45E-4	2.87E-6	1.15E-6	1.90E-6	60%
						233	229	376	369		-326	-3.65E-4				
						451	442	520	509		-152	-1.76E-4				
						891	873	809	793		201	2.09E-4				
						1186	1163	993	973		431	4.94E-4				
						1472	1444	1174	1151		657	7.63E-4				
1.320	40	40	4	5.0	5.1	1682	1649	1848	1812	2305	-571	-4.26E-4	2.87E-6	7.55E-7	1.02E-6	74%
						3525	3456	3239	3175		1004	7.34E-4				
						2854	2798	2715	2662		421	3.57E-4				
						1184	1161	1472	1444		-996	-7.39E-4				
						1463	1434	1697	1664		-750	-6.00E-4				
1.650	40	40	4	5.0	5.1	2413	2366	3197	3135	7235	-4474	-2.01E-3	2.87E-6	4.31E-7	5.07E-7	85%
						3177	3114	3816	3741		-3799	-1.64E-3				
						4707	4615	5075	4976		-2435	-9.41E-4				
						8333	8169	8182	8022		858	3.86E-4				
						9765	9574	9407	9223		2159	9.17E-4				
						11160	10942	10595	10387		3422	1.45E-3				

Table B.10: Detailed WWC data for 2.5 m PZ / 2.5 m HEPD.

CO <sub>2</sub> Loading	T	P <sub>tot</sub>	Q <sub>liquid</sub>	Q <sub>gas</sub>	Q <sub>gas,wet</sub>	P <sub>CO<sub>2</sub>,in,dry</sub>	P <sub>CO<sub>2</sub>,in,wet</sub>	P <sub>CO<sub>2</sub>,out,dry</sub>	P <sub>CO<sub>2</sub>,out,wet</sub>	P <sub>CO<sub>2</sub>*</sub>	(P <sub>CO<sub>2</sub>-P<sub>CO<sub>2</sub>*</sub>)<sub>LM</sub></sub>	N <sub>CO<sub>2</sub></sub>	k <sub>g</sub>	K <sub>g</sub>	k <sub>g</sub> '	K <sub>g</sub> /k <sub>g</sub> '
mol CO <sub>2</sub> /mol PZ	°C	psig	ml/s	StdL/min	StdL/min	Pa	Pa	Pa	Pa	Pa	Pa	mol/s m <sup>2</sup>	mol/s Pa m <sup>2</sup>	mol/s Pa m <sup>2</sup>	mol/s Pa m <sup>2</sup>	%
0.600	40	20	4	5.0	5.2	24	23	64	62	132	-88	-1.61E-4	4.57E-6	1.75E-6	2.84E-6	62%
						56	54	82	80		-64	-1.07E-4				
						159	154	151	146		18	3.28E-5				
						86	83	103	99		-40	-6.76E-5				
						188	182	170	164		41	7.43E-5				
						228	221	197	191		73	1.25E-4				
0.690	40	40	4	5.0	5.1	158	155	881	864	510	-284	-3.43E-4	2.87E-6	1.16E-6	1.94E-6	60%
						297	292	1237	1213		-176	-2.04E-4				
						292	286	751	736		285	3.32E-4				
						377	370	984	965		570	6.48E-4				
1.140	40	40	4	5.0	5.1	453	444	779	763	1630	-1018	-8.34E-4	2.87E-6	8.10E-7	1.13E-6	72%
						958	939	1142	1120		-596	-4.72E-4				
						2360	2314	2172	2129		587	4.83E-4				
						2832	2776	2522	2473		987	7.92E-4				
1.380	40	40	4	5.0	5.1	2522	2473	3167	3105	6375	-3577	-1.65E-3	2.87E-6	4.37E-7	5.15E-7	85%
						3280	3216	3770	3697		-2912	-1.25E-3				
						4046	3966	4396	4310		-2232	-8.98E-4				
						7695	7545	7496	7349		1069	5.12E-4				
						8408	8243	8106	7948		1716	7.72E-4				
						9124	8946	8747	8576		2381	9.65E-4				

Table B.11: Detailed WWC data for 2.5 m PZ / 2.5 m DEA-PDL.

CO <sub>2</sub> Loading	T	P <sub>tot</sub>	Q <sub>liquid</sub>	Q <sub>gas</sub>	Q <sub>gas,wet</sub>	P <sub>CO<sub>2</sub>,in,dry</sub>	P <sub>CO<sub>2</sub>,in,wet</sub>	P <sub>CO<sub>2</sub>,out,dry</sub>	P <sub>CO<sub>2</sub>,out,wet</sub>	P <sub>CO<sub>2</sub>*</sub>	(P <sub>CO<sub>2</sub>-P<sub>CO<sub>2</sub>'</sub>)<sub>LM</sub></sub>	N <sub>CO<sub>2</sub></sub>	k <sub>g</sub>	K <sub>g</sub>	k <sub>g</sub> '	K <sub>g</sub> /k <sub>g</sub> '
mol CO <sub>2</sub> /mol PZ	°C	psig	ml/s	StdL/min	StdL/min	Pa	Pa	Pa	Pa	Pa	Pa	mol/s m <sup>2</sup>	mol/s Pa m <sup>2</sup>	mol/s Pa m <sup>2</sup>	mol/s Pa m <sup>2</sup>	%
0.759	40	20	4	5.0	5.2	110	107	142	138	208	-85	-1.28E-4	4.57E-6	1.51E-6	2.25E-6	67%
						72	70	114	111		-117	-1.72E-4				
						310	300	280	271		77	1.20E-4				
						141	136	163	158		-60	-9.17E-5				
						263	255	249	241		40	5.70E-5				
1.119	40	40	4	5.0	5.1	302	296	517	506	1027	-620	-5.50E-4	2.87E-6	8.74E-7	1.26E-6	70%
						679	665	779	764		-310	-2.58E-4				
						1335	1309	1252	1227		239	2.12E-4				
						1472	1444	1354	1327		355	3.04E-4				
1.383	40	40	4	5.0	5.1	2500	2451	3224	3161	8320	-5507	-1.85E-3	2.87E-6	3.31E-7	3.74E-7	89%
						5531	5423	5863	5748		-2731	-8.50E-4				
						11952	11718	11537	11312		3191	1.06E-3				
						10519	10313	10293	10092		1880	5.79E-4				
						13988	13714	13328	13067		5064	1.69E-3				

Table B.12: Detailed WWC data for 2.5 m PZ / 2.5 m Tropine.

CO <sub>2</sub> Loading	T	P <sub>tot</sub>	Q <sub>liquid</sub>	Q <sub>gas</sub>	Q <sub>gas,wet</sub>	P <sub>CO<sub>2</sub>,in,dry</sub>	P <sub>CO<sub>2</sub>,in,wet</sub>	P <sub>CO<sub>2</sub>,out,dry</sub>	P <sub>CO<sub>2</sub>,out,wet</sub>	P <sub>CO<sub>2</sub>*</sub>	(P <sub>CO<sub>2</sub>-P<sub>CO<sub>2</sub>*</sub>)<sub>LM</sub></sub>	N <sub>CO<sub>2</sub></sub>	k <sub>g</sub>	K <sub>g</sub>	k <sub>g</sub> '	K <sub>g</sub> /k <sub>g</sub> '
mol CO <sub>2</sub> /mol PZ	°C	psig	ml/s	StdL/min	StdL/min	Pa	Pa	Pa	Pa	Pa	Pa	mol/s m <sup>2</sup>	mol/s Pa m <sup>2</sup>	mol/s Pa m <sup>2</sup>	mol/s Pa m <sup>2</sup>	%
0.870	40	20	4	5.0	5.2	47	46	65	63	96	-41	-7.05E-5	4.57E-6	1.80E-6	2.95E-6	61%
						24	23	51	50		-59	-1.11E-4				
						78	76	84	81		-17	-2.32E-5				
						132	127	120	116		25	4.83E-5				
						154	149	134	130		43	8.11E-5				
						174	169	149	144		60	1.02E-4				
1.140	40	20	4	5.0	5.2	153	148	223	217	444	-260	-2.85E-4	4.57E-6	1.11E-6	1.47E-6	76%
						666	646	618	599		177	1.93E-4				
						202	196	261	253		-219	-2.37E-4				
						291	282	332	322		-141	-1.67E-4				
						945	916	830	804		413	4.63E-4				
1.320	40	40	4	5.0	5.1	302	296	665	652	1748	-1266	-9.31E-4	2.87E-6	6.95E-7	9.17E-7	76%
						747	732	982	963		-896	-6.03E-4				
						2194	2151	2074	2033		341	3.09E-4				
						2873	2817	2617	2565		938	6.56E-4				
						3548	3478	3152	3090		1528	1.01E-3				
						1485	1456	1553	1523		-257	-1.75E-4				
1.470	40	40	4	5.0	5.1	2455	2406	3062	3002	7340	-4630	-1.55E-3	2.87E-6	3.22E-7	3.63E-7	89%
						3250	3186	3736	3663		-3910	-1.25E-3				
						4027	3948	4404	4318		-3204	-9.65E-4				
						12065	11829	11537	11312		4225	1.35E-3				
						9200	9020	9011	8835		1585	4.83E-4				
						10670	10461	10293	10092		2933	9.65E-4				

Table B.13: Detailed WWC data for 1.07 m DGA® / 1.93 m MAE / 7 m DMAEE.

CO <sub>2</sub> Loading	T	P <sub>tot</sub>	Q <sub>liquid</sub>	Q <sub>gas</sub>	Q <sub>gas,wet</sub>	PCO <sub>2,in,dry</sub>	PCO <sub>2,in,wet</sub>	PCO <sub>2,out,dry</sub>	PCO <sub>2,out,wet</sub>	PCO <sub>2</sub> *	(PCO <sub>2</sub> -PCO <sub>2</sub> *) <sub>LM</sub>	N <sub>CO2</sub>	k <sub>g</sub>	K <sub>g</sub>	k <sub>g</sub> '	K <sub>g</sub> /k <sub>g</sub> '
mol CO <sub>2</sub> /mol alkalinity	°C	psig	ml/s	StdL/min	StdL/min	Pa	Pa	Pa	Pa	Pa	Pa	mol/s m <sup>2</sup>	mol/s Pa m <sup>2</sup>	mol/s Pa m <sup>2</sup>	mol/s Pa m <sup>2</sup>	%
0.106	40	20	4	5.0	5.2	18	18	59	57	152	-113	-1.64E-4	4.57E-6	1.37E-6	1.95E-6	70%
						41	40	73	70		-96	-1.27E-4				
						95	92	112	108		-51	-6.66E-5				
						222	216	203	197		54	7.72E-5				
						262	254	233	226		87	1.18E-4				
						304	295	264	256		122	1.62E-4				
0.188	40	40	4	5.0	5.1	116	113	368	361	1083	-840	-6.47E-4	2.87E-6	7.39E-7	9.95E-7	74%
						223	219	437	429		-754	-5.48E-4				
						430	421	590	579		-579	-4.10E-4				
						1780	1745	1610	1578		575	4.34E-4				
						2160	2118	1904	1867		904	6.56E-4				
0.240	40	40	4	5.0	5.1	1003	983	1357	1331	2945	-1782	-9.07E-4	2.87E-6	4.99E-7	6.04E-6	83%
						1501	1471	1765	1730		-1340	-6.76E-4				
						1979	1941	2145	2103		-921	-4.25E-4				
						3819	3745	3684	3612		731	3.48E-4				
						3369	3303	3295	3231		321	1.88E-4				
						4860	4765	4543	4454		1660	8.11E-4				
0.292	40	40	4	5.0	5.1	2507	2458	2952	2894	5875	-3194	-1.14E-3	2.87E-6	3.49E-7	3.98E-7	88%
						3280	3216	3631	3560		-2483	-8.98E-4				
						4796	4702	4928	4831		-1107	-3.38E-4				
						7707	7556	7488	7341		1571	5.60E-4				
						9124	8946	8747	8576		2882	9.65E-4				
						6259	6136	6214	6092		238	1.16E-4				
0.350	40	40	4	5.0	5.1	5471	5364	5908	5793	10198	-4617	-1.12E-3	2.87E-6	2.38E-7	2.59E-7	92%
						7692	7541	7918	7763		-2544	-5.79E-4				
						9087	8909	9200	9020		-1233	-2.90E-4				
						13913	13640	13611	13345		3292	7.72E-4				
						12555	12310	12367	12125		2018	4.83E-4				

Table B.14: Detailed WWC data for 2.5 m DGA<sup>®</sup> / 2.5 m MAE / 10 m DMAEE.

CO <sub>2</sub> Loading	T	P <sub>tot</sub>	Q <sub>liquid</sub>	Q <sub>gas</sub>	Q <sub>gas,wet</sub>	P <sub>CO<sub>2</sub>,in,dry</sub>	P <sub>CO<sub>2</sub>,in,wet</sub>	P <sub>CO<sub>2</sub>,out,dry</sub>	P <sub>CO<sub>2</sub>,out,wet</sub>	P <sub>CO<sub>2</sub>*</sub>	(P <sub>CO<sub>2</sub>-P<sub>CO<sub>2</sub>*</sub>)<sub>LM</sub></sub>	N <sub>CO<sub>2</sub></sub>	k <sub>g</sub>	K <sub>g</sub>	k <sub>g</sub> '	K <sub>g</sub> /k <sub>g</sub> '
mol CO <sub>2</sub> /mol alkalinity	°C	psig	ml/s	StdL/min	StdL/min	Pa	Pa	Pa	Pa	Pa	Pa	mol/s m <sup>2</sup>	mol/s Pa m <sup>2</sup>	mol/s Pa m <sup>2</sup>	mol/s Pa m <sup>2</sup>	%
0.150	40	20	4	5.0	5.2	79	76	93	90	118	-34	-5.79E-5	4.57E-6	1.76E-6	2.87E-6	62%
						170	165	155	150		39	6.08E-5				
						246	239	204	197		99	1.73E-4				
						209	203	178	172		68	1.27E-4				
0.253	40	20	4	5.0	5.2	255	248	336	326	612	-324	-3.25E-4	4.57E-6	1.06E-6	1.37E-6	77%
						389	377	449	435		-205	-2.42E-4				
						938	909	864	837		259	2.96E-4				
						1080	1047	983	953		386	3.91E-4				
0.320	40	40	4	5.0	5.1	1389	1361	1137	1115	2902	-932	-5.47E-4	2.87E-6	5.68E-7	7.08E-6	80%
						3597	3527	1602	1571		983	7.05E-4				
						3167	3105	3322	3257		626	3.86E-4				
						4796	4702	3016	2957		2086	1.08E-3				
						1704	1671	4374	4288		-646	-4.25E-4				
0.364	40	40	4	5.0	5.1	956	937	1601	1569	4915	-3653	-1.65E-3	2.87E-6	4.35E-7	5.12E-7	85%
						1878	1841	2334	2288		-2845	-1.17E-3				
						7582	7434	7179	7038		2315	1.03E-3				
						8069	7911	7612	7463		2766	1.17E-3				
0.426	40	40	4	5.0	5.1	8333	8169	8559	8391	11070	-2788	-5.79E-4	2.87E-6	2.04E-7	2.19E-7	93%
						9690	9500	9803	9611		-1514	-2.90E-4				
						11726	11496	11688	11459		408	9.65E-5				
						13762	13493	13573	13308		2329	4.83E-4				
						12442	12199	12367	12125		1091	1.93E-4				

Table B.15: Detailed WWC data for 0.75 m DGA® / 1.35 m MAE / 4.9 m DMAEE.

CO <sub>2</sub> Loading	T	P <sub>tot</sub>	Q <sub>liquid</sub>	Q <sub>gas</sub>	Q <sub>gas,wet</sub>	P <sub>CO<sub>2</sub>,in,dry</sub>	P <sub>CO<sub>2</sub>,in,wet</sub>	P <sub>CO<sub>2</sub>,out,dry</sub>	P <sub>CO<sub>2</sub>,out,wet</sub>	P <sub>CO<sub>2</sub>*</sub>	(P <sub>CO<sub>2</sub>-P<sub>CO<sub>2</sub>'</sub>)<sub>LM</sub></sub>	N <sub>CO<sub>2</sub></sub>	k <sub>g</sub>	K <sub>g</sub>	k <sub>g</sub> '	K <sub>g</sub> /k <sub>g</sub> '
mol CO <sub>2</sub> /mol alkalinity	°C	psig	ml/s	StdL/min	StdL/min	Pa	Pa	Pa	Pa	Pa	Pa	mol/s m <sup>2</sup>	mol/s Pa m <sup>2</sup>	mol/s Pa m <sup>2</sup>	mol/s Pa m <sup>2</sup>	%
0.131	40	40	4	5.0	5.1	90	89	140	137	248	-134	-1.26E-4	2.87E-6	9.54E-7	1.43E-6	67%
						314	308	295	289		50	4.83E-5				
						410	402	362	355		129	1.23E-4				
						138	135	173	170		-94	-9.17E-5				
0.171	40	40	4	5.0	5.1	408	400	451	442	560	-138	-1.09E-4	2.87E-6	7.74E-6	1.06E-6	73%
						320	314	385	377		-213	-1.65E-4				
						724	710	684	671		129	1.02E-4				
						869	852	794	778		253	1.93E-4				
0.260	40	40	4	5.0	5.1	995	976	1248	1224	2414	-1310	-6.47E-4	2.87E-6	4.85E-7	5.83E-6	83%
						1478	1449	1642	1610		-882	-4.20E-4				
						1942	1904	2025	1985		-468	-2.12E-4				
						2850	2795	2786	2732		348	1.64E-4				
						3495	3427	3325	3260		927	4.34E-4				
						3752	3678	3529	3460		1152	5.70E-4				
0.330	40	40	4	5.0	5.1	2304	2259	2685	2632	5360	-2911	-9.75E-4	2.87E-6	3.41E-7	3.87E-7	88%
						3816	3741	4019	3941		-1517	-5.21E-4				
						4630	4539	4743	4650		-764	-2.90E-4				
						6078	5959	5999	5881		559	2.03E-4				
						6775	6643	6621	6491		1205	3.96E-4				
						7465	7319	7213	7072		1833	6.47E-4				
0.420	40	40	4	5.0	5.1	5252	5149	5735	5623	11020	-5631	-1.24E-3	2.87E-6	2.13E-7	2.29E-7	93%
						8144	7985	8370	8206		-2923	-5.79E-4				
						12291	12051	12178	11940		974	2.90E-4				
						13649	13382	13460	13197		2268	4.83E-4				
						14931	14638	14667	14380		3487	6.76E-4				
						8936	8761	9124	8946		-2165	-4.83E-4				

Table B.16: Detailed WWC data for 2.1 m DGA<sup>®</sup> / 4.9 m DMAEE.

CO <sub>2</sub> Loading	T	P <sub>tot</sub>	Q <sub>liquid</sub>	Q <sub>gas</sub>	Q <sub>gas,wet</sub>	P <sub>CO<sub>2</sub>,in,dry</sub>	P <sub>CO<sub>2</sub>,in,wet</sub>	P <sub>CO<sub>2</sub>,out,dry</sub>	P <sub>CO<sub>2</sub>,out,wet</sub>	P <sub>CO<sub>2</sub>*</sub>	(P <sub>CO<sub>2</sub>-P<sub>CO<sub>2</sub>*</sub>)<sub>LM</sub></sub>	N <sub>CO<sub>2</sub></sub>	k <sub>g</sub>	K <sub>g</sub>	k <sub>g</sub> '	K <sub>g</sub> /k <sub>g</sub> '
mol CO <sub>2</sub> /mol alkalinity	°C	psig	ml/s	StdL/min	StdL/min	Pa	Pa	Pa	Pa	Pa	Pa	mol/s m <sup>2</sup>	mol/s Pa m <sup>2</sup>	mol/s Pa m <sup>2</sup>	mol/s Pa m <sup>2</sup>	%
0.120	40	40	4	5.0	5.1	26	26	59	58	132	-89	-8.40E-5	2.87E-6	8.85E-7	1.28E-6	69%
						89	87	101	99		-39	-3.28E-5				
						213	209	189	185		64	6.37E-5				
						319	312	268	262		154	1.30E-4				
0.200	40	40	4	5.0	5.1	1561	1530	1403	1375	700	750	4.05E-4	2.87E-6	5.38E-7	6.61E-7	81%
						494	484	535	525		-195	-1.06E-4				
						296	290	373	366		-371	-1.98E-4				
						201	197	295	289		-455	-2.39E-4				
						984	965	935	917		240	1.25E-4				
						403	396	461	452		-275	-1.49E-4				
0.300	40	40	4	5.0	5.1	6176	6055	5889	5774	3530	2382	7.34E-4	2.87E-6	3.03E-7	3.39E-7	89%
						5460	5353	5260	5157		1723	5.12E-4				
						2470	2421	2594	2543		-1047	-3.19E-4				
						1697	1663	1904	1867		-1763	-5.31E-4				
0.381	40	40	4	5.0	5.1	3111	3050	3514	3445	8070	-4820	-1.03E-3	2.87E-6	2.05E-7	2.21E-7	93%
						5373	5268	5569	5460		-2705	-5.02E-4				
						11047	10831	10821	10609		2649	5.79E-4				
						12442	12199	12141	11903		3979	7.72E-4				

Table B.17: Detailed WWC data for 1.75 m DGA® / 1.75 m MAE / 3.5 m DMAEE at 20 °C.

CO <sub>2</sub> Loading	T	P <sub>tot</sub>	Q <sub>liquid</sub>	Q <sub>gas</sub>	Q <sub>gas,wet</sub>	P <sub>CO<sub>2</sub>,in,dry</sub>	P <sub>CO<sub>2</sub>,in,wet</sub>	P <sub>CO<sub>2</sub>,out,dry</sub>	P <sub>CO<sub>2</sub>,out,wet</sub>	P <sub>CO<sub>2</sub>*</sub>	(P <sub>CO<sub>2</sub></sub> -P <sub>CO<sub>2</sub>*</sub> ) <sub>LM</sub>	N <sub>CO<sub>2</sub></sub>	k <sub>g</sub>	K <sub>g</sub>	k <sub>g</sub> '	K <sub>g</sub> /k <sub>g</sub> '
mol CO <sub>2</sub> /mol alkalinity	°C	psig	ml/s	StdL/min	StdL/min	Pa	Pa	Pa	Pa	Pa	Pa	mol/s m <sup>2</sup>	mol/s Pa m <sup>2</sup>	mol/s Pa m <sup>2</sup>	mol/s Pa m <sup>2</sup>	%
0.170	20	40	4	5.0	5.0	28	28	25	24	16	10	9.65E-6	2.82E-6	1.21E-6	2.13E-6	57%
						0	0	6	6		-12	-1.54E-5				
						31	31	25	25		12	1.54E-5				
						40	39	31	31		19	2.22E-5				
0.270	20	40	4	5.0	5.0	51	51	61	60	86	-30	-2.51E-5	2.82E-6	6.99E-7	9.29E-7	75%
						70	70	74	73		-15	-8.69E-6				
						219	217	188	187		115	7.92E-5				
						175	174	155	154		77	5.31E-5				
0.350	20	40	4	5.0	5.0	126	125	168	167	360	-214	-1.08E-4	2.82E-6	5.05E-7	6.15E-7	82%
						228	227	253	251		-121	-6.18E-5				
						520	517	492	489		142	7.34E-5				
						620	616	575	571		233	1.16E-4				
0.430	20	40	4	3.0	3.0	837	832	961	955	1500	-604	-1.91E-4	1.83E-6	2.91E-7	3.46E-7	84%
						532	528	694	689		-889	-2.49E-4				
						2093	2080	1991	1978		527	1.56E-4				
						2598	2582	2413	2398		987	2.84E-4				

Table B.18: Detailed WWC data for 1.75 m DGA<sup>®</sup> / 1.75 m MAE / 3.5 m DMAEE at 40 °C.

CO <sub>2</sub> Loading	T	P <sub>tot</sub>	Q <sub>liquid</sub>	Q <sub>gas</sub>	Q <sub>gas,wet</sub>	P <sub>CO<sub>2</sub>,in,dry</sub>	P <sub>CO<sub>2</sub>,in,wet</sub>	P <sub>CO<sub>2</sub>,out,dry</sub>	P <sub>CO<sub>2</sub>,out,wet</sub>	P <sub>CO<sub>2</sub>*</sub>	(P <sub>CO<sub>2</sub>-P<sub>CO<sub>2</sub>'</sub>)<sub>LM</sub></sub>	N <sub>CO<sub>2</sub></sub>	k <sub>g</sub>	K <sub>g</sub>	k <sub>g</sub> '	K <sub>g</sub> /k <sub>g</sub> '
mol CO <sub>2</sub> /mol alkalinity	°C	psig	ml/s	StdL/min	StdL/min	Pa	Pa	Pa	Pa	Pa	Pa	mol/s m <sup>2</sup>	mol/s Pa m <sup>2</sup>	mol/s Pa m <sup>2</sup>	mol/s Pa m <sup>2</sup>	%
0.170	40	40	4	5.0	5.1	23	23	55	54	99	-59	-8.11E-5	2.87E-6	1.39E-6	2.67E-6	52%
						31	31	60	59		-53	-7.34E-5				
						56	55	75	73		-34	-4.83E-5				
						140	137	123	121		29	4.34E-5				
						164	160	138	136		48	6.47E-5				
0.270	40	40	4	5.0	5.1	192	188	310	304	635	-386	-3.04E-4	2.87E-6	8.01E-7	1.11E-6	72%
						285	280	383	375		-305	-2.49E-4				
						929	910	856	839		238	1.87E-4				
						980	961	891	874		280	2.29E-4				
0.350	40	40	4	5.0	5.1	676	662	2843	2787	2225	-1414	-7.51E-4	2.87E-6	5.16E-7	6.29E-7	82%
						1263	1238	3748	3674		-893	-4.71E-4				
						969	950	2715	2662		497	3.28E-4				
						1447	1419	3503	3434		1326	6.27E-4				
0.430	40	40	4	3.0	3.1	1991	1952	2899	2843	7430	-5020	-1.40E-3	1.86E-6	2.74E-7	3.21E-7	85%
						9011	8835	8785	8613		1291	3.48E-4				
						11123	10905	10557	10350		3190	8.69E-4				
						4102	4022	4638	4547		-3138	-8.22E-4				

Table B.19: Detailed WWC data for 1.75 m DGA<sup>®</sup> / 1.75 m MAE / 3.5 m DMAEE at 60 °C.

CO <sub>2</sub> Loading	T	P <sub>tot</sub>	Q <sub>liquid</sub>	Q <sub>gas</sub>	Q <sub>gas,wet</sub>	P <sub>CO<sub>2</sub>,in,dry</sub>	P <sub>CO<sub>2</sub>,in,wet</sub>	P <sub>CO<sub>2</sub>,out,dry</sub>	P <sub>CO<sub>2</sub>,out,wet</sub>	P <sub>CO<sub>2</sub>*</sub>	(P <sub>CO<sub>2</sub>-P<sub>CO<sub>2</sub>*</sub>)<sub>LM</sub></sub>	N <sub>CO<sub>2</sub></sub>	k <sub>g</sub>	K <sub>g</sub>	k <sub>g</sub> '	K <sub>g</sub> /k <sub>g</sub> '
mol CO <sub>2</sub> /mol alkalinity	°C	psig	ml/s	StdL/min	StdL/min	Pa	Pa	Pa	Pa	Pa	Pa	mol/s m <sup>2</sup>	mol/s Pa m <sup>2</sup>	mol/s Pa m <sup>2</sup>	mol/s Pa m <sup>2</sup>	%
0.170	60	40	4	5.0	5.3	1463	1386	1191	1128	690	537	6.95E-4	2.98E-6	1.25E-6	2.16E-6	58%
						528	500	596	564		-176	-1.74E-4				
						226	214	417	395		-399	-4.88E-4				
						961	911	873	827		155	2.27E-4				
0.270	60	40	4	5.0	5.3	986	934	1734	1643	3865	-2560	-1.92E-3	2.98E-6	7.18E-7	9.46E-7	76%
						1436	1360	2028	1921		-2213	-1.52E-3				
						5418	5132	5086	4817		1102	8.50E-4				
						6926	6560	6278	5946		2375	1.66E-3				
0.350	60	40	4	5.0	5.3	3725	3528	5116	4846	9670	-5456	-3.56E-3	2.98E-6	6.42E-7	8.19E-7	78%
						4475	4239	5674	5374		-4841	-3.07E-3				
						5972	5657	6858	6496		-3577	-2.27E-3				
						12367	11713	11914	11285		1820	1.16E-3				

Table B.20: Detailed WWC data for 2 m PZ / 3 m HMPD at 0.157 mol CO<sub>2</sub> /mol alkalinity.

CO <sub>2</sub> Loading	T	P <sub>tot</sub>	Q <sub>liquid</sub>	Q <sub>gas</sub>	Q <sub>gas,wet</sub>	P <sub>CO<sub>2</sub>,in,dry</sub>	P <sub>CO<sub>2</sub>,in,wet</sub>	P <sub>CO<sub>2</sub>,out,dry</sub>	P <sub>CO<sub>2</sub>,out,wet</sub>	P <sub>CO<sub>2</sub>*</sub>	(P <sub>CO<sub>2</sub>-P<sub>CO<sub>2</sub>*</sub>)<sub>LM</sub></sub>	N <sub>CO<sub>2</sub></sub>	k <sub>g</sub>	K <sub>g</sub>	k <sub>g</sub> '	K <sub>g</sub> /k <sub>g</sub> '
mol CO <sub>2</sub> /mol alkalinity	°C	psig	ml/s	StdL/min	StdL/min	Pa	Pa	Pa	Pa	Pa	Pa	mol/s m <sup>2</sup>	mol/s Pa m <sup>2</sup>	mol/s Pa m <sup>2</sup>	mol/s Pa m <sup>2</sup>	%
0.157	20	40	4	5	5.03	0	0	11	10	19.55	-14	-2.70E-5	2.82E-6	1.72E-6	4.43E-6	39%
						9	9	14	14		-8	-1.16E-5				
						36	36	28	28		12	1.93E-5				
						29	29	25	24		7	1.16E-5				
						31	31	25	25		8	1.54E-5				
						11	11	15	15		-6	-9.65E-6				
0.157	40	40	4	5	5.1	0	0	71	70	128.7	-89	-1.82E-4	2.87E-6	1.91E-6	5.72E-6	33%
						77	76	104	102		-38	-6.95E-5				
						53	52	92	91		-55	-1.01E-4				
						252	247	189	186		84	1.61E-4				
						202	198	165	162		49	9.46E-5				
0.157	60	40	4	5	5.28	0	0	321	304	685	-518	-8.22E-4	2.98E-6	1.59E-6	3.42E-6	47%
						234	221	451	427		-351	-5.55E-4				
						448	424	569	539		-198	-3.12E-4				
						1069	1012	910	862		245	4.06E-4				
						1572	1489	1201	1137		611	9.51E-4				
0.157	80	60	4	5	5.51	0	0	1818	1650	3535	-2624	-3.41E-3	2.28E-6	1.29E-6	2.97E-6	43%
						1756	1594	2729	2478		-1454	-1.82E-3				
						5654	5133	4799	4357		1168	1.60E-3				
						6802	6176	5494	4988		1988	2.45E-3				
0.157	100	60	4	5	6.22	0	0	6230	5004	12825	-10117	-1.17E-2	2.54E-6	1.11E-6	1.96E-6	56%
						6920	5558	10143	8147		-5877	-6.04E-3				
						24921	20017	21368	17163		5646	6.66E-3				
						30585	24566	25230	20265		9428	1.00E-2				

Table B.21: Detailed WWC data for 2 m PZ / 3 m HMPD at 0.257 mol CO<sub>2</sub> /mol alkalinity.

CO <sub>2</sub> Loading	T	P <sub>tot</sub>	Q <sub>liquid</sub>	Q <sub>gas</sub>	Q <sub>gas,wet</sub>	P <sub>CO<sub>2</sub>,in,dry</sub>	P <sub>CO<sub>2</sub>,in,wet</sub>	P <sub>CO<sub>2</sub>,out,dry</sub>	P <sub>CO<sub>2</sub>,out,wet</sub>	P <sub>CO<sub>2</sub>*</sub>	(P <sub>CO<sub>2</sub>-P<sub>CO<sub>2</sub>*</sub>)<sub>LM</sub></sub>	N <sub>CO<sub>2</sub></sub>	k <sub>g</sub>	K <sub>g</sub>	k <sub>g</sub> '	K <sub>g</sub> /k <sub>g</sub> '
mol CO <sub>2</sub> /mol alkalinity	°C	psig	ml/s	StdL/min	StdL/min	Pa	Pa	Pa	Pa	Pa	Pa	mol/s m <sup>2</sup>	mol/s Pa m <sup>2</sup>	mol/s Pa m <sup>2</sup>	mol/s Pa m <sup>2</sup>	%
0.257	20	40	4	5	5.03	0	0	35	34	90	-71	-8.88E-5	2.82E-6	1.12E-6	1.86E-6	60%
						51	51	62	62		-33	-2.90E-5				
						38	38	57	56		-42	-4.63E-5				
						195	194	158	157		84	9.46E-5				
						255	253	200	199		134	1.41E-4				
						146	145	124	123		43	5.79E-5				
0.257	40	40	4	5	5.1	0	0	186	183	480	-381	-4.77E-4	2.87E-6	1.18E-6	1.99E-6	59%
						141	139	267	261		-275	-3.21E-4				
						255	250	334	327		-189	-2.01E-4				
						694	680	616	604		159	1.98E-4				
						905	887	758	743		330	3.76E-4				
						973	954	796	780		380	4.54E-4				
0.257	60	40	4	5	5.28	0	0	1033	978	2568	-2040	-2.65E-3	2.98E-6	1.27E-6	2.22E-6	57%
						1184	1121	1742	1650		-1162	-1.43E-3				
						3944	3735	3473	3289		926	1.21E-3				
						5659	5360	4562	4321		2232	2.81E-3				
0.257	80	60	4	5	5.51	0	0	4917	4465	11972	-9567	-9.22E-3	2.28E-6	9.63E-7	1.67E-6	58%
						25281	22955	20905	18981		8848	8.21E-3				
						36455	33101	27547	25013		16761	1.67E-2				
0.257	100	60	4	5	6.22	0	0	14417	11580	43550	-37462	-2.70E-2	2.54E-6	6.24E-7	8.27E-7	75%
						25178	20224	30791	24732		-20992	-1.05E-2				
						87738	70473	79809	64104		23596	1.49E-2				
						77543	62285	71931	57777		16377	1.05E-2				

Table B.22: Detailed WWC data for 2 m PZ / 3 m HMPD at 0.377 mol CO<sub>2</sub> /mol alkalinity.

CO <sub>2</sub> Loading	T	P <sub>tot</sub>	Q <sub>liquid</sub>	Q <sub>gas</sub>	Q <sub>gas,wet</sub>	PCO <sub>2,in,dry</sub>	PCO <sub>2,in,wet</sub>	PCO <sub>2,out,dry</sub>	PCO <sub>2,out,wet</sub>	PCO <sub>2</sub> *	(PCO <sub>2</sub> -PCO <sub>2</sub> <sup>*</sup> ) <sub>LM</sub>	N <sub>CO<sub>2</sub></sub>	k <sub>g</sub>	K <sub>g</sub>	k <sub>g</sub> '	K <sub>g</sub> /k <sub>g</sub> '
mol CO <sub>2</sub> /mol alkalinity	°C	psig	ml/s	StdL/min	StdL/min	Pa	Pa	Pa	Pa	Pa	Pa	mol/s m <sup>2</sup>	mol/s Pa m <sup>2</sup>	mol/s Pa m <sup>2</sup>	mol/s Pa m <sup>2</sup>	%
0.377	20	40	4	5	5.03	0	0	106	105	416	-361	-2.70E-4	2.82E-6	6.57E-7	8.57E-7	77%
						104	103	168	167		-280	-1.64E-4				
						258	257	293	292		-141	-8.98E-5				
						584	581	547	544		146	9.46E-5				
						692	688	630	626		239	1.59E-4				
0.377	40	40	4	5	5.1	0	0	607	595	2468	-2157	-1.55E-3	2.87E-6	7.54E-7	1.02E-6	74%
						505	495	1018	998		-1709	-1.31E-3				
						1063	1042	1437	1408		-1234	-9.56E-4				
						3273	3209	3084	3024		644	4.83E-4				
						4411	4325	3936	3859		1613	1.22E-3				
0.377	60	40	4	5	5.28	0	0	2741	2596	11073	-9717	-7.02E-3	2.98E-6	6.58E-7	8.44E-7	78%
						9351	8856	9803	9285		-1995	-1.16E-3				
						5912	5599	7111	6735		-4884	-3.07E-3				
						19832	18784	18022	17070		6818	4.63E-3				
						24281	22998	21491	20355		10548	7.14E-3				
0.377	80	60	4	5	5.51	0	0	10658	9678	43380	-38338	-2.00E-2	2.28E-6	4.10E-7	4.99E-7	82%
						36197	32867	37484	34036		-9917	-2.41E-3				
						19566	17766	24612	22348		-23248	-9.46E-3				
						87069	79058	79294	71999		32019	1.46E-2				
						77337	70222	71880	65266		24280	1.02E-2				

Table B.23: Detailed WWC data for 2 m PZ / 3 m HMPD at 0.444 mol CO<sub>2</sub> /mol alkalinity.

CO <sub>2</sub> Loading	T	P <sub>tot</sub>	Q <sub>liquid</sub>	Q <sub>gas</sub>	Q <sub>gas,wet</sub>	P <sub>CO<sub>2</sub>,in,dry</sub>	P <sub>CO<sub>2</sub>,in,wet</sub>	P <sub>CO<sub>2</sub>,out,dry</sub>	P <sub>CO<sub>2</sub>,out,wet</sub>	P <sub>CO<sub>2</sub>*</sub>	(P <sub>CO<sub>2</sub>-P<sub>CO<sub>2</sub>*</sub>)<sub>LM</sub></sub>	N <sub>CO<sub>2</sub></sub>	k <sub>g</sub>	K <sub>g</sub>	k <sub>g</sub> '	K <sub>g</sub> /k <sub>g</sub> '
mol CO <sub>2</sub> /mol alkalinity	°C	psig	ml/s	StdL/min	StdL/min	Pa	Pa	Pa	Pa	Pa	Pa	mol/s m <sup>2</sup>	mol/s Pa m <sup>2</sup>	mol/s Pa m <sup>2</sup>	mol/s Pa m <sup>2</sup>	%
0.444	20	40	4	5	5.03	0	0	195	194	1150	-1050	-5.00E-4	2.82E-6	4.46E-7	5.30E-7	84%
						437	435	546	542		-660	-2.77E-4				
						630	626	709	705		-484	-2.04E-4				
						1812	1800	1700	1690		593	2.85E-4				
						2933	2915	2658	2642		1625	7.05E-4				
0.444	40	40	4	5	5.1	0	0	1161	1139	6556	-5969	-2.97E-3	2.87E-6	4.65E-7	5.54E-7	84%
						3405	3338	3940	3863		-2948	-1.37E-3				
						4604	4514	4902	4806		-1893	-7.63E-4				
						13008	12753	11914	11681		5644	2.80E-3				
						10633	10424	9992	9796		3545	1.64E-3				
						24093	23621	21265	20849		15638	7.24E-3				
0.444	60	40	4	5	5.28	0	0	4279	4053	25560	-23475	-1.10E-2	2.98E-6	3.88E-7	4.46E-7	87%
						35970	34068	34763	32925		7923	3.09E-3				
						12819	12142	14554	13784		-12579	-4.44E-3				
						17570	16641	18550	17570		-8446	-2.51E-3				
						54859	51959	51127	48424		24589	9.56E-3				
						45056	42674	42379	40139		15813	6.85E-3				

Table B.24: Detailed WWC data for 2 m PZ / 3 m HMPD at 0.521 mol CO<sub>2</sub> /mol alkalinity.

CO <sub>2</sub> Loading	T	P <sub>tot</sub>	Q <sub>liquid</sub>	Q <sub>gas</sub>	Q <sub>gas,wet</sub>	P <sub>CO<sub>2</sub>,in,dry</sub>	P <sub>CO<sub>2</sub>,in,wet</sub>	P <sub>CO<sub>2</sub>,out,dry</sub>	P <sub>CO<sub>2</sub>,out,wet</sub>	P <sub>CO<sub>2</sub>*'</sub>	(P <sub>CO<sub>2</sub>-P<sub>CO<sub>2</sub>'</sub>)<sub>LM</sub></sub>	N <sub>CO<sub>2</sub></sub>	k <sub>g</sub>	K <sub>g</sub>	k <sub>g</sub> '	K <sub>g</sub> /k <sub>g</sub> '
mol CO <sub>2</sub> /mol alkalinity	°C	psig	ml/s	StdL/min	StdL/min	Pa	Pa	Pa	Pa	Pa	Pa	mol/s m <sup>2</sup>	mol/s Pa m <sup>2</sup>	mol/s Pa m <sup>2</sup>	mol/s Pa m <sup>2</sup>	%
0.521	20	40	4	5	5.03	0	0	445	442	3610	-3384	-1.14E-3	2.82E-6	2.91E-7	3.24E-7	90%
						2277	2263	2402	2387		-1284	-3.19E-4				
						1165	1158	1421	1413		-2322	-6.56E-4				
						5558	5523	5343	5310		1804	5.50E-4				
						6715	6673	6368	6329		2888	8.88E-4				
						4442	4414	4362	4335		764	2.03E-4				
0.521	40	40	4	5	5.1	0	0	1731	1697	15730	-14865	-4.43E-3	2.87E-6	2.71E-7	2.99E-7	91%
						7047	6909	7805	7652		-8444	-1.94E-3				
						3258	3194	4524	4436		-11904	-3.24E-3				
						24131	23658	23339	22882		7533	2.03E-3				
						29598	29018	28278	27724		12630	3.38E-3				
						21831	21403	21227	20812		5372	1.54E-3				
0.521	60	40	4	5	5.28	0	0	5165	4892	47170	-44679	-1.32E-2	2.98E-6	2.32E-7	2.51E-7	92%
						24206	22926	25752	24390		-23504	-3.96E-3				
						12932	12249	15873	15034		-33509	-7.53E-3				
						64511	61101	63154	59815		13278	3.48E-3				
						73183	69315	71449	67672		21313	4.44E-3				

## Appendix C: Thermal Degradation Data for DGA<sup>®</sup>/DMAEE

The following tables give the detailed thermal degradation data for DGA<sup>®</sup>/DMAEE at variable conditions.

Table C.1: Thermal degradation of 5 m DGA<sup>®</sup> with 0.2 mol H<sup>+</sup>/mole alkalinity at 150 °C.

<b>Time (day)</b>	<b>DGA (mmol/kg)</b>
0.0	3286
1.0	3285
3.1	3267
7.0	3268
13.8	3307

Table C.2: Thermal degradation of 5 m DMAEE with 0.2 mol H<sup>+</sup>/mole alkalinity at 150 °C, along with the formation of MAEE and QUAT.

<b>Time (day)</b>	<b>DMAEE</b>	<b>MAEE</b>	<b>QUAT</b>	<b>Sum</b>
	<b>(mmol/kg)</b>			
0.0	3097	0	0	3097
1.0	2978	46	40	3064
3.1	2870	121	119	3110
7.0	2654	156	153	2963
13.8	2499	152	151	2801

Table C.3: Degradation of 7 m DGA<sup>®</sup> with 0.3 mol CO<sub>2</sub>/mole alkalinity at 150 °C, along with the formation of morpholine.

Time (day)	DGA	Morpholine	Sum
	(mmol/kg)		
0.0	3882	0	3882
5.2	3596	0	3596
12.4	3453	14	3467
22.3	3501	28	3529
35.4	3445	49	3494

Table C.4: Thermal degradation of 5 m DGA<sup>®</sup>/5 m DMAEE with 0.2 mol H<sup>+</sup>/mole alkalinity at 175 °C, along with the formation of MAEE.

Time (day)	DGA	DMAEE	MAEE	Sum
	(mmol/kg)			
0.0	2059	2081	0	4141
2.8	1637	1657	1048	4343
9.8	1358	1250	1605	4212
17.0	1301	1180	1639	4120

Table C.5: Thermal degradation of 2.5 m DGA<sup>®</sup>/7.5 m DMAEE with 0.2 mol H<sup>+</sup>/mole alkalinity at 175 °C, along with the formation of MAEE.

Time (day)	DGA	DMAEE	MAEE	Sum
	(mmol/kg)			
0.0	1028	3167	0	4195
2.8	628	2550	1010	4187
9.8	464	2344	1311	4119
17.0	423	2220	1284	3926

Table C.6: Thermal degradation of 7.5 m DGA<sup>®</sup>/2.5 m DMAEE with 0.2 mol H<sup>+</sup>/mole alkalinity at 175 °C, along with the formation of MAEE.

Time (day)	DGA	DMAEE	MAEE	Sum
	(mmol/kg)			
0.0	3287	1107	0	4395
2.8	2946	886	468	4300
9.8	2632	607	974	4213
17.0	2547	518	1182	4247

Table C.7: Degradation of 5 m DGA<sup>®</sup>/5 m DMAEE with 0.4 mol CO<sub>2</sub>/mole alkalinity at 150 °C, along with the formation of MAEE and other minor products.

Time (day)	DGA	DMAEE	MAEE	M-Morph	QUAT	Sum
	(mmol/kg)					
0.0	2050	1921	0	0	0	3970
1.0	1863	1807	60	0	33	3762
3.1	1732	1711	179	0	62	3684
7.0	1610	1588	367	0	71	3636
13.8	1538	1540	583	65	49	3775
20.7	1443	1434	683	109	41	3710
32.9	1276	1287	779	186	28	3556

Table C.8: Degradation of 5 m DGA<sup>®</sup>/5 m DMAEE with 0.3 mol CO<sub>2</sub>/mole alkalinity at 150 °C, along with the formation of MAEE and other minor products.

Time (day)	DGA	DMAEE	MAEE	M-Morph	QUAT	Sum
	(mmol/kg)					
0.0	2071	1965	0	0	0	4036
4.0	1828	1784	210	0	47	3869
13.6	1638	1631	538	0	28	3835
20.8	1520	1528	688	64	21	3822
31.9	1401	1456	835	38	13	3743

Table C.9: Degradation of 5 m DGA<sup>®</sup>/5 m DMAEE with 0.3 mol CO<sub>2</sub>/mole alkalinity at 135 °C, along with the formation of MAEE and other minor products.

Time (day)	DGA	DMAEE	MAEE	M-Morph	QUAT	Sum
	(mmol/kg)					
0.0	2011	1782	0	0	0	3793
13.6	1727	1618	198	0	58	3601
20.8	1662	1594	286	0	50	3591
31.9	1627	1559	397	0	38	3621
58.0	1499	1414	600	0	33	3547

## References

- Adeosun, A., Hadri, N. El, Goetheer, E., Abu-, M.R.M., 2013. Absorption of CO<sub>2</sub> by Amine Blends Solution: An Experimental Evaluation. *Int. J. Eng. Sci.* 3, 12–23.
- Al-Juaied, M., Rochelle, G.T., 2006. Absorption of CO<sub>2</sub> in Aqueous Diglycolamine. *Ind. Eng. Chem. Res.* 45, 2473–2482.
- Alvis, R.S., Hatcher, N. a, Weiland, R.H., Rd, J., 2012. CO<sub>2</sub> Removal from Syngas Using Piperazine - Activated MDEA and Potassium Dimethyl Glycinate 20–23.
- Anslyn, E. V., Dougherty, D.A., 2006. *Modern Physical Organic Chemistry*. University Science Books.
- Arlinda Fejzo Ciftja, 2015. personal communication.
- Astarita, G., Savage, D.W., Bisio, A., 1983. *Gas Treating with Chemical Solvents*. John Wiley & Sons Inc, New York.
- Ayub, Z.H., 2003. Plate Heat Exchanger Literature Survey and New Heat Transfer and Pressure Drop Correlations for Refrigerant Evaporators. *Heat Transf. Eng.* 24, 3–16.
- Bedell, S.A., Worley, C.M., Al-Horr, R.S., McCrery, D.A., 2010. Quaternaries as Intermediates in the Thermal and Oxidative Degradation of Alkanolamines. *Ind. Eng. Chem. Res.* 49, 7147–7151.
- Bishnoi, S., Rochelle, G.T., 2002. Absorption of Carbon Dioxide in Aqueous Piperazine/Methyldiethanolamine. *AIChE J.* 48, 2788–2799.
- Bishnoi, S., Rochelle, G.T., 2000. Absorption of Carbon Dioxide into Aqueous Piperazine: Reaction Kinetics, Mass Transfer and Solubility. *Chem. Eng. Sci.* 55, 5531–5543.
- Bottoms, R.R., 1933. Process for separating acidic gases.
- Brookes, P., Lawley, P.D., 1961. The Alkylation of Guanosine and Guanylic Acid. *J.Chem.Soc.* 3923–3927.
- Cai, Z., Xie, R., Wu, Z., 1996. Binary Isobaric Vapor–Liquid Equilibria of Ethanolamines + Water. *J. Chem. Eng. Data* 41, 1101–1103.

- Catalanotti, E., Hughes, K.J., Porter, R.T.J., Price, J., Pourkashanian, M., 2014. Evaluation of Performance and Cost of Combustion-Based Power Plants with CO<sub>2</sub> Capture in the United Kingdom. *Environ. Prog. Sustain. Energy* 33, 1425–1431.
- Chang, D., Feiten, H.-J., Engesser, K.-H., van Beilen, J.B., Witholt, B., Li, Z., 2002. Practical Syntheses of N-Substituted 3-Hydroxyazetidines and 4-Hydroxypiperidines by Hydroxylation with *Sphingomonas* sp. HXN-200. *Org. Lett.* 4, 1859–1862.
- Chen, X., Cloosmann, F., Rochelle, G.T., 2011. Accurate Screening of Amines by the Wetted Wall Column. *Energy Proc.* 4, 101–108.
- Chen, X., Rochelle, G.T., 2011. Aqueous Piperazine Derivatives for CO<sub>2</sub> Capture: Accurate Screening by a Wetted Wall Column. *Chem. Eng. Res. Des.* 89, 1693–1710.
- Chowdhury, F.A., Yamada, H., Higashii, T., Goto, K., Onoda, M., 2013. CO<sub>2</sub> Capture by Tertiary Amine Absorbents: A Performance Comparison Study. *Ind. Eng. Chem. Res.* 52, 8323–8331.
- Chowdhury, F.A., Yamada, H., Matsuzaki, Y., Goto, K., Higashii, T., Onoda, M., 2014. Development of Novel Synthetic Amine Absorbents for CO<sub>2</sub> Capture. *Energy Proc.* 63, 572–579.
- Clark, V.R., Herzog, H.J., 2014. Assessment of the US EPA's determination of the role for CO<sub>2</sub> capture and storage in new fossil fuel-fired power plants. *Environ. Sci. Technol.* 48, 7723–7729.
- Cloosmann, F., Nguyen, T., Rochelle, G.T., 2009. MDEA/Piperazine as a Solvent for CO<sub>2</sub> Capture. *Energy Proc.* 1, 1351–1357.
- Cloosmann, F.B., 2011. Oxidation and Thermal Degradation of Methyldiethanolamine/Piperazine in CO<sub>2</sub> Capture. PhD dissertation, The University of Texas at Austin.
- Conway, W., Yang, Q., James, S., Wei, C.-C., Bown, M., Feron, P., Puxty, G., 2014. Designer Amines for Post Combustion CO<sub>2</sub> Capture Processes. *Energy Proc.* 63, 1827–1834.
- Da Silva, E.F., Hoff, K.A., Booth, A., 2013. Emissions from Postcombustion CO<sub>2</sub> Capture Plants; An Overview. *Energy Proc.* 37, 784–790.

- Dai, N., Mitch, W.A., 2013. Influence of Amine Structural Characteristics on N-nitrosamine Formation Potential Relevant to Postcombustion CO<sub>2</sub> Capture Systems. *Environ. Sci. Technol.* 47, 13175–13183.
- Davis, J., Rochelle, G., 2009. Thermal Degradation of Monoethanolamine at Stripper Conditions. *Energy Proc.* 1, 327–333.
- Davis, J.D., 2009. Thermal Degradation of Aqueous Amines Used for Carbon Dioxide Capture. The University of Texas at Austin.
- Du, Y., Li, L., Namjoshi, O., Voice, A.K., Fine, N.A., Rochelle, G.T., 2013. Aqueous Piperazine/N-(2-aminoethyl) piperazine for CO<sub>2</sub> Capture. *Energy Proc.* 37, 1621–1638.
- Du, Y., Wang, Y., Rochelle, G.T., 2016b. Thermal Degradation of Piperazine/4-Hydroxy-1-methylpiperidine for CO<sub>2</sub> Capture. *Prep.*
- Du, Y., Wang, Y., Rochelle, G.T., 2016a. Thermal Degradation of Novel Piperazine-based Amine Blends for CO<sub>2</sub> Capture. *Prep.*
- Du, Y., Yuan, Y., Rochelle, G.T., 2016c. CO<sub>2</sub> Capacity and Absorption rate of Novel Piperazine-based Amine Blends for Flue Gas CO<sub>2</sub> Capture. *Prep.*
- Du, Y., Yuan, Y., Rochelle, G.T., 2016d. Volatility of Amines for CO<sub>2</sub> Capture. *Prep.*
- Dugas, R.E., 2009. Carbon Dioxide Absorption, Desorption, and Diffusion in Aqueous Piperazine and Monoethanolamine. PhD dissertation, The University of Texas at Austin.
- Eide-Haugmo, I., Brakstad, O.G., Hoff, K.A., Sørheim, K.R., da Silva, E.F., Svendsen, H.F., 2009. Environmental Impact of Amines. *Energy Proc.* 1, 1297–1304.
- Eide-Haugmo, I., Lepaumier, H., Einbu, A., Vernstad, K., Da Silva, E.F., Svendsen, H.F., 2011. Chemical Stability and Biodegradability of New Solvents for CO<sub>2</sub> Capture. *Energy Proc.* 4, 1631–1636.
- EPA, 2015a. Inventory of U.S. Greenhouse Gas Emissions and Sinks: 1990-2014.
- EPA, 2015b. Carbon Pollution Emission Guidelines for Existing Stationary Sources: Electric Utility Generating Units.

- Fakstorp, J., Speggers, G., Theander, O., Zackrisson, M., Ernster, L., Diczfalusy, E., 1958. Bifunctional Amines and Ammonium Compounds. VII. Basic Strength of Some Tert. Amino Alkyl Ethers. *Acta Chem. Scand.* 12, 350–350.
- Finkenrath, M., 2012. Carbon Dioxide Capture from Power Generation – Status of Cost and Performance. *Chem. Eng. Technol.* 35, 482–488.
- Frailie, P.T., 2014. Modeling of Carbon Dioxide Absorption/Stripping by Aqueous Methyl-diethanolamine/Piperazine. PhD dissertation, The University of Texas at Austin.
- Freeman, S.A., 2011. Thermal Degradation and Oxidation of Aqueous Piperazine for Carbon Dioxide Capture. PhD dissertation, The University of Texas at Austin.
- Freeman, S.A., Davis, J., Rochelle, G.T., 2010a. Degradation of Aqueous Piperazine in Carbon Dioxide Capture. *Int. J. Greenh. Gas Control* 4, 756–761.
- Freeman, S.A., Dugas, R.E., Van Wagener, D.H., Nguyen, T., Rochelle, G.T., 2010b. Carbon Dioxide Capture with Concentrated, Aqueous Piperazine. *Int. J. Greenh. Gas Control* 4, 119–124.
- Freeman, S.A., Rochelle, G.T., 2012a. Thermal Degradation of Aqueous Piperazine for CO<sub>2</sub> Capture. 1. Effect of Process Conditions and Comparison of Thermal Stability of CO<sub>2</sub> Capture Amines. *Ind Eng Chem Res* 51, 7719–7725.
- Freeman, S.A., Rochelle, G.T., 2012b. Thermal Degradation of Aqueous Piperazine for CO<sub>2</sub> Capture: 2. Product Types and Generation Rates. *Ind. Eng. Chem. Res.* 51, 7726–7735.
- Freeman, S.A., Rochelle, G.T., 2011. Thermal Degradation of Piperazine and its Structural Analogs. *Energy Proc.* 4, 43–50.
- Gangarapu, S., Marcelis, A.T.M., Zuilhof, H., 2013. Carbamate Stabilities of Sterically Hindered Amines from Quantum Chemical Methods: Relevance for CO<sub>2</sub> Capture. *ChemPhysChem* 14, 3936–43.
- Goto, K., Okabe, H., Chowdhury, F.A., Shimizu, S., Fujioka, Y., Onoda, M., 2011. Development of Novel Absorbents for CO<sub>2</sub> Capture from Blast Furnace Gas. *Int. J. Greenh. Gas Control* 5, 1214–1219.
- Grob, C.A., 1985. Inductive Charge Dispersal in Quinuclidinium Ions. Polar Effects, Part 13. *Helv. Chim. Acta* 68, 882–886.

- Haines, J.A., Reese, C.B., Todd, Lord, 1962. The Methylation of Guanosine and Related Compounds with Diazomethane. *J. Chem. Soc.* 5281–5288.
- Hamborg, E.S., Niederer, J.P.M., Versteeg, G.F., 2007. Dissociation Constants and Thermodynamic Properties of Amino Acids Used in CO<sub>2</sub> Absorption from (293 to 353) K. *J. Chem. Eng. Data* 52, 2491–2502.
- Hamborg, E.S., Versteeg, G.F., 2009. Dissociation Constants and Thermodynamic Properties of Amines and Alkanolamines from (293 to 353) K. *J. Chem. Eng. Data* 54, 1318–1328.
- Hatchell, D., 2015. Thermal Degradation and Corrosion of Amines for CO<sub>2</sub> Capture. The University of Texas at Austin.
- Hatchell, D., Namjoshi, O., Fischer, K., Rochelle, G.T., 2014. Thermal Degradation of Linear Amines for CO<sub>2</sub> Capture. *Energy Proc.* 63, 1558–1568.
- Haubrock, J., Hogendoorn, J.A., Versteeg, G.F., 2007. The Applicability of Activities in Kinetic Expressions: A More Fundamental Approach to Represent the Kinetics of the System—Salt in terms of Activities. *Chem. Eng. Sci.* 62, 5753–5769.
- Hine, J., Mookerjee, P.K., 1975. Structural effects on rates and equilibria. XIX. Intrinsic hydrophilic character of organic compounds. Correlations in terms of structural contributions. *J. Org. Chem.* 40, 292–298.
- Hofmann, K., 1953. *Chemistry of Heterocyclic Compounds: Imidazole and Its Derivatives*. Interscience Publishers, Inc.
- Hook, R.J., 1997. An Investigation of Some Sterically Hindered Amines as Potential Carbon Dioxide Scrubbing Compounds. *Ind. Eng. Chem. Res.* 36, 1779–1790.
- HOWTON, D.R., 1945. 1,3-DIMETHYLPYPERIDONE-4. *J. Org. Chem.* 10, 277–282.
- Hu, W., Frenkel, D., Mathot, V.B.F., 2002. Free Energy Barrier for Single-chain Melting and Crystallization 7.
- Huang, Q., Bhatnagar, S., Remias, J.E., Selegue, J.P., Liu, K., 2013. Thermal Degradation of Amino Acid Salts in CO<sub>2</sub> Capture. *Int. J. Greenh. Gas Control* 19, 243–250.
- IPCC, 2014. Summary for Policymakers, in: Field, C.B., Barros, V.R., Dokken, D.J., Mach, K.J., M.D., M., Bilir, T.E., Chatterjee, M., Ebi, K.L., Estrada, Y.O., Genova, R.C., Girma, B., Kissel, E.S., Levy, A.N., MacCracken, S., Mastrandrea, P.R.,

White, L.L. (Eds.), *Climate Change 2014: Impacts, Adaptation, and Vulnerability. Part A: Global and Sectoral Aspects. Contribution of Working Group II to the Fifth Assessment Report of the Intergovernmental Panel on Climate Change*. Cambridge University Press, Cambridge, United Kingdom and New York, NY, USA.

Jencks, W.P., Carriuolo, J., 1959. Imidazole Catalysis: III. General Base Catalysis and the Reactions of Acetyl Imidazole with Thiols and Amines. *J. Biol. Chem.* 234, 1280–1285.

Kato, K., Jingu, S., Ogawa, N., Higuchi, S., 2002. Differentiation Between Isomeric Oxidative Metabolites of a Piperidine-containing Drug by Liquid Chromatography-tandem Mass Spectrometry with Stable-isotope Tracer Technique. *Biomed. Chromatogr.* 16, 25–30.

Khakharia, P., 2015. *Aerosol-based Emission, Solvent Degradation, and Corrosion in Post Combustion CO<sub>2</sub> Capture*. Master Thesis. Technische Universiteit Delft, the Netherlands.

Kim, I., Svendsen, H.F., Børresen, E., 2008. Ebulliometric Determination of Vapor–Liquid Equilibria for Pure Water, Monoethanolamine, N - Methyl-diethanolamine, 3-(Methylamino)-propylamine, and Their Binary and Ternary Solutions. *J. Chem. Eng. Data* 53, 2521–2531.

Knuutila, H., Juliussen, O., Svendsen, H.F., 2010. Kinetics of the Reaction of Carbon Dioxide with Aqueous Sodium and Potassium Carbonate Solutions. *Chem. Eng. Sci.* 65, 6077–6088.

Kochetkov, N.K., Budovskii, E.I., 1972. *Organic Chemistry of Nucleic Acids, Part B*. Plenum Press, New York.

Kohl, A.L., Nielsen, R., 1997. *Gas Purification*. Gulf Professional Publishing.

Kumar, G., Kundu, M., 2012. Solubility of CO<sub>2</sub> in Aqueous Blends of (N-methyl-2-ethanolamine+N-methyl-diethanolamine) and (N-methyl-2-ethanolamine+2-amino-2-methyl-1-propanol). *J. Chem. Eng. Data* 57, 3203–3209.

Larsen, B.L., Rasmussen, P., Fredenslund, A., 1987. A Modified UNIFAC Group-contribution Model for Prediction of Phase Equilibria and Heats of Mixing. *Ind. Eng. Chem. Res.* 26, 2274–2286.

Lenard, J.-L., Rousseau, R.W., Teja, A.S., 1990. Vapor-Liquid Equilibria for Mixtures of 2-aminoethanol+ water. *AIChE Symp. Ser.* 86, 1–5.

- Lepaumier, H., Picq, D., Carrette, P., 2009. New Amines for CO<sub>2</sub> Capture. I. Mechanisms of Amine Degradation in the Presence of CO<sub>2</sub>. *Ind. Eng. Chem. Res.* 48, 9061–9067.
- Li, H., Li, L., Nguyen, T., Rochelle, G.T., Chen, J., 2013. Characterization of Piperazine/2-Aminomethylpropanol for Carbon Dioxide Capture. *Energy Proc.* 37, 340–352.
- Li, H., Moullec, Y. Le, Lu, J., Chen, J., Marcos, J.C.V., Chen, G., 2014a. Solubility and Energy Analysis for CO<sub>2</sub> Absorption in Piperazine Derivatives and their Mixtures. *Int. J. Greenh. Gas Control* 31, 25–32.
- Li, H., Moullec, Y. Le, Lu, J., Chen, J., Marcos, J.C.V., Chen, G., 2014b. Solubility and Energy Analysis for CO<sub>2</sub> Absorption in Piperazine Derivatives and their Mixtures. *Int. J. Greenh. Gas Control* 31, 25–32.
- Li, L., 2015. Carbon Dioxide Solubility and Mass Transfer in Aqueous Amines for Carbon Capture. PhD dissertation, The University of Texas at Austin.
- Li, L., Li, H., Namjoshi, O., Du, Y., Rochelle, G.T., 2013a. Absorption Rates and CO<sub>2</sub> Solubility in New Piperazine Blends. *Energy Proc.* 37, 370–385.
- Li, L., Voice, A.K., Li, H., Namjoshi, O., Nguyen, T., Du, Y., Rochelle, G.T., 2013b. Amine Blends using Concentrated Piperazine. *Energy Proc.* 37, 353–369.
- Li, Z., Chang, D., Witholt, B., 2004. Process for Preparing n-substituted 4-hydroxypiperidines by Enzymatic Hydroxylation.
- Liu, H., 2015. Oxidative Degradation of Amine Solvents for CO<sub>2</sub> Capture. The University of Texas at Austin.
- Liu, H., Namjoshi, O., Rochelle, G.T., 2014. Oxidative Degradation of Amine Solvents for CO<sub>2</sub> Capture. *Energy Proc.* 63, 1546–1557.
- Long, F.A., McDevit, W.F., 1952. Activity Coefficients of Nonelectrolyte Solutes in Aqueous Salt Solutions. *Chem. Rev.* 51, 119–169.
- Luo, S.-N., Strachan, A., Swift, D.C., 2004. Nonequilibrium Melting and Crystallization of a Model Lennard-Jones System. *J. Chem. Phys.* 120, 11640–9.
- Ma, X., Kim, I., Beck, R., Knuutila, H., Andreassen, J.P., 2012. Precipitation of Piperazine in Aqueous Piperazine Solutions with and without CO<sub>2</sub> Loadings. *Ind. Eng. Chem. Res.* 51, 12126–12134.

- Maraš, N., Polanc, S., Kočevar, M., 2012. Ring-opening Reactions of 1,4-diazabicyclo[2.2.2]octane (DABCO) Derived Quaternary Ammonium Salts with Phenols and Related Nucleophiles. *Org. Biomol. Chem.* 10, 1300.
- Mazari, S.A., Ali, B.S., Jan, B.M., Saeed, I.M., Nizamuddin, S., 2015. An Overview of Solvent Management and Emissions of Amine-based CO<sub>2</sub> Capture Technology. *Int. J. Greenh. Gas Control* 34, 129–140.
- McElvain, S.M., McMahan, R.E., 1949. Piperidine Derivatives. XXI. 4-Piperidone, 4-Piperidinol and Certain of their Derivatives. *J. Am. Chem. Soc.* 71, 901–906.
- Mousavi, M., Mohammadalizadeh, M., Khosravan, A., 2011. Theoretical Investigation of Corrosion Inhibition Effect of Imidazole and its Derivatives on Mild Steel using Cluster Model. *Corros. Sci.* 53, 3086–3091.
- Müller-Schwarze, D., Silverstein, R.M. (Eds.), 1980. *Chemical Signals*. Springer US, Boston, MA.
- Mullin, J.W., 2001. *Crystallization*. Butterworth-Heinemann.
- Murai, S., Kato, Y., Maezawa, Y., Muramatsu, T., Saito, S., 2013. Novel Hindered Amine Absorbent for CO<sub>2</sub> Capture. *Energy Proc.* 37, 417–422.
- Namjoshi, O., 2015. Thermal Degradation of PZ-Promoted Tertiary Amines for CO<sub>2</sub> Capture. PhD dissertation, The University of Texas at Austin.
- Namjoshi, O., Li, L., Du, Y., Rochelle, G.T., 2013. Thermal Degradation of Piperazine Blends with Diamines. *Energy Proc.* 37, 1904–1911.
- Nguyen, T., 2013. Amine Volatility in CO<sub>2</sub> Capture. PhD dissertation, The University of Texas at Austin.
- Nguyen, T., Hilliard, M., Rochelle, G.T., 2010. Amine Volatility in CO<sub>2</sub> Capture. *Int. J. Greenh. Gas Control* 4, 707–715.
- Nielsen, P.T., Li, L., Rochelle, G.T., 2013. Piperazine Degradation in Pilot Plants. *Energy Proc.* 37, 1912–1923.
- Nozaki, Y., Gurd, F.R.N., Chen, R.F., Edsall, J.T., 1957. The Association of 4-Methylimidazole with the Ions of Cupric Copper and Zinc; with Some Observations on 2,4-Dimethylimidazole. *J. Am. Chem. Soc.* 79, 2123–2129.

- Oexmann, J., Kather, A., 2010. Minimising the regeneration heat duty of post-combustion CO<sub>2</sub> capture by wet chemical absorption: The misguided focus on low heat of absorption solvents. *Int. J. Greenh. Gas Control* 4, 36–43.
- Oyenekan, B.A., Rochelle, G.T., 2007. Alternative Stripper Configurations for CO<sub>2</sub> Capture by Aqueous Amines. *AIChE J.* 53, 3144–3154.
- Paoletti, P., Stern, J.H., Vacca, A., 1965. Thermochemical Studies. XV. 1 Thermodynamics of Protonation of Triethylenediamine, Triethylamine, Trimethylamine, and Ammonia in Aqueous Solution at 25 °. *J. Phys. Chem.* 69, 3759–3762.
- Pappa, G.D., Anastasi, C., Voutsas, E.C., 2006. Measurement and Thermodynamic Modeling of the Phase Equilibrium of Aqueous 2-amino-2-methyl-1-propanol Solutions. *Fluid Phase Equilib.* 243, 193–197.
- Plaza, J.M., 2011. Modeling of Carbon Dioxide Absorption using Aqueous Monoethanolamine, Piperazine and Promoted Potassium Carbonate. PhD dissertation, The University of Texas at Austin.
- Puxty, G., Rowland, R., Allport, A., Yang, Q., Bown, M., Burns, R., Maeder, M., Attalla, M., 2009. Carbon Dioxide Postcombustion Capture: A Novel Screening Study of the Carbon Dioxide Absorption Performance of 76 Amines. *Environ. Sci. Technol.* 43, 6427–6433.
- Radzisewski, B., 1882. Ueber Glyoxalin und seine Homologe. *Berichte der Dtsch. Chem. Gesellschaft* 15, 2706–2708.
- Robinson, K., McCluskey, A., Attalla, M., 2011. The Effect Molecular Structural Variations has on the CO<sub>2</sub> Absorption Characteristics of Heterocyclic Amines. *Energy Proc.* 4, 224–231.
- Rochelle, G.T., 2012. Thermal Degradation of Amines for CO<sub>2</sub> Capture. *Curr. Opin. Chem. Eng.* 1, 183–190.
- Rochelle, G.T., 2009. Amine Scrubbing for CO<sub>2</sub> Capture. *Science* 325, 1652–4.
- Rochelle, G.T., Chen, E., Freeman, S.A., Van Wagener, D., Xu, Q., Voice, A.K., 2011. Aqueous Piperazine as the New Standard for CO<sub>2</sub> Capture Technology. *Chem. Eng. J.* 171, 725–733.

- Rubin, E.S., Chen, C., Rao, A.B., 2007. Cost and performance of fossil fuel power plants with CO<sub>2</sub> capture and storage. *Energy Policy* 35, 4444–4454.  
doi:10.1016/j.enpol.2007.03.009
- Salkuyeh, Y.K., Mofarahi, M., 2012. Comparison of MEA and DGA Performance for CO<sub>2</sub> Capture under Different Operational Conditions. *Int. J. Energy Res.* 36, 259–268.
- Sandler, S.R., Delgado, M.L., 1969. Reinvestigation of the Reaction of Piperazine with Aldehydes. *J. Polym. Sci. Part A-1 Polym. Chem.* 7, 1373–1378.
- Seo, D.J., Hong, W.H., 2000. Effect of Piperazine on the Kinetics of Carbon Dioxide with Aqueous Solutions of 2-Amino-2-methyl-1-propanol. *Ind. Eng. Chem. Res.* 39, 2062–2067.
- Shannon, M.S., Bara, J.E., 2011. Properties of Alkylimidazoles as Solvents for CO<sub>2</sub> Capture and Comparisons to Imidazolium-based Ionic Liquids. *Ind. Eng. Chem. Res.* 50, 8665–8677.
- Shao, R., Stangeland, A., 2009. Amines Used in CO<sub>2</sub> Capture-Health and Environmental Impacts.
- Sherman, B., Ciftja, A.F., Rochelle, G.T., 2016. Thermodynamic and Mass Transfer Modeling of Carbon Dioxide Absorption into Aqueous 2-piperidineethanol.
- Silva, E.F., Grimstvedt, A., Vevelstad, S.J., Einbu, A., Vernstad, K., Svendsen, H.F., Zahlsen, K., 2012. Understanding 2-Ethanolamine Degradation in Postcombustion CO<sub>2</sub> Capture. *Ind. Eng. Chem. Res.* 51, 13329–13338.
- Silvia Pérez-Casas, Moreno-Esparza, R., Costas, M., Patterson, D., 1991. Effect of steric hindrance and  $\pi$  electrons on alcohol self-association. *J. Chem. Soc., Faraday Trans.* 87, 1745–1750.
- Simond, M.R., Ballerat-Busserolles, K., Coulier, Y., Rodier, L., Coxam, J.Y., 2012. Dissociation constants of protonated amines in water at temperatures from 293.15 K to 343.15 K. *J. Solution Chem.* 41, 130–142.
- Singh, P., 2011. Amine based solvent for CO<sub>2</sub> absorption “From molecular structure to process.” University of Twente.
- Song, H.-J., Park, S., Kim, H., Gaur, A., Park, J.-W., Lee, S.-J., 2012. Carbon Dioxide Absorption Characteristics of Aqueous Amino Acid Salt Solutions. *Int. J. Greenh. Gas Control* 11, 64–72.

- Spencer, J.N., Bodner, G.M., Rickard, L.H., 2010. *Chemistry: Structure and Dynamics*. John Wiley & Sons.
- Strazisar, B.R., Anderson, R.R., White, C.M., 2003. Degradation Pathways for Monoethanolamine in a CO<sub>2</sub> Capture Facility. *Energy and Fuels* 17, 1034–1039.
- Tomizaki, K.Y., Shimizu, S., Onoda, M., Fujioka, Y., 2010. Heats of Reaction and Vapor-Liquid Equilibria of Novel Chemical Absorbents for Absorption/Recovery of Pressurized Carbon Dioxide in Integrated Coal Gasification Combined Cycle-Carbon Capture and Storage Process. *Ind. Eng. Chem. Res.* 49, 1214–1221.
- Treybig, D.S., 1989. Process for the Reaction of Piperazine, and Derivatives thereof, with Glyoxal, and Derivatives thereof. U.S. patent 4837324.
- Voice, A.K., 2013. Amine Oxidation in Carbon Dioxide Capture by Aqueous Scrubbing. PhD dissertation, The University of Texas at Austin.
- Xu, Q., Rochelle, G.T., 2011. Total Pressure and CO<sub>2</sub> Solubility at High Temperature in Aqueous Amines. *Energy Proc.* 4, 117–124.
- Xu, S., Otto, F.D., Mather, A.E., 1993. Dissociation constants of some alkanolamines. *Can. J. Chem.* 71, 1048–1050.
- Xu, S., Wang, Y., Otto, F.D., Mather, A.E., 1992. Physicochemical properties of 2-piperidineethanol and its aqueous solutions. *J. Chem. Eng. Data* 37, 407–411.
- Yamada, H., Shimizu, S., Okabe, H., Matsuzaki, Y., Chowdhury, F. a., Fujioka, Y., 2010. Prediction of the basicity of aqueous amine solutions and the species distribution in the amine-H<sub>2</sub>O-CO<sub>2</sub> system using the COSMO-RS method. *Ind. Eng. Chem. Res.* 49, 2449–2455.
- Yuan, Y., Du, Y., Rochelle, G.T., 2016. Hybrid amine/physical solvent in aqueous solution for CO<sub>2</sub> capture.
- Zhou, S., Chen, X., Nguyen, T., Voice, A.K., Rochelle, G.T., 2010. Aqueous Ethylenediamine for CO<sub>2</sub> Capture. *ChemSusChem* 3, 913–918.